

CO-REGULATION OF ENDOTHELIAL AND MYOGENIC CELL FATES THROUGH INTERCELLULAR CROSSTALK IN SKELETAL MUSCLE

Présentée le 1^{er} octobre 2021

Faculté des sciences de la vie
Programme doctoral en biotechnologie et génie biologique

pour l'obtention du grade de Docteur ès Sciences

par

Umji LEE

Acceptée sur proposition du jury

Prof. B. E. Ferreira De Sousa Correia, président du jury
Dr J. Feige, Prof. B. D. Cosgrove, directeurs de thèse
Prof. P. Muñoz-Cánoves, rapporteuse
Prof. P. Castets, rapporteuse
Prof. K. De Bock, rapporteuse

Thesis Committee

Prof. Bruno Correia (President of Jury)

Dr. Jerome Feige (Director)

Prof. Benjamin Cosgrove (Director)

Prof. Katrien De Bock

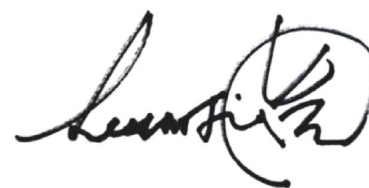
Prof. Pura Muñoz-Canoves

Prof. Perrine Castets

Umji Lee

Ithaca
14850, New York
United States of America

05 August 2021
EPF Lausanne, Switzerland

A handwritten signature in black ink, appearing to read 'Umji Lee', with a large circular flourish at the end.

Co-regulation of Endothelial and Myogenic Cell Fates Through Intercellular Crosstalk in Skeletal Muscle

Abstract

Skeletal muscle is one of the most dynamic organs in the human body, which has a vigorous potential to regenerate and adapt to environmental changes. Depending on environments, skeletal muscle enables essential life activities to survive by controlling movement and metabolism. The functional and structural adaptations of skeletal muscle crosstalk with other physiological systems enabling nutrition and oxygen delivery, and the elimination of metabolic waste products. The work in this dissertation focuses on the intercellular signals produced by myogenic cells to dynamically remodel skeletal muscle during exercise or muscle repair, and the reciprocal signals from the local niche and the systemic environment that regulate myogenic cell fate and metabolism according to physiological needs. This complex crosstalk is dissected in three specific chapters where we study the crosstalk of myogenic cells with endothelial cells and the vasculature to coordinate local niche interactions and systemic crosstalks. First, we demonstrate that an exercise-induced myokine called apelin is produced by muscle fiber and mediates intercellular signaling to endothelial cells through the apelin receptor. In addition, through a yeast one-hybrid screen of transcription factor binding to the apelin promoter, we identified the myogenic transcription factor TEA domain family member 1 (*Tead1*) as a regulator of *ApIn* transcription. We observed via single-cell transcriptomic analysis of regenerating skeletal muscle that *ApInr* (Apelin receptor) is enriched in muscle endothelial cells, whereas *Tead1* is enriched in myogenic cells. Myofiber-specific over-expression of *Tead1* suppresses apelin secretion at the whole-body level, and apelin secretion via *Tead1* knock-down in muscle cells stimulates endothelial cell proliferation in co-cultures. By showing that apelin peptide supplementation in vivo enhances endothelial cell expansion following muscle injury, we conclude that paracrine crosstalk in which apelin secretion controlled by *Tead1* in myogenic cells influences endothelial remodeling during skeletal muscle repair.

Secondly, we show how tissue-resident support cells affect muscle progenitor activation in different metabolic environments. Skeletal muscle progenitors (SKMP) reside in close

proximity to supportive cell types in the stem cell niche and dynamically interact with each other to adapt to environmental changes. Here, we studied how different niche cell types affect SKMPs in response to glyceic levels. Using co-cultures of SKMPs and niche cells, we discovered that endothelial cells synergistically enhance SKMP proliferation in a low glyceic environment, while fibroblasts and macrophages had no effect. We observed that the crosstalk between SKMPs and endothelial cells was mediated by direct cell-cell contacts independent of soluble paracrine signals. Transcriptomic analysis revealed that the endothelial alpha/beta hydrolase N-Myc Downstream Regulated1 (NDRG1) is induced by a low glyceic environment and is associated with biological adhesion. SKMPs co-cultured with NdrG1 knock-down endothelial cells lose their synergistic functional relationship in response to glucose levels. Therefore, our findings suggest that NdrG1 is a key mediator of endothelial cell-mediated glyceic control of SKMPs and provides a link between systemic energy levels and the skeletal muscle stem cell niche.

Lastly, I developed intravital imaging to monitor muscle stem cells and vasculature to deepen the anatomical and kinetic understanding of the intercellular crosstalk between vascular networks and muscle stem cells (MuSCs) in vivo. To that end, we optimized the long-lasting- chronic window frame to optically access hindlimb muscle during recovery, developed an endogenous endothelial cell labeling system, and monitored MuSC engraftment after cell transplantation in a living animal. We discovered that most of the muscle stem cells successfully engrafted were located in close proximity of the vasculature and endothelial niche. This approach offers a great promise for the development of a robust tool to monitor muscle repair dynamics in real-time with spatial information of the vascular network. Altogether, my dissertation chapters bring together a complementary set of cellular mechanisms with reciprocal co-regulatory effects between myogenic and endothelial cell fates and established a competitive tool to investigate them in a living animal.

Co-régulation du destin des cellules endothéliales et myogéniques par diaphonie intercellulaire dans le muscle squelettique

Résumé

Le muscle squelettique est l'un des organes les plus dynamiques du corps humain, qui a un potentiel vigoureux pour se régénérer et s'adapter aux changements environnementaux. Selon les environnements, le muscle squelettique permet aux activités vitales essentielles de survivre en contrôlant les mouvements et le métabolisme. Les adaptations fonctionnelles et structurelles du muscle squelettique se croisent avec d'autres systèmes physiologiques permettant la nutrition et l'apport d'oxygène, et l'élimination des déchets métaboliques. Le travail de cette thèse se concentre sur les signaux intercellulaires produits par les cellules myogéniques pour remodeler dynamiquement le muscle squelettique pendant l'exercice ou la réparation musculaire, et les signaux réciproques de la niche locale et de l'environnement systémique qui régulent le destin et le métabolisme des cellules myogéniques en fonction des besoins physiologiques. Cette diaphonie complexe est disséquée dans trois chapitres spécifiques où nous étudions la diaphonie des cellules myogéniques avec les cellules endothéliales et le système vasculaire pour coordonner les interactions de niche locales et les diaphonies systémiques. Premièrement, nous démontrons qu'une myokine induite par l'exercice appelée apéline est produite par la fibre musculaire et médie la signalisation intercellulaire vers les cellules endothéliales via le récepteur de l'apéline. En outre, grâce à un criblage de levure mono-hybride du facteur de transcription se liant au promoteur de l'apéline, nous avons identifié le membre de la famille du domaine du facteur de transcription myogénique TEA 1 (Tead1) en tant que régulateur de la transcription *Apln*. Nous avons observé via une analyse transcriptomique unicellulaire du muscle squelettique en régénération que *Aplnr* (récepteur Apelin) est enrichi en cellules endothéliales musculaires, tandis que *Tead1* est enrichi en cellules myogéniques. La surexpression de *Tead1* spécifique aux myofibres supprime la sécrétion d'apéline au niveau du corps entier, et la sécrétion d'apéline via *Tead1* knock-down dans les cellules musculaires stimule la prolifération des cellules endothéliales dans les co-cultures. En montrant que la supplémentation en peptide apéline *in vivo* améliore l'expansion des cellules endothéliales après une lésion musculaire, nous concluons que la paracrine croisée dans laquelle la

sécrétion d'apéline contrôlée par Tead1 dans les cellules myogéniques influence le remodelage endothélial pendant la réparation des muscles squelettiques.

Deuxièmement, nous montrons comment les cellules de soutien résidentes dans les tissus affectent l'activation des progéniteurs musculaires dans différents environnements métaboliques. Les progéniteurs des muscles squelettiques (SKMP) résident à proximité immédiate des types de cellules de soutien dans la niche des cellules souches et interagissent dynamiquement les uns avec les autres pour s'adapter aux changements environnementaux. Ici, nous avons étudié comment différents types de cellules de niche affectent les SKMP en réponse aux niveaux glycémiques. En utilisant des co-cultures de SKMP et de cellules de niche, nous avons découvert que les cellules endothéliales améliorent de manière synergique la prolifération de SKMP dans un environnement à faible indice glycémique, tandis que les fibroblastes et les macrophages n'ont aucun effet. Nous avons observé que la diaphonie entre les SKMP et les cellules endothéliales était médiée par des contacts directs cellule-cellule indépendants des signaux paracrines solubles. L'analyse transcriptomique a révélé que l'hydrolase endothéliale alpha/bêta N-Myc Downstream Regulated1 (NDRG1) est induite par un environnement à faible indice glycémique et est associée à une adhésion biologique. Les SKMP co-cultivés avec des cellules endothéliales knock-down *Ndr1* perdent leur relation fonctionnelle synergique en réponse aux niveaux de glucose. Par conséquent, nos résultats suggèrent que *Ndr1* est un médiateur clé du contrôle glycémique à médiation cellulaire endothéliale des SKMP et fournit un lien entre les niveaux d'énergie systémique et la niche des cellules souches du muscle squelettique.

Enfin, j'ai développé l'imagerie intravitale pour surveiller les cellules souches musculaires et le système vasculaire afin d'approfondir la compréhension anatomique et cinétique de la diaphonie intercellulaire entre les réseaux vasculaires et les cellules souches musculaires (MuSC) *in vivo*. À cette fin, nous avons optimisé le cadre de la fenêtre chronique de longue durée pour accéder optiquement au muscle des membres postérieurs pendant la récupération, développé un système de marquage des cellules endothéliales endogènes et surveillé la prise de greffe MuSC après transplantation cellulaire chez un animal vivant. Nous avons découvert que la plupart des cellules souches musculaires greffées avec succès étaient situées à proximité du système vasculaire et de la niche endothéliale. Cette approche offre une grande promesse pour le développement d'un outil robuste pour

surveiller la dynamique de réparation musculaire en temps réel avec des informations spatiales du réseau vasculaire. Au total, les chapitres de ma thèse rassemblent un ensemble complémentaire de mécanismes cellulaires avec des effets de corégulation réciproques entre les destins des cellules myogéniques et endothéliales et ont établi un outil compétitif pour les étudier chez un animal vivant.

Acknowledgments

You can not hope to build a better world without improving the individuals. To that end, each of us must work for our own improvement and, at the same time share general responsibility for all humanity, our particular duty being to aid those to whom we think we can be most useful.

- Marie Sklodowska 1867-1984

As I remember, when I was at my elementary school, I often spoke that I would like to become an artist in the future. A lot of accidental events in my life brought me into the art of measuring life activity and converting the art into a scientific hypothesis. Five years of my Ph.D. taught me that science is not just measurements and equations but is iterative empirical observations and recursive corrections on my hypothesis. And I learned keeping the enthusiasm during this iteration will make a scientist. However, to keep motivated amid the small and big failures for 5 years was extremely hard. Every time I am facing the small and big hurdles, I had so much luck with my mentors, teachers, colleagues, and friends who help me keep going without losing my enthusiasm. I sincerely thank all the people who worked with me and talked with me during this time.

My intellectual development and scientific thinking owe a huge deal to my two advisors **Dr. Jerome Feige** and **Dr. Benjamin Cosgrove**. I sincerely thank Dr. Feige and Prof. Cosgrove for allowing me to carry out my exciting Ph.D. projects under their guidance and for providing the tools and invaluable advice to enrich my research and scientific education. I am indebted to all their support and help on scientific growth but also for showing me a lot of inspiration what is a good leader-like. It was a great privilege to work with them. They have been the most influencing advisors in both professional and personal aspects of my career and gave exceptional scientific supervision during my time at EPFL and Cornell University. They advised me each study, which was not only for a big picture design or results but also brings important details and messages from the moment I started to design an experiment. I have learned a great deal from them how to logically and constructively approach scientific questions. I believe their mentorship and advice are necessary factors in finishing my Ph.D. Beyond my Ph.D. project supervision, their encouragement and passion for learning and communicating with other scientists in the field, have guided me in many aspects. The encouragement to attend scientific conferences whenever there is a related conference or seminar and also leading the Muscle Science Talk Series, which is not only helpful to broaden the knowledge but also it is a huge contribution

to the field of muscle biology. I sincerely learned a lot from my supervisors and feel lucky to work at both places.

I would like to express my deep appreciation to **Prof. Florian Bentzinger** for supporting and advising me with helpful discussion and collaboration. I feel extremely lucky to meet him as my first mentor, which led me to muscle biology. Thanks to him, I could learn not only basic muscle techniques and science but also the attitude to draw a big picture from a sketch. He was my first mentor and will be my mentor forever. I will always admire him for his energy and enthusiasm for science. Besides my mentors, I thank my thesis committee members for their serve and contribution to my Ph.D. thesis. **Prof. Bruno Correia, Prof. Pura Muñoz-Canoves, Prof. Katrien De Bock**, and **Prof. Perrine Castets**, I am very honored to have their input and have an opportunity to share my Ph.D. works with them as I always admired their works in the field of study.

I also extremely thank Swiss National Science Foundation and the selection committee for the mobility fellowship, which gave me an incredible opportunity to carry on my Ph.D. with a unique project including multi-photon microscope modalities in pioneering university. I had a lot of luck from many scientific foundations supporting my education from my master's to here. Without their support, this higher education and studying abroad would have just remained in my dream. I would like to thank Mogam Science Foundation to believe and see my potential as well as Swiss National Science Foundation for allowing me to build this amazing experience. I deeply acknowledge their decision.

To my colleagues as well as my friends, thank them for all their time and support, encouragement, sharing mindful visions, and jokes during the experiments and my endeavors. Sitting on the biosafety cabinet for a long time, fighting with so many different cells could be joyful when we were doing it together. Both in and out of the lab, I have learned a lot from each of them, they were my teachers and mentors. **Hannah Fong, David McKellar, Charles Heinke, Emily Laurilliard, Paula Petella, Lauren Walter, Alex Loiben**, and **Andrea De Michele**, I appreciate them for creating an environment where freely ask and cooperate, and I truly learn synergy when people work together and help each other. They were the people who made my Ph.D., which can be difficult sometimes, much easier. I am deeply grateful to all the precious bonds forged at Cornell. In addition, I also would like to thank **Prof. Nishimura** and her lab members **Dr. Chi-Yong Eom, Nichole Biliotta, Dr. David Small**, and **Aron Mok** in Chris Xu's lab taught me and helped me with various steps related to intravital imaging techniques in chapter 5.

I also would like to express special gratitude to all the Feige lab members and collaborators at Nestle Institute of Health Sciences. I could be exposed to state-of-the-art technology and various screening skills in muscle research thanks to them. **Sonia Karaz, Omid Mashinchian, Tanja Sonntag, Gabriele Dammone, Dr. Eugenia Migliavacca, Dr. Gabriele Civiletto, Joris Michaud, Dr. Pascal Stuelsatz, Sara Ancel, Anna Weiser, Philip Rein, Maria Deak, Caterina Collodet, and Minji Huh.** I sincerely thank them all who not only taught me techniques but also gave priceless advice for my future career and gave me enormous emotional support. They always gave me valuable advice and brought up great ideas on my project. Without their detailed instructions, I would not have been able to perform the projects properly in particular with Section 3. I appreciate their work which became the basis of my project and helped my experiments using high-content screening. **Deplancke's group**, especially **Julie Russeil** and **Prof. Bart Deplancke** to give me supervision and various feedback with helpful advice related to transcription factor study as well as teaching me yeast one-hybrid techniques on Section 3. I would be able to start my Ph.D. smoothly thanks to them.

Most of all, I sincerely thank my family and friends for their enormous support no matter where I am, no matter what I try to do, and how I want to do it. **Seongsik Lee, Inja Kim, Yeji Lee, Junglang Gu, Areum Yuhan, Jinhae Lee, Siyu Liu, Dr. Melina Scholze, Garazi Monzo Contreras, Dr. Radek Jankele, Oh-Hyeon Choung, Jisoo Park, Dr. Jane Yi, and Changwoo Seo.** I sincerely appreciate that you have been always on my side and truly believed I can make my choice right. Without their supports and trust, I could not be able to get back up again every time I stumble. Some of them I met as Ph.D. students or master students became doctors. I do not recall how much coffee we have had so far, over the coffee, they always inspired me in multiple aspects of life. Their scientific thoughts and passion brought me a lot of crazy ideas and my fun life activities continuously and strongly, which still make my scientific motivation to be going on. I would not have been able to continue my Ph.D. or science without their support and love. I sincerely thank them all.

Now, I am exceptionally honored to announce that I will be moving to another step to commence my new life as a scientist. These short paragraphs would not be sufficient to give my acknowledgment to everyone who has been instrumental to my studying from the moment I imagined 5 years ago until today. For all the people who constantly cheer me up, I deeply bow my head to your dedication.





Contents

Abstract	2
Résumé	4
Acknowledgments	7
Contents	11
Section 1: Introduction	13
1.1 Skeletal Muscle Structure and Functions	13
1.2 Myokines: Endocrine Function of Skeletal Muscle	18
1.3 Muscle Stem Cells in Muscle Regeneration	20
1.4 Muscle Stem Cell Niche	23
1.5 Muscle Atrophy in Aging.....	34
Section 2: Statement of Research	38
2.1. Investigating transcriptional regulation of apelin	39
2.2 Investigating functional relationship between myogenic progenitors and supportive cells with glycemic control	45
2.3 Developing intravital imaging of vasculature and satellite cells.....	50
Section 3 A Tead1-Apelin axis directs paracrine communication from myogenic to endothelial cells in skeletal muscle	55
3.1 Introduction.....	58
3.2 Results:	60
3.3 Discussion and Conclusion	79

Section 4 Endothelial-myogenic progenitor cell crosstalk is regulated by glycemic levels via endothelial Ndrp1	94
4.1 Introduction.....	98
4.2 Results:	100
4.3 Discussion and Conclusion	112
Section 5 Intravital imaging of vasculature and muscle progenitors in skeletal muscle of live mice	125
5.1 Introduction.....	128
5.2 Results:	130
5.3 Discussion and Conclusion	136
Section 6: Perspective.....	138
6.1 Summary and Perspective.....	138
6.2 Future Directions	140
Appendix.....	142
The Exerkine Apelin Reverses Age-associated Sarcopenia	142
Bibliography	147
Curriculum Vitae	171

Section 1: Introduction

1.1 Skeletal Muscle Structure and Functions

1.1.1 Skeletal Muscles of Human Body

The musculoskeletal system is one of the most abundant components of vertebrate animals and has evolved to enable movement specialization and adapt to environments dynamically. It enables life activity to make it possible for them to survive in different environments by controlling the movement of individuals to seek food and adapting metabolism (Flück and Hoppeler, 2003). As a major component of the human body, skeletal muscle accounts for approximately 40-50 percent of body mass and contains 50-70% of body proteins (Frontera and Ochala, 2015; Karagounis and Hawley, 2010). Energy expenditure of skeletal muscle varies dramatically depending on the physical activity rates of individuals. During the resting time, it usually accounts for 20% of energy expenditure, but it can account for 90% of whole-body O₂ consumption during the high-loaded rates exercise (Brooks, 1997; Wahren et al., 1971; Zurlo et al., 1990). In this regard, malfunctioning skeletal muscle can skew the whole body bioenergetics and contribute to metabolic syndromes such as obesity, hyperglycemia, and dyslipidemia, which increases the risk of type 2 diabetes mellitus and cardiovascular diseases (Cornier et al., 2008; Kim and Kim, 2020; Lakka et al., 2002; Rubio-Ruiz et al., 2019)

Around 650 types of skeletal muscles are spread symmetrically throughout the human body. Individual skeletal muscle is connected to the skeletons and the somatic nervous system, which is controlled by the central nervous system; hence it is contracted by voluntary control under consciousness. It primarily controls body movement, sustains posture, speaking, and breathing at will (**Figure 1.1**)(Frontera and Ochala, 2015). The central nervous system control somatic peripheral motor neurons which recruit each muscle independently. The disruption of the nervous system through motor neuron damages or genetic mutations of motor-neuron-related proteins can lead to severe muscle fasciculations, progressive muscle weakness, and muscle atrophy such as spinal muscular atrophy (SMA), amyotrophic lateral sclerosis (ALS), and Charcot-Marie Tooth disease (CMT) (Bowerman et al., 2018; Cafforio et al., 2005; Szigeti and Lupski, 2009; Zarei et al., 2015). Depending on its supporting bones, degeneration or dysfunction of a certain muscle are also closely involved

in the pathogenesis of degenerative bone, joint and connective tissue disorders. For instance, the interspinal and exterior erector lumbar muscles surrounding the lumbar spine contribute to the stability of the lumbar spine, and improving those muscle functions could prevent herniated disk (HNP) and chronic lower back pain (Deyo and Mirza, 2016; Hirayama et al., 2006; Jeon et al., 2016; Stoll et al., 2001). In addition, periarticular and hip muscles such as the gluteus maximus and gluteus medius muscles are closely involved in the pathogenesis of osteoarthritis (OA) by contributing to joint stability while creating a vicious cycle with diseased muscle mass from OA (**Figure 1.1**) (Hurley, 1999; Krishnasamy et al., 2018; Pisters et al., 2014; Shorter et al., 2019).

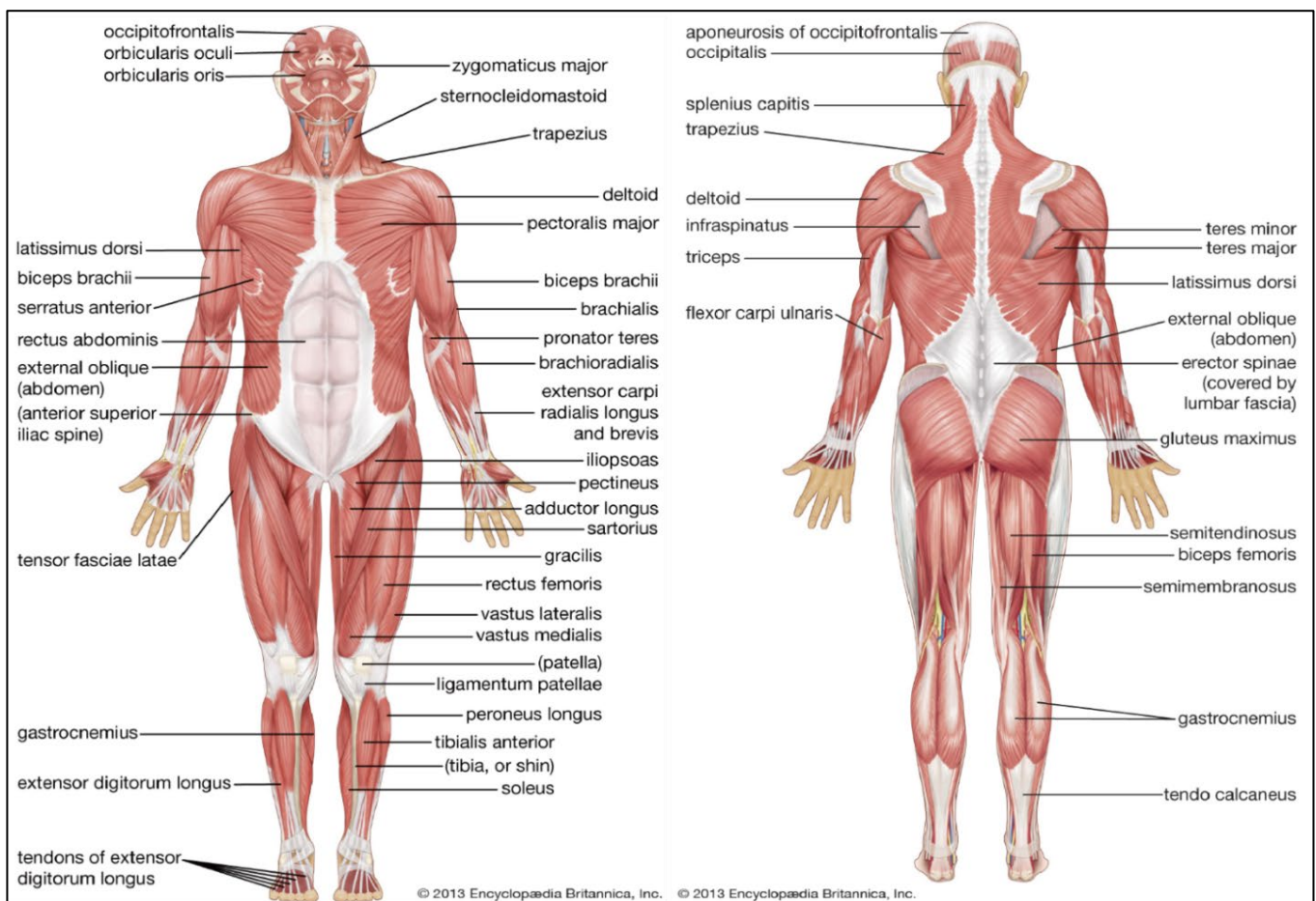


Figure 1.1 Major Human Skeletal Muscular Anatomy (Source of the figures: Encyclopaedia Britannica Inc.)

Figure 1.1 This figure was reproduced from Encyclopaedia Britannica and is copyright of the Encyclopaedia Britannica Inc.

1.1.2 Skeletal Muscle Contractility and Major Components

The functionality of skeletal muscle is integrally linked to the precisely organized muscle structure, which enables muscle contraction-relaxation in a hundred milliseconds. Each skeletal muscle is composed of muscle fibers, blood vessels, and connective tissue. The outer connective tissue is called **fascia** or **epimysium**, which connects the muscle fibers to tendons. Parts of epimysium infiltrate inward muscle and transforms into **perimysium** or **endomysium**, covering the separate bundles of muscle fibers, called **fascicles** which are grouped as hundred or a thousand muscle fibers (Figure 2). In the endomysium area, blood vessels and nerves are largely abundant, which are essential for the primary function of muscle, contraction. A set of arteries and veins is generally located alongside a nerve that penetrates the entire muscle in the epimysium area. Endomysium provides the pathway of capillaries and peripheral nerves, withholds the forces generated from fibers, and protects the surrounding tissues.

A muscle fiber is a single cylindrical fused-muscle cells and an individual fiber is composed of multiple micro-organelles, which provide critical elements for efficient contraction-relaxation cycles. A fiber is enveloped by a transparent tubular sheath called **sarcolemma**, and it separates the muscle cells from the endomysial connective tissue. Parts of the sarcolemma branch and penetrate myofibril bundles and form **transverse tubules** (T-tubules), sheathing around myofibrils and providing a specialized structure for excitation-contraction coupling. **Myofibrils** are the basic unit of the myofiber which assemble in parallel and grouped contractile elements. The gaps between the myofibril bundles are filled with small organelles that provide necessary elements instantly for myofibril contraction such as **sarcoplasmic reticulum**, mitochondria, and sarcoplasm (fluid) (Roberts et al., 2020). In particular, the net structure of sarcoplasmic reticulum enables the recruitment of myofibril bundles through Ca^{2+} release to contract simultaneously without delay when the motor unit is polarized in a few milliseconds (**Figure 2**). Contractions occur when **actin filaments** (thin filament) slide onto **myosin filaments** (thick filament) in a myofibril, and this actin-myosin filament complex is called **sarcomere** and serves as a basic unit of contraction (Frontera and Ochala, 2015). Sarcomere contraction is triggered by the Ca^{2+} diffusion emanated from sarcoplasmic reticulum. Upon binding Ca^{2+} , troponin moves tropomyosin away exposing the head of myosin, which contains actin-binding site and ATPase, hence it acts as a cross-bridge between the myofilaments (Figure 2) (Clarke, 2010; Huxley and Niedergerke, 1954;

Lehman et al., 1994). Because the pulling motion of actin filaments requires ATP to attach to myosin heavy chains, the mitochondrial function is essential to provide sufficient energy to myofibril contraction. Therefore, this topographical composition and its components are critical to enabling rapid muscle recruitment and muscle function (**Figure 2**).

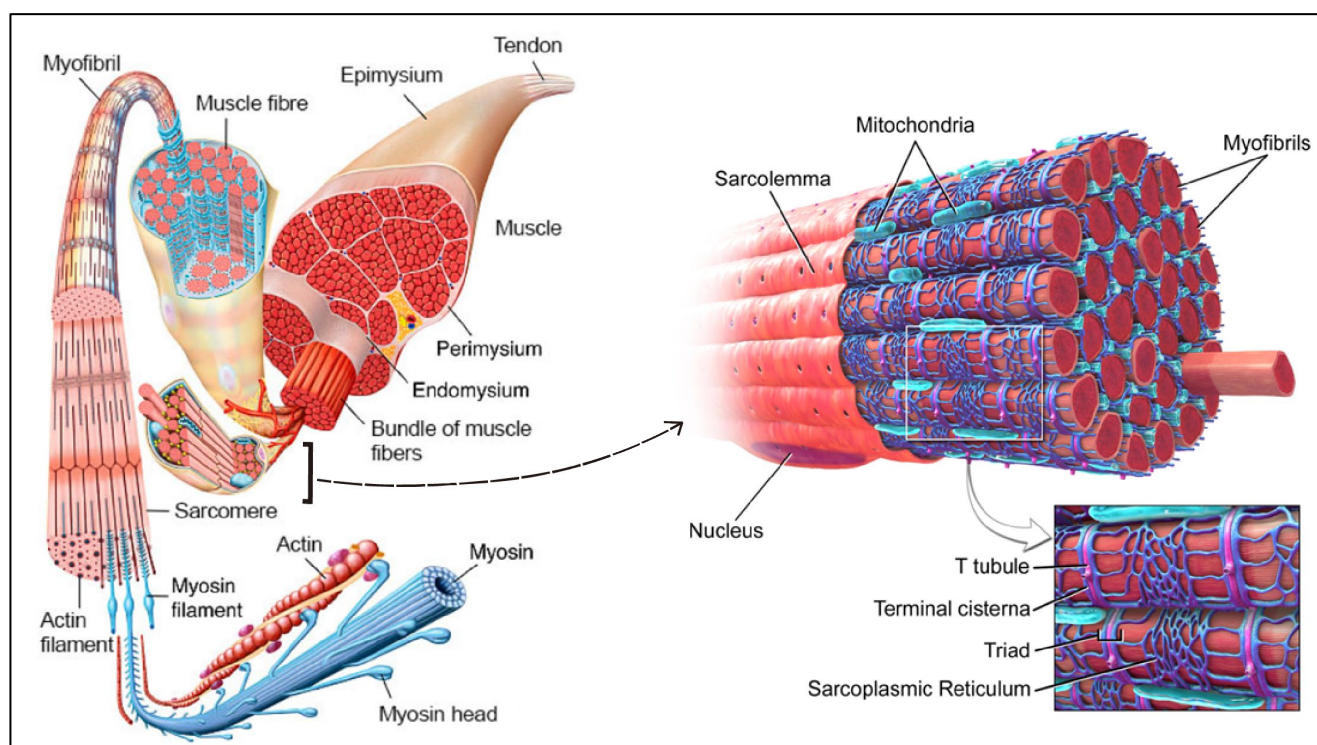


Figure 1.2. Geometry of skeletal muscle and components (This figure was modified from figures from Frank Geisler and from (Bluce Blaus, 2014) and are copyright of MediDesign and, Medical Gallery)

Figure 1.2 This figure was modified from Frank Geisler and Bluce Blaus (2014) and is copyright of the MediDesign and Medical Gallery.

1.1.3 Physiological Function of Skeletal Muscle

As the most abundant organ in the human body, skeletal muscle plays multifaceted roles in physiological functions that extend beyond the mechanical function to other various vital functions including metabolic homeostasis. Mainly, skeletal muscles are defined by their mechanical function, which converts chemical energy into physical energy such as generating motion and sustaining body postures by contraction-relaxation of muscle fibers. Moreover, skeletal muscle is largely responsible for whole-body metabolism (Bracy et al., 1995; Mul et al., 2015; Wolfe, 2006; Yang, 2014). Together with the liver, skeletal muscle plays a role in storing essential nutrients such as amino acids, fatty acids, and carbohydrates while supplying them to other organs or catabolizing them to maintain body homeostasis including blood glucose level (Mul et al., 2015; Wolfe, 2006). Furthermore, skeletal muscle regulates body temperature by non-shivering thermogenesis, producing approximately 85 percent of the heat in a body (Periasamy et al., 2017).

Although its primary functions are mainly known to dictate mobility and metabolic homeostasis, recent studies describe skeletal muscle as a secretory organ, releasing hormone-like substances, which implies that skeletal muscle exerts endocrine and paracrine functions to influence other physiological systems (Gomarasca et al., 2020; Pedersen, 2013; Pedersen and Febbraio, 2012). Muscle fiber secretome includes several hundred peptides. In particular, the small proteins or proteoglycan peptides released by muscle fibers during contraction are called **myokines** or **exerkines**, and they exert various crucial functions on other organs such as adipose tissue, liver, pancreas, bones, brain through blood vessel as well as muscle itself (Eadie et al., 2005; Gomarasca et al., 2020; Pedersen, 2013; Pedersen and Febbraio, 2012; Ramis et al., 2021; Yang, 2014). Therefore, studying the myokines is logical to understand the health benefits of physical exercise.

1.2 Myokines: Endocrine Function of Skeletal Muscle

The combinatorial techniques of proteomics and bioinformatics are used to study myokines and have allowed the identification of a hundred putative myokines (Catoire et al., 2014; Kwon et al., 2020). In addition, the contractile in-vitro myotube model is often used to validate the up-regulated proteins in response to electrical pulse stimulation (EPS) derived from C2C12 or human myoblasts (Catoire et al., 2014; Farmawati et al., 2013; Kwon et al., 2020; Pourteymour et al., 2017). Earlier, myostatin, LIF, IL-6, IL-7 were identified as myokines, which exert autocrine effects of myogenesis and muscle hypertrophy or atrophy (Broholm et al., 2008; Pedersen and Febbraio, 2012). Later, the sub-set of myokines such as BDNF, IL-6, IGF-1, FGF-2, FSTL-1, and irisin were also found to exert systemic effects in brain function, fat oxidation, brown fat development as well as endothelial function in the vascular system (Miranda et al., 2019; Ouchi et al., 2008; Pedersen, 2013)

Although the detailed mechanism remains unclear, more recently, different types of myokines were described to be up-regulated in response to the different types of exercise training. For instance, after intensive-short term training, ADAMTS1, APOLD1, LIF, CCL2, CX3CL1, FGF6, CXCL2, SERPINE1, ANGPTL4, CSF1, CYR61, and VEGFA are up-regulated and these molecules are canonically characterized as cytokines, chemokines, or ECM and vascular-related factors (Catoire et al., 2014; Görgens et al., 2015; Pourteymour et al., 2017). On the other hand, long-term exercise largely induces various ECM-related proteins such as COL1A, COL3A, COL4A, COL6A, OGN, BGN, ADAMTS7, MXRA5 taking approximately 20 percent of total up-regulated genes (Hjorth et al., 2015).

However, there are discrepancies of selective myokines between the exercise protocols, and only a limited number of myokines overlap among those that are previously identified as up-regulated during exercise, which makes it difficult to find the best pharmacological target for muscular or metabolic diseases. Furthermore, it is difficult to know which types of physiological changes are critical to providing the health benefits of physical exercise. Of relevance to disease intervention, focusing on the myokines that are altered in aging could be an alternative strategy to find the best target of intervention, in which muscular dysfunctionality is frequently observed.

Kwon et al described 13 myokines that are affected by aging (Kwon et al., 2020). Alongside a muscular functional decline in aging, secretion of myokines including decorin, IGF-1, IL-15, CXCL12, BMP-7, sestrin, SPARC, irisin, VEGF-A, and apelin are notably reduced whereas IL-6 and myostatin increase (Görgens et al., 2015; Leal et al., 2018; Puchert et al., 2016). Among those myokines, sestrin, IL-15, and irisin are known to increase muscle performance by regulating metabolism in AMPK or PGC1 α dependant pathways (Crane et al., 2015; Lee et al., 2013). Interestingly, a subset of myokines such as decorin, IGF-1, BMP-7, and SPARC are known to be primarily associated with cartilage, tendons, or osteogenesis by controlling the extracellular matrix, yet also positively regulate skeletal muscle hypertrophic pathways while mediating various myogenic factors like actin, follistatin, Myod1, myogenin, atrogin1, and MuRF1 (Jørgensen et al., 2017; Kanzleiter et al., 2014; Kim et al., 2016a; Liu et al., 2010; Ripamonti and Hari Reddi, 1997, 1997; Salmon and Daughaday, 1957; Trombetta et al., 2010; Winbanks et al., 2013; Xu et al., 2018).

Similarly, several myokines such as CXCL12, VEGF-A, and apelin are well defined predominantly as angiogenic factors, which regulate cardiovascular health through controlling blood pressure, cardiac contractility, and angiogenesis, but also enhance muscle function (Brzoska et al., 2012; Han et al., 2008a; Puchert et al., 2016; Szokodi et al., 2002a; Tatemoto et al., 2001; Vinel et al., 2018; Yamada et al., 2019; Zhang et al., 2016). The findings suggest that myokines have binary or multiple effects on the various muscle resident cells and dynamically use muscle niche to improve myofibers in adaptation to environments. Based on this notion, investigating more about the function of myokines in the intercellular crosstalk must be intriguing and the underlying signal mediating these effects remains to be further explained. In addition, from a therapeutic point of view, investigating the mechanisms that decline in aged muscle in which muscle wasting and weakness are frequently observed, is a potential approach to find targets that mitigate the relevant aging-related symptoms by targeting autocrine and paracrine signals.

1.3 Muscle Stem Cells in Muscle Regeneration

Muscle contractile activities, accidents and, volumetric muscle loss by surgical resection can cause local or massive muscle damage. Although small local damage on the fiber can be healed by the adherence of membrane of muscle fibers, the repair capacity largely relies on the function of adult stem cells that are undifferentiated myogenic cells located around the muscle fibers called muscle stem cells (MuSCs) or satellite cells (Brack and Rando, 2012; Kuang and Rudnicki, 2008). These satellite cells reside between the basal lamina and the sarcolemma of muscle fibers in a typically quiescent state but can be activated in response to muscle injury and environmental changes. Following activation, MuSCs proliferate to amplify the pool of myogenic progeny that will then enter the differentiation process and fuse with damaged myofibers or form new myofibers to repair and maintain tissue homeostasis (Jejurikar and Kuzon, Jr., 2003; Yablonka-Reuveni, 2011). While the vast majority of the MuSC progeny directly contributes to muscle repair, at least some can self-renew, thereby meeting the criteria of bona fide resident stem cells (Collins et al., 2005).

The states of MuSCs and their progenitors are defined at the molecular level by the fine-tune temporal expression of transcription factors and cell cycle regulators, providing a balance between quiescence, proliferation, differentiation, and renewal (Brack and Rando, 2012). This coordinated regulation involves the myogenic regulatory factors (MRFs) that are expressed in a temporally ordered manner (**Figure 1.3**). MRFs are the master players, which regulate myogenesis whether during embryogenesis or at the adult stage (Hernandez-Torres et al., 2017). In the lineage of myogenic differentiation, the two paired box transcription factors Pax3 and Pax7 are the most well-studied regulators of myogenesis (Buckingham, 2007; Halevy et al., 2004; Relaix et al., 2005)). In particular, transcription factor Pax7 is expressed in adult myogenic progenitors and has been demonstrated to maintain the MuSC stemness and stem cell pool (von Maltzahn et al., 2013). Many studies demonstrated that transplantation of Pax7 expressing cells contribute to new and existing fibers and Pax7⁺ cells are sufficient to repair muscle fibers after injury while the dysregulation of Pax7 impairs MuSC survival and muscle regeneration; hence it has been conveniently used as a marker of skeletal muscle progenitors (Halevy et al., 2004; Zammit et al., 2006; Lepper et al., 2011; Sambasivan et al., 2011; Ancel et al., 2021).

Following stimulus, homeostatic Pax7⁺ cells undergo asymmetric division and start to express myogenic transcription factors such as Myf5 or MyoD, which indicate the activated state of MuSCs. A subset of the populations diverges into Pax7⁺Myf⁻ or Pax7⁺MyoD⁻, which are returning to quiescent MuSC. The activated Pax7⁺Myf5⁺ or Pax7⁺MyoD⁺ progenitors are further differentiated to Pax7⁻Myf5⁻MyoD⁺Myog⁺ committing myocytes or expressing late MRFs such as MRF4 and MRF6 (Ancel et al., 2021; Tedesco et al., 2010). At this stage, myogenic progenitors exit from the active cell cycle and terminate differentiation, while being aligned to fuse to existing myofibers or form new multi-nucleated syncytium (Chargé and Rudnicki, 2004; Zammit et al., 2006). Ultimately, the functionally mature-myofibers re-establish contractile components such as myosin heavy chain (Myh1), Desmin, and (Des) α -actin (Acta1).

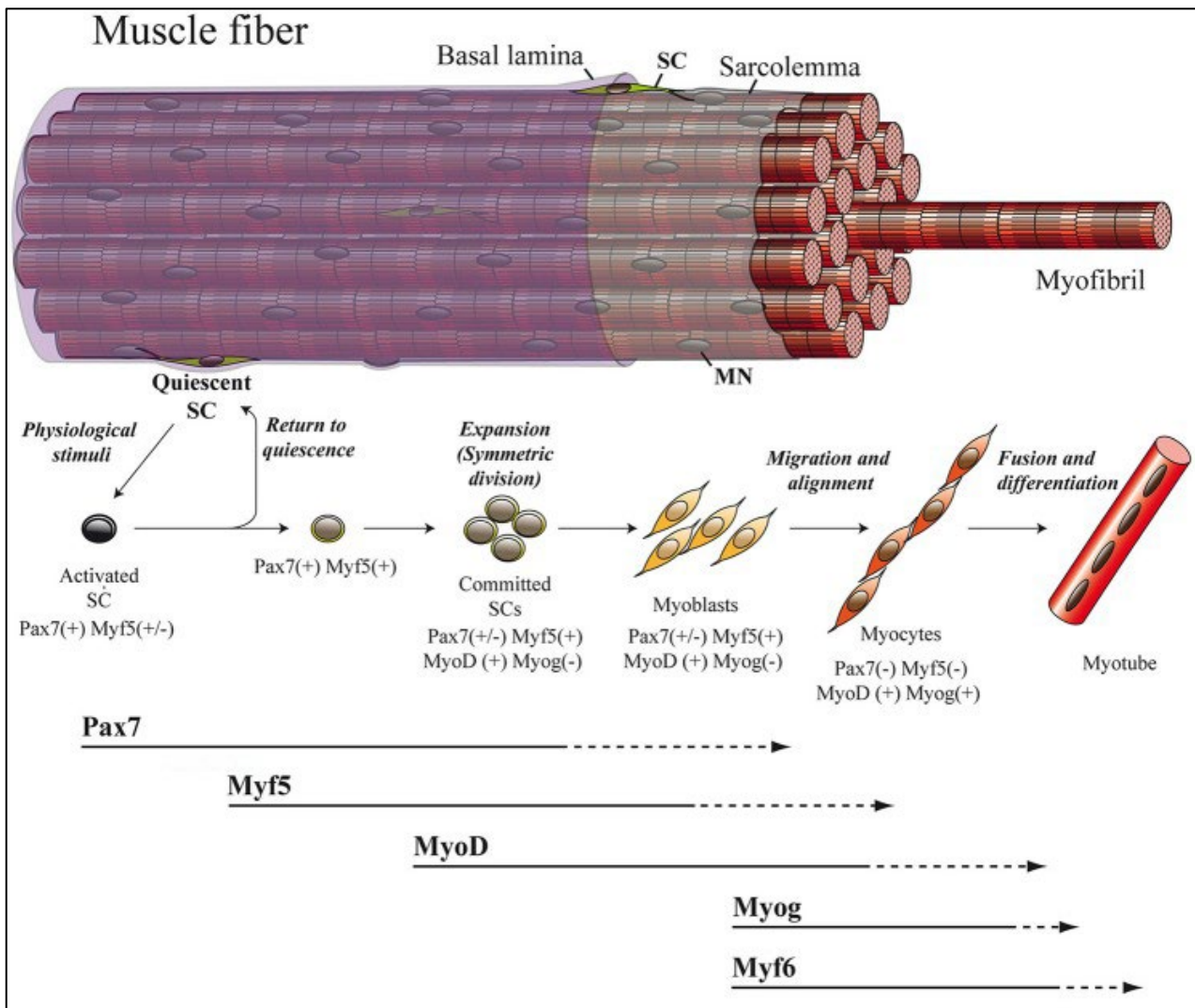


Figure 1.3. Adult myogenesis (Adapted from Hernandez-Torres et al., 2017) The overall myogenic differentiation pathway includes the activation of quiescent SCs, commitment to differentiation, proliferation, fusion to form myotubes, and ultimately maturation into myofibers. SC, satellite cell; MN, myonucleus (Hernandez-Torres et al., 2017).

Figure 1.3 The figure was adapted from *Frontier in Cell and Developmental Biology* (Hernandez-Torres et al., 2017) and is copyright of the Frontiers Media S.A.

1.4 Muscle Stem Cell Niche

1.4.1 Muscle stem cell membrane receptors

Skeletal muscle stem cells (MuSCs) are surrounded by a complex microenvironment called niche, and the homeostasis and fate decisions of myogenic progenitors are orchestrated by intrinsic and extrinsic signals that are mediated through cell-cell, cell-matrix, and paracrine signals from the niche (Cosgrove et al., 2009; Kuang and Rudnicki, 2008; Reilly and Engler, 2010). Particularly, MuSCs express various surface receptors and receive these biologically active cues through ligand-receptor interactions that transduce intracellular cell fate regulatory signals (**Figure 1.4**) (Abreu, 2018; Yin et al., 2013a). Quiescent MuSCs are known to express several surface receptors such as integrin receptors $\alpha 7$ and $\beta 1$ (Itga7, Itgb2), which have been emphasized to develop cell-sorting and labeling strategies (Blanco-Bose et al., 2001; Rozo et al., 2016; Yao et al., 1996). Beyond the use of purification MuSC from muscle tissues, Itga7 and Itgb2 provide stability of adhesive molecules by dynamically interacting with extracellular matrix (ECM) proteins such as laminin, collagen IV, fibronectin and they dictate the cell quiescence. They also integrate with fibroblast growth factor 2 (Fgf2) to regulate proliferation and myogenic differentiation (Urciuolo et al., 2013; Yao et al., 1996).

Notch (1-4) and adhesion-related receptors such as M-cad, N-cad, NCAM, and VCAM-1, are highly abundant in MuSCs and tightly control satellite cell quiescence by providing powerful adhesive molecules on the membrane (**Figure 1.4**). For instance, when Notch receptors bind delta/jagged ligands (Dll1,4 and Jag1,2), MuSCs remain in the quiescence state by transducing Hes and Hey which are repressors of MyoD but when it is interrupted, MuSCs enter cell-cycle while promoting asymmetric division (Buas and Kadesch, 2010; Conboy and Rando, 2002). Recent studies showed an additional notch-regulatory mechanism, explaining that kruffer-like factor 7 (KLF5) induced by Notch signaling up-regulates cycle-dependent kinase inhibitor (CDKI) p21 in which p57 migrate to the nucleus while triggering cell-cycle exit (Mademtzoglou et al., 2018; Relaix et al., 2021; Wang et al., 2016). Similarly, M-cad, a calcium-dependent cell adhesion molecule, encoded by *Cdh15* maintains MuSC quiescence by providing a homophilic interaction with myofiber (Goel et al., 2017; Irintchev et al., 1994; Krauss et al., 2005). Conversely, other adhesion molecules such as neural cell adhesion molecule (NCAM), N-cadherin (N-cad), and VCAM-1 provide MuSC

with tight-junction to other tissue-resident cells in niche while participating in cell migration or activation in response to the tissue damage rather than supporting adhesion to myofibers (Covault and Sanes, 1986; Irintchev et al., 1994; Jesse et al., 1998).

Several cytokine-related receptors are also found on the MuSC membrane and regulate MuSC fates (**Figure 1.4**) (Abreu, 2018; Yin et al., 2013a). For example, C-X-C chemokine receptor type 4 (CXCR4) that is expressed on the MuSC membrane, promotes muscle regeneration by being involved in myogenic progenitor migration by binding its ligand CXCL12 (SDF-1) (Brzoska et al., 2012). Intriguingly, CXCL12 has a dual binding affinity to proteoglycan syndecan 4 (Sdc4) and is present in the bone marrow and hematopoietic stem cells (Charnaux et al., 2005; Ratajczak, 2003). CXCL12 is previously noted as a myokine and widely studied as an angiogenic factor, indicating its potential function in intercellular crosstalk with the blood and myogenic populations (Brzoska et al., 2012; Collins et al., 2017; Ho et al., 2010; Puchert et al., 2016; Ratajczak, 2003; Yamada et al., 2019). Moreover, CD34, often used as a marker of MuSCs given its specificity, co-expresses with Myf5, which indicates that they are activated MuSCs rather than quiescent MuSC although the initial study suggests the majority of CD34⁺/Myf5⁺ cells are defined as quiescent satellite cells (Beauchamp et al., 2000). CD34 can be activated by CXCL12 and promotes proliferation and satellite cell migration (Alfaro et al., 2011; Brzoska et al., 2012). Furthermore, CD34 serves not only as a receptor but also has dual functions as a ligand for vascular selectins on human hematopoietic progenitors (AbuSamra, 2015; Alfaro et al., 2011; Beauchamp et al., 2000). Although the specific mechanism is unclear, accumulated evidence shows that the niche ligand signals potentially coming from non-myogenic tissue-resident cells are essential for myogenic cell fate decisions.

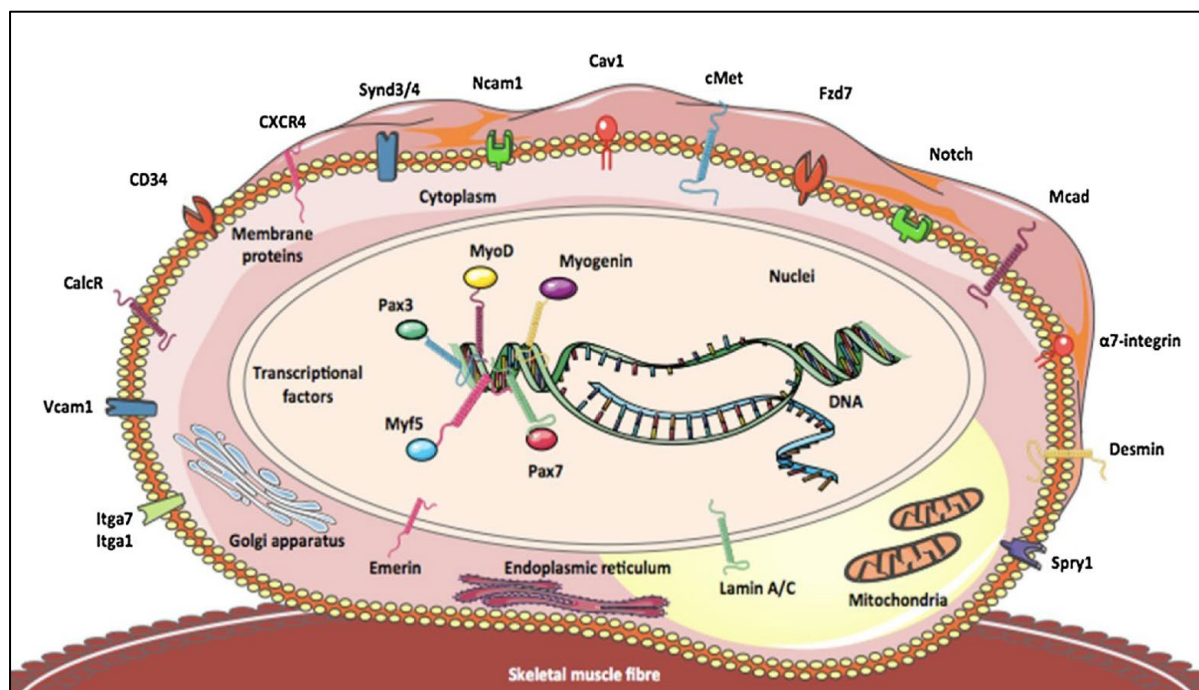


Figure 1.4. Muscle stem cell membrane surface expressing receptors (Abreu, 2018).

Surface proteins of muscle stem cells that are identified to be involved in myogenic cell fate decision. Lists of membrane proteins include Synd3/4 indicating syndecans 3 and 4, M-cadherin (Mcad), calcitonin receptor (CalcR), C-X-C chemokine receptor type 4 (CXCR4), calveolin-1(Cav1), α 7- and β 1- integrains (Itga7, Itb1) neural cell adhesion molecule1 (Ncam1), vascular cell adhesion molecule 1 (Vcam1) and CD34.

Figure 1.4 The figure was adapted from Frontier in Cell and Developmental Biology (Hernandez-Torres et al., 2017) and is copyright of the Frontiers Media S.A.

1.4.2 Muscle stem cell niche and tissue-resident cells

Dynamic changes in tissue-resident cell population and myogenic cell fates are notably observed in the muscle regeneration process upon tissue damage. Along the time of recovery, different cells types are recruited at the site of injury to coordinate the distinctive roles in muscle reconstitution (**Figure 1.5**) (Bentzinger et al., 2013; Yin et al., 2013a).

At the onset of injury, detection of necrotic lesions, activating neighboring cells by multiple-inflammatory signaling, clearing the necrotic cells, and inflammation resolution are coordinated by resident immune cells with the incorporation of circulating monocytes. Initially, the injury site is instantly detected by the resident **innate leukocytes** such as **mast cells** and **neutrophils** while turning into Ly6G⁺/Cd11b⁺ phagocytic **granulocytes** and secreting numerous pro-inflammatory cytokines such as TNF- α , histamine, IL-6, and IL-1 β (Auffray et al., 2007; Galli et al., 2011; Gibbs et al., 2001; Tidball, 2017; Ziemkiewicz et al., 2021). Whereas the pro-inflammatory chemoattractants from neutrophils including IL-8, MIP-1 α , and MCP-1 promote other neutrophil and **monocyte** extravasation, the activated phagocytes clear damaged cells and cellular debris (Scapini et al., 2000; Yang and Hu, 2018). Those inflammatory signals from neutrophils also serve dual functions in regulating myogenic cells. Especially, adequate amounts of TNF- α and IL-6 are reported to provoke satellite cell proliferation by activating the MAPK/p38a pathway, which leads to silencing *Pax7* and *Notch1* thereby exit the cell cycle of quiescence (Chen et al., 2007a). Neutrophils start to appear after an hour and can be present for a week (Ziemkiewicz et al., 2021).

Later around the first two days of recovery, the **pro-inflammatory M1-like macrophages** differentiated from Ly6C⁺ monocytes infiltrate and dominantly construct the pro-inflammatory microenvironment in the lesion. Particularly, the polarized M1-like macrophages emanate interferon- γ (IFN- γ), which inhibits the muscle differentiation by activating the JAK-STAT1 pathway where *Myog* is down-regulated (Londhe and Davie, 2013; Tidball, 2017). Subsequently or concurrently, the subset of monocytes with a lower level of Ly6C differentiate to **anti-inflammatory M2-like macrophages** and secrete anti-inflammatory cytokines which include IL-10, IL-4, TGF- β , IGF-1 as well as VEGF. These anti-inflammatory factors are particularly involved in the progress of myogenesis while closely interacting with differentiating myoblasts or myocytes (Saclier et al., 2013). In the

contrast to the similar result of the role of pro-inflammatory M1-like macrophages in hindering myogenic differentiation and fusion, M2 polarized macrophages are secreting factors that have a paradoxical function on myogenesis. For instance, while IGF-1 is enhancing muscle stem cell proliferation in hypoxia, which is a close condition of the regenerating muscle, under normoxia condition, it promotes myogenic differentiation (Duan et al., 2010). Nevertheless, the majority of the anti-inflammatory signals such as IL-4 and TGF- β and the consensus of anti-inflammatory cytokine functions have been established to increase myogenic differentiation and reinforce the myogenic fusion while the protein supplementation results in muscle hypertrophy (Chang et al., 2019; Girardi et al., 2021; Saclier et al., 2013). The other regulatory mechanism of M2-like macrophage in muscle regeneration presents in ECM proteins they exude. They produce a higher amount of ColVI, fibronectin, which eventually link to muscle stem cell fate decisions (Gratchev et al., 2001; Schnoor et al., 2008; Urciuolo et al., 2013).

Further, some evidence shows that Cd4⁺ **Treg cells** may express tissue-specific amphiregulin which acts as an immune suppressor by directly binding to its receptor epithelial growth factor receptor (EGFR) (Burzyn et al., 2013; Zaiss et al., 2015). Although various other adaptive immune cells such as T cells, B cells, and NK cells are also found in the regenerating muscle, the functional analysis showing which particular signals they mediate and the direct relationship with myogenesis remains scant (McKellar et al., 2020a). Collectively, the immune cells substantially contribute to the muscle regeneration throughout the initial response to the injury to regulating myogenesis, which tightly adhered to the transition of M1 and M2 polarization.

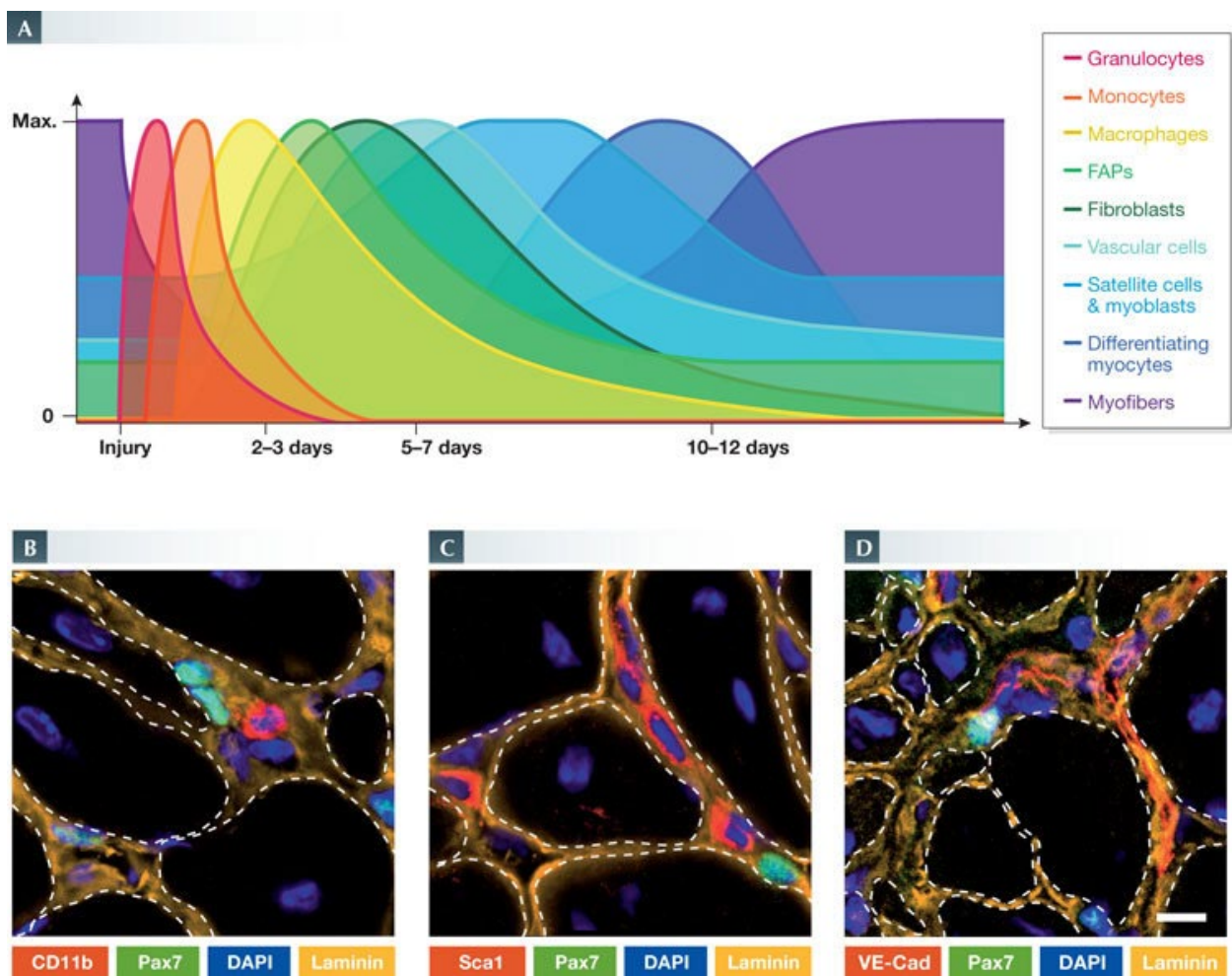


Figure 1.5. Participation of non-myogenic cell types in muscle regeneration (Bentzinger et al., 2013). (A) The relative presence of immune, fibrotic, vascular, and myogenic cell types after muscle injury. (B–D) Immunofluorescence images of muscle tissue sections from regenerating mouse muscles. In their niche, Pax7-positive cells (green) are close to various non-myogenic cells (red): (B) CD11b-positive leukocytes; (C) Sca1-positive interstitial cells; and (D) VE-Cad-positive endothelial cells. Laminin staining is shown in orange and nuclei are labeled with DAPI (blue). Scale bar, 10 μ m.

Figure 1.5 The figure was reproduced from EMBO Reports (Bentzinger et al., 2013) and is copyright of the European Molecular Biology Organization Journal.

Fibrogenic mesenchymal stromal cells are abundant cells in skeletal muscle and dynamically transformed to sub-populations during muscle reconstruction while changing the surrounding extracellular matrix composition thereby essential for connective tissue remodeling and control muscle stem cell fate and myogenesis. The transition of ECM components is particularly important because it preserves the structure of the anatomical position of degenerative fibers until the formation of the muscle fibers and innervation is complete. Intravital imaging showed that remnant ECM surrounding muscle fiber, which is named as 'ghost fiber' after muscle injury can guide the directionality of myogenic progenitors and newly forming muscle fiber during regeneration (Webster et al., 2016a)

The main populations of fibrogenic mesenchymal stromal cells are **fibroblasts** and **fibro/adipogenic progenitor cells** (FAP). In particular, FAPs are capable to differentiate into multi-distinctive cell types, which are not limited to fibroblasts, and adipocytes. They even potentially diverge to tenocytes, which are further committed to forming cartilage or bone (Uezumi et al., 2010; Wosczyzna et al., 2012). **FAPs** are known to exclusively express PDGFR α with CD34 and Sca-1 on the cell membrane but with the absence of CD45, CD31, and α -7 integrin, thereby being distinguished by hematopoietic stem cells and satellite cells (Low et al., 2017). FAPs are mainly in charge of fibrosis and fat accumulation and stay closely adjacent to blood vessels in the interstitial endomysium area (Joe et al., 2010; Olson and Soriano, 2009). Upon muscle injury, they are activated to proliferate rapidly and maximized their population around 3-4 days of repair and return to the quiescent again after a week to 9 days (**Figure 1.5**)(Joe et al., 2010; Pretheeban et al., 2012). During regeneration, FAPs also positively contribute to myogenesis by supporting MuSC through various ECM and secretory signals (Joe et al., 2010). These signals include collagen isoforms, connective tissue growth factor (CTGF), WNT inducible signaling pathway protein (WISP-1), and TGF- β which are pro-fibrotic but also act directly on satellite cells (Contreras et al., 2016; Joe et al., 2010; Lukjanenko et al., 2019; Theret et al., 2021; Uezumi et al., 2011)

Similarly, **fibroblasts** are the main source of ECM proteins and play an essential role in remodeling connective tissue by producing matrix metalloproteinases such as MMP1 and 3; hence controlling myogenesis (Lindner et al., 2012; Murphy et al., 2011; Tomasek et al., 2002). They also express PDGFR α as FAPs, but co-express transcription factor 4 (TCF-4) and have distinctive functional relationships with myogenic progenitors. Whereas FAPs are more prone to facilitate myogenic differentiation to satellite cells, Tcf-4⁺ fibroblasts hinder pre-mature differentiation of Pax7⁺ cells (Murphy et al., 2011). During the repair process, fibroblasts are mostly populated at day 5 post-injury, in which satellite cells also start to

appear (**Figure 1.6**) (Bentzinger et al., 2013). Although they are a major part of the muscle stem cell niche and crucial for muscle regeneration, the heterogeneity of fibroblasts and FAPs and their complicated interplay with myogenic cells are often discrepant and largely remain unknown.

Endothelial cells or blood vessel forming cells are one of the main muscle-tissue resident cells. During homeostasis, they mainly reside as blood vessels and serve trophic functions to skeletal muscle such as delivering oxygen, and nutrition, while eliminating the toxic byproducts from heavy muscle activities such as carbon dioxide, lactic acids, and excess inflammation (Clark et al., 2000; Duscha et al., 1999; Lin et al., 2014). Interestingly, quiescent Pax7⁺ satellite cells were found very close to CD31⁺ or vWF⁺ endothelial cells in histology (Christov et al., 2007a). In agreement with this finding, intravital imaging using Pax7^{tdT}: Flt1^{gfp} labeled transgenic mice reveal that quiescent Pax7⁺ cells are highly juxtavascular showing that around 80 percent of satellite cells are localized directly in the contact with Flt1⁺ blood vessel cells (**Figure 1.6**)(Verma et al., 2018a). Additionally, the loss of proximity resulted in the decreased number of muscle stem cells and thereby impair muscle repair (Verma et al., 2018a). The intriguing part of this intercellular crosstalk between Pax7⁺ muscle stem cells and Flt1⁺ endothelial cells is mediated by the combinatorial signals between a paracrine signal of Vegfa and a juxtacrine signal of the Dll4-Notch pathway (Verma et al., 2018a). During muscle reconstruction after muscle injury, capillary density was highest at 7 days post-injury, and the delayed capillary formation due to lack of CCL2 lead to a substantial decrease in the cross-section of muscle fibers, which is supported by the proportional relationship between capillary density and muscle size in the previous study (Luque et al., 1995; Ochoa et al., 2007). Additionally, endothelial cells also indirectly regulate myogenesis by producing lactate which contributes to the polarization of macrophages to M2-like macrophages (Zhang et al., 2020).

More direct evidence of crosstalk between endothelial cells and myogenic cells can be found in an in-vitro experiment. Direct co-culture of satellite cells with endothelial cells which express the high level of platelet-derived growth factor-BB (PDGF-BB) and bFGF increased the proliferation of myogenic progenitors (Christov et al., 2007a). Moreover, endothelial-related Ang1/Tie-2 signaling mediates the transition of satellite cells into quiescence (Abou-Khalil et al., 2009; Mounier et al., 2011). Inversely, the differentiating myogenic cells are highly angiogenic, which promote endothelial cell expansion and their capillary structure formation (Christov et al., 2007a; Rhoads et al., 2009). This evidence implicates they might have reciprocal co-regulation between myogenic and endothelial cells.

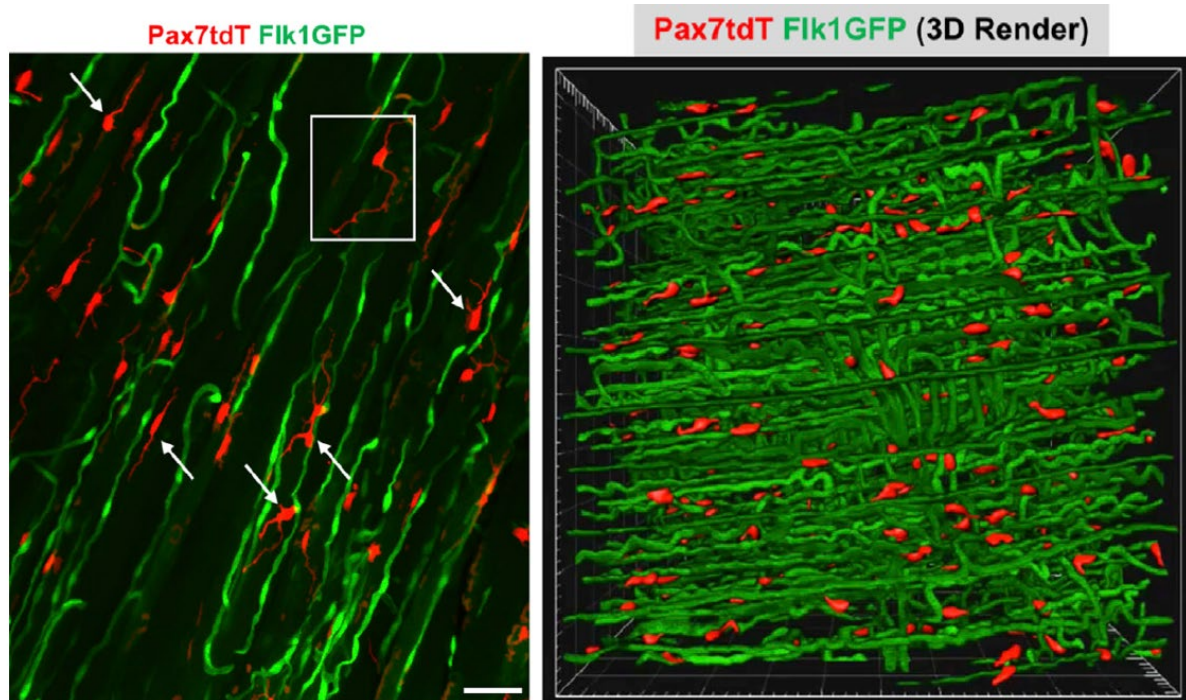


Figure 1.6. Tissue cleared MuSCs and ECs in skeletal muscle from genetic reporter mice (Pax7tdT:Flk1GFP)(Verma et al., 2018a). (Left) Maximum intensity project of reporter mice for MuSCs (Pax7tdT) and capillary ECs (Flk1GFP) after tissue clearing: scale bar 50nm. (Right) Snapshot of segmented MuSCs (Pax7tdT), and ECs (Flk1gfp) in soleus muscle. Immunofluorescence images of muscle tissue sections from regenerating mouse muscles.

Figure 1.6 The figure was reproduced from Cell Stem Cell (Verma et al., 2018a) and is copyright of the Cell Press Journal.

On these grounds, we learn that successful muscle repair is the consequence of the precisely fine-tuned interplay between myogenic cells and non-myogenic cells in both temporal and spatial ways. However, the understanding of complex ligand-receptor networks driving heterogeneous cell type interactions in the skeletal muscle niche is still limited. Which specific cell types produce the ligands and receptors? What are the conditions that activating the ligands? How do they functionally interact with the receptors of which sub-populations in muscle adaptation or regeneration? What are the consequences of the interaction? To understand the complex functional relationship between niche and myogenic cells the field needs to explore answer those questions.

1.4.3 Tissue-resident cells and single-cell RNA sequencing

The recent development of in-depth single-cell RNA sequencing analysis captured and characterized extended sub-populations of tissue-resident cells and facilitate the knowledge of the potential cell-stem cell interaction by deciphering the ligand-receptor transcriptomics (**Figure 1.7**)(Armingol et al., 2021; De Micheli et al., 2020; Macosko et al., 2015; Zheng et al., 2017). With that, we could add the muscle tissue-resident non-myogenic cells which are defined by the various sub-types of immune cells like innate M1, M2 and adaptive immune cells, fibroblast/adipogenic cells, neural cells, and various components of vessel forming cells such as smooth muscle cells, and endothelial cells (**Figure 1.7**) (De Micheli et al., 2020; Macosko et al., 2015; McKellar et al., 2020a; Saber et al., 2020; Zheng et al., 2017). Notably, it also changes the conventional notions of the sub-cell types in the tissue-resident cells and their marker expressions. In particular, fibroblasts and FAPs populations are extended or merged by stem-like FAPs, adipogenic FAPs, and pro-remodeling FAPs with a subtle difference of cell marker expression. Probably, what we have known so far, might need to be annotated differently following further studies on their functional relationship. Although the functional relationship between specific cell types and their dynamic changes in transcriptomics during muscle repair has not been yet unequivocally elucidated, it might be an advantageous strategy to take this advance of technology to further dissect the signals related to intercellular crosstalk.

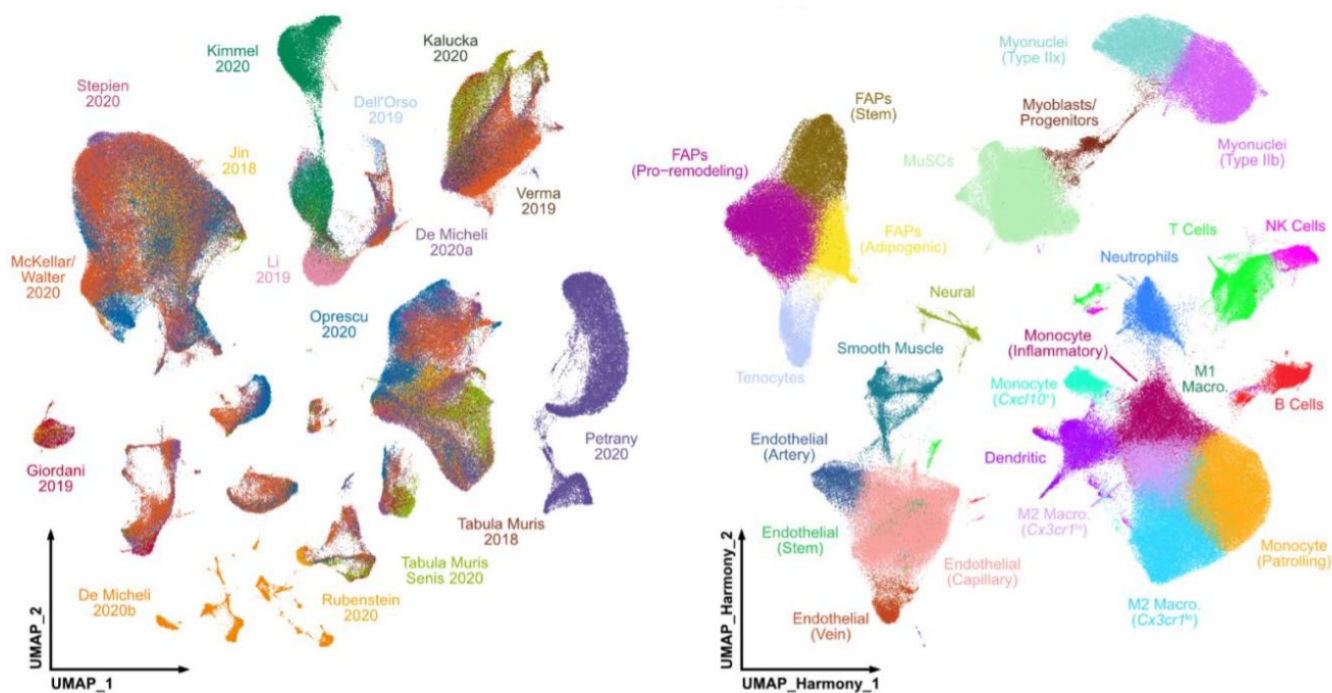


Figure 1.7. 102 scRNAseq and snRNAseq publicly available dataset integration (McKellar et al., 2020b). (Left) UMAP projection of the 102 datasets colored by the source with name and year of publication (Right) UMAP representation of sub-populations in skeletal muscle after quality filtering and batch-correction (Harmony) colored by cell type.

Figure 1.7 The figure was reproduced from BioRxiv (McKellar et al., 2020b) and is copyright of the Cold Spring Harbor Laboratory.

1.5 Muscle Atrophy in Aging

1.5.1 Prevalence of muscle atrophy in aging

With increasing life span, aging-related health issues became more prevalent. Aging is a complex and multifactorial process leading to numerous chronic diseases such as diabetes, cancers, cardiovascular, and arthritic disease (Rubio-Ruiz et al., 2019; Zierer et al., 2016). Muscle-related pathologies account for 7.5% of the diseases over 60 years of age and are estimated to affect 50% of people older than 80 years of age (Dawson A, 2016). Sarcopenia, a gradual loss of skeletal muscle mass and function, is an inevitable process associated with the loss of life quality while increasing the risk of mortality in elderly individuals (Dorrens and Rennie, 2003; Janssen et al., 2004). Sarcopenia is clinically defined as an age-dependent decline in walking speed or grip strength associated with low muscle mass. From the ages of 20 to 80, Vastus lateralis muscle mass is diminished by 40 percent and affects 5-30% of adults over 65 years with the prevalence increasing to as high as 50 % in persons over the age of 80 years (von Haehling et al., 2010, Dorrens and Rennie, 2003; Lexell, 1995).

Due to the various functions of skeletal muscle, a decline in skeletal muscle mass and function could result in devastating life quality and often lead to life-threatening challenges in addition to other negative pathogenic issues such as metabolic syndrome or impaired glucose homeostasis (Marcell, 2003). Currently available treatments, only include a moderate amount of exercise and nutritional management without any biological diagnoses or medical treatments (Hawley et al., 2006; Parise and Yarasheski, 2000).

1.5.2 Causes of muscle atrophy in aging

Although specific biological diagnoses or medical treatments remain to be further investigated, several negative changes in aging that are commonly found in sarcopenic patients and diverse aging animal models have been reported. First, one's **lifestyle or physical activity** is one of the most important factors associated with muscle wasting. For

example, individuals who have more sedentary behavior have a higher risk to develop sarcopenia than individuals who have a vivacious lifestyle. In addition, physical inactivity is closely linked with the pathogenesis of other chronic diseases. Negative energy balance or energy depletion that leads to inactive behavior is often pointed out as a consequence of **imbalanced protein synthesis and degradation** in skeletal muscle (Carbone et al., 2012). Indeed, excessive protein consumption above the recommended protein allowance was demonstrated to ameliorate the loss of muscle mass by regulating muscle anabolism and proteolysis.

Perturbation in the nervous system and thereby the motor unit loss and incomplete innervation with defective neuromuscular junction substantially affect the whole muscle contractility in aging (Castets et al., 2020; Larsson and Ansved, 1995; Pannérec et al., 2016). At a fiber level, **atrophy of type II muscle fibers** expressing fast myosin isoform is a hallmark of aging and occurs at a higher frequency than in slow muscle fiber type (type I fiber) (Brocca et al., 2017; Karlsen et al., 2019; Larsson et al., 1978; Vinel et al., 2018).

The gender differences and preferential atrophy between females and males come from the **alteration of sex hormones** in aging. Particularly sex steroids such as androgens, estrogen, and progesterone have been reported to decline in aging and directly influence the pathophysiology of muscular function by systemically affecting multiple muscle function-related organs and satellite cells (Collins et al., 2018, 2019; Kim et al., 2016b; Maggio et al., 2012; Tanideh et al., 2014).

Furthermore, the multi-ethnic human transcriptomic profiles showed that a significant **reduction in mitochondrial-related genes** such as $ERR\alpha/PGC-1\alpha/NRF1$ is commonly featured in the biopsy from sarcopenia patients across their ethnicities (Migliavacca et al., 2019). Given muscle contractility is highly dependent on bioenergetics and energy availability, accumulated mutations in mitochondrial-related genes and, thereby, its dysfunction leads to impairment of muscle function and the whole-body system.

Muscle stem cell depletion which leads to regeneration failure after volumetric muscle injury is one of the causes of acute decline muscle mass in aging. Many studies have shown that there is an age-associated decline in MuSC numbers, self-renewal and differentiation function (Kuang and Rudnicki, 2008; Shefer et al., 2010). This decline causes the impaired muscle regeneration, reduced muscle performance, and increased muscle fibrosis, which slowly stiffens the tissue and leads to the loss of contractile function (Brack et

al., 2007; Fry et al., 2015). The impaired regenerative capability can not successfully be recovered from the acute volumetric muscle injury from surgery or accidents which leave post-traumatic atrophy. Other than regenerative capacity, muscle stem cell depletion can also result in voluntary physical inactivity which creates a vicious cycle of muscle atrophy although whether the increase in the number of muscle stem cells can change the elder's lifestyle remains to be investigated (Englund et al., 2020).

The aging of muscle stem cells is influenced by both complex relationships between cell-intrinsic and extrinsic factors (Bengal et al., 2017; Blau et al., 2015; Brack and Rando, 2012; Cosgrove et al., 2014a). The perturbations in the p38 MAPK, SMAD, FGF, pRb, Stat3, β -catenin, p16 together with senescence-related proteins such as p21 signaling have been noted at a cell-intrinsic level while aberrant activation in MuSC niche is shown to impact the MuSC function and muscle regeneration in aged MuSCs (**Figure 1.8**) (Blau et al., 2015; Cosgrove et al., 2014a; Muñoz-Cánoves et al., 2020). Overall, dysfunction in aged muscle is closely intertwined with diverse causes both at cell-intrinsic and -extrinsic factors, and the future development of an effective intervention of sarcopenia should consider that systemic and local alteration in aging.

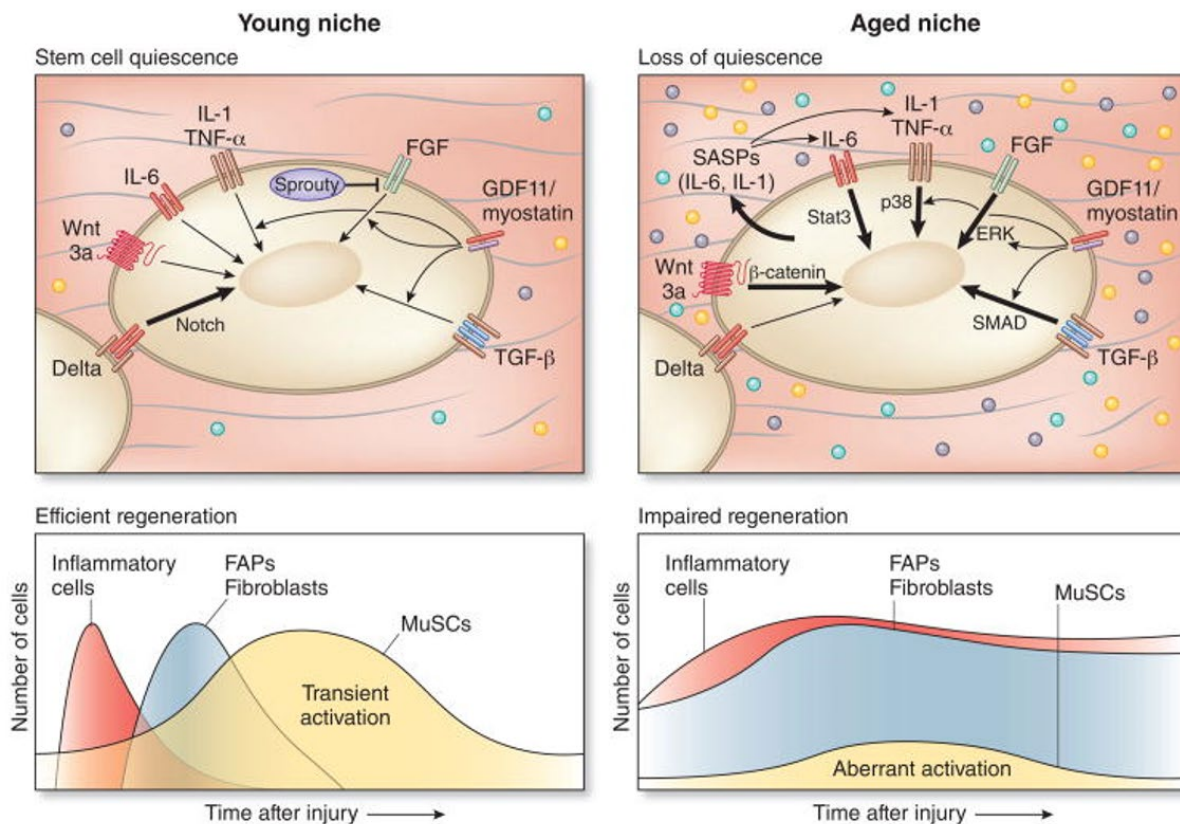


Figure 1.8. The intrinsic and extrinsic changes of muscle stem cells in tissue homeostasis during aging (Blau et al., 2015). The comparison between young muscle niche (Left) and aged muscle niche (Right) in quiescence (Upper) and in muscle regeneration after muscle injury (Bottom). Aged muscle niche shows aberrant activation of tissue-resident populations along the time after injury between young niche and aged niche.

Figure 1.8 The figure was reproduced from Nature Medicine (Blau et al., 2015) and is copyright of the Springer Nature.

Section 2: Statement of Research

2.1. Investigating transcriptional regulation of apelin

2.1.1 Myokine apelin as anti-aging factor

Exercise is one of the most powerful ways to increase muscle function. Various human training trials and animal experiments have shown that physical activity and performance in exhaustion conditions increase running time and speed while reversing aging-related phenotypes in various tissues. Overall, various animal experimental data indicate that the exercise regimen promoted enhanced performance together with metabolic improvement.

Apelin is produced in skeletal muscle in response to muscle contraction during exercise. Apelin has recently emerged as a modulator of muscle physiology and as a therapeutic target for muscle and metabolic diseases (Besse-Patin et al., 2014; Castan-laurell et al., 2012; Kadoglou et al., 2012; Rai et al., 2017). Particularly, plasma apelin and mRNA were significantly increased by long-term aerobic exercise such as cycling, running, treadmill, ladder, and swimming after 8 weeks of training (Besse-Patin et al., 2014; Zhang et al., 2006). Apelin regulates various physiological processes including metabolism, cardiac contractility, blood pressure, and participates in several pathological processes of metabolic syndrome such as diabetes and obesity (Boucher et al., 2005; Li et al., 2006; Szokodi et al., 2002a; Tatemoto et al., 2001; Zhang et al., 2016). It increases blood glucose level stability between rest, exhaustion, and recovery states, which improves the pre-diabetic condition and also relieves hypertension homeostasis in rats (Zhang et al., 2006). Further, a combination of apelin treatment and pre-exercise reduces fibrotic and inflammatory cells after ischemia-reperfusion injury in rats, showing the protective function in cardiac cells (Nazari and Chehelcheraghi, 2020).

In humans, apelin is produced as a 77 amino acid pre-pro peptide, which is cleaved by endopeptidases, then converted into the mature peptides, apelin-36, apelin-17, and apelin-13 (Japp and Newby, 2008; Nyimanu et al., 2019; Tatemoto et al., 1998). Apelin signals by binding to the G protein-coupled apelin receptor (APLNR, angiotensin receptor-like 1) and intra-cellular coupling to $G_{\alpha i}$. Downstream to this receptor complex, apelin signaling diverges on several signaling pathways such as phosphoinositol 3-kinase (PI3K),

phospholipase C (PLC), AMPK, and mitogenic extracellular signal-regulated kinase (ERK) in skeletal muscle (**Figure 2.1**) (Besse-Patin et al., 2014; Chapman et al., 2014; Szokodi et al., 2002b).

Systemic apelin levels and local apelin and its receptor expression in cardiac, aorta, renal, hepatic, lung tissue decline with aging (Rai et al., 2017). The exogenous administration of the apelin peptide ameliorates various age-related pathologies such as cardiac hypertrophy and insulin resistance (Attane et al., 2012; Rai et al., 2017; Vinel et al., 2019). Particularly, apelin (-/-) deficient mice show much severe abnormality in muscle function together with aging, and downregulation of apelin and its receptor (apelin receptor) accelerated the age-related cardiovascular features as it mediates senescence-promoting transcription factors (Rai et al., 2017). Taken together, apelin has the potential to be a strong anti-aging factor while raising the investigation of using apelin as a pharmacological target to extend healthspan.

As part of my Ph.D., we investigated the plasma level of apelin in sarcopenia patients and the local production in skeletal muscle with aging (**Appendix**)(Vinel et al., 2018). We investigated which specific phenotypes are related to the apelin signals in mice. In particular, we demonstrate that apelin signaling is perturbed in myogenic cells in aging and the effect of apelin in muscle regenerative function.

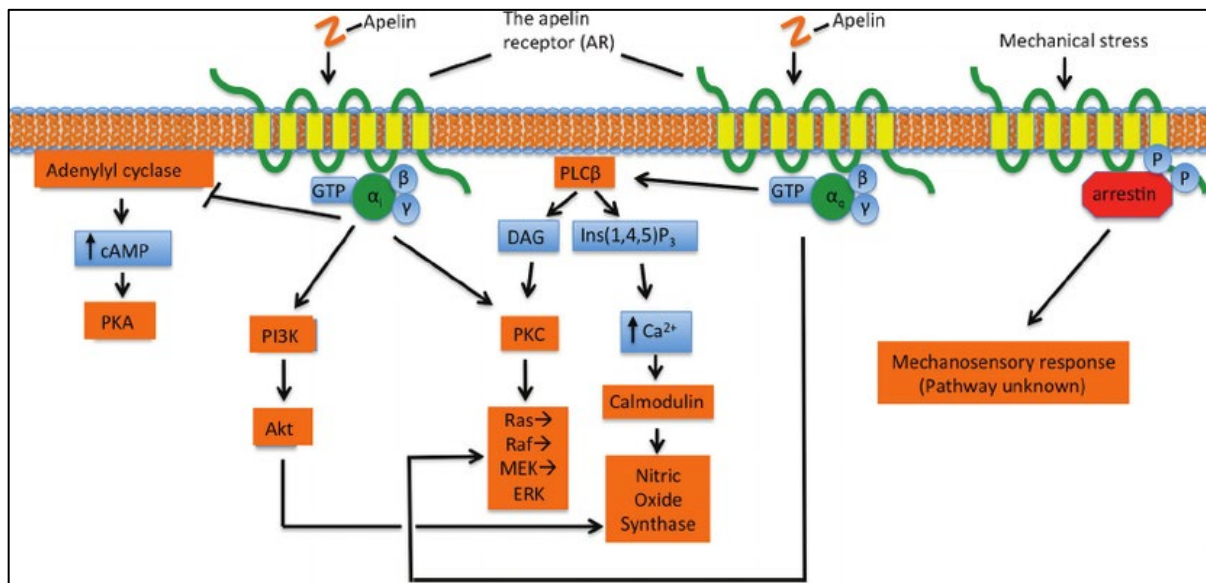


Figure 2.1. Signaling pathways induced by activation of APLNR (Chapman et al., 2014). Activated signals in the presence of apelin. Apelin receptor (APLNR) couples to Gi protein and activates phosphoinositol 3-kinase (PI3K), Akt, and Protein kinase C (PKC), thereby leading to activation of mitogenic extracellular signal-regulated kinase (ERK) pathway. Alternatively, activation of Gq protein through APJ activates phospholipase C (PLC) inducing diacylglycerol (DAG) and inositol 1,4,5-triphosphate (Ins(1,4,5)P₃) production.

Figure 2.1 The figure was reproduced from *Biochemistry and Cell Biology* (Chapman et al., 2014) and is copyright of the Canadian Science Publishing.

2.1.2 Transcriptional regulation of apelin

The transcriptional regulation of the *Ap1n* promoter directly influences its circulating levels. HIF and USF have been identified as transcription factors regulating apelin transcription based on targeted hypotheses (Han et al., 2008b; Wang et al., 2006). For instance, the APLN gene core promoter region has been characterized in humans and rats (-100/+74bp for human -207/-1bp for rat) and a binding site for upstream stimulatory factor (USF) has first been reported (Wang et al., 2006). Another identified activator of APLN phospho-Stat3 was found at promoter between -198/-195bp, which implicates that apelin expression can be induced by the inflammation-dependent manner within the gastrointestinal tract (Han et al., 2008).

Notably, in skeletal muscle tissue, various dietary factors and metabolic signals are reported to induce apelin expression (Bertrand et al., 2013; Lv et al., 2013; Mazzucotelli et al., 2008). A significant increase in apelin expression was observed after 24 hours of treatment with 100 μ M dietary eicosapentaenoic acid (EPA) supplement in ERK1/2 dependent manner both in vivo and in vitro using myotube (14days of C2C12 differentiated)(Bertrand et al., 2013). In another study, apelin mRNA and peptide secretion was increased in response to PGC-1 α in human white adipocytes (Mazzucotelli et al., 2008). The induction of PGC-1 α was either through forskolin and isobutylmethylxhe (IBMX) or cold exposure increased the apelin expression in a cAMP-dependent manner (Mazzucotelli et al., 2008).

Furthermore, apelin precursor peptide expression is increased by synthetic retinoid Am80 through recruiting retinoic acid receptor- α (RAR α) to the apelin promoter by interacting with Kruppel-like factor 5 (KLF5) and stimulating protein 1 (Sp1) in rat vascular smooth muscle cells (VSMCs) (Lv et al., 2013). Hence, we could infer that the regulatory elements of apelin transcription vary a lot ranging from cellular glucose and lipid metabolism to inflammatory signals in various tissue cell types.

However, the backgrounds remain several questions to answer further. Which specific network of transcription factors coordinates apelin expression in skeletal muscle? What are the specific cell types in skeletal muscle that are most relevant to apelin production in exercise? As a secreted protein, can endogenous regulation of apelin influence paracrine

communication? If apelin does, what are the specific cell types which serve as recipients, and what are the consequences of the ligand-receptor signaling? My goal is, therefore, to determine the function of apelin in skeletal muscle and the upstream target mediating apelin expression to discover new strategies to target sarcopenia and muscle diseases.

2.1.3 Detailed research plan of project

To achieve this goal, we suggest two approaches. In the first investigation, we plan to discover transcription factors interacting with the apelin promoter and driving apelin transcription. In this study, we performed a systematic evaluation of transcription factors regulating the apelin promoter using a yeast one-hybrid (Y1H) screen with a library containing 745 mammalian transcription factors (Gubelmann et al., 2013). Through this approach, we demonstrate a novel regulator of apelin expression in myofibers in vitro and in vivo. Secondly, we suggest finding the major cell types expressing apelin and apelin receptor to identify specific cell types that are involved in the paracrine function of apelin. This is achieved by using single-cell RNAseq analysis of healthy and regenerating muscle. Lastly, we present a specific phenotype that apelin treatment or modulation of apelin production by a novel factor in a specific cell type drives a paracrine effect during muscle repair.

Specifically, our detailed experimental aims include; the identification of putative promoter sites driving active apelin expression by performing a dual luciferase assay [**Aim 1**] (**Figure 11**). Then, we screen for 745 transcription factors for the discovery of novel regulators interacting with the apelin promoter using Yeast 1 hybrid screening [**Aim 2**]. The positive hits from Y1H are validated by ChIP-qPCR in-vitro and causative relationships are determined both in-vitro and in-vivo [**Aim 3**]. Next, we analyze the single-cell RNAseq to identify the major cell types expressing apelin and apelin receptor in regenerating muscle [**Aim 4**] and elucidate the involved pathways from a transcription factor to phenotypes on muscle in vitro [**Aim 5**] and find the phenotypes involved and therapeutic intervention in vivo [**Aim 6**]. Ultimately, our strategies will increase our knowledge of the molecular regulation of apelin signaling in health and disease and contribute to the development of novel therapeutic approaches to treat sarcopenia and other conditions where apelin signaling is defective.

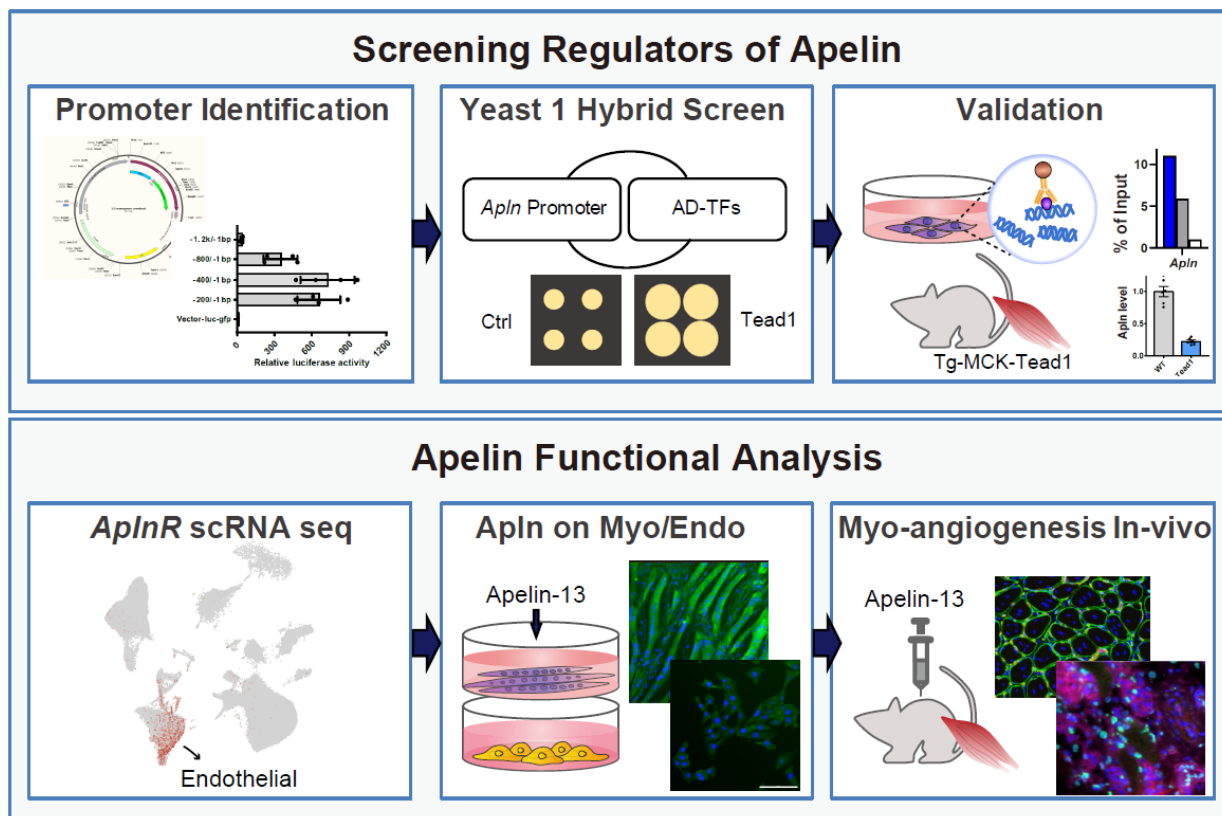


Figure 2.2. Schematic illustration of specific aims of the project. [1] Dual-luciferase assay to discover active promoter region regulating apelin transcription [2] Screening Y1H for 760 transcription factors to discover new transcription factors interacting with the apelin promoter and driving apelin transcription [3] Among the Hits from Y1H, validating the binding affinity of TFs and promoter using ChIP-qPCR and finding causative relation with apelin transcription in skeletal muscle [4] Finding the *ApIn*/*ApInr* signaling mediates cell-specific phenotype by incorporating scRNAseq transcriptomics [5] Identifying the functional relationship that *ApIn*/*ApInr* mediate cell-type-specific phenotypes in vitro. [6] Performing the functional assay on myo-angiogenesis to validate in vivo.

2.2 Investigating functional relationship between myogenic progenitors and supportive cells with glycemic control

2.2.1 Satellite cells and the tissue-resident cells

Satellite cells or skeletal muscle progenitors (SKMPs) are located contiguously with other muscle tissue-resident cells and dynamically interact with each other to maintain, repair the tissue and adapt to environmental changes throughout life. Homeostasis and fate decisions of SKMPs are orchestrated by various tissue-resident cells in the stem cell niche (Bentzinger et al., 2013; Mashinchian et al., 2018; Thomas et al., 2015). Recent in-depth single-cell transcriptomic analysis captured and characterized extended sub-populations of tissue-resident cells such as immune cells, neurons, adipocytes, fibroblast-like cells, and endothelial cells, and smooth muscle cells (De Micheli et al., 2020; Macosko et al., 2015; McKellar et al., 2020a; Saber et al., 2020; Zheng et al., 2017). However, our mechanistic understanding of how these specific cell types influence SKMP function remains limited.

2.2.2 Glucose metabolism in skeletal muscle and satellite cell activation

Skeletal muscle contraction is mediated by dynamic changes in diffusion and the active transport of Ca^{2+} , which requires a massive amount of adenosine triphosphate (ATP). Energy supply is, therefore, critical to muscle function and subject to the metabolism of glucose and fatty acid substrates (Berger et al., 1976; Hänninen and Atalay, 1998; Rose and Richter, 2005). Depending on load and fitness, muscle fibers utilize different modes of ATP synthesis either through anaerobic cytosolic glycolysis or mitochondrial oxidation (Brooks, 1998). The intensity and duration of exercise exponentially increase glucose utilization in muscle and recruit fast-twitch muscle fibers (Brooks, 1997; Wahren et al., 1971; Williams et al., 1995). Since skeletal muscle is one of the most glucose-consuming tissues, it can account for 75-89% of total carbohydrate oxidation during high-intensity exercise (Brooks, 1997; Wahren et al., 1971).

Muscle stem cells can be activated in response to the different environments in muscle adaptation such as mechanical stimulation from work-load endurance exercise and metabolic pathways and oxygen availability. These environmental factors have been known to provoke muscle stem cell activation with higher expression of Pax7, MyoD, Sirt1, Cxcr4, and Spry1 (Abreu, 2018; Abreu et al., 2017; Crane et al., 2015; Fulco et al., 2008; Theret et al., 2017). Current knowledge about satellite cell activation and expansion during the endurance exercise mainly regards AMPK, Sirt1, Oxphos, and ROS-related pathways through mitochondria, which then activates satellite cell self-renewal commitment (Abreu, 2018; Crane et al., 2015; Theret et al., 2017). Moreover, the metabolic adaptation mediated by metabolites from non-myogenic cell types can indirectly be linked to the improvement of satellite cell functions. For instance, lactate, pH, HIF related-signaling induction from endothelial cells enhance satellite cell function through macrophage polarization while different muscle adaptation processes (**Figure 2.3**) (Nalbandian et al., 2020; Zhang et al., 2020). Although metabolism possesses a critical part of muscle stem cell fates, the specific mechanism of muscle stem cell expansion from metabolic adaptation remains unclear.

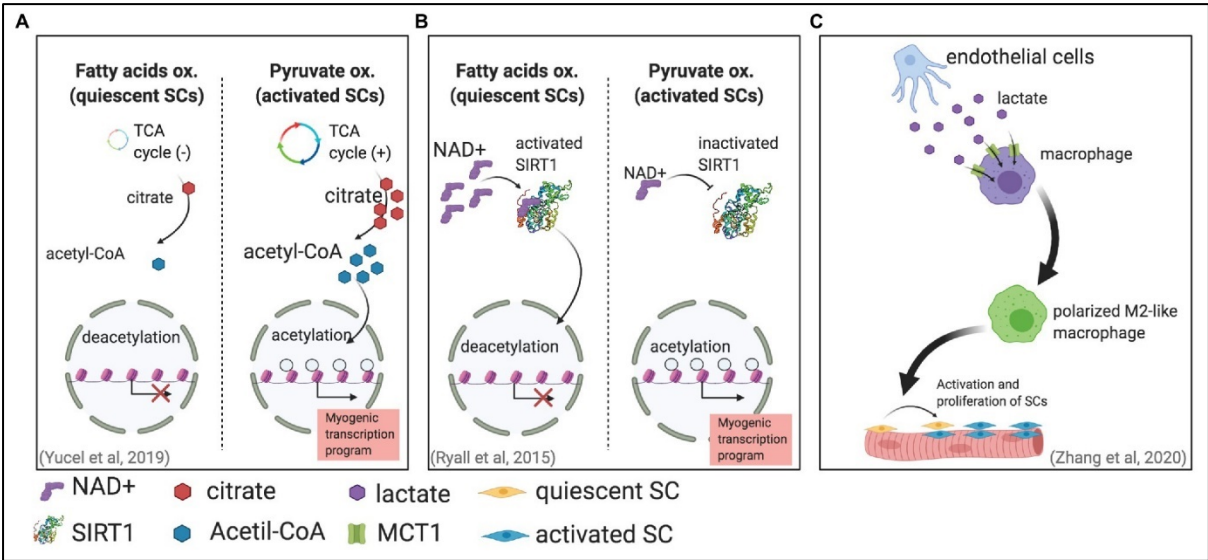


Figure 2.3. Metabolism in muscle stem cell fate decision (Nalbandian et al., 2020). (A) MuSC activation by pyruvate metabolism through TCA cycle activation, which produces more citrate and acetyl-CoA (Yucel et al., 2019) (B) MuSC activation by pyruvate oxidation, reducing the available NAD⁺ and hence reducing Sirt1 activity (Ryall et al., 2015) (C) Endothelial-lactate mediated MuSC activation by M2-like macrophage polarization (Zhang et al., 2020).

Figure 2.3 The figure was reproduced from *Frontiers in Physiology* (Nalbandian et al., 2020) and is copyright of the *Frontiers*.

Interestingly, recent results suggest that SKMPs *in-vitro* do not require high levels of glucose and become impaired under these conditions (Furuichi et al., 2021). In agreement with these findings, excessive blood sugar levels, which are frequently observed in diabetic patients, decrease the myogenic potential of SKMPs and can lead to the development of myopathic changes (D'Souza et al., 2013). Conversely, *in-vivo* caloric restriction has been shown to enhance SKMP function by boosting mitochondrial activity and stimulates muscle regeneration (Cerletti et al., 2012). SKMPs undergo metabolic reprogramming depending on their activation state and utilize distinct metabolic systems and substrates (Ryall, 2013; Ryall et al., 2015). While proliferating SKMPs mainly rely on mitochondrial respiration for ATP production, differentiating cells demand more glucose (Ahsan et al., 2020; Yucel et al., 2019). Hence, glucose metabolism is closely linked to SKMP function.

Moreover, glucose metabolism impacts various functions of other cell populations present in skeletal muscle. For instance, bone-marrow-derived macrophages become more pro-inflammatory and show lower phagocytosis activity with high glucose treatment (Pavlou et al., 2018; Van den Bossche et al., 2017). High glucose treatment decreases migration and proliferation of fibroblasts, which causes the delayed wound healing (Buranasin et al., 2018; Xuan et al., 2014). Endothelial proliferation, permeability, and regenerative function of EC progenitors are also found to be altered by glycemic control (Baumgartner-Parzer et al., 1995; Chen et al., 2007b; Hempel et al., 1997).

In this regard, my specific questions are straightforward yet to be determined. How do glycemic changes affect skeletal muscle progenitors? How do the glycemic changes affect skeletal muscle stem cell niche? What are the consequences in the functional crosstalks between the non-myogenic tissue-resident cells and myogenic progenitors in different metabolic environments? What is the specific mechanism in this metabolic adaptation? Can we use the inter-cellular mediators to boost the function of myogenic progenitors? In this chapter, therefore, we proposed to investigate the niche-dependent metabolic effects of glycemic levels.

2.2.3 Detailed research plan of project

To investigate which specific types of muscle resident cells are involved in this muscle stem cell activation and how the crosstalk is mediated in different glycemic levels, we utilized in-vitro co-culture models, engineered endothelial cell co-transplantation, and single-cell RNAseq data. Our specific aims include identifying specific neighboring cells in muscle tissue that directly give a positive effect on muscle stem cell function using a direct co-culture model and high-content screening in-vitro (**figure 2.4**) [Aim 1]. Then, we find the metabolic effect on SKMPs with its supportive cells by glycemic control [Aim 2]. Next, we try to find the specific molecular signals that potentially mediate the intercellular crosstalk by performing microarray and comparing scRNAseq data [Aim 3]. Then the potential mediators are validated in-vitro and in-vivo [Aim 4].

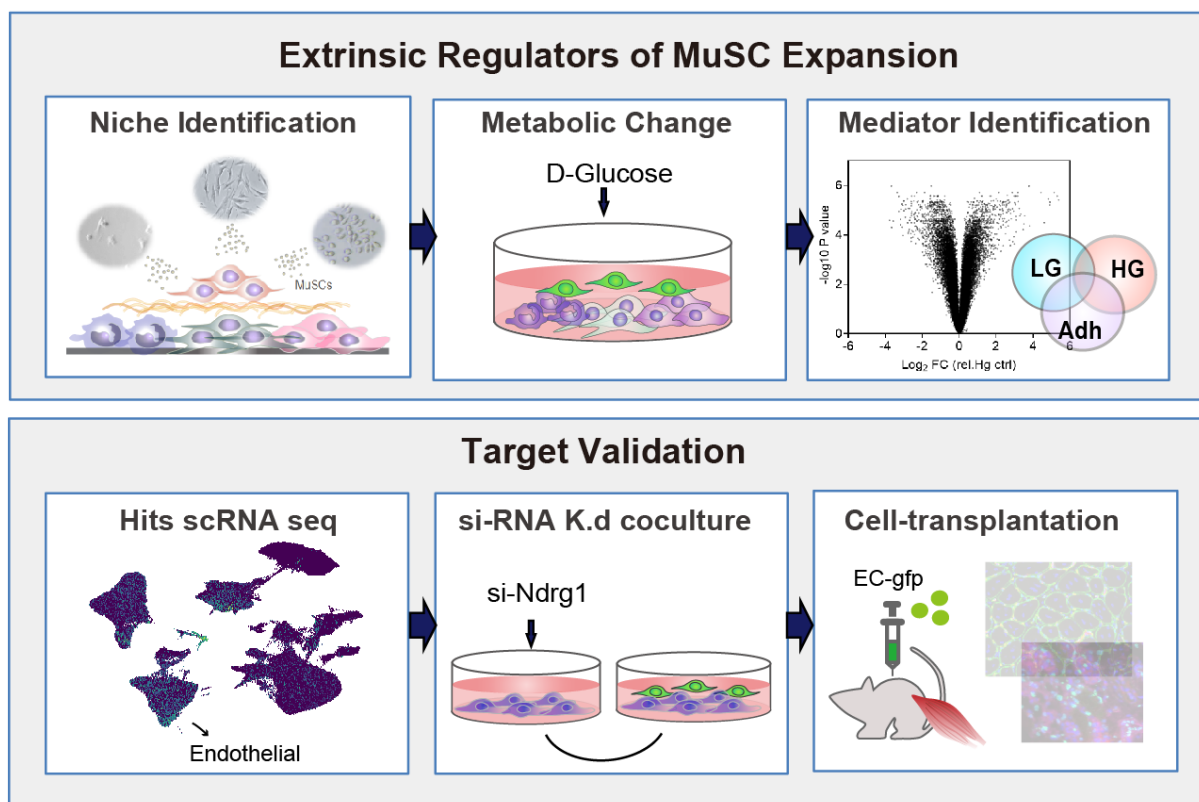


Figure 2.4. Schematic illustration of specific aims of the project. [1] Identifying specific neighboring cells in muscle tissue that directly give a positive effect on muscle stem cell function using High-Content-Screening [2] Discovery of metabolic effect on SKMPs and its supportive cells [3] Finding the specific molecular signals that mediate the crosstalk using combinational analysis of microarray and [4] single-cell RNAseq [5] Validating the signals using the loss of function models in vitro [6] Discovering the phenotypes in muscle in-vivo.

2.3 Developing intravital imaging of vasculature and satellite cells

2.3.1 Vasculature in skeletal muscle

Skeletal muscle is intensely vascularized and vasculature primarily gives a trophic bed to skeletal muscle via local vasodilation depending on the demands of metabolism. The vascular tone is responsively regulated by the instant and transient signals during exercise. In particular, metabolic demands, oxygen levels, neuronal transmitters, and inner polarization within the vessel compartment by mechanical compression from muscle are well described to induce functional hyperemia (Bockman, 1983; Clifford et al., 2006; Hamann et al., 2004). Not only the local hyperemia, but exercise can also regulate the remodeling of vascularization by actively producing angiogenic signalings. Nitric oxide (NO) signaling together with eNOS, nNOS, ROS from enzymatic production from NAD(P)H oxidase in skeletal muscle remodels the microvasculature and the secretion of the vascular endothelial growth factor (VEGF) by myofibers can stimulate endothelial cell expansion and regulates myo-angiogenesis (Bloor, 2005; Gorski and De Bock, 2019).

2.3.2 Endothelial cells and satellite cells in muscle regeneration

The rapid remodeling of blood vessels during muscle repair is essential as the spatiotemporal coordination of angiogenesis and myogenesis is key to rebuild functional vascularized myofibers following muscle injury to ensure efficient oxygen and nutrient supply to muscle fibers (Chazaud, 2020; Lazure et al., 2020; Whitham and Febbraio, 2016). In recent discoveries, the other aspects of the roles of capillaries or vessel-forming cells were highlighted in the maintenance and regulation of satellite cells. For instance, quiescent muscle stem cells have been shown to attract endothelial cells by secreting local VEGF in the niche to keep the proximity to the vasculature and thereby the quiescence (Verma et al., 2018b). During regeneration, vascular remodeling supports muscle stem cell expansion and

commitment to myogenesis through the secretion of IGF-1, HGF, bFGF, and PDGF-BB (Christov et al., 2007a). Beyond these signals, microvascular and skeletal muscle stem cell expansion and hypertrophy after exercise are frequently observed but we still have the lack of direct evidence *in-vivo* (Nederveen et al., 2017; Snijders et al., 2017). Therefore, the understanding of the complex inter-cellular crosstalk between muscle stem cells and microvasculature in skeletal muscle requires further investigation in a Spatio-temporal manner.

2.3.3 Non-invasive imaging for *in-vivo* stem cell research

Recent advances in imaging techniques combined with genetically labeled fluorescent markers have allowed closer inspections into the function of stem cells and biological processes *in vivo*. For example, Cosgrove et al. showed that muscle stem cells from older mice have intrinsic defects by monitoring transplanted stem cell engraftment using *in vivo* bioluminescence imaging (**Figure 2.5**) (Cosgrove et al., 2014b). This study has revealed that the intrinsic inhibition of p38 α / β in MuSCs from old mice allows efficient engraftment into the functional MuSC compartment without interfering viability of mice (Cosgrove et al., 2014b). Such findings suggest a new strategy for quantitative measurement of muscle stem cell function in a non-invasive way.

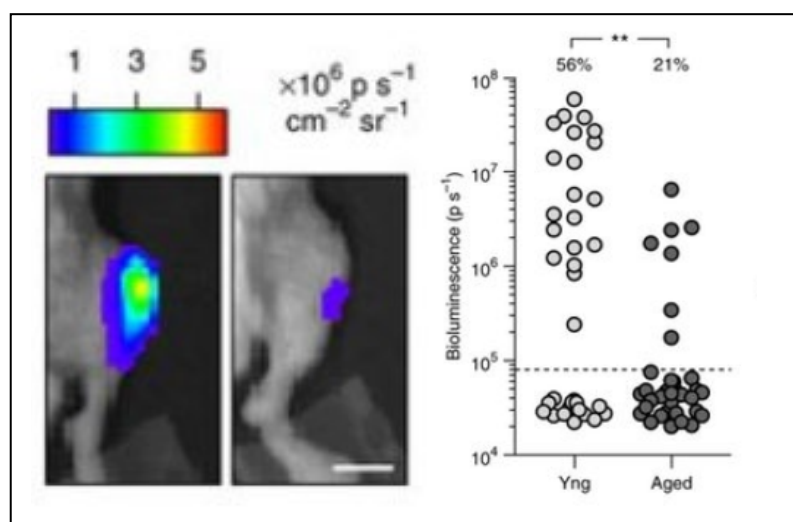


Figure 2.5. The measurement of engraftment success using bioluminescence (Cosgrove et al., 2014b)

Figure 2.5 The figure was reproduced from *Nature Medicine* (Cosgrove et al., 2014a) and is copyright of the Springer Nature.

Multiphoton microscopy has opened a new door for observation of stem cell growth, proliferation, and stability without tissue disruption in a living animal, which was not possible with conventional imaging techniques. For example, two-photon microscopy uses a near-infrared (NIR) laser, which penetrates deep tissue by using the light excitation at 800 - 1300nm. A greater wavelength results in less scattering of photons on a specimen, which is mainly caused by Rayleigh scattering ($1/\lambda^4$) and Mie scattering ($1/\lambda^{0.5}$), hence, it achieves a deep real-time optical readout of living specimens to a micrometer scale level without sacrificing the animal (Benninger and Piston, 2013).

Two-photon imaging has been applied to monitor diverse human and animal stem cells. Researchers have successfully characterized cell morphology, behavior, and metabolic activity in cancer cells and human mesenchymal stem cells (Rice et al., 2010; Uchugonova et al., 2008). More recently, a joint work by Shen and Nishimura group's at Cornell University monitored the vasculature system to study cortical blood flow in Alzheimer's disease from seconds to several week-timescales (**Figure 2.6**)(Cruz Hernández et al., 2019). Another example combining this approach showed a real-time recovery process of injured intestinal stems cells using *in vivo* two-photon microscopy, which revealed that local damage was recovered by the rearrangements of pre-existing cells, and this ability was reduced in aged animals (**Figure 2.7**)(Choi et al., 2018).

This groundbreaking technical achievement is a perfect technique to answer our biological questions. Can we observe the dynamics of muscle stem cells in regenerating vasculature after muscle injury? How do MuSCs integrate the action from the regulatory circuitry of the vascular niche? How stem cells change the behavior as incomplete vascular remodeling is happening? Can we permanently restore the stem cells to a normal function by using vascular niche? This is my vision for the future trajectory of studying muscle stem cells and regeneration. My goal is, therefore, to build the imaging strategy to dynamically and quantitatively evaluate tissue regenerative processes in living animals. This approach will improve stem cell-targeted regenerative medicine therapies to treat muscle aging and degeneration.

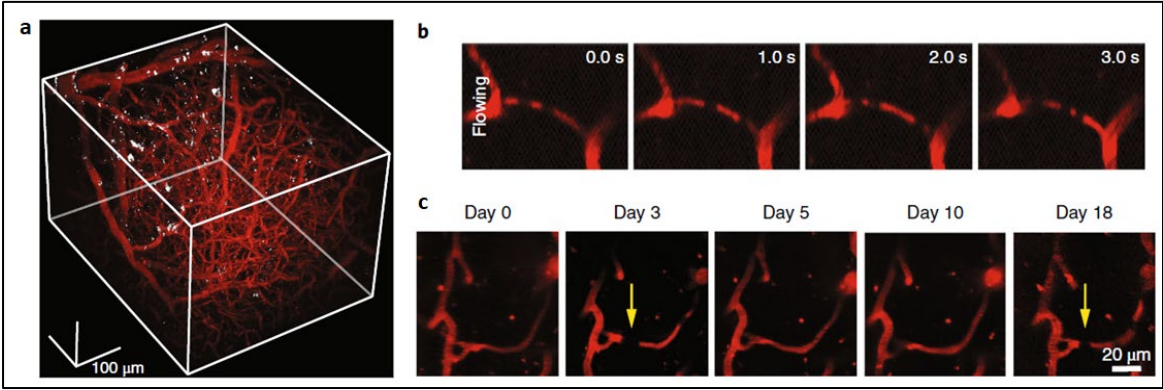


Figure 2.6. 2PEF imaging of mouse cortical vasculature revealed a higher fraction of plugged capillaries in APP/PS1 mice (Cruz Hernández et al., 2019). **a**, Rendering of 2PEF image stack **b**, Individual brain capillaries (red; Texas Red dextran) in seconds **c**, 2PEF images of the same capillary flow over several weeks.

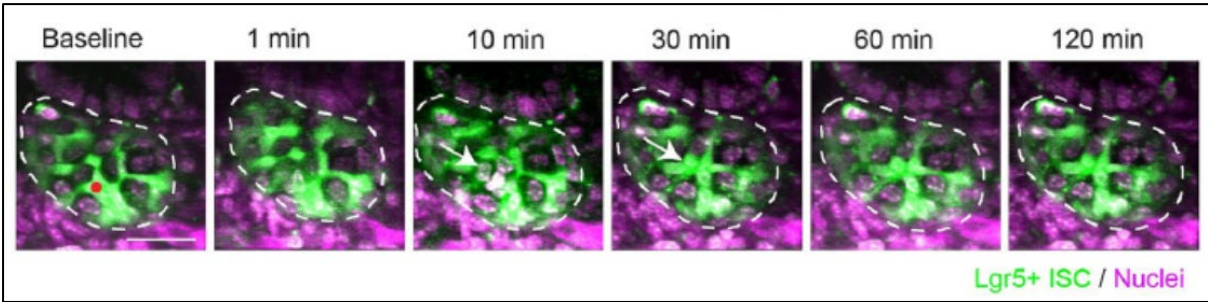


Figure 2.7. Recovery dynamics of intestinal stem cells (GFP labeled) after laser ablation (at Baseline) (Choi et al., 2018).

Figure 2.6 was reproduced from Nature Neurosciences (Cruz Hernández et al., 2019) and Figure 2.7 was reproduced from Scientific Reports (Choi et al., 2018) are copyright of the Springer Nature.

2.3.3 Detailed research plan of project

In this part of my project, I sought to develop intravital imaging to monitor muscle stem cells and vasculature to deepen the anatomical and kinetic understanding of the intercellular crosstalk between vascular networks and muscle stem cells. I propose to use multiphoton microscopy and observe them in the skeletal muscle of mice. Our specific aims included optimizing the chronic or long-lasting window to be able to optically access to hindlimb muscle over the days of recovery [**Aim 1**], developing endogenous endothelial cells labeling system [**Aim 2**], and optimizing visualize muscle stem cells and vasculature in muscle tissue in a living animal [**Aim 3**]. This multidisciplinary approach offers a great promise for the development of a robust in vivo tool to monitor muscle repair dynamics in real-time and will give the basement of monitoring muscle stem cells and their interaction with their native niche.

Section 3

A Tead1-Apelin axis directs paracrine communication from myogenic to endothelial cells in skeletal muscle

A Tead1-Apelin axis directs paracrine communication from myogenic to endothelial cells in skeletal muscle

Umji Lee^{1,2,3}, Pascal Stuelsatz¹, Sonia Karaz¹, David W. McKellar², Julie Russeil³, Maria Deak¹, Iwijn De Vlaminck², Christoph Lepper⁴, Bart Deplancke³, Benjamin D. Cosgrove², and Jerome N. Feige^{1,3,*}

¹ Nestlé Institute of Health Sciences,
Nestlé Research,
Lausanne, Switzerland

² Meinig School of Biomedical Engineering,
Cornell University,
Ithaca, New York, USA

³ School of Life Sciences,
École Polytechnique Fédérale de Lausanne (EPFL),
Lausanne, Switzerland

⁴ Department of Physiology & Cell Biology,
The Ohio State University College of Medicine,
Columbus, Ohio, USA

* Corresponding author:
jerome.feige@rd.nestle.com

Abstract

Apelin is a myokine that regulates skeletal muscle plasticity and metabolism and declines during aging. The molecular mechanisms regulating Apelin levels and the paracrine actions of Apelin signaling within the skeletal muscle are poorly understood. Through a yeast one-hybrid screen of transcription factor binding to the Apelin promoter, we identified the myogenic transcription factor TEA domain family member 1 (*Tead1*) as a novel regulator of *Apln* transcription. We observed via single-cell transcriptomic analysis of regenerating skeletal muscle that *Ap1nr* (Apelin receptor) is enriched in muscle endothelial cells, whereas *Tead1* is enriched in myogenic cells. Knock-down of *Tead1* stimulates the secretion of Apelin from muscle cells *in vitro* and myofiber-specific over-expression of *Tead1* suppresses apelin secretion *in vivo*. Apelin secretion via *Tead1* knock-down in muscle cells stimulates endothelial cell proliferation *in vitro* co-cultures and Apelin peptide supplementation enhances endothelial cell expansion following muscle injury *in vivo*. Our work describes novel paracrine crosstalk in which Apelin secretion is controlled by *Tead1* in myogenic cells and influences endothelial remodeling during skeletal muscle repair.

Keywords: Apelin; Tead1; Skeletal muscle; regeneration; stem cells; endothelial cells; single-cell RNAseq

Author contribution:

As a primary author, I have led the project by designing and performing the experiments, interpreting the results, and writing the manuscript.

Current status of the project:

Submitted to iScience Journal, in revision.

3.1 Introduction

Skeletal muscle is a plastic tissue with intrinsic capacity for structural and functional adaptations in response to nutrition, physical activity, and various physiological needs of the body. In particular, muscle physiology adapts to different types of exercise training but also declines in muscle-wasting conditions which can arise from genetic monogenic mutations causing muscular dystrophies, chronic diseases such as cancer or COPD, aging, traumatic or sports injuries, or simply inactivity during immobilization or prolonged bed rest (Egerman and Glass, 2014; Sartori et al., 2021). At the cellular level, the ability to contract is tightly controlled by the number of contractile proteins and the bioenergetic capacity of myofibers, but also by local cellular interactions with motoneurons and blood vessels as well as endocrine signals from the rest of the body. In addition, skeletal muscle can be repaired when damaged during pathological conditions owing to a tissue-resident population of stem cells called satellite cells (Ancel et al., 2021; Fuchs and Blau, 2020; Yin et al., 2013b).

Secretion of myokines by myofibers and paracrine communication within skeletal muscle has emerged as an active mechanism through which muscle physiology and repair are coordinated through cross-talk with satellite cells, immune cells, fibro-adipogenic progenitors, and endothelial cells which regulate angiogenesis and remodel the vasculature to ensure efficient oxygen and nutrient supply to muscle fibers (Chazaud, 2020; Lazure et al., 2020; Mashinchian et al., 2018; Whitham and Febbraio, 2016). Exercise training is well described to remodel vascularization of skeletal muscle via mechanisms involving paracrine secretion of the vascular endothelial growth factor (VEGF) by myofibers, which stimulates endothelial cells and regulates angiogenesis (Bloor, 2005; Gorski and De Bock, 2019). The remodeling of blood vessels during muscle repair is also a topic of active investigation as the spatiotemporal coordination of angiogenesis and myogenesis is key to rebuild functional vascularized myofibers during tissue repair following muscle injury. Muscle stem cells have been shown to attract endothelial cells by secreting local VEGF in the niche (Verma et al., 2018b). Macrophages invading muscle after tissue injury were also recently described to modulate endothelial cell remodeling via secretion of lactate (Zhang et al., 2020). Conversely, vascular remodeling during muscle repair supports muscle stem cell expansion and commitment to myogenesis (Christov et al., 2007a). Beyond the identification of these first signals, the understanding of the complex inter-cellular crosstalk between muscle fibers, muscle stem cells, and endothelial cells requires further investigation.

Apelin (APLN) is a small peptide regulating paracrine and endocrine communication in adipose tissue and the cardiovascular system. *Apln* is produced in skeletal muscle in response to exercise and contraction and has recently emerged as a modulator of muscle physiology and as a therapeutic target for muscle and metabolic diseases (Besse-Patin et al., 2014; Castan-laurell et al., 2012; Kadoglou et al., 2012; Rai et al., 2017). In humans, apelin is produced as a 77 amino acid pre-pro peptide, which is cleaved by endopeptidases, then converted into the mature peptides, apelin-36, apelin-17, and apelin-13 (Japp and Newby, 2008; Nyimanu et al., 2019; Tatemoto et al., 1998). *Apln* signals by binding to the G protein-coupled apelin receptor (APLNR, angiotensin receptor-like 1) and intra-cellular coupling to *G α i*. Downstream to this receptor complex, apelin signaling diverges on several signaling pathways such as phosphoinositol 3-kinase (PI3K), phospholipase C (PLC), AMPK, and mitogenic extracellular signal-regulated kinase (ERK) in skeletal muscle (Besse-Patin et al., 2014; Chapman et al., 2014; Szokodi et al., 2002b). Systemic apelin levels and local production by muscle decline with aging and an exogenous administration of the apelin peptide ameliorates age-associated pathologies such as cardiac hypertrophy, insulin resistance, and sarcopenia (Attane et al., 2012; Rai et al., 2017; Vinel et al., 2018, 2019).

The transcriptional regulation of the *Apln* promoter directly influences its circulating levels, and HIF and USF have been identified as transcription factors regulating apelin transcription based on targeted hypotheses (Han et al., 2008b; Wang et al., 2006). It remains, however, unclear which network of transcription factors coordinates apelin expression in skeletal muscle and how the endogenous regulation of apelin expression influences paracrine communication. In this study, we performed a systematic evaluation of transcription factors regulating the apelin promoter using a yeast one-hybrid (Y1H) screen with a library containing 745 mammalian transcription factors (Gubelmann et al., 2013). Through this approach, we identified TEA domain family member 1 (Tead1) as a regulator of apelin expression in myofibers in vitro and in vivo. Finally, single-cell RNAseq analysis of healthy and regenerating muscle identified endothelial cells as the major cell type expressing *Aplnr*. Based on this observation, we demonstrate that apelin treatment or modulation of apelin production by Tead1 in myofibers drives endothelial remodeling and angiogenesis during muscle repair through paracrine signaling.

3.2 Results:

3.2.1 Tead1 interacts with the apelin gene promoter in myogenic cells.

To gain insight into the transcriptional mechanisms of *Apln* regulation, we investigated cis-regulatory elements of the *Apln* precursor gene (*Apln*) and its regulatory transcription factors. Classic methods to discover TF-DNA interactions, such as gel-shift assay and reporter assay combined with promoter deletion do not easily scale to a high-throughput evaluation of TF-DNA interactions. Hence, we adopted a yeast one-hybrid (Y1H) method, which allows to probe interactions between TFs and DNA sequences of interest at a large scale (Gubelmann et al., 2013). To identify a putative promoter region for *Apln*, we examined the epigenetic regulatory signatures and sequence conservation of its 5' upstream region in the WashU Epigenome Browser (**Figure 3.S1A**). The conservation score between 20 mammalian species described in (Miller et al., 2007; Zhou and Wang, 2012) is high within the -400bp region upstream of the *Apln* transcriptional start site (TSS). Similarly, this region is enriched in H3K9ac and H3K4me3 histone marks and EP300 binding based on public ChIP-seq analyses (Gates et al., 2017; Liang et al., 2004), suggesting that it may contain the core *Apln* promoter. To determine the transcriptional activity of the *Apln* promoter region, we performed dual reporter gene assays in C2C12 myoblast cells (**Figure 3.S1B**). -200/-1bp and -400/-1bp fragments of the *Apln* promoter showed the highest transcriptional activity, confirming that this proximal promoter contains the core activating elements for *Apln* transcription.

We then performed Y1H screens of different *Apln* promoter regions. Yeast lines containing the respective *Apln* promoter fragments were each mated with a library of yeast strains, each containing a prey vector that encodes one out of 745 mouse transcription factors that are fused to the Gal4 activation domain. Positive TF-*Apln* promoter fragment interactions were then identified based on the ability of the respective diploid yeast to grow on a selective plate (**Figure 3.1A** and (Gubelmann et al., 2013)). Among the positive Y1H interactions with the -200/-1bp *Apln* promoter region, we identified six TFs (Tead1, Zic3, Barx1, Zfp319, Gcm2, and Zdhc9) out of the 745 candidates in the TF ORF library (**Figure 3.1B-C**). Binding of the same six TFs was detected for the -400/-1bp *Apln* promoter (**Figure 3.S1C-D**), and longer promoter fragments did not result in further binding of additional TFs (data not shown).

To prioritize the relevance of the candidate apelin promoter binding-TFs to skeletal muscle physiology, we compared the mRNA expression of the six TFs in mouse and human tissues using datasets in the bioGPA portal (Su et al., 2004; Wu et al., 2013). *Tead1*, *Zfp319*, *Zdhhc9*, and *Barx1* expression were all detectable in skeletal muscle from both mice and humans (**Figure 3.1D**). *Tead1*, *Zfp319*, and *Zdhhc9* were also expressed in C12C12 myoblasts (**Figure 3.1E**) and were selected for functional validation through siRNA knock-down. Knock-down of *Zdhhc9* did not influence *Apln* expression in C2C12 cells and knock-down of *Zfp319* reduced *Apln* mRNA but did not influence apelin peptide secretion (**Figure 3.S2A-F**).

Given that *Zdhhc9* and *Zfp319* have never been linked to muscle biology, while *Tead1* was previously established to influence myogenesis (Joshi et al., 2017; Southard et al., 2016; Tsika et al., 2008), we then tested whether *Tead1* binds and regulates the *Apln* promoter in myogenic cells. In chromatin immunoprecipitation (ChIP) experiments, we found that *Tead1* specifically binds to the proximal *Apln* promoter (**Figure 3.1G**), as well as regulatory regions of the previously reported TEAD1 target genes *Ankrd1* and *Ctgf* (Stein et al., 2015). The binding of *Tead1* to the apelin promoter was reduced upon siRNA knockdown of *Tead1* (**Figure 3.1F-G**). Functionally, the siRNA knockdown of *Tead1* increased the activity of an apelin promoter-luciferase reporter (**Figure 3.1H**), highlighting that *Tead1* represses the *Apln* promoter in muscle cells as also previously reported in other cell types (Kim et al., 2015).

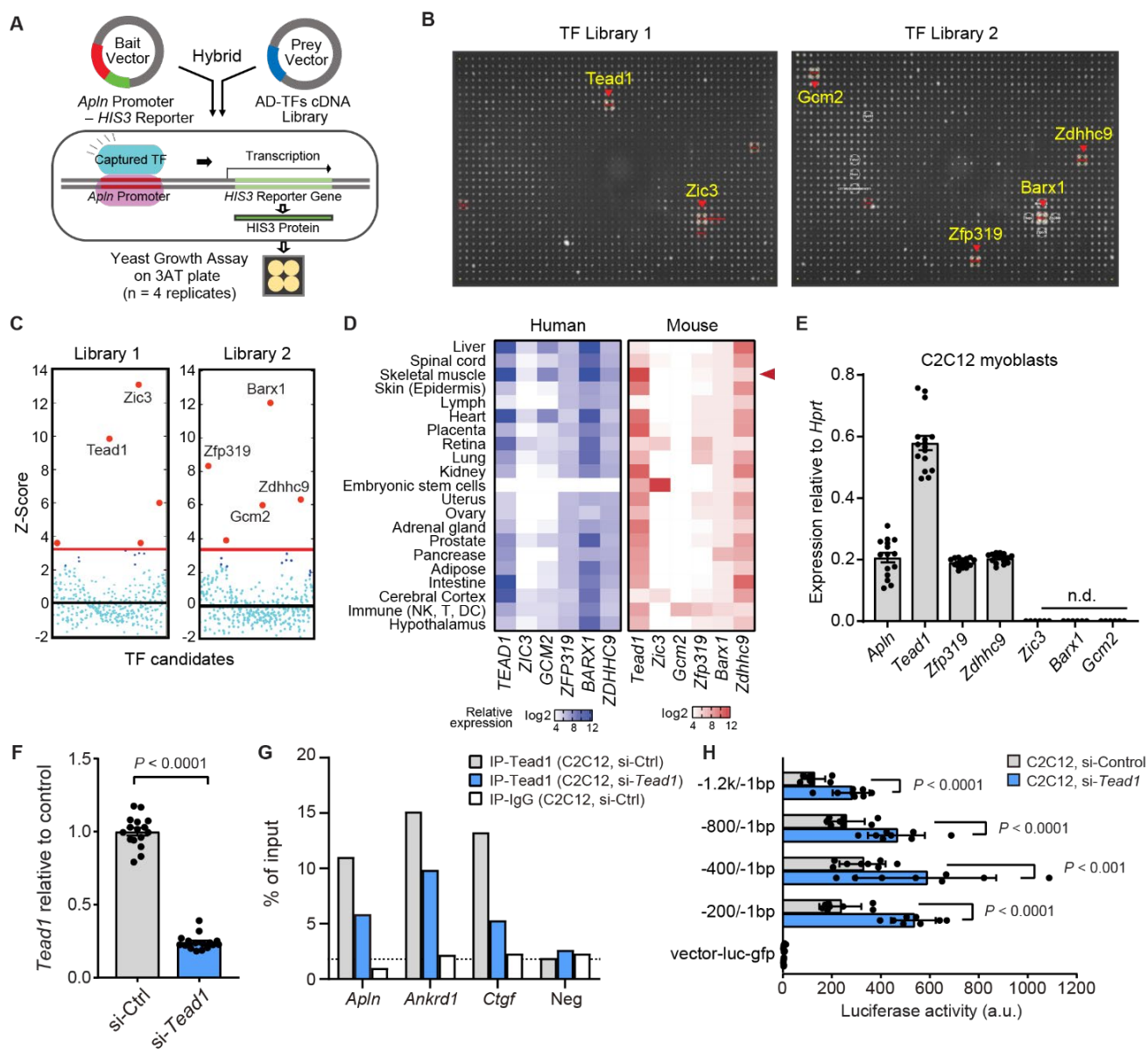


Figure 3.1. A transcription factor screen identifies Tead1 as a direct regulator of apelin transcription. (A) Overview of the yeast one-hybrid (Y1H) assay to screen 745 transcription factors for their ability to interact with the *Apelin* (*Apln*) promoter. Binding of a transcription factor is read-out via expression of the *HIS3* reporter which enables yeast growth on a selective 3AT-containing medium plate. (B) Y1H screen results using the -200/-1bp fragment of the mouse *Apln* promoter as bait and 745 mouse TFs as prey (n = 4 replicates per tested TF, hence the formation of a quadrant in case of a positive interaction). (C) Z-score-normalized Y1H spot intensities for all 745 TFs. Six TFs with Z-scores above the background threshold (red line) are noted here and in (B). (D) Relative mRNA expression of the six TF candidates in bulk mRNA profiling of human and mouse tissues. Microarray data for human (left) from the GeneAtlas UI33A and mouse (right) from the GeneAtlas MOE430 of the bioGPS gene annotation portal. n = 2 replicates per tissue. Expression data are normalized

and presented in a log₂-scaled heatmap by species. **(E)** mRNA expression of *Apln* and the six TFs in C2C12 myoblasts measured by RT-qPCR relative to *Hprt*. n.d., not detected. Mean \pm standard error of mean (s.e.m.) of n = 16 replicates. **(F)** mRNA expression of *Tead1* in C2C12 myoblasts transfected with scrambled control or *Tead1* targeted siRNAs for 3 d. n = 16 replicates. **(G)** ChIP-qPCR assay of *Tead1* testing for binding to known target promoters (*Ctgf*, *Ankrd1*), *Apln* promoter (-177/-77bp), or a random negative control in C2C12 myoblasts treated with either scrambled control or *Tead1*-targeted siRNA for 3 d. ChIP was performed with *Tead1* or IgG control antibodies and qPCR was normalized to IP input. n = 1 biological replicate. **(H)** Luciferase activity of five *Apln* promoter fragments transfected into C2C12 myoblasts at D3 with scrambled or *Tead1* siRNA. Vector control contains no *Apln* promoter. Mean \pm s.e.m. of n = 8 biological replicates. *P* values are reported from two-tailed, unpaired t-tests between siRNA conditions.

3.2.2 Tead1 suppresses apelin secretion in muscle.

The *Apln* peptide is a myokine previously documented to be produced by skeletal muscle during contraction (Vinel et al., 2018). *Apln* is also expressed in myogenic cells (Latroche et al., 2017)(Vinel et al., 2018), and induced at the transcript and protein levels during myogenic differentiation (**Figure 3.2A-B**). To evaluate if Tead1 regulates the endogenous *Apln* promoter, we performed *Tead1* knockdown by siRNA in muscle cells. The *Apln* transcript and peptide levels were significantly increased by 50 and 24%, respectively, when Tead1 was knocked down (**Figure 3.2C-D**; **Figure 3.1F**).

The repression of apelin by Tead1 in myofibers was then tested *in vivo* by analyzing *Apln* levels in mice overexpressing Tead1 specifically in mature myofibers under the control of the muscle creatine kinase (MCK) promoter (**Figure 3.2E-I**) (Southard et al., 2016; Tsika et al., 2008). Consistent with the *in vitro* data, myofiber-specific Tead1 overexpression resulted in lower levels of *Apln* mRNA and peptide in skeletal muscle (**Figure 3.2F-H**). Overexpression of Tead1 in myofibers also reduced systemic *Apln* levels in serum (**Figure 3.2I**), demonstrating that the regulation of the *Apln* gene by Tead1 in muscle directly influences systemic levels of *Apln* in the circulation and that skeletal muscle is a direct contributor to circulating *Apln* levels.

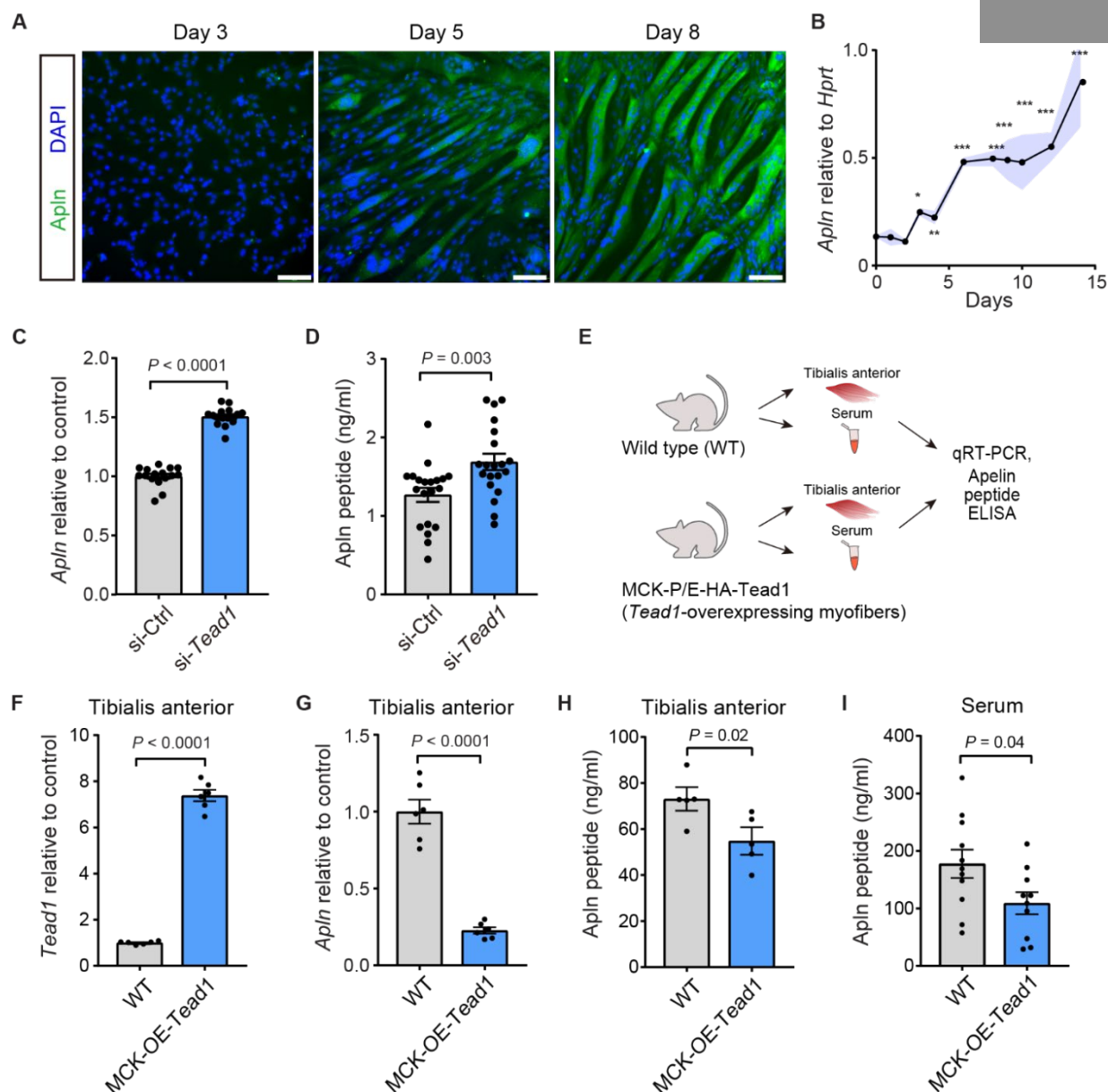


Figure 3.2. Apelin is repressed by Tead1 in muscle cells *in vitro* and *in vivo*. (A) Immunostaining of ApIn protein during C2C12 myotube differentiation. Scale bars, 100 μ m. (B) Quantification of ApIn mRNA by RT-qPCR during C2C12 myotube differentiation relative to *Hprt* using $2^{-\Delta\Delta C_t}$ method. $n = 4$ cell culture replicates per time point. (C-D) Quantification of apelin mRNA by RT-qPCR (C) or apelin peptide in supernatant by ELISA (D) in C2C12 myoblasts transfected with scrambled control or *Tead1* targeted siRNAs for 3d. $n = 16-20$ replicates per condition (E-I) Analysis of *Tead1* and in adult mice over-expressing *Tead1* in skeletal muscle myofibers under the muscle creatine kinase (MCK) promoter (MCK-OE-*Tead1* mice), compared to WT C57BL6 controls. (F-G) *Tead1* mRNA (F) and *ApIn* mRNA (G) expression levels measured by RT-qPCR and normalized to *Hprt* in tibialis anterior (TA) muscles. $n = 6$ mice per condition. (H-I) ApIn peptide concentration measured by ELISA in TA muscles (H) or serum (I). $n = 5$ mice per condition for TA ; $n = 11$ mice per condition for serum. All data are presented as mean \pm s.e.m., and P values are reported from two-tailed, unpaired t-tests between conditions. * $P < 0.05$, ** $P < 0.01$, *** $P < 0.001$.

3.2.3 *Tead1-Apln-Aplnr* expression patterns suggest paracrine signaling to endothelial cells.

The recovery of skeletal muscle following tissue damage is essential to maintain muscle mass and strength and relies on coordinated expansion and differentiation of myogenic and non-myogenic cell types (Bentzinger et al., 2013). Our previous work demonstrating that apelin promotes muscle regeneration (Vinel et al., 2018) prompted us to examine how *Tead1* and *Apln* signaling crosstalk in the niche during muscle repair by analyzing a notexin-induced muscle regeneration single-cell RNA sequencing dataset previously reported (De Micheli et al., 2020). In this dataset analyzing mononucleated cells, *Apln* expression in mature multinucleated myofibers cannot be captured as *Apln* is induced during terminal phases of myogenic differentiation after myogenic fusion and maturation (**Figure 3.2A-B**). Out of the mononucleated niche cells analyzed, low levels of apelin expression were detected in endothelial and smooth muscle cells (**Figure 3.3A-B**).

Conversely, *Tead1* was weakly expressed in most non-immune cell clusters, including in the myogenic progenitor cell (*Myod1*⁺) cluster, compared to all non-myogenic cells at 7 days post-injury (d.p.i.; false discovery-adjusted $P = 2.2 \times 10^{-164}$). To understand how apelin secretion signals during muscle regeneration, we analyzed which recipient cells from the muscle stem cell niche express the apelin receptor at 0-7 d.p.i. in this dataset (**Figures 3.3A-B** and **Figure 3.S3**). *Aplnr* expression was detected in the capillary (*Kdr*⁺ *Pecam1*⁺) and vein (*Vwf*⁺ *Pecam1*⁺) endothelium cell clusters at most time points. At 7 d.p.i., *Aplnr* was enriched in all endothelial cells relative to all non-endothelial cells (false discovery-adjusted $P = 0.038$).

To confirm the specificity of *Apln* and *Aplnr* expression in the niche and identify simple cell culture models to study apelin signaling across the niche, we analyzed the expression of *Apln* and *Aplnr* mRNA and protein in endothelial cells and myotubes *in vitro*. As expected from the single-cell RNAseq, *Aplnr* is specifically expressed by mouse C166 yolk sac-derived endothelial cells (Wang et al., 1996), while apelin is specifically expressed by C2C12 myotubes (**Figure 3.3C-D**). Given that *Aplnr* is highly enriched in endothelial cells, we hypothesized that *Apln* may regulate endothelial cell behavior and angiogenesis following muscle injury.

To evaluate this possibility, the dynamics of apelin production and endothelial cell remodeling were measured in an *in vivo* model of muscle regeneration (**Figure 3.3E-G**).

Transient activation of *Apln* expression during muscle regeneration directly mirrored the dynamics of CD31/Pecam1⁺ endothelial cells remodeling, with both apelin expression and CD31⁺ endothelial cells peaking in the initial phases of muscle repair at 3 d.p.i. (**Figure 3.3F;H-I**). Thus, apelin receptor is enriched in endothelial cells and the timing of apelin production correlates with endothelial remodeling during tissue repair.

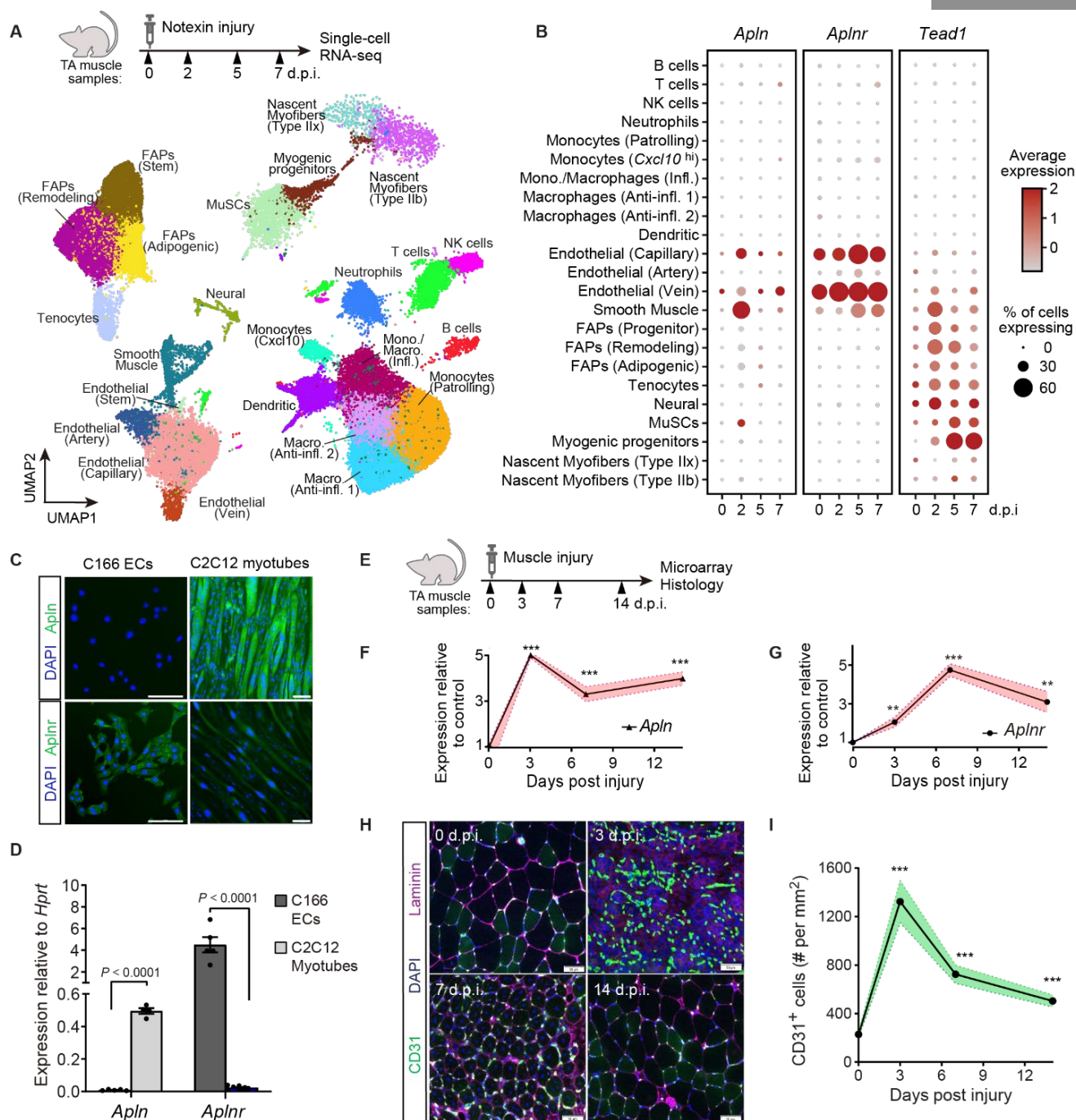


Figure 3.3. *Apln*, *Aplnr*, and *Tead1* expression dynamics in regenerating skeletal muscle. (A-B) Single-cell RNA-sequencing analysis of a notexin injury response in TA muscle adult mice. TA muscle samples from 0, 2, 5, and 7 days post-injury (d.p.i.) with $n = 2-3$ mice per time-point were analyzed from De Micheli et al (2020) (A) UMAP projection of scRNAseq data demonstrating cell-type annotations of clusters using markers shown in Figure S3. (B) Dot plots showing expression of *Apln*, *Aplnr*, and *Tead1* by cell-type cluster and time-point. Dot size shows frequency of cells expressing non-zero transcript level. Dot color shows average expression level. (C-D) *In vitro* expression of *Apln* and *Aplnr* protein by immunofluorescence (C) and mRNA by qRT-PCR (D) in C166 endothelial cells (ECs) and

C2C12 myotubes differentiated for 8d. $n = 5$ for C166 ECs; $n = 4$ for C2C12 myotubes. Scale bar, $100\ \mu\text{m}$. **(E-I)** Regeneration of TA muscles of adult WT mice after IM injection of glycerol analyzed at 0, 3, 7, and 14 d.p.i. by gene expression microarray and immunohistology. **(E)** Experimental overview. **(F-G)** *Apln* and *Apnr* mRNA levels from transcriptomic analyses, normalized and presented as fold-change relative to mean of 0 d.p.i. Data are mean \pm s.e.m. of $n = 5$ (0, 14 d.p.i.) and $n = 6$ (3, 7 d.p.i.) mice. **(H)** Representative images of CD31 and Laminin immunostaining in regenerating muscle samples at 0, 3, 7, and 14 d.p.i. Scale bar, $50\ \mu\text{m}$. **(I)** Quantification of CD31⁺ endothelial cells per cross-sectional area. Data are mean \pm s.e.m. of $n = 5$ TA muscles. In **(F-G)** and **(I)**, P values are reported by two-tailed unpaired t -test compared to 0 d.p.i.; with * $P < 0.05$, ** $P < 0.01$, *** $P < 0.001$.

3.2.4 Apelin stimulates endothelial remodeling during muscle regeneration.

To examine if ApIn directly regulates endothelial cell remodeling, we treated C166 ECs as well as the mouse EOMA hemangioendothelioma EC line with the recombinant bioactive ApIn-13 peptide for 5 days and observed increased endothelial cell expansion with both EC lines (**Figure 3.4A-B**) (Obeso et al., 1990). We next asked if ApIn signaling influences angiogenesis during muscle regeneration in vivo. Based on the prior report of reduced ApIn production during aging (Vinel et al., 2018), we examined the effect of daily ApIn-13 administration at 0.5 $\mu\text{mol/kg/day}$ in aged mice following cardiotoxin-induced muscle injury (**Figure 3.4C**). ApIn-13 treatment increased the abundance of CD31⁺ endothelial cells by IHC and elevated *Pecam1* expression by bulk muscle RT-qPCR at both 3 and 7 d.p.i. compared to vehicle-treated controls (**Figure 3.4D-F**). These data indicate that ApIn signaling induces the proliferation of endothelial cells and acts as a pro-angiogenic factor during the early stage of muscle regeneration.

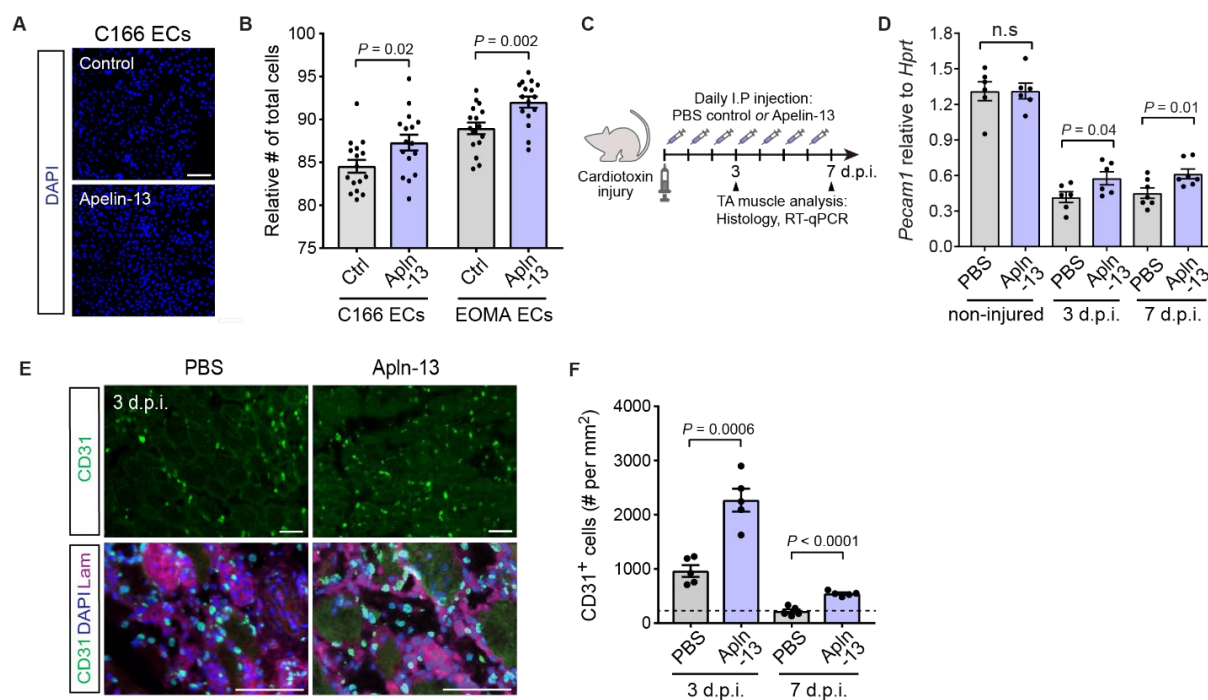


Figure 3.4. ApIn promotes endothelial cell remodeling *in vitro* and *in vivo*. (A-B) EC expansion of C166 and EOMA lines treated for 5d with the recombinant ApIn-13 peptide at 10 μ M. (A) Representative images of DAPI staining of C166 ECs. Scale bar, 100 μ m. (B) Quantification of the total number of C166 and EOMA cells treated with ApIn compared to control medium. (n = 16 cell culture replicates per group). (C-F) Daily ApIn-13 administration at 0.5 μ mol/kg/day for 7d in aged mice following cardiotoxin-induced injury in TA muscle. (D) Expression of *Pecam1* mRNA by RT-qPCR in whole TA muscles at 3 and 7 d.p.i. and non-injured TA muscles (n = 6-7 TA muscles per group). (E) Representative images of CD31 and Laminin immunostaining in CTX-injured TA muscles at 3 d.p.i. Scale bar, 50 μ m. (F) Quantification of CD31⁺ endothelial cells at 3 and 7 d.p.i. in regenerating regions (n = 5 TA muscles per group). Dashed line indicates basal level of CD31⁺ cell per mm² in non-injured TA muscles.

3.2.5 Tead1-Apelin axis regulates endothelial remodeling during muscle regeneration.

Given the prior findings, we hypothesized that the paracrine communication between myogenic cells and endothelial cells via ApIn may be modulated by myogenic Tead1. We tested this in a co-culture system with GFP-expressing C166 ECs cultured directly on pre-differentiated C2C12 myotubes, with or without Tead1 depletion by siRNA (**Figure 3.5A**). After 3d of co-culture, EC growth reflected by total GFP⁺ cell area was enhanced in co-cultures on si-*Tead1* C2C12 myotubes compared to C2C12 myotubes (**Figure 3.5B-C**). To test if this co-culture effect acts via direct or secreted factors, we assayed C166 EC expansion in the presence of transferred conditioned media from C2C12 myotube monocultures starting at 3 days of differentiation and continued daily (**Figure 3.5D**). In this system, we found that the conditioned medium from si-*Tead1* treated C2C12 myotubes enhanced C166 EC cell growth compared to the conditioned medium from control C2C12 cultures, suggesting that Tead1-regulated secreted factor(s) mediate the myogenic-endothelial cell communication effect (**Figure 3.5E**). We next tested if this cell communication occurs through ApInr. To test, we treated si-*ApInr* on GFP⁺ECs and ML221 compounds which is a known ApInr antagonist in the co-culture system (Maloney et al., 2010). In the presence of si-*ApInr* and ML221, the paracrine effect was attenuated in the co-culture with si-*Tead1* myotube, suggesting that Tead1 regulated myogenic-endothelial crosstalk is partially mediated by ApIn-ApInr signaling (**Figure 3.5F-I**).

Finally, we examined MCK-OE-Tead1 mice to test if Tead1-overexpressing myofibers, which exhibit reduced ApIn levels (**Figure 3.2E-I**), influence endothelial phenotypes *in vivo* after muscle injury (**Figure 3.5J-M**). In MCK-OE-Tead1 transgenic muscles, the basal levels of mRNA expression of the canonical endothelial genes *Pecam1*, *Icam1*, and *Tek* (also known as *Tie2*) and the CD31⁺ ECs frequency in IHC were decreased (**Figure 3.5K-M**). Notably, the endothelial infiltrated numbers in the regenerating region at 3 and 7 d.p.i were delayed in the MCK-OE-Tead1 mice. This observation demonstrates that Tead1 acts by suppressing pro-angiogenic paracrine secretion from myofibers, and establishes the Tead1-ApIn regulation in myofibers as a contributing mechanism to myogenic-endothelial cross-talk during muscle regeneration.

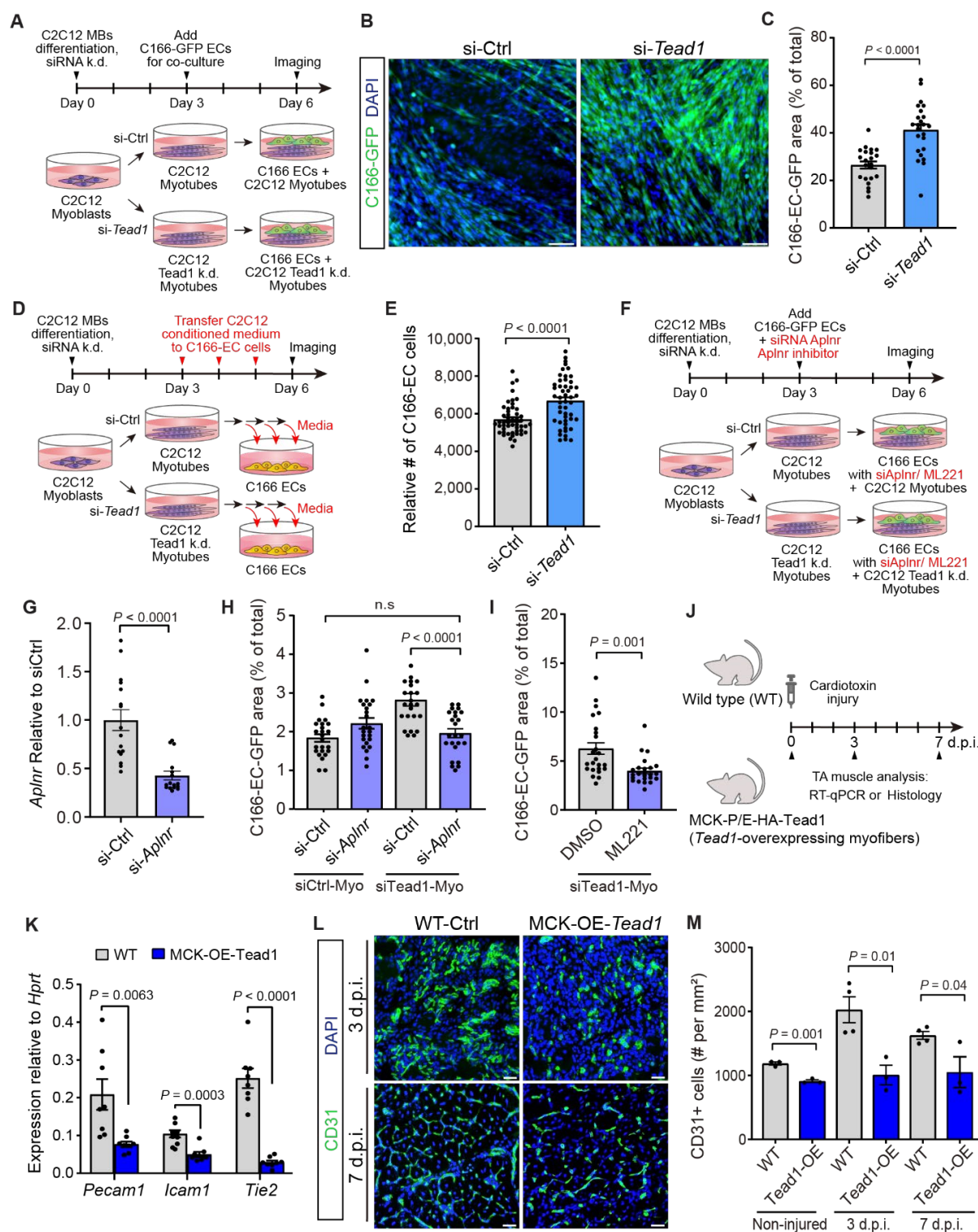
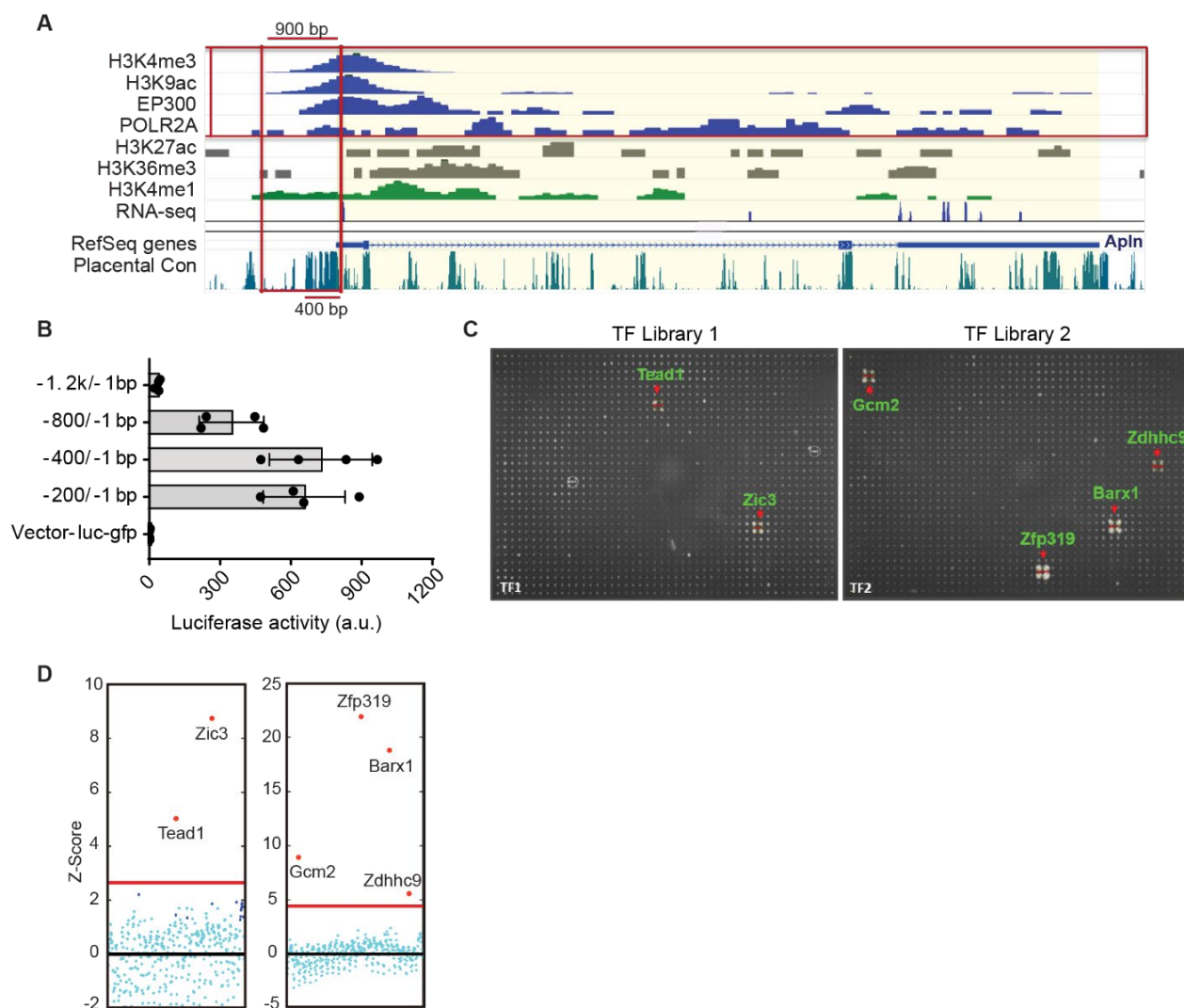


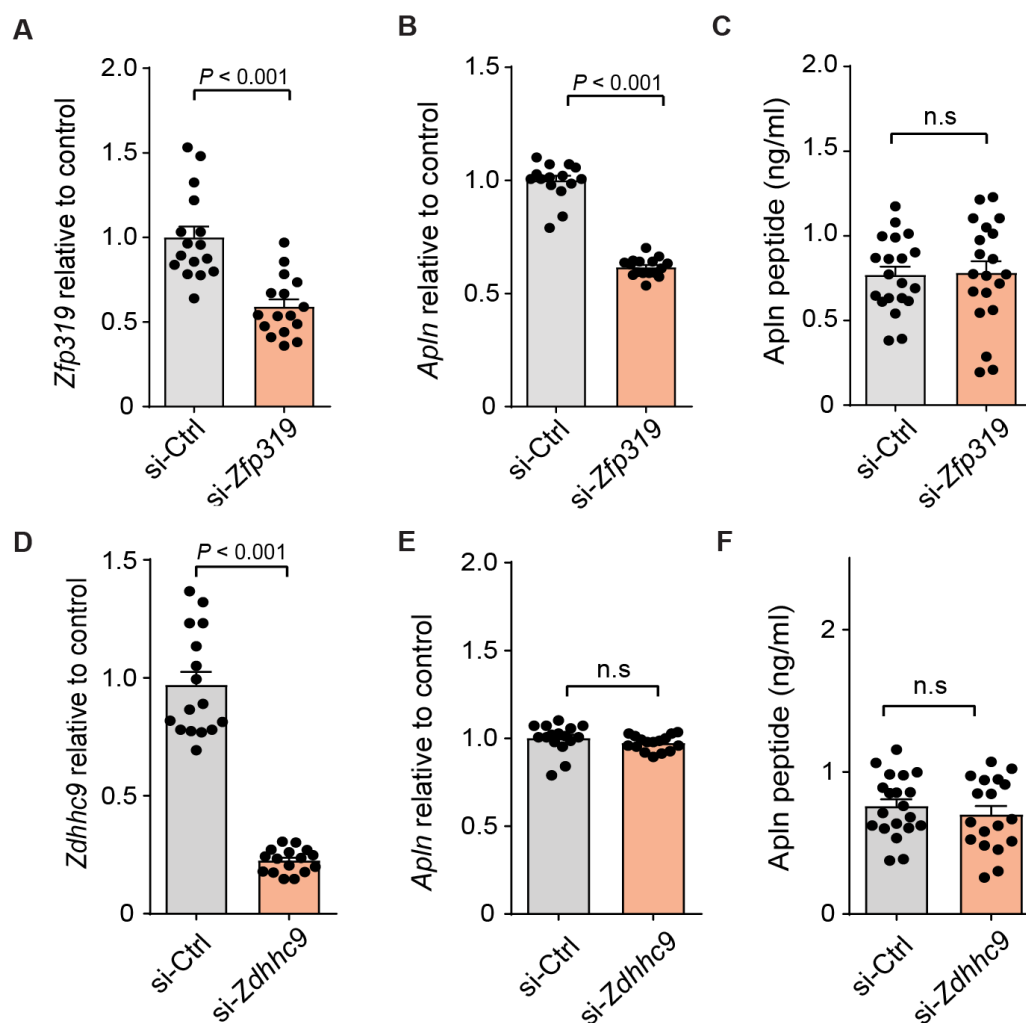
Figure 3.5. Myogenic Tead1 inhibits myogenic-endothelial cross-talk. (A-C) Co-culture of GFP expressing C166 ECs with myotubes derived from C2C12 myoblasts transfected with scrambled control or *Tead1* targeted siRNAs for 3d. **(B)** Representative images of C166-GFP EC and C2C12 co-cultures at 6d, with DAPI counter-stain. Scale bar, 100 μ m. **(C)** Quantification of the total GFP+ cell area relative to total image area. (n = 24 cell culture

replicates per group). **(D-E)** Culture of C166 ECs in presence of conditioned medium harvested from myotubes derived from C2C12 myoblasts transfected with scrambled control or *Tead1* targeted siRNAs. Conditioned media were collected from myotube cultures and applied daily to C166 EC cultures for 3 days. **(E)** Quantification of the number of C166 ECs per well in conditioned medium from control and *Tead1* siRNA treated C2C12 myotubes. (n = 49 wells cell culture replicates per group). **(F-I)** Co-culture of GFP expressing C166 ECs with myotubes derived from C2C12 myoblasts transfected with scrambled control or *Tead1* targeted siRNAs in presence of *Aplnr* siRNAs or *Aplnr* inhibitor (ML221). **(G)** *Aplnr* expression after transfection of siRNAs targeted *Aplnr* compared to si-scrambled control (n=16 per group). **(H)** Quantification of the total GFP+ cell area relative to total image area after si*Aplnr* k/d (n = 24 per group). **(I)** Quantification of the total GFP+ cell area relative to total image area after 10 μ M ML221 (*Aplnr* inhibitor) compared to DMSO control (n = 24 per group). **(J-M)** Analysis of MCK-*Tead1* overexpressing mice following cardiotoxin-induced injury in TA muscle compared to WT controls. **(K)** Expression of *Pecam1*, *Icam1*, and *Tek* (*Tie2*) mRNA by RT-qPCR in tibialis anterior muscles isolated from adult myofiber specific *Tead1*-overexpressing mice (MCK-OE-*Tead1*) compared to WT C57BL6 controls. (n = 4 mice per group). **(L)** Representative images of CD31 immunostaining in CTX-injured TA muscles at 3, 7 d.p.i. Scale bar, 50 μ m. **(M)** Quantification of CD31⁺ endothelial cells at non-injured, 3 and 7 d.p.i. in regenerating regions (n = 3-4 TA muscles per group). All graphs are reported as mean \pm s.e.m. and *P* values are reported from two-tailed, unpaired t-test between the conditions.

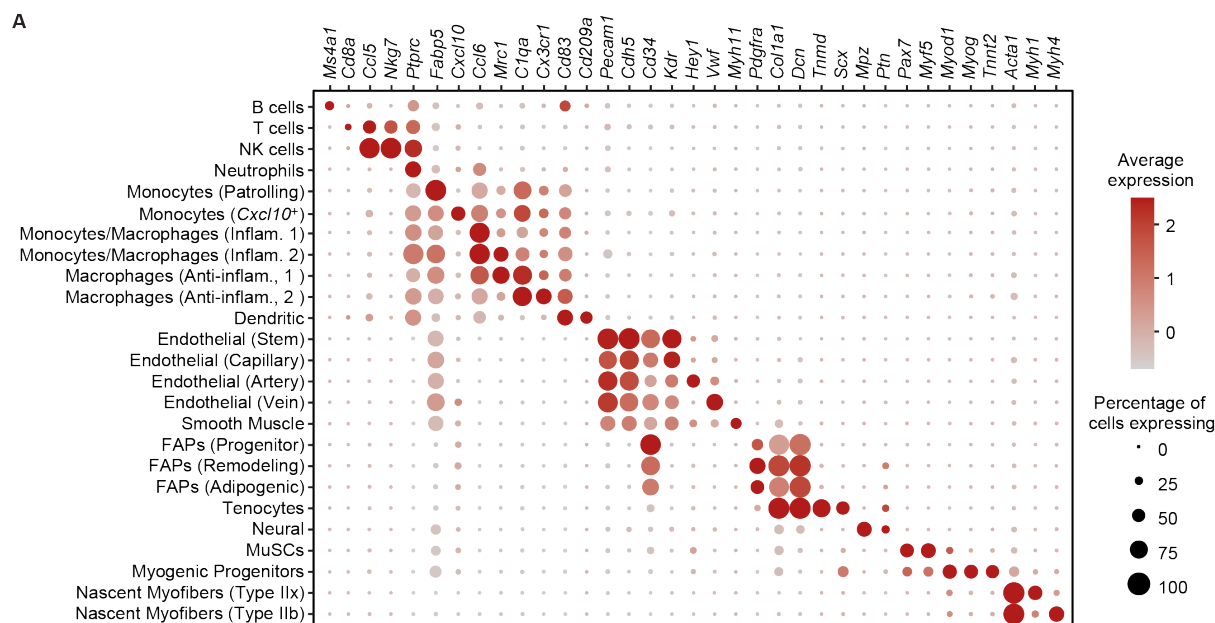
3.2.5 Supplementary Figures



Supplementary Figure 3.1. Characterization of the Apelin promoter and identification of transcription factors in Yeast 1 Hybrid screen. (A) Epigenomic annotation near the TSS of Apelin precursor gene (*ApIn*) in mouse ES-Bruce4 cells from the WashU Epigenome Browser. Tag densities (blue) of proximal promoter markers H3K4me3, H3K9ac, EP300, and POLR2A by ChIP-seq are highlighted (top). Placental Con represents the conservation score between 20 mammalian species available from WashU Epigenome Browser (Miller et al., 2007) **(B)** Nano luciferase activity of four putative *ApIn* promoter regions and no-promoter vector transfected into C2C12 cells, normalized by co-transfected firefly luciferase activity. Mean \pm s.e.m. of $n = 4$ cell culture replicates per group. **(C)** Y1H screen growth cluster results using -400/-1bp fragment of *Athe pln* promoter mated with two TF libraries. **(D)** Z-score-normalized Y1H spot intensities for all 745 TF-promoter interactions using -400/-1bp promoter fragments.

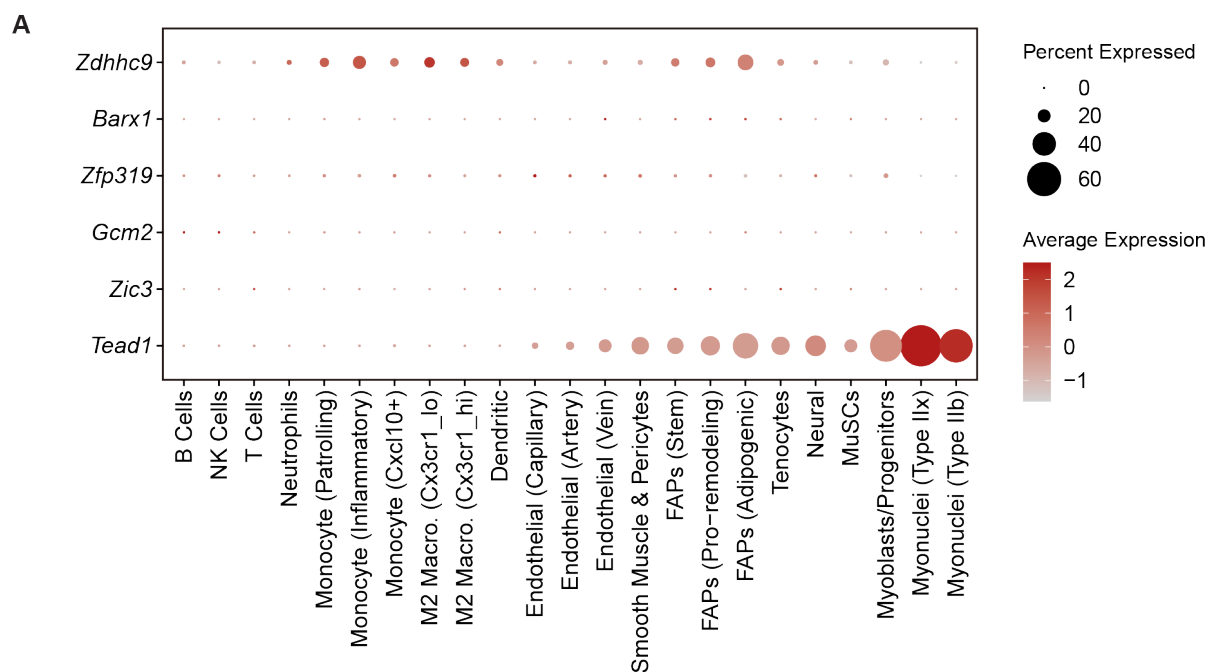


Supplementary Figure 3.2. Effects of Zfp319 and Zdhhc9 on apelin in C2C12 cells. (A-B) *Zfp319* (A) and *Apln* (B) mRNA expression measured by RT-qPCR in C2C12 myoblasts transfected with scrambled control or *Zfp319* targeted siRNA for 3 d, $n = 16$ cell culture replicates per condition. (C) *Apln* peptide concentration in culture medium measured by enzyme immunoassay (EIA) after 3 d culture from the same experiment. $n = 20$ cell culture supernatants per condition. (D-E) *Zdhhc9* (D) and *Apln* (E) mRNA expression in C2C12 myoblasts transfected with scrambled control or *Zdhhc9* targeted siRNA for 3 d, $n = 16$ cell culture replicates per condition. (F) *Apln* peptide concentration in culture medium measured by enzyme immunoassay (EIA) after 3 d culture from the same experiment. $n = 20$ from one experiment. For all panels, data are presented as mean \pm s.e.m., and P values are reported from two-tailed, unpaired t-tests between conditions.



Supplementary Figure 3.3. Expression profiles of single-cell RNA-sequencing clusters.

(A) Dot plots representing marker gene expression used to characterize cell clusters in the single-cell RNA-sequencing muscle regeneration data set from **Figure 3C-E**. Cell clustering was performed using SNN and annotations were manually determined based on these gene expression patterns. For each gene/cluster combination, the average expression level is shown in red color and the fraction of cells with non-zero expression is shown as the dot size. Some clusters shown here are not plotted in **Figure 3E** if not consistently observed at different time-points in the dataset.



Supplementary Figure 3.4. Expression profiles of six transcription factors in Y1H from single-cell and nucleus RNA-sequencing datasets. (A) Dot plots representing cell-specific TF gene expression from integrated 102 publically-available single-cell or nucleus RNA-sequencing datasets by harmony batch-correction (McKellar et al., 2020a).

3.3 Discussion and Conclusion

Serum and muscle apelin decline during aging in humans and low apelin levels associate with loss of muscle mass and strength in older people (Vinel et al., 2018). Pre-clinical studies have shown the therapeutic potential of apelin supplementation as the apelin-13 injection in aged mice could increase muscle strength and physical performance and boost regeneration after muscle injury (Vinel et al., 2018). These proof-of-concept observations bear promising therapeutic potential, but the applicability in humans is limited by the short half-life of the apelin peptide and the fact that it is not orally bioavailable. Stabilized apelin peptides and synthetic small molecule agonists of the Apln receptor constitute possible alternatives but understanding the endogenous regulatory pathways that modulate apelin production endogenously will allow developing parallel strategies to modify local production specifically in target tissues.

In this study, we used a screen of 745 mammalian transcription factors to identify novel transcriptional regulators of apelin expression. Out of 4 confirmed screening hits, we characterize Tead1 as a bona fide regulator of apelin expression in myogenic cells using functional assays in vitro and in vivo. Tead1 has been shown to regulate the expression of several skeletal muscle-specific genes (Joshi et al., 2017; Qiu et al., 2011). Myofiber-specific overexpression of *Tead1* induces a switch to a slow muscle contractile phenotype in vivo (Tsika et al., 2008), and induces hyperplasia of muscle stem cells (Southard et al., 2016). Although Tead1 generally activates transcription by recruiting coactivators like Yap-Taz (Huh et al., 2019; Stein et al., 2015), repressive actions of Tead1 have been previously reported via co-repressor recruitment and coactivator squelching (Kim et al., 2015). In this study, we demonstrated that Tead1 binds to the apelin promoter in myotubes and knock-down of *Tead1* is sufficient to boost apelin transcription and secretion, demonstrating that an endogenous repressive tone limits apelin secretion in muscle cells. Conversely, mice with myofiber-specific overexpression of Tead1 have reduced muscle and serum apelin concentrations, highlighting that the regulation of apelin by Tead1 is also at play in vivo and that skeletal muscle is a dominant contributor to systemic apelin levels.

To understand how apelin signals across the multiple cell types communicate to efficiently maintain and repair skeletal muscle, we analyzed the Tead1-Apln-AplnR regulatory network using recent single-cell RNAseq datasets of the muscle stem cell niche.

Consistent with previous reports (Latroche et al., 2017; Vinel et al., 2018), apelin was secreted by myogenic cells and myofibers and to some extent in endothelial and smooth muscle populations. Although the ApInR mRNA was not detected in myogenic cells by scRNAseq as the low expression of this GPCR cannot be captured with the sensitivity of scRNAseq, Apelin can signal in an autocrine fashion in myogenic cells as these muscle stem cells express the ApInR protein at sufficient levels to drive myogenic commitment (Latroche et al., 2017; Vinel et al., 2018). Consistent with these observations, apelin production increases *in vivo* after muscle injury, and systemic apelin injection further stimulates muscle stem cell amplification and myofiber repair after a muscle injury (Vinel et al., 2018). Our scRNAseq analysis also detected very strong enrichment of the ApInR mRNA in various endothelial cell populations during muscle regeneration, highlighting that endothelial cells are active receiving cells for Apelin signals in the niche.

The injured muscle stem cell niche is a hypoxic environment and the efficient coupling of myogenesis and angiogenesis is required to rebuild functional myofibers with adequate vascularization for oxygen and nutrient supply (Barnouin et al., 2017; Drouin et al., 2019; Duscha et al., 1999; Latroche et al., 2015; Luque et al., 1995). In particular, muscle stem cells and their myogenic progeny attract endothelial cells and orchestrate re-vascularization during tissue repair (Christov et al., 2007a; Latroche et al., 2015, 2017). Apelin has been previously reported to regulate angiogenesis and vascular formation during development and adult physio-pathology in tissues like the heart or the retina (Kidoya and Takakura, 2012; Wu et al., 2017), and was identified as a mediator of the cross-talk between myogenic and endothelial cells in skeletal muscle using the loss of function approaches (Latroche et al., 2017).

Our experiments with the recombinant apelin peptide further link apelin signaling to endothelial remodeling in muscle, and open translational opportunities by proving that apelin-mediated activation of angiogenesis can be further enhanced beyond its endogenous tone through therapeutic activation of apelin signaling *in vivo*. Importantly, our co-culture, conditioned medium and myofiber specific overexpression experiments also establish directionality in the apelin-mediated myogenic-angiogenic crosstalk by proving that Tead1 regulation of apelin in myogenic cells directly modulates endothelial cells. Considering that capillarization in skeletal muscle positively correlates with myofiber size and function (Barnouin et al., 2017; Takahashi et al., 2002), our results support a model where the regulation of endothelial cell remodeling and angiogenesis by apelin contributes to the

reported benefits of apelin treatment on muscle mass and muscle strength (Vinel et al., 2018).

Collectively, our experiments establish a novel regulatory pathway controlling apelin secretion where Tead1 transcriptionally controls *Apln* expression in myofibers to regulate endothelial remodeling via paracrine communication. This regulation highlights that the beneficial effects of *Apln* during muscle regeneration are mediated by inter-cellular paracrine communication across the niche and further strengthen the importance of myogenesis-angiogenesis coupling during muscle repair.

Section 3 Methods

Cell growth and differentiation

C2C12 cells were harvested in a growth medium formulated with 20% of heat-inactivated Fetal Bovine Serum (FBS) and 1% penicillin and streptomycin (Pen/Strep) in DMEM with or without glutamax supplemented (Blau et al., 1985; Yaffe and Saxel, 1977). For the myotube differentiation, 5% horse serum was added to DMEM with 1%Pen/Strep, and media was changed daily. For the endothelial cell growth assay, we used C166 (ATCC) and EOMA (ATCC) endothelial cells from ATCC and cultured them in DMEM supplemented with 20% FBS and 1% Pen/Strep (Obeso et al., 1990; Wang et al., 1996).

Dual reporter assay

C2C12 cells were co-transfected with the apelin promoter plasmid fused with the nano-luciferase encoding gene and a plasmid with the constitutively active cytomegalovirus (CMV) promoter conjugated with firefly luciferase. Stop&Glo reagents were purchased from Promega. Three days after transfection, cells were washed with PBS and lysed. After 15 minutes of incubation, 65µl of the lysate (supernatant) were mixed with ONE GLO EX firefly luciferase detection reagent and measured luminescence with the integration time of one minute. Subsequently, 65µl of NanoDLR STOP&GLO was added and luminescence was measured after being mixed on an orbital shaker. The activity of NanoLuc was normalized based on the constitutively active firefly luciferase activity.

Yeast one-hybrid screen

A large-scale library of TF Open Reading Frame (ORF) clones (768 mouse TFs) was created as described previously (Gubelmann et al., 2013). For bait construction, four different sizes of the *Ap1n* promoter region were selected as described in the promoter characterization section. Those promoter fragments were inserted into a yeast-compatible pMW2 vector containing the *HIS3* gene with the Gibson assembly kit (NEB) after which bait-*HIS3* reporter yeast lines were generated, as described previously (Gubelmann et al., 2013). Yeast lines that showed minimal background reporter expression were then selected for mating with the compatible mouse TF ORF yeast library whereby each interaction is tested in quadruplicate, also as described (Gubelmann et al., 2013). After one week of incubation, positive TF-DNA interactions were then identified in a semi-automated fashion based on growth on a selective yeast plate containing 3-amino-1,2,4-triazole (3AT) using “transcription factor-DNA interaction detection in yeast (TIDY)” software (Hens et al., 2011a). In short, TIDY calculates the intensity values of each quadrant (i.e. four replicates of the same, tested

protein-DNA interaction) and groups these into 10 clusters. Among these clusters, the highest intensity value of the largest cluster, which most likely represents the bulk of negative interactions, was used as the background threshold. Then, the TF yeast quadrants whose intensity values are above at least 20% of the background value are selected as positive hits.

Knock-down experiments

C2C12 myoblasts were harvested without pen/strep 24 hours before transfection and the cells were split and distributed at 1000 per well in 96-well plate. When the cells were in the suspension, the complex of transfection reagent RNAiMax (ThermoFisher) with the siRNAs was directly added to the cells. The siRNAs were synthesized by Dharmacon (cat# L-048419-01-0005 for si-Tead1, L-058018-01-0005 for Zdhhc9, L-059731-01-0005 for Zfp319), and we used scrambled siRNAs for the negative control (cat#D-001810-10-50). After 3 days of incubation, mRNA or protein were extracted and the following experiments were performed.

Chromatin Immunoprecipitation (ChIP) qPCR Assay

Cells were treated with siRNAs as described in Knock-down experiments and harvested until 100% confluency. Cells were fixed with 1% formaldehyde, and nuclei were prepared with Covaris truChIP Chromatin Shearing Kit (Cat# SKU:500465) by following the manual for “high cell” from the producer. The extracted chromatin was sonicated for 90 seconds using Covaris E220 (5% duty cycle and intensity 4). Immunoprecipitation was performed using Magna ChIP A/G kit from Millipore Sigma (Cat# 17-10085) and 10 μ g of chromatin was incubated with 1 μ g of anti-Tead1 (Cat# 610922 BD Biosciences) or IgG (Cat# Magna 0014) which were pre-incubated with 20 μ l of magnetic beads overnight at 4°C. Followed by low salt, high salt, Lici, and TE washing steps with immunoprecipitation using a magnetic rack as described in the manual of Magna ChIP kit, DNA was eluted, reverse-crosslinked at 65°C overnight, and purified using Minielute PCR column purification from Qiagen (Cat#28004). For quantitative PCR, Maxima Sybr Green/ROX qPCR master mix (K0221 Thermo scientific) was used and performed on ViiA 7 Real-Time PCR system (Life Technologies). *Ankrd1*, *Ctgf*, *Apln*, *Neg* primers were used for quantitative PCR detection as followed.

Gene	Forward Primer	Reverse Primer	Genomic Coordinates
<i>Ankrd1</i>	GAGGGGAGGACAAGCTAACC	CGATGTGATCACCACCAAAG	chr10:92681001–92681083

<i>Ctgf</i>	GCCAATGAGCTGAATGGAGT	CAATCCGGTGTGAGTTGATG	Chr6:132272566-132272653
<i>ApIn</i>	CTCTCCCTCTTCCTGCCTC	TTTTGTAGCTTGTGGTTTGGC	chr X:48034975 - 48034875
<i>Neg-control</i>	ACCAACACTCTTCCCTCAGC	TTATTTTGGTTCAGGTGGTTGA	Chr10:60902566-60902665

Real-Time quantitative PCR

Total RNA was extracted with the miRNeasy mini kit (Qiagen) or Fastlane cell multiplex kit (Qiagen). TaqMan probes and the FastLane Cell Multiplex NR Kit (Qiagen) were used to measure RNA levels. Following real-time quantitative PCR, the expression level of target gene mRNA was analyzed with a ddCT algorithm and normalized to a reference gene, *Hprt*. The TaqMan probes used are listed in the resources table.

Protein extraction

After TA muscle is harvested, samples were weighed and calculated the lysis buffer as 10 μ l per mg of tissue. The lysis buffer was formulated with 50mM Tris-HCl (pH 7.5), 1mM EDTA, 1mM EGFA, 0.27 M Sucrose, 1% Triton X-100, 20mM Glycerol-2-phosphate disodium, 50mM NaF, and 5mM Na₄P₂O₇ with a proteinase inhibitor cocktail (Roche, #11697498001). The samples were homogenized by polytron and incubated on ice with the lysis buffer for 30 mins. The protein was obtained by transferring the supernatant after spinning down the samples with a centrifuge at 3500g with 4°C for 5 mins and the concentration of protein was further determined by bicinchoninic acid assay (Peirce #23225)

Elisa detection of the apelin peptide

Following protein extraction, the apelin peptide was measured with the EIA kit (Phoenix pharmaceuticals cat# EK-057-23). 5mg of protein from samples in 50 μ l of lysis buffer were distributed on the immuno-plates, which were pre-coated with secondary antibody and 25 μ l of the biotinylated peptide. After 2 hours of incubation, the biotinylated peptide was catalyzed by streptavidin-horseradish peroxidase solution for one hour. TMB substrate solution was added for one hour at room temperature. Then, the reaction was terminated with 2N HCl. The concentration of apelin peptide was detected by absorbance at 450nm and then quantified based on a standard curve.

Quantification of myocyte and fusion index

C2C12 myoblasts or FACs-isolated satellite cells were cultured in a growth medium until 80% confluent or 1000 cells per well, respectively. Media was then changed to the differentiation

medium. After 5 days of incubation, the cells were fixed (4% paraformaldehyde for 15 minutes) and permeabilized (0.5% PBTX for 15 minutes). After blocking with 1% horse serum, the primary antibody for anti-mouse myosin heavy chain (Millipore, 1/200) was incubated for one hour at room temperature. Then, the secondary antibody with Hoechst (goat anti-mouse A488 1:1000, Hoechst 33342 1:5000) was incubated for one hour. Images were acquired by metaXpress (Molecular Devices) and quantified by the automated cell counting software in the metaXpress platform. The margin of the plates was removed in the software. Then, the fusion index was calculated as the number of MyHC expressing cells divided by the total number of nuclei (DAPI).

Gene expression analysis with single-cell RNA sequencing data

Previously reported single-cell RNA sequencing data was prepared as described in McKellar et al, *bioRxiv*, 2020 (McKellar et al., 2020a). Briefly, raw reads were aligned to the mm10 reference genome using Cellranger version 3.1.0. Count matrices generated by Cellranger were analyzed using Seurat, version 3.1.5 (Butler et al., 2018). Cells with fewer than 1000 transcripts detected or greater than 30% of transcripts mapping to mitochondrial genes were removed from the analysis. The batch correction was performed using harmony, version 1.0 (Korsunsky et al., 2019a). After batch correction, clustering was performed via Seurat (FindClusters) using default parameters. Each cluster was labeled based on canonical gene expression. To minimize batch effects in gene expression values, but retain the clustering resolution enabled through the large-scale resource, only samples from Gene Expression Omnibus accession numbers GSE143435, GSE143437, and GSE159500 were subset out and used for this analysis. After quality filtering and subsetting, 67,985 cells were used.

Histology of endothelial cell infiltration in muscle tissue

Mouse muscle samples were dissected, embedded in OCT, and frozen in liquid nitrogen-cooled isopentane. Samples were then sectioned at 10 μ m on a cryostat and fixed with 4% paraformaldehyde for 15min at room temperature. After permeabilization with cold 100% methanol for 6 minutes, blocking was performed with 4% BSA for 3 hours. Following blocking, primary antibodies, rat anti-mouse CD31 (BD Biosciences), chicken anti-mouse laminin (LS Bio) were incubated at 4°C overnight at 1:500. Secondary antibodies with Hoechst (goat anti-rat A488 1/2000, goat anti-chicken-A647 1/200, Hoechst 1/5000) were incubated for one hour at room temperature. Subsequently, the stained sections were mounted and imaged using a 10X objective on an Olympus VS120 fluorescence slide scanner and quantified in three randomly selected injured areas of each sample using the

VS-ASV 2.8 software. The total number of endothelial cells was quantified as the total number of CD31+/DAPI+ nuclei per area analyzed.

Statistical Analysis

Statistical significance (P-value) for quantitative PCR, luciferase activity, cell quantification data were assessed using Student's t-test, two-way ANOVA in the software GraphPad Prism 7 to 9.

KEY RESOURCES TABLE

REAGENT or RESOURCE	SOURCE	IDENTIFIER
Antibodies		
Anti-Myosin Heavy Chain antibody, clone A4.1025	Millipore	Cat#05-716 RRID:AB_309930
Anti-Tead1 (TEF-1 Pure)	BD Biosciences	Cat# 610922 RRID:AB_398237
Anti-IgG	Millipore	Cat# Magna 0014
Anti-APJ receptor antibody	Abcam	Cat# ab214369
Anti-Apelin antibody	Abcam	Cat# ab125213 RRID:AB_10999708
Anti-Laminin antibody	LS Bio	Cat# LS-C96142 RRID:AB_2033342
Anti-CD31 (Pecam1) antibody	BD Biosciences	Cat# 557355 RRID:AB_396660
Critical Commercial Assays		
One-Glo Firefly Luciferase Detection Kit	Promega	Cat# E8120
Nano-Glo Dual-Luciferase Detection Kit	Promega	Cat# N1620
Glo-lysis Buffer	Promega	Cat# E2661
Lipofectamine RNAiMax	Thermofisher	Cat# S-006-100
Apelin EIA kit	Phoenix pharmaceuticals	Cat# EK-057-23
Gibson assembly kit	NEB	Cat# E5510
FastLane cell multiplex NR kit	Qiagen	Cat# 216713
miRNeasy Mini Kit	Qiagen	Cat# 217004
Covaris truChIP chromatin shearing kit	Covaris	Cat# SKU:500465
Magna ChIP A/G kit	Millipore/Sigma	Cat#17-10085
Minielute DNA purification kit	Qiagen	Cat# 28004
Maxima Sybr Green/ROX master mix	Thermo Scientific	Cat# K0221
Chemicals, Peptides, and Recombinant Proteins		
Recombinant Phy Apelin-13	Bachem	Cat# U-01260
Deposited Data		
GeneAtlas UI33A (gcrma) for human samples	bioGPS	N/A
GeneAtlas MOE430 (gcrma) for mouse tissues	bioGPS	N/A
GSE 81096	GEO	(Lukjanenko et al., 2013)
GSE 143435, GSE 143437, GSE 159500	GEO	(McKellar et al., 2020a)
Experimental Models: Cell Lines		

C2C12 myoblast cell line	ATCC	Cat# CRL1772 RRID:CVCL_0188
C166 endothelial cell line	ATCC	Cat# CRL2581 RRID:CVCL_6581
EOMA endothelial cell line	ATCC	Cat# CRL2586 RRID:CVCL_3507
C166GFP endothelial cell line	ATCC	Cat# CRL2583 RRID:CVCL_6582
Experimental Models: Organisms/Strains		
C57BL/6	Jackson	Cat# 000664 RRID:IMSR_JAX:000664
Oligonucleotides		
si-RNA scramble pool	Dharmacon	Cat# D-001810-10-50
si-Tead1 pool	Dharmacon	Cat# L-048419-01-0005
si-Zdhhc9 pool	Dharmacon	Cat# L-058018-01-0005
si-Zfp319 pool	Dharmacon	Cat# L-059731-01-0005
Apln taqman probe	Life Technologies	Mm00443562_m1
Hprt taqman probe	Life Technologies	Mm00446968_m1
Tead1 taqman probe	Life Technologies	Mm00493507_m1
Barx1 taqman probe	Life Technologies	Mm01353100_m1
Zic3 taqman probe	Life Technologies	Mm00494362_m1
Zdhhc9 taqman probe	Life Technologies	Mm00552609_m1
Gcm2 taqman probe	Life Technologies	Mm00492312_m1
Pecam1 taqman probe	Life Technologies	Mm01242576_m1
Icam 1 taqman probe	Life Technologies	Mm00516023_m1
Tek (Tie2) taqman probe	Life Technologies	Mm00443243_m1
Recombinant DNA		
N/A		
Software and Algorithms		
SnapGene	Snapgene	N/A
metaXpress	Molecular Devices	N/A
VS-ASW FL software	Nikon	N/A
MetaXpress software	Molecular Devices	N/A
NIS-Elements	Nikon	N/A
GraphPad Prism Software version 7-9	GraphPad	N/A
ApE	ApE	N/A
Transcription factor-DNA interaction detection in yeast (TIDY)	(Hens et al., 2011b)	https://updeplasrv1.epfl.ch/software/
Other		
Seurat, version 3.1.5	(Butler et al., 2018)	
Harmony, version 1.0	(Korsunsky et al., 2019a)	

Lead contact & material availability

Further information and requests for resources and reagents should be directed to and will be fulfilled where possible by the lead contact, Jerome Feige (jerome.feige@rd.nestle.com). All unique/stable reagents generated in this study are available from the lead contact without restriction.

ACKNOWLEDGEMENTS

This study was funded by Nestlé, EPFL Institutional Support, SNSF grant 310030_182655, SNSF Doc. Mobility grant_P1ELP3_187970, and the National Institutes of Health award R01AG058630. We also thank Joris Michaud, Eugenia Migliavacca, Cedric Gobet, Mathieu Membrez, Omid Mashinchian, Gabrielle Dammone, Tanja Sonntag, Caterina Collodet, Guillaume Jacot for technical supports and helpful discussions.

AUTHOR CONTRIBUTIONS

U.L. designed and performed experiments and analyzed results. B.D., B.D.C, and J.N.F. designed and supervised the study. P.S., S.K., J.R., M.D., C.L. performed experiments and generated critical experimental tools. D.W.M. performed single-cell RNAseq data analysis. U.L., P.S., B.D.C, and J.N.F. wrote the manuscript.

COMPETING INTERESTS

U.L., P.S., S.K., M.D. and J.N.F. are or were employees of the Société des Produits Nestlé S.A.

Section 3 References

Ancel, S., Stuelsatz, P., and Feige, J.N. (2021). Muscle Stem Cell Quiescence: Controlling Stemness by Staying Asleep. *Trends Cell Biol.*

Attane, C., Foussal, C., Le Gonidec, S., Benani, A., Daviaud, D., Wanecq, E., Guzman-Ruiz, R., Dray, C., Bezaire, V., Rancoule, C., et al. (2012). Apelin Treatment Increases Complete Fatty Acid Oxidation, Mitochondrial Oxidative Capacity, and Biogenesis in Muscle of Insulin-Resistant Mice. *Diabetes* 61, 310–320.

Barnouin, Y., McPhee, J.S., Butler-Browne, G., Bosutti, A., De Vito, G., Jones, D.A., Narici, M., Behin, A., Hogrel, J.-Y., and Degens, H. (2017). Coupling between skeletal muscle fiber size and capillarization is maintained during healthy aging. *J. Cachexia Sarcopenia Muscle* 8, 647–659.

Bentzinger, C.F., Wang, Y.X., Dumont, N.A., and Rudnicki, M.A. (2013). Cellular dynamics in the muscle satellite cell niche. *EMBO Rep.* 14, 1062–1072.

Besse-Patin, A., Montastier, E., Vinel, C., Castan-Laurell, I., Louche, K., Dray, C., Daviaud, D., Mir, L., Marques, M.-A., Thalamas, C., et al. (2014). Effect of endurance training on skeletal muscle myokine expression in obese men: identification of apelin as a novel myokine. *Int. J. Obes.* 38, 707–713.

Blau, H.M., Pavlath, G.K., Hardeman, E.C., Chiu, C.-P., Silberstein, L., Webster, S.G., Miller, S.C., and Webster, C. (1985). Plasticity of the Differentiated State. *Science* 230, 758–766.

Bloor, C.M. (2005). Angiogenesis during exercise and training. *Angiogenesis* 8, 263–271.

Butler, A., Hoffman, P., Smibert, P., Papalexi, E., and Satija, R. (2018). Integrating single-cell transcriptomic data across different conditions, technologies, and species. *Nat. Biotechnol.* 36, 411–420.

Castan-laurell, I., Dray, C., Knauf, C., Kunduzova, O., and Valet, P. (2012). Apelin, a promising target for type 2 diabetes treatment? *Trends Endocrinol. Metab.* 23, 234–241.

Chapman, N.A., Dupré, D.J., and Rainey, J.K. (2014). The apelin receptor: Physiology, pathology, cell signalling, and ligand modulation of a peptide-activated class A GPCR. *Biochem. Cell Biol. Biochim. Biol. Cell.* 92, 431–440.

Chazaud, B. (2020). Inflammation and Skeletal Muscle Regeneration: Leave It to the Macrophages! *Trends Immunol.* 41, 481–492.

Christov, C., Chrétien, F., Abou-Khalil, R., Bassez, G., Vallet, G., Authier, F.-J., Bassaglia, Y., Shinin, V., Tajbakhsh, S., Chazaud, B., et al. (2007). Muscle Satellite Cells and Endothelial Cells: Close Neighbors and Privileged Partners. *Mol. Biol. Cell* 18, 1397–1409.

De Micheli, A.J., Laurilliard, E.J., Heinke, C.L., Ravichandran, H., Fraczek, P., Soueid-Baumgarten, S., De Vlaminck, I., Elemento, O., and Cosgrove, B.D. (2020). Single-Cell Analysis of the Muscle Stem Cell Hierarchy Identifies Heterotypic Communication Signals Involved in Skeletal Muscle Regeneration. *Cell Rep.* 30, 3583-3595.e5.

- Drouin, G., Couture, V., Lauzon, M.-A., Balg, F., Faucheux, N., and Grenier, G. (2019). Muscle injury-induced hypoxia alters the proliferation and differentiation potentials of muscle resident stromal cells. *Skelet. Muscle* 9, 18.
- Duscha, B.D., Kraus, W.E., Keteyian, S.J., Sullivan, M.J., Green, H.J., Schachat, F.H., Phippen, A.M., Brawner, C.A., Blank, J.M., and Annex, B.H. (1999). Capillary density of skeletal muscle. *J. Am. Coll. Cardiol.* 33, 1956–1963.
- Egerman, M.A., and Glass, D.J. (2014). Signaling pathways controlling skeletal muscle mass. *Crit. Rev. Biochem. Mol. Biol.* 49, 59–68.
- Fuchs, E., and Blau, H.M. (2020). Tissue Stem Cells: Architects of Their Niches. *Cell Stem Cell* 27, 532–556.
- Gates, L.A., Shi, J., Rohira, A.D., Feng, Q., Zhu, B., Bedford, M.T., Sagum, C.A., Jung, S.Y., Qin, J., Tsai, M.-J., et al. (2017). Acetylation on histone H3 lysine 9 mediates a switch from transcription initiation to elongation. *J. Biol. Chem.* 292, 14456–14472.
- Gorski, T., and De Bock, K. (2019). Metabolic regulation of exercise-induced angiogenesis. *Vasc. Biol.* 1, H1–H8.
- Gubelmann, C., Waszak, S.M., Isakova, A., Holcombe, W., Hens, K., Iagovitina, A., Feuz, J., Raghav, S.K., Simicevic, J., and Deplancke, B. (2013). A yeast one-hybrid and microfluidics-based pipeline to map mammalian gene regulatory networks. *Mol. Syst. Biol.* 9, 682.
- Han, S., Wang, G., Qi, X., Lee, H.M., Englander, E.W., and Greeley, G.H. (2008). A possible role for hypoxia-induced apelin expression in enteric cell proliferation. *Am. J. Physiol.-Regul. Integr. Comp. Physiol.* 294, R1832–R1839.
- Hens, K., Feuz, J.-D., Isakova, A., Iagovitina, A., Massouras, A., Bryois, J., Callaerts, P., Celniker, S.E., and Deplancke, B. (2011). Automated protein-DNA interaction screening of *Drosophila* regulatory elements. *Nat. Methods* 8, 1065–1070.
- Huh, H.D., Kim, D.H., Jeong, H.-S., and Park, H.W. (2019). Regulation of TEAD Transcription Factors in Cancer Biology. *Cells* 8.
- Japp, A.G., and Newby, D.E. (2008). The apelin–APJ system in heart failure: Pathophysiological relevance and therapeutic potential. *Biochem. Pharmacol.* 75, 1882–1892.
- Joshi, S., Davidson, G., Le Gras, S., Watanabe, S., Braun, T., Mengus, G., and Davidson, I. (2017). TEAD transcription factors are required for normal primary myoblast differentiation in vitro and muscle regeneration in vivo. *PLOS Genet.* 13, e1006600.
- Kadoglou, N.P.E., Vrabas, I.S., Kapelouzou, A., Lampropoulos, S., Sailer, N., Kostakis, A., Liapis, C.D., and Angelopoulou, N. (2012). The impact of aerobic exercise training on novel adipokines, apelin and ghrelin, in patients with type 2 diabetes. *Med. Sci. Monit. Int. Med. J. Exp. Clin. Res.* 18, CR290–CR295.
- Kidoya, H., and Takakura, N. (2012). Biology of the apelin-APJ axis in vascular formation. *J. Biochem. (Tokyo)* 152, 125–131.

Kim, M., Kim, T., Johnson, R.L., and Lim, D.-S. (2015). Transcriptional Co-repressor Function of the Hippo Pathway Transducers YAP and TAZ. *Cell Rep.* 11, 270–282.

Korsunsky, I., Millard, N., Fan, J., Slowikowski, K., Zhang, F., Wei, K., Baglaenko, Y., Brenner, M., Loh, P., and Raychaudhuri, S. (2019). Fast, sensitive and accurate integration of single-cell data with Harmony. *Nat. Methods* 16, 1289–1296.

Latroche, C., Gitiaux, C., Chrétien, F., Desguerre, I., Mounier, R., and Chazaud, B. (2015). Skeletal Muscle Microvasculature: A Highly Dynamic Lifeline. *Physiology* 30, 417–427.

Latroche, C., Weiss-Gayet, M., Muller, L., Gitiaux, C., Leblanc, P., Liot, S., Ben-Larbi, S., Abou-Khalil, R., Verger, N., Bardot, P., et al. (2017). Coupling between Myogenesis and Angiogenesis during Skeletal Muscle Regeneration Is Stimulated by Restorative Macrophages. *Stem Cell Rep.* 9, 2018–2033.

Lazure, F., Blackburn, D.M., Corchado, A.H., Sahinyan, K., Karam, N., Sharanek, A., Nguyen, D., Lepper, C., Najafabadi, H.S., Perkins, T.J., et al. (2020). Myf6/MRF4 is a myogenic niche regulator required for the maintenance of the muscle stem cell pool. *EMBO Rep.* 21, e49499.

Liang, G., Lin, J.C.Y., Wei, V., Yoo, C., Cheng, J.C., Nguyen, C.T., Weisenberger, D.J., Egger, G., Takai, D., Gonzales, F.A., et al. (2004). Distinct localization of histone H3 acetylation and H3-K4 methylation to the transcription start sites in the human genome. *Proc. Natl. Acad. Sci. U. S. A.* 101, 7357–7362.

Luque, E., Peña, J., Martin, P., Jimena, I., and Vaamonde, R. (1995). Capillary Supply During Development of Individual Regenerating Muscle Fibers. *Anat. Histol. Embryol.* 24, 87–89.

Mashinchian, O., Pisconti, A., Le Moal, E., and Bentzinger, C.F. (2018). Chapter Two - The Muscle Stem Cell Niche in Health and Disease. In *Current Topics in Developmental Biology*, D. Sassoon, ed. (Academic Press), pp. 23–65.

McKellar, D.W., Walter, L.D., Song, L.T., Mantri, M., Wang, M.F.Z., Vlaminc, I.D., and Cosgrove, B.D. (2020). Strength in numbers: Large-scale integration of single-cell transcriptomic data reveals rare, transient muscle progenitor cell states in muscle regeneration. *BioRxiv* 2020.12.01.407460.

Miller, W., Rosenbloom, K., Hardison, R.C., Hou, M., Taylor, J., Raney, B., Burhans, R., King, D.C., Baertsch, R., Blankenberg, D., et al. (2007). 28-Way vertebrate alignment and conservation track in the UCSC Genome Browser. *Genome Res.* 17, 1797–1808.

Nyimanu, D., Kay, R.G., Sulentic, P., Kuc, R.E., Ambery, P., Jermutus, L., Reimann, F., Gribble, F.M., Cheriyan, J., Maguire, J.J., et al. (2019). Development and validation of an LC-MS/MS method for detection and quantification of in vivo derived metabolites of [Pyr 1]apelin-13 in humans. *Sci. Rep.* 9, 19934.

Obeso, J., Weber, J., and Auerbach, R. (1990). A hemangioendothelioma-derived cell line: its use as a model for the study of endothelial cell biology. *Lab. Investig. J. Tech. Methods Pathol.* 63, 259–269.

Qiu, H., Wang, F., Liu, C., Xu, X., and Liu, B. (2011). TEAD1-dependent expression of the FoxO3a gene in mouse skeletal muscle. *BMC Mol. Biol.* 12, 1.

Rai, R., Ghosh, A.K., Eren, M., Mackie, A.R., Levine, D.C., Kim, S.-Y., Cedernaes, J., Ramirez, V., Procissi, D., Smith, L.H., et al. (2017). Downregulation of the Apelinergic Axis Accelerates Aging, whereas Its Systemic Restoration Improves the Mammalian Healthspan. *Cell Rep.* 21, 1471–1480.

Sartori, R., Romanello, V., and Sandri, M. (2021). Mechanisms of muscle atrophy and hypertrophy: implications in health and disease. *Nat. Commun.* 12, 330.

Southard, S., Kim, J.-R., Low, S., Tsika, R.W., and Lepper, C. (2016). Myofiber-specific TEAD1 overexpression drives satellite cell hyperplasia and counters pathological effects of dystrophin deficiency. *ELife* 5, e15461.

Stein, C., Bardet, A.F., Roma, G., Bergling, S., Clay, I., Ruchti, A., Agarinis, C., Schmelzle, T., Bouwmeester, T., Schübeler, D., et al. (2015). YAP1 Exerts Its Transcriptional Control via TEAD-Mediated Activation of Enhancers. *PLoS Genet.* 11.

Su, A.I., Wiltshire, T., Batalov, S., Lapp, H., Ching, K.A., Block, D., Zhang, J., Soden, R., Hayakawa, M., Kreiman, G., et al. (2004). A gene atlas of the mouse and human protein-encoding transcriptomes. *Proc. Natl. Acad. Sci. U. S. A.* 101, 6062–6067.

Szokodi, I., Tavi, P., Földes, G., Voutilainen-Myllylä, S., Ilves, M., Tokola, H., Pikkarainen, S., Piihola, J., Rysä, J., Tóth, M., et al. (2002). Apelin, the novel endogenous ligand of the orphan receptor APJ, regulates cardiac contractility. *Circ. Res.* 91, 434–440.

Takahashi, A., Kureishi, Y., Yang, J., Luo, Z., Guo, K., Mukhopadhyay, D., Ivashchenko, Y., Branellec, D., and Walsh, K. (2002). Myogenic Akt Signaling Regulates Blood Vessel Recruitment during Myofiber Growth. *Mol. Cell. Biol.* 22, 4803–4814.

Tatemoto, K., Hosoya, M., Habata, Y., Fujii, R., Kakegawa, T., Zou, M.X., Kawamata, Y., Fukusumi, S., Hinuma, S., Kitada, C., et al. (1998). Isolation and characterization of a novel endogenous peptide ligand for the human APJ receptor. *Biochem. Biophys. Res. Commun.* 251, 471–476.

Verma, M., Asakura, Y., Murakonda, B.S.R., Pengo, T., Latroche, C., Chazaud, B., McLoon, L.K., and Asakura, A. (2018). Muscle Satellite Cell Cross-Talk with a Vascular Niche Maintains Quiescence via VEGF and Notch Signaling. *Cell Stem Cell* 23, 530-543.e9.

Vinel, C., Lukjanenko, L., Batut, A., Deleruyelle, S., Pradère, J.-P., Le Gonidec, S., Dortignac, A., Geoffre, N., Pereira, O., Karaz, S., et al. (2018). The exerkin apelin reverses age-associated sarcopenia. *Nat. Med.* 24, 1360–1371.

Vinel, C., Schanstra, J.P., Boizard, F., Péreira, O., Auriou, J., Dortignac, A., Breuil, B., Feuillet, G., Nkuipou-Kenfack, E., Zürgbig, P., et al. (2019). Apelin affects the mouse aging urinary peptidome with minimal effects on kidney. *Sci. Rep.* 9, 10647.

Wang, G., Qi, X., Wei, W., Englander, E.W., and Greeley, G.H. (2006). Characterization of the 5'-regulatory regions of the rat and human apelin genes and regulation of breast apelin by USF. *FASEB J.* 20, 2639–2641.

- Wang, S.J., Greer, P., and Auerbach, R. (1996). Isolation and propagation of yolk-sac-derived endothelial cells from a hypervascular transgenic mouse expressing a gain-of-function *fps/fes* proto-oncogene. *In Vitro Cell. Dev. Biol. Anim.* 32, 292–299.
- Whitham, M., and Febbraio, M.A. (2016). The ever-expanding myokinome: discovery challenges and therapeutic implications. *Nat. Rev. Drug Discov.* 15, 719–729.
- Wu, C., Macleod, I., and Su, A.I. (2013). BioGPS and MyGene.info: organizing online, gene-centric information. *Nucleic Acids Res.* 41, D561-565.
- Wu, L., Chen, L., and Li, L. (2017). Apelin/APJ system: A novel promising therapy target for pathological angiogenesis. *Clin. Chim. Acta Int. J. Clin. Chem.* 466, 78–84.
- Yaffe, D., and Saxel, O. (1977). Serial passaging and differentiation of myogenic cells isolated from dystrophic mouse muscle. *Nature* 270, 725–727.
- Yin, H., Price, F., and Rudnicki, M.A. (2013). Satellite cells and the muscle stem cell niche. *Physiol. Rev.* 93, 23–67.
- Zhang, J., Muri, J., Fitzgerald, G., Gorski, T., Gianni-Barrera, R., Masschelein, E., D’Hulst, G., Gilardoni, P., Turiel, G., Fan, Z., et al. (2020). Endothelial Lactate Controls Muscle Regeneration from Ischemia by Inducing M2-like Macrophage Polarization. *Cell Metab.* 31, 1136-1153.e7.
- Zhou, X., and Wang, T. (2012). Using the Wash U Epigenome Browser to examine genome-wide sequencing data. *Curr. Protoc. Bioinforma.* Ed. Board Andreas Baxevanis AI 0 10, Unit10.10.

Section 4

Endothelial-myogenic progenitor cell crosstalk is regulated by glycemic levels via endothelial Ndrp1

Endothelial-myogenic progenitor cell crosstalk is regulated by glycemic levels via endothelial Ndrp1

Umji Lee^{1,2,3}, Hannah Fong¹, David W. McKellar¹, Charles Heinke¹, Emily Laurillard¹,
Jerome N. Feige^{2,3}, C. Florian Bentzinger^{3,4}, Benjamin D. Cosgrove^{1*}

1. Meinig School of Biomedical Engineering
Cornell University
Ithaca, New York, USA
2. School of Life Sciences
École Polytechnique Fédérale de Lausanne (EPFL)
Lausanne, Switzerland
3. Nestlé Institute of Health Sciences
Lausanne, Switzerland
4. Department de pharmacologie et physiologie
Centre de Recherche du CHUS
Faculté de médecine et des sciences de la santé
Université de Sherbrooke
Sherbrooke, QC, Canada

* Corresponding author:
Benjamin D. Cosgrove, PhD
Email: bdc68@cornell.edu

Abstract

Background

Skeletal muscle progenitors (SKMPs) reside in close proximity to supportive cell types in the stem cell niche and dynamically interact with each other to adapt to environmental changes. Although systemic energy levels play a critical role in regulating muscle strength and SKMP function, it remains unknown how these signals are integrated by the niche. Here, we studied how different niche cell types affect SKMPs in response to glycemic levels.

Methods

To determine whether common niche cell types such as macrophages, fibroblasts, or endothelial cells have differential effects on SKMPs in response to energy availability, we analyzed co-cultures in low- and high-glucose media. Using transcriptomics we identified a regulatory effector of the glycemic response in endothelial cells and studied its role in controlling SKMP self-renewal function using siRNA.

Results

We discovered that endothelial cells synergistically enhanced SKMP proliferation in a low-glycemic environment, while fibroblasts and macrophage co-culture had no effect. Crosstalk between SKMPs and endothelial cells was mediated by direct cell-cell interaction and could not be reproduced through conditioned media transfer of soluble paracrine factors. Transcriptome analysis revealed that the endothelial α/β hydrolase N-Myc downstreamregulated 1 (Ndr1) is induced by a low-glycemic environment and is associated with biological adhesion. SKMPs co-cultured with Ndr1 knock-down endothelial cells lose their synergistic functional relationship in response to altered glucose levels.

Conclusion

Our findings suggest that Ndr1 is a key mediator of endothelial cell-mediated glycemic control of SKMPs and provides a link between systemic energy levels and the skeletal muscle stem cell niche.

Keywords: *Skeletal Muscle Progenitors; Intercellular Metabolism; Cell-Stem Cell Interaction; ar Metabolism; Cell-Stem Cell Interaction; Endothelial Ndr1;*

Personal contribution:

As a first author, I had led the project, designed and performed the experiments, interpreted the results, and wrote the manuscript.

Current status of the project:

In submission to Skeletal Muscle Journal

4.1 Introduction

Skeletal muscle is a dynamic tissue, which has a vigorous potential to regenerate and adapt to environmental changes. Maintenance and regeneration of skeletal muscle primarily rely on the function of undifferentiated adult stem cells that reside beneath the basal lamina of muscle fibers in the satellite cell position. Skeletal muscle progenitors (SKMPs) are typically quiescent but can be activated in response to external stimuli such as traumatic injury and physical activity. In response, SKMPs proliferate and differentiate to form new myofibers and maintain muscle homeostasis (Dumont et al., 2015; Chakkalakal et al., 2012, 2014; Shea et al., 2010; Schultz, 1996). Defects in SKMP function associated with skeletal muscle disease or aging can severely reduce the regenerative capability of the tissue.

Homeostasis and fate decisions of SKMPs are orchestrated by various tissue-resident cells in the stem cell niche (Bentzinger et al., 2013; Mashinchian et al., 2018; Thomas et al., 2015). Recent in-depth single-cell transcriptomic analyses captured and characterized extended sub-populations of tissue-resident cells such as immune cells, neurons, adipocytes, fibroblast-like cells and endothelial cells, and smooth muscle cells (De Micheli et al., 2020; Macosko et al., 2015; McKellar et al., 2020a; Saber et al., 2020; Zheng et al., 2017). However, our mechanistic understanding of how these specific cell types influence SKMP function remains limited.

Skeletal muscle contraction is mediated by dynamic changes in diffusion and the active transport of Ca^{2+} , which requires a massive amount of adenosine triphosphate (ATP). Thus, energy supply is critical to muscle function and subject to the metabolism of glucose and fatty acid substrates (Berger et al., 1976; Hänninen and Atalay, 1998; Rose and Richter, 2005). Depending on load and fitness, muscle fibers utilize different modes of ATP synthesis either through anaerobic cytosolic glycolysis or mitochondrial oxidation (Brooks, 1998). The intensity and duration of exercise exponentially increase glucose utilization in muscle and recruit fast-twitch muscle fibers (Brooks, 1997; Wahren et al., 1971; Williams et al., 1995). Since skeletal muscle is one of the most glucose-consuming tissues, it can account for 75-89% of total carbohydrate oxidation during high-intensity exercise (Brooks, 1997; Wahren et al., 1971).

Interestingly, recent results suggest that SKMPs *in-vitro* do not require high levels of glucose and become impaired under these conditions (Furuichi et al., 2021). In agreement with these findings, excessive blood sugar levels frequently observed in diabetic patients, decrease the myogenic potential of SKMPs and can lead to the development of myopathic changes (D'Souza et al., 2013). Conversely, *in-vivo* caloric restriction has been shown to enhance SKMP function by boosting mitochondrial activity and stimulates muscle regeneration (Cerletti et al., 2012). SKMPs undergo metabolic reprogramming depending on their activation state and utilize distinct metabolic systems and substrates (Ryall, 2013; Ryall et al., 2015). While proliferating SKMPs mainly rely on mitochondrial respiration for ATP production, differentiating cells demand more glucose (Ahsan et al., 2020; Yucel et al., 2019). Hence, glucose metabolism is closely linked to SKMP function.

Likewise, glucose metabolism impacts various functions of other cell populations present in skeletal muscle. For instance, bone-marrow-derived macrophages become more pro-inflammatory and show a lower phagocytosis activity under high glucose conditions (Pavlou et al., 2018; Van den Bossche et al., 2017). High glucose treatment decreases the migration and proliferation of fibroblasts, which causes delayed wound healing (Buranasin et al., 2018; Xuan et al., 2014). Moreover, endothelial cell proliferation, permeability, and the regenerative function of vascular progenitors depend on glucose levels (Baumgartner-Parzer et al., 1995; Chen et al., 2007b; Hempel et al., 1997). These observations support the notion that glycemic levels also affect regulatory cell types in the SKMP niche. Here, we investigated niche-dependent metabolic effects of differential glucose levels and identify alpha/beta hydrolase N-Myc Downstream Regulated1 (Ndr1) in endothelial cells as a regulator of SKMP function in low glycemic conditions.

4.2 Results:

4.2.1 Endothelial cells stimulate SKMP proliferation in a low-glycemic environment

Immune cells, fibroblasts, and endothelial cells represent the majority of cell types identified in single-cell transcriptomics of skeletal muscle tissue (De Micheli et al., 2020). To assess whether macrophages (Macs), endothelial cells (ECs), or fibroblasts (Fibs) affect the proliferation of Pax7 positive (Pax7+) SKMPs we maintained them for three days in co-culture in standard myoblast media containing 4.5g glucose/L (**Fig. 1a,b**). We observed a significant increase in both Pax7+ and proliferating EdU+/Pax7+ SKMPs were cultured in the presence of ECs compared to SKMPs in mono-culture (**Fig. 1c-e**).

We next examined whether the altered availability of glucose affects Pax7+ SKMPs in mono-culture. We observed that high glucose levels reduced total cell numbers and EdU incorporation in Pax7+ SKMPs (**Supplementary Fig. 1a-d**). Interestingly, co-culture with ECs stimulated the proliferation of Pax7+ SKMPs in response to decreasing levels of glucose far beyond the effect observed in mono-cultures (**Fig. 1f,l**). While co-culture with Fibs slightly increased total SKMP numbers it did not lead to increased EdU incorporation (**Fig. 1g,j**). Conversely, co-culture of Macs inhibited EdU incorporation in SKMPs in media with increased glucose levels (**Fig. 1h,k**). These observations demonstrate that ECs have pro-proliferative effects on SKMPs in a low glycemic environment.

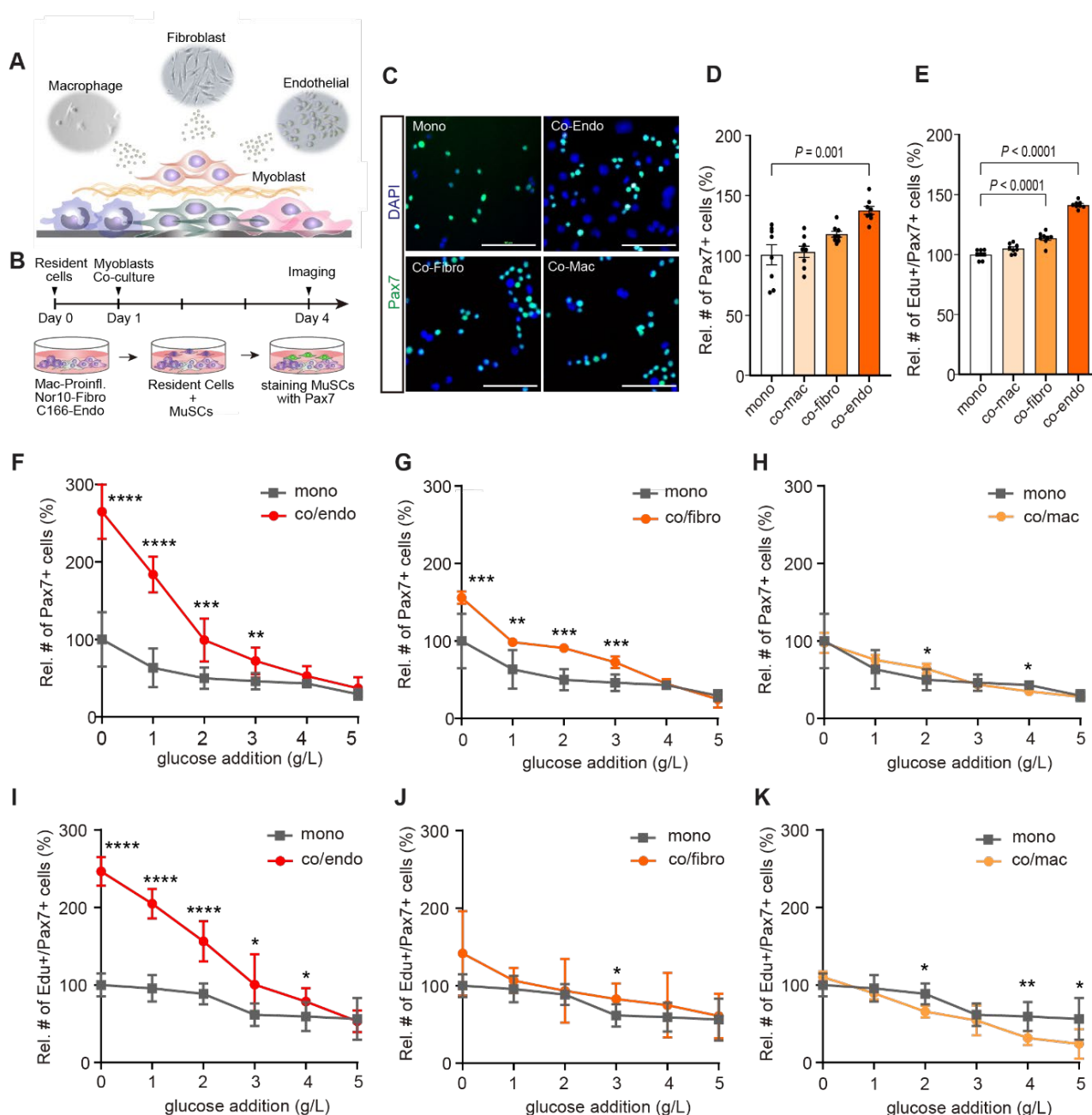


Figure 4.1. Hypoglycemic conditions stimulate SKMP proliferation through endothelial cells. **a,b.** Overview of in-vitro co-culture experimental models of niche cell types with SKMPs. **c.** Representative images of Pax7 immunostaining of SKMP mono- or co-cultures with endothelial cells (ECs), fibroblasts (Fibs), and macrophages (Macs). Scale bar = 100 μ m. **d-e.** Quantification of the number of Pax7+ and Edu+/Pax7+ SKMPs in mono- or co-culture with ECs, Fibs, or Macs. **f-k.** Quantification of the number of Pax7+ and Edu+/Pax7+ SKMPs in mono- or co-culture with ECs, Fibs, or Macs depending on glucose concentration. All data are presented as means \pm s.e.m.

4.2.2 SKMP and EC crosstalk under low glucose conditions is mediated by direct cell-cell interactions

To test whether soluble factors are responsible for the interactions between niche cell types and SKMPs, we prepared a conditioned medium from Macs, Fibros, and ECs. Subsequently, we incubated SKMPs for 3 days with the conditioned media and assessed effects on cell number and EdU incorporation (**Fig. 2a**). Interestingly, the number of Pax7+ and Pax7+/EdU+ SKMPs was not affected by any of the conditioned media (**Fig. 2b-d**). Even conditioned media that were four-fold concentrated did not affect SKMPs (**Supplementary Fig. 2a-c**). These data suggest that crosstalk between niche cell types and SKMPs occurs through insoluble factors or cell-cell contacts.

To better understand the nature of energy-dependent pro-proliferative signals presented by ECs, we profiled them by microarray under low- and high-glucose conditions. Genes with p-value <0.0001 and a fold change >3 were selected as differentially regulated (**Fig. 3e**). Amongst 181 low glucose-induced genes, 17 genes were of the gene ontology biological adhesion (**Fig. 2f,g**). To confirm their relevance *in-vivo* we compared these 17 genes to single-cell RNA-sequencing analysis of mouse skeletal muscle tissue (**Fig. 2h**). We observed that the genes *Ndr1*, *Ackr3*, *Igf2*, *Gbp2* were expressed by skeletal muscle resident ECs.

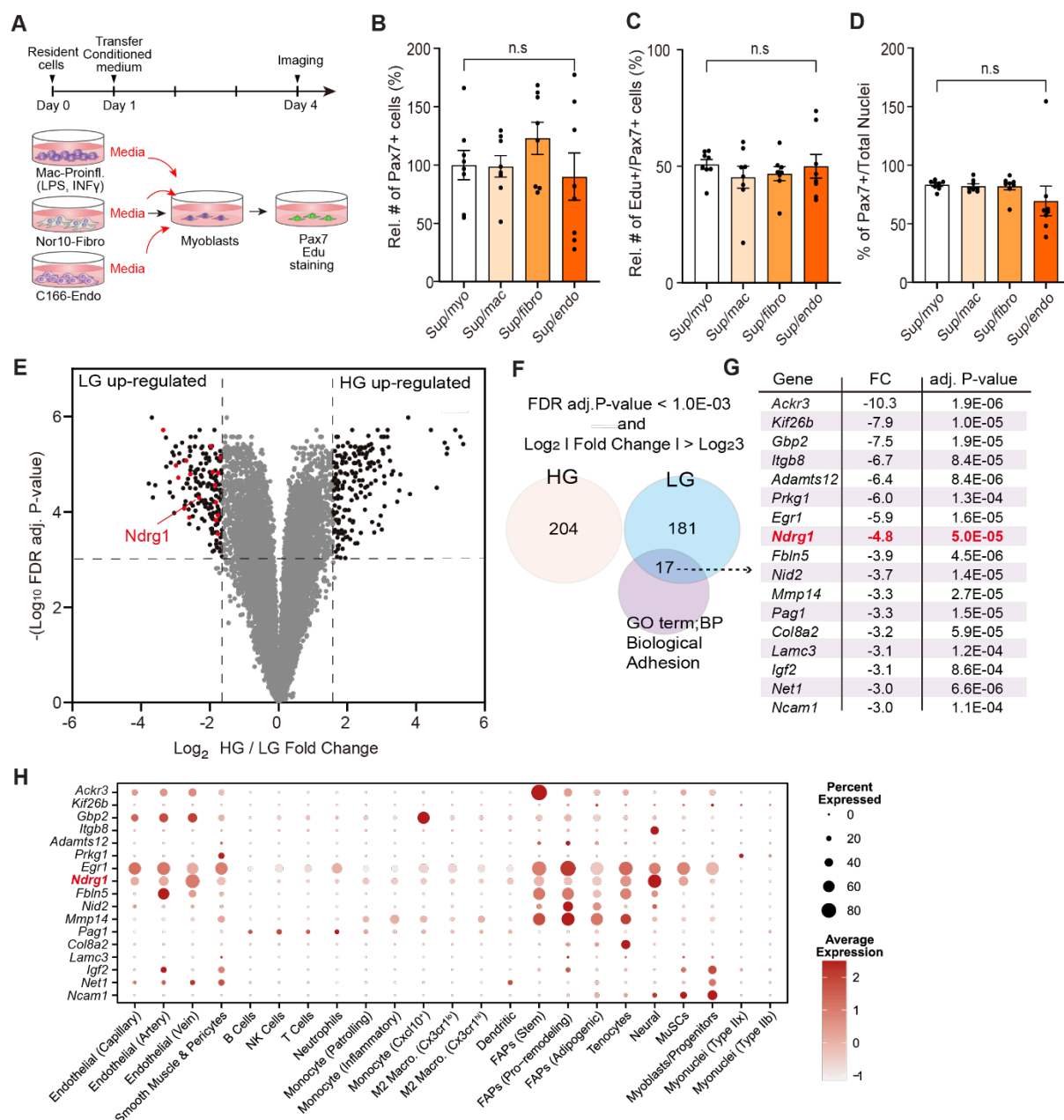


Figure 4.2. Low glucose regulates adhesion-related mechanisms in ECs. **a.** Scheme outlining SKMP culture in conditioned media collected from Macs, Fibs, and ECs. **b-d.** Quantification of the number of Pax7+, Edu+/Pax7+, Pax7+/total nuclei in SKMPs cultured in conditioned media supernatant (Sup). Data are presented as means \pm s.e.m. Statistical significance was determined using the Student t-test compare with sup/myo control. * $P < 0.05$, ** $P < 0.01$, *** $P < 0.001$, **** $P < 0.0001$. **e.** Volcano plot for differentially expressed genes in ECs cultured in low- or high-glucose medium. Genes with a p-value < 0.0001 , fold change > 3 are colored in black and 17 genes related to the gene ontology (GO) biological adhesion are colored in red. **f.** Venn diagram of the differentially expressed genes in ECs in low- (LG) and high-glucose (HG) and the genes belonging to the GO term biological

adhesion. **g.** Biological adhesion-related genes up-regulated in ECs in low glucose medium. FC = Fold change. **h.** Dot plots showing the expression of biological adhesion-related genes up-regulated in ECs under low-glucose conditions *in-vitro* by cell-type clusters from single-cell RNA-sequencing analysis of adult mouse skeletal muscle from De Micheli et al. (2020).

4.2.3 *Ndr*1 expression in ECs is induced under low glyceic conditions

To test whether the mRNA levels of *Ndr*1, *Ackr3*, *Igf2*, *Gbp2* in ECs are responsive to differential energy availability we assessed their induction under low- and high-glucose conditions by quantitative PCR. Notably, expression of *Ndr*1 expression was induced 6-fold in ECs cultured under low glyceic conditions (**Fig. 3a**). *Ndr*1 (N-Myc Downstream Regulated 1) is annotated by alpha/beta hydrolase which involves in regulating tight and adhesion junction molecules (Gon et al., 2017). Furthermore, *Ndr*1 mRNA levels progressively increased over 6 days of culture in low-glucose conditions, while it remained stable in high-glyceic media (**Fig. 3b,c**). Western blots confirmed that low glucose also led to higher *Ndr*1 levels in ECs on the protein level (**Fig. 3d,e**). Lastly, we observed that *Ndr*1 immunostaining was dramatically increased under low-glucose conditions in ECs (**Fig. 3f**).

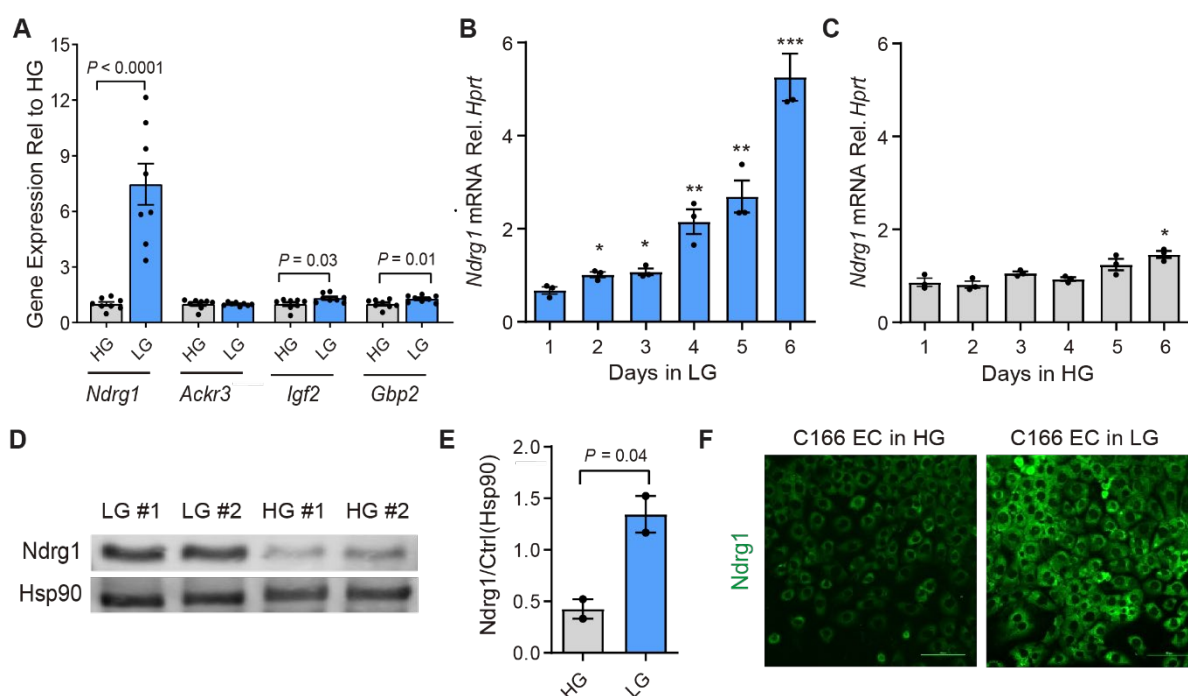


Figure 3. Endothelial NdrG1 is upregulated under low-glycemic conditions. **a.** Glucose-dependent gene expression of *NdrG1*, *Ackr3*, *Igf2*, and *Gbp2* in ECs measured by quantitative PCR. **b,c.** *NdrG1* mRNA expression in ECs in low- or high-glucose media over six days. *Hprt* was used as a housekeeper. All graphs are presented as means \pm s.e.m. Statistics were analyzed using Students t-test compared to Day1 condition * $P < 0.05$, ** $P < 0.01$, *** $P < 0.001$, **** $P < 0.0001$. **d,e.** *NdrG1* protein expression and gray value quantification determined by western blot of ECs cultured in low- or high-glucose media. *Hsp90* is shown as a housekeeper. **f.** Representative images of *NdrG1* immunostaining in ECs cultured in low- and high-glucose media. Scale bar = 100 μ m. All graphs are presented as means \pm s.e.m. Binary comparisons were analyzed using Students t-test * $P < 0.05$, ** $P < 0.01$, *** $P < 0.001$, **** $P < 0.0001$.

4.2.4 Ndr1 is required for SKMP-EC crosstalk

To determine the role of Ndr1 in EC-SKMP crosstalk, we performed siRNA knockdown, which efficiently reduced mRNA and protein levels on ECs (**Fig. 4a-c**). Co-cultured with Ndr1 knock-down ECs in low glyceic medium significantly reduced the number of Pax7⁺ cells when compared to scrambled siRNAs (siCtrl) or SKMP monoculture (**Fig. 4d-f**). Therefore, Ndr1 in ECs is required for the pro-proliferative effects of a low glyceic environment on SKMPs.

Validating our findings with closer models in skeletal muscle might be necessary to recapitulate physiological relevance with *in vivo* systems. Hence, we tested our experiments using primary endothelial cells (pECs) isolated from mouse skeletal muscle. *Ndr1* mRNA levels were also found to be significantly higher in pECs cultured in low glucose and its expression increased progressively during long-term culture under low glyceic conditions (**Fig. 5a,b**). In agreement with these findings, immunostaining of pECs revealed increased protein levels under low-glucose conditions (**Fig. 5c**). The siRNAs effectively downregulated *Ndr1* expression in pECs compared to the control condition and prevented the pro-proliferative effect in low glyceic co-culture with SKMPs (**Fig. 5d-g**). Altogether, we demonstrate that ECs integrate energy levels through Ndr1 to control SKMP proliferation

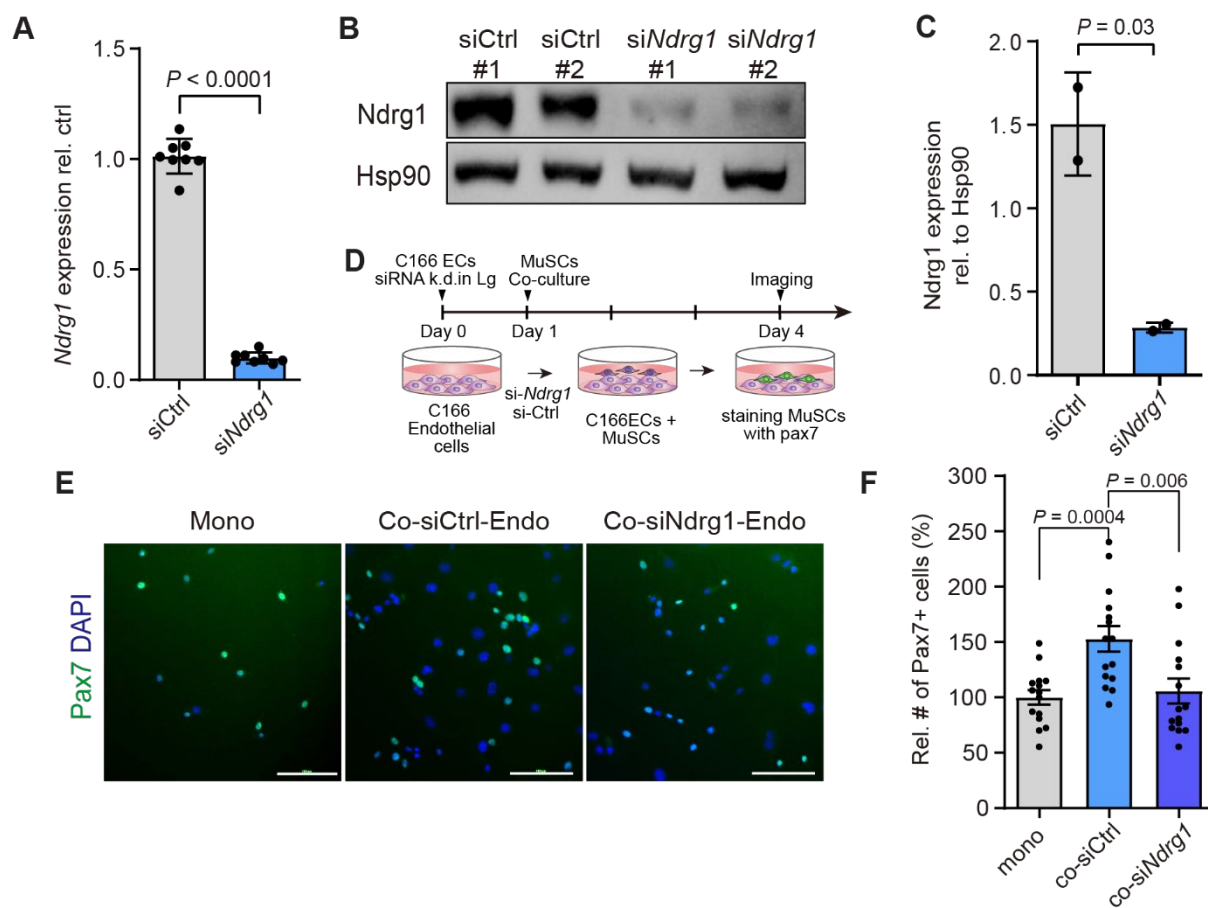


Figure 4.4. Knockdown of Endothelial NdrG1 under low-glucose conditions prevents the pro-proliferative effects of ECs on SKMPs. **a.** mRNA expression after transfection of siNdrG1 or a scrambled siRNA (siCtrl) in ECs. **b,c.** NdrG1 protein levels and western blot gray value quantification after siNdrG1 or siCtrl transfection of ECs. **d-f.** Experimental outline, representative images, and quantification of Pax7+ cells in SKMP mono-culture and in the presence of ECs treated with siNdrG1 and siCtrl in low glucose medium. Scale bar = 100 μ m. All data are reported as means \pm s.e.m. Binary comparisons were analyzed using Student's t-test. * $P < 0.05$, ** $P < 0.01$, *** $P < 0.001$, **** $P < 0.0001$.

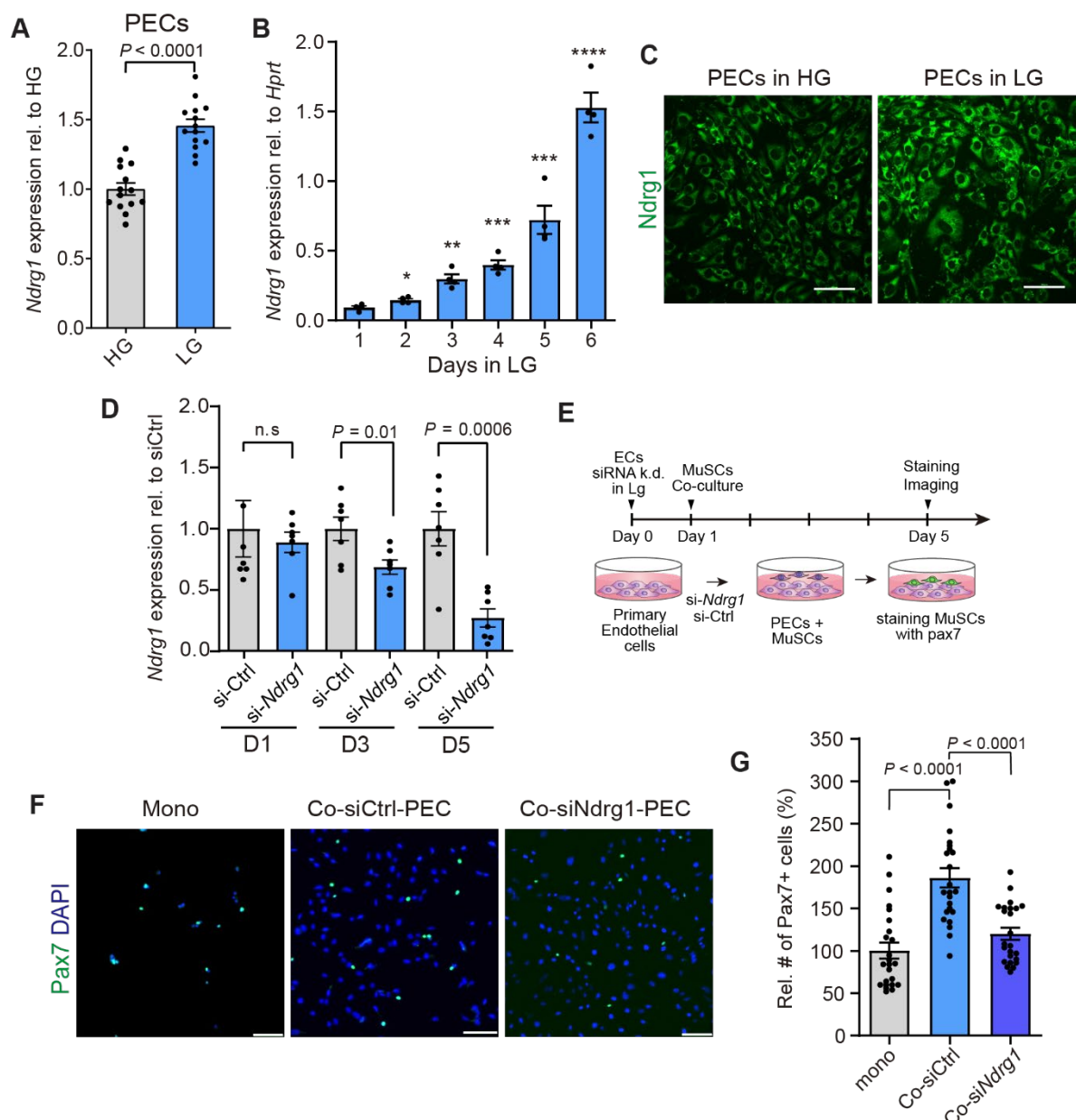
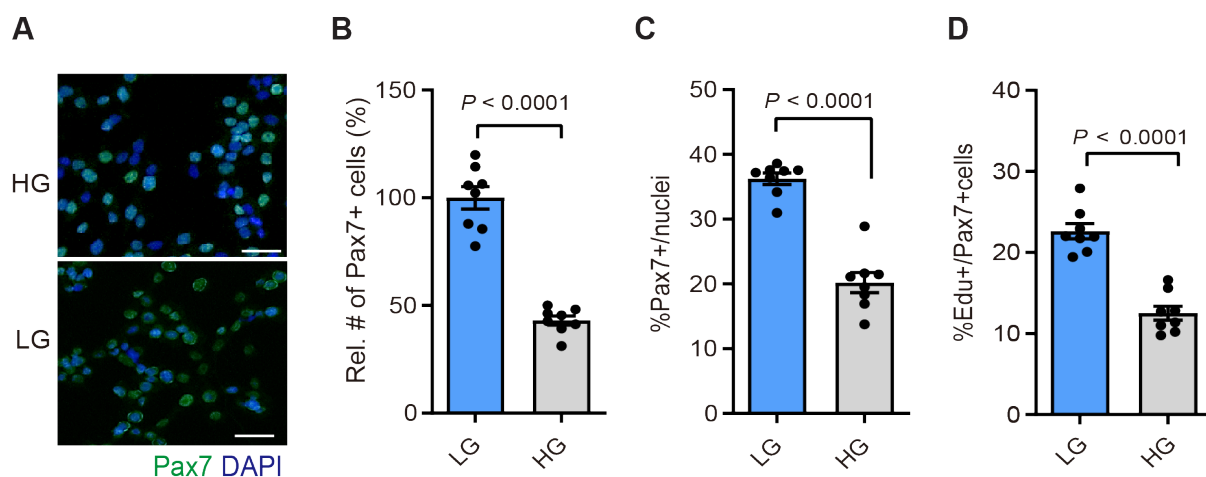
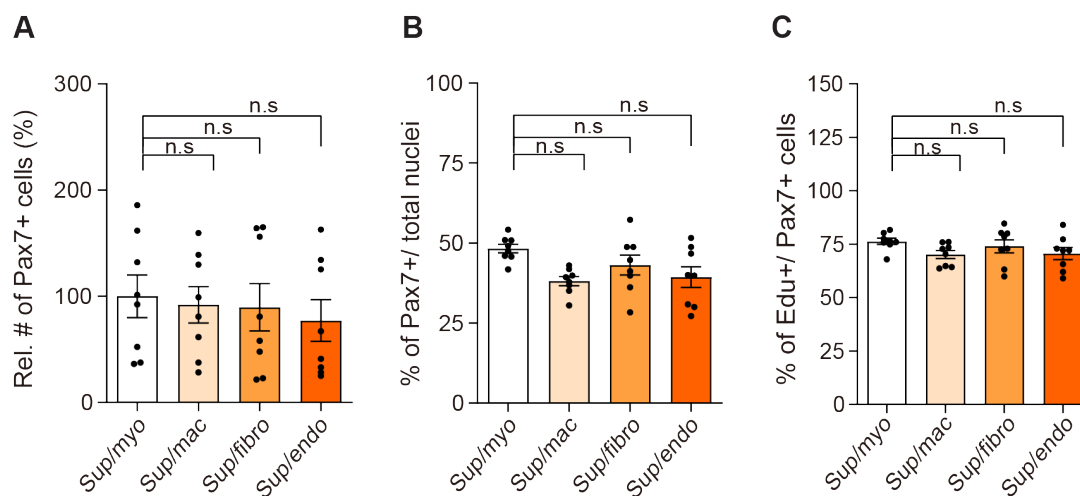


Figure 4.5. NdrG1 in primary endothelial response to low-glucose conditions and is required for controlling SKMP function. **a,b.** Glucose-dependent gene expression of *NdrG1*, primary ECs (pECs) measured by quantitative PCR. *Hprt*. was used as a housekeeper. **b.** Representative images of *NdrG1* immunostaining in pECs cultured in low and high-glucose media **d.** mRNA expression after transfection of siNdrG1 or siCtrl in pECs over five days of culture. **e-g.** Experimental outline, representative images, and quantification of Pax7+ cells in SKMP mono-culture and the presence of pECs treated with siNdrG1 and siCtrl in low glucose medium. Scale bar = 100 μ m. All data are reported as means \pm s.e.m. Binary comparisons were analyzed using Students t-test and multiple comparisons using ANOVA with Bonferroni correction. * $P < 0.05$, ** $P < 0.01$, *** $P < 0.001$, **** $P < 0.0001$.

Section 4. Supplementary Data



Supplementary Figure 1. High glucose affects SKMP proliferation. **a.** Representative Pax7 immunostaining images of SKMPs cultured in low- (LG) or high-glucose media. **b-d.** Quantification of the number of Pax7+, Edu+/Pax7+, Pax7+/total nuclei in SKMPs cultured in low- and high-glucose. Scale bar = 100 μ m. All data are reported as means \pm s.e.m. Significance was determined using Students t-test. * $P < 0.05$, ** $P < 0.01$, *** $P < 0.001$, , **** $P < 0.0001$.



Supplementary Figure 4.2. Four-fold concentrated niche-cell conditioned media do not affect SKMP proliferation. a-d. Quantification of the number of Pax7+, Edu+/Pax7+, Pax7+/total nuclei in cultures exposed to conditioned media supernatant (Sup) collected from Macs, Fibs, ECs, and SKMPs. Data are presented as means \pm s.e.m. and n.s represents non-significant with P values > 0.05 , reported from two-tailed, unpaired t-test between the conditions.

4.3 Discussion and Conclusion

During adult myogenesis, supportive cells provide essential instructive signals to SKMPs. In particular, blood vessel reconstitution by EC recruitment prior to fiber regeneration is critical for shunting oxygen, nutrients, and growth factors from the systemic circulation (Barnouin et al., 2017; Drouin et al., 2019; Duscha et al., 1999; Egginton, 2001; Luque et al., 1995). In addition, reciprocal regulatory interactions between SKMPs and ECs have been reported. SKMPs send angiogenic paracrine signals to ECs (Christov et al., 2007b; Verma et al., 2018a). Vice-versa, ECs appear to regulate MuSC function through EC-derived delta-like ligand, which mediates juxtacrine interaction with Notch signaling in MuSCs (Verma et al., 2018a). Interestingly, changes in vascular density correlate with pathological skeletal muscle diseases such as muscular dystrophy (Christov et al., 2007a; Ennen et al., 2013; Latroche et al., 2015, 2017; Matsakas et al., 2013). Thus ECs represent potential therapeutic targets to stimulate SKMP function.

Here, we report an EC-mediated metabolic control mechanism of SKMP proliferation. Consistent with previous reports, we observed an inhibitory effect of glucose on SKMP expansion in mono-culture (Furuichi et al., 2021). Moreover, the permissive effects of a low glycemic environment on SKMP proliferation are dramatically enhanced in the presence of ECs, while Fibs or Macs do not have such effects. Importantly, Cerletti et al. showed that short-term caloric restriction enhances SKMP function in skeletal muscles of young and old animals (Cerletti et al., 2012). Our results suggest that these effects are at least partially mediated by ECs in the SKMP niche.

We observed that EC-dependent metabolic reprogramming of SKMPs does not depend on soluble factors. Thus, juxtacrine signals appear to be more prominent in endothelial cell-stem cell crosstalk. In agreement with this observation, in-vivo deep-tissue imaging using Pax7 and the EC maker Flk1 showed that the function of Pax7⁺ cells depends on their distance to microvessels (Verma et al., 2018a). Using transcriptomics, we identified Ndrp1 as a low-glucose responsive gene required for EC-mediated SKMP stimulation. Ndrp1 is a highly conserved alpha/beta hydrolase and functions as a tumor suppressor by regulating glucose metabolism-related enzymes in epithelial cells (Liu et al., 2017; Melotte et al., 2010; Stein et al., 2004). Interestingly, live-cell imaging showed that Ndrp1 mediates recycling of the adhesion molecule E-cadherin in the Golgi apparatus (Choudhury et al.,

2005; Kachhap et al., 2007). Moreover, NdrG1 can recruit the GTPase Rab4a and regulates the extra- and intracellular trafficking of various membrane proteins including tight and adhesion junction molecules (Goueli et al., 2012; Kachhap et al., 2007). Therefore, it is conceivable that NdrG1 also regulates adhesion molecules mediating EC-SKMP interactions in response to low-glucose conditions.

Conclusion

In conclusion, we demonstrate that endothelial Ndrp1 mediates EC-SKMP crosstalk in response to glucose levels. Our results support the notion that the vascular stem cell niche integrates systemic energy levels through ECs to control SKMP function. Nevertheless, we only focus on endothelial Ndrp1 function on EC-SKMP crosstalk in response to glucose levels. To make the conclusive results, we will need to prove the solid mechanism how and what specific adhesion molecules that Ndrp1 upregulates.

Section 4 Methods

Mice

All animal protocols were approved by The Cornell University Institutional Animal Care and Use Committee (IACUC) and experiments were performed in compliance with the institutional guidelines. Animals used for SKMP isolation were 3-6 months old male and female C57BL/6J mice (Jackson Laboratory, 000664).

SKMP isolation

Freshly dissected mouse hindlimb muscles were placed in 8 mg/mL collagenase D (Roche, 11088882001) in DMEM and incubated at 37°C for 15 mins. The tissue was then mechanically dissociated using the gentleMACS dissociator (Miltenyi Biotec, 130-093-235). After adding 10 U/mL dispase II in DMEM (Roche, 39307800), the tissues were incubated again at 37°C for 40 min. Digested tissues were filtered using a 100 µm strainer followed by a 40 µm strainer. After the filtrate was spun down at 582 xg for 7 min at 4°C and the cells were resuspended in RBC lysis buffer (IBI, 89135-030) for 5 min to remove red blood cells. After spinning down again, cells were resuspended in FACS buffer (2.5% horse serum, 2mM EDTA in PBS) containing biotinylated lineage antibodies: 1:500 biotin anti-CD45 (Biolegend, 103104-BL), 1:200 biotin anti-CD31 (Biolegend, 102404-BL), 1:200 biotin anti-CD11b (Biolegend, 101204-BL), biotin anti-Sca1 (Biolegend, 108104-BL), and incubated for 25 mins on ice. Streptavidin-coated magnetic microbeads (Miltenyi Biotec, 130-048-102) were added to each tube at a dilution of 1:80 and incubated on ice for 10 mins. The cells were then loaded into prewashed LD separation columns (Miltenyi Biotec, 130-042-901) and placed in a QuadroMACS magnetic separator (Miltenyi Biotec, 130-090-976). After two washes with FACS buffer, the lineage negative cells were recovered and resuspended in fluorescent antibody solution for 25 mins: 1:70 eFluor450 anti-CD34 (Invitrogen, **48-0341-80**), **1:500** AlexaFluor647 anti- α 7-integrin (Ablab, 67-0010-05), and 1:90 Streptavidin-PE-Cy7 (Biolegend, 405206). Cells were then diluted with FACS buffer, spun down, and resuspended in 200-300 µL FACS buffer with 1 µL propidium iodide (Life Technologies, P3566). Sorting was performed using a FACSAria Fusion Sorter (BD, 656700), selecting for Lin-/PI-/Alpha 7+/CD34+ cells.

Cell maintenance

Following FACS sorting, SKMPs were seeded and maintained in tissue culture plates pre-coated with collagen (Life Technologies, A1048301). SKMPs were grown in Ham's F-10 medium (Corning, 10-070-CV) supplemented with 20% heat-inactivated fetal bovine serum (FBS), 5ng/ml b-FGF(Life Technologies, PMG0035), and 1% pen/strep (Thermo Scientific, 15140122). SKMPs were passaged with 0.25% Trypsin (Corning, 25-053-CI) and seeded at a density of 2.000 cells/cm². Mouse skeletal muscle-derived fibroblasts (ATCC, NOR-10) were cultured in DMEM (Corning, 10-0130-CM) containing 1% Pen/Strep and 20% FBS. Mouse yolk sac-derived endothelial cells (ATCC, C166) were maintained in 10% FBS containing growth medium DMEM (4.5g/L glucose). Mouse ascites-derived monocytes (ATCC, J774.1A) were grown in DMEM with 10% FBS. Mouse muscle derived-primary endothelial cells (Cell Biologics, C57-6220) were maintained with EndoGro-MV VEGF medium (Cell Biologics, SCME003-M1168) on gelatine (Sigma, G1393) pre-coated plates.

Macrophage polarization

J774.1A monocytes were used and seeded at 0.2x10⁶/cm². Macrophage polarization was induced using 20ng/ml Interferon-gamma (INF- γ , Sigma-Aldrich, I4777) and 100ng/ml of lipopolysaccharide (LPS) from E.coli 011184 (Sigma-Aldrich, L2630) for 24 hours in monocyte media. Subsequently, the cells were washed for further co-culture experiments.

Co-culture assays and conditioned media

Endothelial cells, fibroblasts, or polarized macrophages were plated 96 well-plates at 1000 cells per well. After 24 hours of incubation, 1000 SKMPs per well were added to the different cell types for co-culture. Subsequently, the cells were maintained SKMP medium for 24 hours. For low glucose conditions, no glucose medium (DMEM 0g glucose, Thermofisher, 11966025) with 20% FBS and 1mM of sodium pyruvate were supplemented. After 3-4 days of treatment, the cells were fixed, stained, and analyzed. Conditioned media were obtained from mono-cultures of the different cell types after 3 days in the cell-type growth medium.

Proliferation assay

Cells were treated with 5-ethynaly-2'-deoxyuridine (EdU, Life Technologies, C10086) for 2 hours at 10uM before fixation with 4% of Paraformaldehyde (PFA, Electron Microscopy Sciences, 15710) for 15 mins. Fixed cells were blocked with 4% of bovine serum albumin

(BSA, VWR, RLBSA50) following permeabilization for 15 mins. EdU staining was performed as described in the Click-iT EdU imaging kit manual (Life technology, C10340).

Immunofluorescence and imaging

Cells were fixed with 4% of Paraformaldehyde (PFA) for 15 mins and blocked with 4% of bovine serum albumin (BSA) following permeabilization with tween 20 (Millipore Sigma, 9005-64-5) or cold methanol for 15 mins. Primary antibodies of Pax7 (DSHB, Pax7-b) and NdrG1 (Abcam, ab124689) were diluted in blocking buffer at 1:200 and were incubated at 4°C overnight. After three PBS washes, the cells were exposed to secondary antibodies and DAPI (ThermoFisher Scientific, 62248) on an agitating plate for 30 mins at room temperature. Stained cells were imaged using a Nikon Ti-E Eclipse inverted confocal microscope (Nikon) or the MetaXpress system (Molecular Devices) and analyzed using software provided by the manufacturer.

Microarrays

RNA for microarray analysis was purified using the Agencourt RNAdvance extraction kit (Beckman Coulter Life Sciences, A32649). Briefly, cells were treated with Proteinase K, lysed, and nuclei acids were isolated with paramagnetic beads from other contaminants. After several washing steps, DNase was added to digest genomic DNA and re-bind the RNA to the beads. After additional washing, RNAs were eluted from magnetic particles.

Gene expression analysis and single-cell RNA sequencing data

Publicly available single-cell and single-nucleus RNA sequencing data was downloaded, aligned, processed, and integrated as described in McKellar et al, *bioRxiv*, 2020 (McKellar et al., 2020b). Briefly, samples were aligned to the mm10 reference genome using Cellranger v3.1.0. Ambient RNA signatures were removed using SoupX v1.4.5 (Young and Behjati, 2018). Doublets were removed using DoubletFinder v2.0 (McGinnis et al., 2019). Samples were then preprocessed using Seurat v3.2.1 (Stuart et al., 2019). Batch correction was performed using Harmony v1.0 (Korsunsky et al., 2019b). Cell types were annotated based on canonical marker gene expression. The code used for processing these data can be found at <https://github.com/mckellardw/scMuscle>.

Knock-down experiments

C166 endothelial cells at 50% confluence were harvested from 96 well plates and siRNAs with transfection reagent RNAiMax (Life Technologies, 13778150) were added to the suspended cells after 5 min incubation. siRNA SMART pools were synthesized by Dharmacon (L-0455-01-0005), and non-specific target si-scramble was used as a negative control (Dharmacon, D-001810-10-50). After 3 days of incubation, mRNA or protein were extracted and quantified by RT-qPCR or western blot. Target sequences are listed in the table below.

siRNA-NdrG1	siRNA-scramble
ACGACAUGAACCCGAGCAA	CGACCGAAAUUGCGAGGAC
UGGAGGUAGUGCACACGUA	CAGAAUAGAUCUAGCUGAG
GCAAGAAGCAGUUCAGCGU	CUACUUUGAAUGCGGACAA
UUAAGUUCUGGACGCUGA	CGUCCAUGCCGUUUGCUUU

Quantitative PCR

Total RNA was extracted using the mRNA extraction kit (Qiagen, 74106). The FastLane cell multiplex NR kit (Qiagen, 216513) or Master mix (Life Technologies, 4444557) were used for TaqMan qPCR using a Roche thermocycler. Taqman probes were purchased from Life Technologies (Hprt: Mm00446968, NdrG1: Mm00440447). *Hprt* was used as a housekeeper.

Western blot

Protein was extracted using a lysis buffer (Biorad, 171304011) containing the protease inhibitor cocktail (0.5mM PMSF, 1mM Benzamidine HCl, 1 µg/ml Leupeptin, 1 µg/ml Pepstatin A, 1mM DTT, 1mM Microcystin-LR, 1mM Sodium Orthovanadate, and 10 µg/ml Aprotinin). After centrifugation of debris, protein concentration was measured using the bicinchoninic acid assay (Pierce Chemical, 23235). SDS-PAGE was run on 10% acrylamide gels. After transfer membranes were blocked using 4% BSA and incubated with primary antibodies against anti-NdrG1 (Abcam, ab124689) and anti-HSP90 (Cell signaling, 4875S). After washing, the membranes were incubated with peroxidase- goat anti-rabbit antibody (Jackson ImmunoResearch, 111-035-045). The Image Lab software (Bio-Rad) was used to quantify protein expression levels.

Statistical Analysis

Data were analyzed using Student's t-test for binary and two-way ANOVA using GraphPad Prism 9.

Lead contact & material availability

Further information and requests for resources and reagents should be directed to and will be fulfilled by the lead contact, Benjamin Cosgrove (bdc68@cornell.edu). All unique/stable reagents generated in this study are available from the lead contact without restriction.

ACKNOWLEDGEMENTS

This study was funded by Nestlé and the National Institutes of Health (R01AG058630). U.L. is supported by SNSF Doc. Mobility fellowship (P1ELP3_187970). C.F.B. is supported by the Canadian Institutes of Health Research (CIHR, PJT-162442), the Natural Sciences and Engineering Research Council of Canada (NSERC, RGPIN-2017-05490), the Fonds de Recherche du Québec - Santé (FRQS, Dossier 36789 and 296357), the ThéCell Network (supported by the FRQS), the Canadian Stem Cell Network, and a research chair of the Centre de Recherche Médicale de l'Université de Sherbrooke (CRMUS). B.D.C. is supported by the National Institutes of Health (R01AG058630). We also thank Genomics Group and FACS Facility for technical supports and helpful discussions.

AUTHOR CONTRIBUTIONS

U.L. designed and performed experiments and analyzed results. C.F.B and B.D.C designed and supervised the study. U.L., H.F., C.H., E.L., performed experiments or generated critical experimental tools. D.W.M. analyzed single-cell transcriptomics. U.L., J.N.F, C.F.B., and B.D.C wrote the manuscript.

COMPETING INTERESTS

J.N.F., U.L, and C.F.B are or were employees of the Société des Produits Nestlé S.A., Switzerland

Section 4 References

1. Dumont NA, Wang YX, von Maltzahn J, Pasut A, Bentzinger CF, Brun CE, et al. Dystrophin expression in muscle stem cells regulates their polarity and asymmetric division. *Nat Med*. 2015;21:1455–63.
2. Chakkalakal JV, Jones KM, Basson MA, Brack AS. The aged niche disrupts muscle stem cell quiescence. *Nature*. 2012;490:355–60.
3. Chakkalakal JV, Christensen J, Xiang W, Tierney MT, Boscolo FS, Sacco A, et al. Early forming label-retaining muscle stem cells require p27kip1 for maintenance of the primitive state. *Development*. 2014;141:1649–59.
4. Shea KL, Xiang W, LaPorta VS, Licht JD, Keller C, Basson MA, et al. Sprouty1 Regulates Reversible Quiescence of a Self-Renewing Adult Muscle Stem Cell Pool during Regeneration. *Cell Stem Cell*. 2010;6:117–29.
5. Schultz E. Satellite Cell Proliferative Compartments in Growing Skeletal Muscles. *Dev Biol*. 1996;175:84–94.
6. Bentzinger CF, Wang YX, Dumont NA, Rudnicki MA. Cellular dynamics in the muscle satellite cell niche. *EMBO Rep*. 2013;14:1062–72.
7. Mashinchian O, Pisconti A, Le Moal E, Bentzinger CF. Chapter Two - The Muscle Stem Cell Niche in Health and Disease. In: Sassoon D, editor. *Curr Top Dev Biol* [Internet]. Academic Press; 2018 [cited 2021 Feb 26]. p. 23–65. Available from: <https://www.sciencedirect.com/science/article/pii/S0070215317300431>
8. Thomas K, Engler AJ, Meyer GA. Extracellular matrix regulation in the muscle satellite cell niche. *Connect Tissue Res*. 2015;56:1–8.
9. De Micheli AJ, Laurillard EJ, Heinke CL, Ravichandran H, Fraczek P, Soueid-Baumgarten S, et al. Single-Cell Analysis of the Muscle Stem Cell Hierarchy Identifies Heterotypic Communication Signals Involved in Skeletal Muscle Regeneration. *Cell Rep*. 2020;30:3583-3595.e5.
10. Macosko EZ, Basu A, Satija R, Nemesh J, Shekhar K, Goldman M, et al. Highly Parallel Genome-wide Expression Profiling of Individual Cells Using Nanoliter Droplets. *Cell*. Elsevier; 2015;161:1202–14.
11. McKellar DW, Walter LD, Song LT, Mantri M, Wang MFZ, Vlaminc ID, et al. Strength in numbers: Large-scale integration of single-cell transcriptomic data reveals rare, transient muscle progenitor cell states in muscle regeneration. *bioRxiv*. Cold Spring Harbor Laboratory; 2020;2020.12.01.407460.
12. Saber J, Lin AYT, Rudnicki MA. Single-cell analyses uncover granularity of muscle stem cells. *F1000Research*. 2020;9.
13. Zheng GXY, Terry JM, Belgrader P, Ryvkin P, Bent ZW, Wilson R, et al. Massively parallel digital transcriptional profiling of single cells. *Nat Commun*. Nature Publishing Group; 2017;8:14049.

14. Berger M, Hagg SA, Goodman MN, Ruderman NB. Glucose metabolism in perfused skeletal muscle. Effects of starvation, diabetes, fatty acids, acetoacetate, insulin and exercise on glucose uptake and disposition. *Biochem J.* 1976;158:191–202.
15. Hänninen O, Atalay M. Oxidative metabolism in skeletal muscle. In: Reznick AZ, Packer L, Sen CK, Holloszy JO, Jackson MJ, editors. *Oxidative Stress Skelet Muscle* [Internet]. Basel: Birkhäuser; 1998 [cited 2021 Jun 2]. p. 29–42. Available from: https://doi.org/10.1007/978-3-0348-8958-2_2
16. Rose AJ, Richter EA. Skeletal Muscle Glucose Uptake During Exercise: How is it Regulated? *Physiology.* American Physiological Society; 2005;20:260–70.
17. Brooks GA. Mammalian fuel utilization during sustained exercise. *Comp Biochem Physiol B Biochem Mol Biol.* 1998;120:89–107.
18. Brooks GA. Importance of the “crossover” concept in exercise metabolism. *Clin Exp Pharmacol Physiol.* 1997;24:889–95.
19. Wahren J, Felig P, Ahlborg G, Jorfeldt L. Glucose metabolism during leg exercise in man. *J Clin Invest.* 1971;50:2715–25.
20. Williams BD, Plag I, Troup J, Wolfe RR. Isotopic determination of glycolytic flux during intense exercise in humans. *J Appl Physiol Bethesda Md* 1985. 1995;78:483–90.
21. Furuichi Y, Kawabata Y, Aoki M, Mita Y, Fujii NL, Manabe Y. Excess Glucose Impedes the Proliferation of Skeletal Muscle Satellite Cells Under Adherent Culture Conditions. *Front Cell Dev Biol* [Internet]. Frontiers; 2021 [cited 2021 Mar 5];9. Available from: <https://www.frontiersin.org/articles/10.3389/fcell.2021.640399/full>
22. D’Souza DM, Al-Sajee D, Hawke TJ. Diabetic myopathy: impact of diabetes mellitus on skeletal muscle progenitor cells. *Front Physiol* [Internet]. Frontiers; 2013 [cited 2021 Jun 3];4. Available from: <https://www.frontiersin.org/articles/10.3389/fphys.2013.00379/full>
23. Cerletti M, Jang YC, Finley LWS, Haigis MC, Wagers AJ. Short-term calorie restriction enhances skeletal muscle stem cell function. *Cell Stem Cell.* 2012;10:515–9.
24. Ryall JG. Metabolic reprogramming as a novel regulator of skeletal muscle development and regeneration. *FEBS J.* 2013;280:4004–13.
25. Ryall JG, Dell’Orso S, Derfoul A, Juan A, Zare H, Feng X, et al. The NAD(+)-dependent SIRT1 deacetylase translates a metabolic switch into regulatory epigenetics in skeletal muscle stem cells. *Cell Stem Cell.* 2015;16:171–83.
26. Ahsan S, Raval MH, Ederer M, Tiwari R, Chareunsouk A, Rodgers JT. Metabolism of glucose and glutamine is critical for skeletal muscle stem cell activation. *bioRxiv.* Cold Spring Harbor Laboratory; 2020;2020.07.28.225847.
27. Yucl N, Wang YX, Mai T, Porpiglia E, Lund PJ, Markov G, et al. Glucose Metabolism Drives Histone Acetylation Landscape Transitions that Dictate Muscle Stem Cell Function. *Cell Rep.* 2019;27:3939–3955.e6.

28. Luo W, Ai L, Wang B-F, Wang L-Y, Gan Y-M, Zhou Y. [Effects of mice macrophages on skeletal muscle cells under high glucose treatment]. *Zhongguo Ying Yong Sheng Li Xue Za Zhi Zhongguo Yingyong Shenglixue Zazhi Chin J Appl Physiol*. 2020;36:124–9.
29. Pavlou S, Lindsay J, Ingram R, Xu H, Chen M. Sustained high glucose exposure sensitizes macrophage responses to cytokine stimuli but reduces their phagocytic activity. *BMC Immunol*. 2018;19:24.
30. Van den Bossche J, O'Neill LA, Menon D. Macrophage Immunometabolism: Where Are We (Going)? *Trends Immunol*. 2017;38:395–406.
31. Buranasin P, Mizutani K, Iwasaki K, Pawaputanon Na Mahasarakham C, Kido D, Takeda K, et al. High glucose-induced oxidative stress impairs proliferation and migration of human gingival fibroblasts. *PLoS ONE*. 2018;13:e0201855.
32. Xuan YH, Huang BB, Tian HS, Chi LS, Duan YM, Wang X, et al. High-Glucose Inhibits Human Fibroblast Cell Migration in Wound Healing via Repression of bFGF-Regulating JNK Phosphorylation. *PLoS ONE*. 2014;9:e108182.
33. Baumgartner-Parzer SM, Wagner L, Pettermann M, Grillari J, Gessl A, Waldhäusl W. High-Glucose–Triggered Apoptosis in Cultured Endothelial Cells. *Diabetes*. American Diabetes Association; 1995;44:1323–7.
34. Chen Y-H, Lin S-J, Lin F-Y, Wu T-C, Tsao C-R, Huang P-H, et al. High Glucose Impairs Early and Late Endothelial Progenitor Cells by Modifying Nitric Oxide–Related but Not Oxidative Stress–Mediated Mechanisms. *Diabetes*. American Diabetes Association; 2007;56:1559–68.
35. Hempel A, Maasch C, Heintze U, Lindschau C, Dietz R, Luft FC, et al. High Glucose Concentrations Increase Endothelial Cell Permeability via Activation of Protein Kinase C α . *Circ Res*. American Heart Association; 1997;81:363–71.
36. McKellar DW, Walter LD, Song LT, Mantri M, Wang MFZ, De Vlaminck I, et al. Strength in numbers: Large-scale integration of single-cell transcriptomic data reveals rare, transient muscle progenitor cell states in muscle regeneration. *bioRxiv*. Cold Spring Harbor Laboratory; 2020;2020.12.01.407460.
37. Young MD, Behjati S. SoupX removes ambient RNA contamination from droplet based single cell RNA sequencing data. *bioRxiv*. Cold Spring Harbor Laboratory; 2018;303727.
38. McGinnis CS, Murrow LM, Gartner ZJ. DoubletFinder: Doublet Detection in Single-Cell RNA Sequencing Data Using Artificial Nearest Neighbors. *Cell Syst*. Cell Press; 2019;8:329–337.e4.
39. Stuart T, Butler A, Hoffman P, Hafemeister C, Papalexi E, Mauck WM, et al. Comprehensive Integration of Single-Cell Data. *Cell*. Elsevier Inc.; 2019;177:1888–1902.e21.
40. Korsunsky I, Millard N, Fan J, Slowikowski K, Zhang F, Wei K, et al. Fast, sensitive and accurate integration of single-cell data with Harmony. *Nat Methods*. 2019;
41. Gon Y, Maruoka S, Kishi H, Kozu Y, Kazumichi K, Nomura Y, et al. NDRG1 is important to maintain the integrity of airway epithelial barrier through claudin-9 expression: NDRG1 maintains epithelial barrier integrity. *Cell Biol Int*. 2017;41:716–25.

42. Barnouin Y, McPhee JS, Butler-Browne G, Bosutti A, De Vito G, Jones DA, et al. Coupling between skeletal muscle fiber size and capillarization is maintained during healthy aging. *J Cachexia Sarcopenia Muscle*. 2017;8:647–59.
43. Drouin G, Couture V, Lauzon M-A, Balg F, Faucheux N, Grenier G. Muscle injury-induced hypoxia alters the proliferation and differentiation potentials of muscle resident stromal cells. *Skelet Muscle*. 2019;9:18.
44. Duscha BD, Kraus WE, Keteyian SJ, Sullivan MJ, Green HJ, Schachat FH, et al. Capillary density of skeletal muscle. *J Am Coll Cardiol*. 1999;33:1956–63.
45. Egginton S. Unorthodox angiogenesis in skeletal muscle. *Cardiovasc Res*. 2001;49:634–46
46. Luque E, Peña J, Martin P, Jimena I, Vaamonde R. Capillary Supply During Development of Individual Regenerating Muscle Fibers. *Anat Histol Embryol*. 1995;24:87–9.
47. Verma M, Asakura Y, Murakonda BSR, Pengo T, Latroche C, Chazaud B, et al. Muscle Satellite Cell Cross-Talk with a Vascular Niche Maintains Quiescence via VEGF and Notch Signaling. *Cell Stem Cell*. 2018;23:530-543.e9.
48. Christov C, Chrétien F, Abou-Khalil R, Bassez G, Vallet G, Authier F-J, et al. Muscle Satellite Cells and Endothelial Cells: Close Neighbors and Privileged Partners. Bronner-Fraser M, editor. *Mol Biol Cell*. 2007;18:1397–409.
50. Ennen JP, Verma M, Asakura A. Vascular-targeted therapies for Duchenne muscular dystrophy. *Skelet Muscle*. 2013;3:9.
51. Latroche C, Gitiaux C, Chrétien F, Desguerre I, Mounier R, Chazaud B. Skeletal Muscle Microvasculature: A Highly Dynamic Lifeline. *Physiology*. American Physiological Society; 2015;30:417–27.
52. Latroche C, Weiss-Gayet M, Muller L, Gitiaux C, Leblanc P, Liot S, et al. Coupling between Myogenesis and Angiogenesis during Skeletal Muscle Regeneration Is Stimulated by Restorative Macrophages. *Stem Cell Rep*. 2017;9:2018–33.
53. Matsakas A, Yadav V, Lorca S, Narkar V. Muscle ERR γ mitigates Duchenne muscular dystrophy via metabolic and angiogenic reprogramming. *FASEB J Off Publ Fed Am Soc Exp Biol*. 2013;27:4004–16.
54. Melotte V, Qu X, Ongenaert M, van Crielinge W, de Bruïne AP, Baldwin HS, et al. The N-myc downstream regulated gene (NDRG) family: diverse functions, multiple applications. *FASEB J*. 2010;24:4153–66.
55. Stein S, Thomas EK, Herzog B, Westfall MD, Rocheleau JV, Jackson RS, et al. NDRG1 Is Necessary for p53-dependent Apoptosis*. *J Biol Chem*. 2004;279:48930–40.
56. Choudhury RR, Hyvola N, Lowe M. Phosphoinositides and membrane traffic at the trans-Golgi network. *Biochem Soc Symp*. 2005;31–8.
57. Kachhap SK, Faith D, Qian DZ, Shabbeer S, Galloway NL, Pili R, et al. The N-Myc down regulated Gene1 (NDRG1) Is a Rab4a effector involved in vesicular recycling of E-cadherin. *PLoS One*. 2007;2:e844.

58. Goueli BS, Powell MB, Finger EC, Pfeffer SR. TBC1D16 is a Rab4A GTPase activating protein that regulates receptor recycling and EGF receptor signaling. *Proc Natl Acad Sci.* 2012;109:15787–92.

Section 5

Intravital Imaging of Vasculature and Muscle Progenitors in Skeletal Muscle of Live Mice

Intravital Imaging of Vasculature and Muscle Progenitors in Skeletal Muscle of Live Mice

Umji Lee^{1,2}, Emily Laurilliard¹, Hannah Fong¹, Aron Mok¹, Chiyong Eom¹, Nicole Biliotta¹,
Nozomi Nishimura¹, Jerome N. Feige², Benjamin D. Cosgrove^{1*}

¹ Meinig School of Biomedical Engineering,
Cornell University,
Ithaca, New York, USA

² School of Life Sciences,
École Polytechnique Fédérale de Lausanne (EPFL),
Lausanne, Switzerland

* Corresponding author:

Benjamin D. Cosgrove, PhD

Email: bdc68@cornell.edu

Abstract

Skeletal muscle is intensively surrounded by vessels that give a trophic bed to skeletal muscle by controlling local hyperemia. Vasculature and vessel compartments in skeletal muscle regulate the myogenesis of muscle progenitors through various signals involved in secreting and adhesive factors. Although muscle stem cell-mediated therapy has been successfully introduced as a model of muscle regeneration studies, these studies have largely been relying on histological analysis at specific time points after sacrificing the animals. Hence, a method for direct visualization of vasculature and muscle progenitors with Spatio-temporal information in a live animal is necessary to understand the complex inter-cellular crosstalk between muscle stem cells and microvasculature in skeletal muscle. Recent advances in multiphoton microscopes combined with genetically labeled fluorescent markers allow deep tissue intravital imaging to understand the function of stem cells and biological processes *in vivo*. Here, we describe a method and the optimization process to label microvasculature and myogenic progenitors during homeostasis after SKMP cell transplantation using a multi-photon microscope.

Key words: Intravital Imaging; Vasculature; Skeletal muscle; Satellite cells; Endothelial cells; Multi-photon microscope

Author contribution:

As a primary author, I designed and performed the experiments, interpreted the results and wrote the manuscript.

Current status of the project:

In preparation

5.1 Introduction

Skeletal muscle is intensely vascularized, which gives a trophic bed to skeletal muscle via local hyperemia depending on the metabolic demands of muscles. Vessels not only supply oxygen and nutrition by the local hyperemia but also contribute to MuSC functions (Latroche et al., 2017). In homeostasis, quiescent muscle stem cells attract endothelial cells by secreting local VEGF in the niche to keep the proximity to the vasculature (Verma et al., 2018b). During muscle reconstruction, re-vascularization supports muscle stem cell expansion and commitment to myogenesis through IGF-1, HGF, bFGF, and PDGF-BB (Christov et al., 2007a). Vascular remodeling and skeletal muscle stem cell expansion after exercise are observed (Nederveen et al., 2017; Snijders et al., 2017). Therefore, the understanding of the complex inter-cellular crosstalk between muscle stem cells and microvasculature in skeletal muscle requires further investigation in a Spatio-temporal manner.

Recent advances in imaging techniques combined with genetically labeled fluorescent markers have allowed closer inspections into the function of stem cells and biological processes *in vivo*. Multiphoton microscopy has been developed to observe stem cell growth, proliferation, and stability without tissue disruption in a living animal. Researchers have successfully characterized cell morphology, behavior, and metabolic activity in cancer cells and human mesenchymal stem cells using two-photon microscopes (Rice et al., 2010; Uchugonova et al., 2008). More recently, the cerebral-vasculature was monitored to study cortical blood flow in Alzheimer's disease from seconds to several week-timescales (Cruz Hernández et al., 2019). Another example combining this approach showed a real-time recovery process of injured intestinal stems cells using *in vivo* two-photon microscopy, which revealed that local damage was recovered by the rearrangements of pre-existing cells, and this ability was reduced in aged animals (Choi et al., 2018).

In this chapter, I optimized the intravital imaging to monitor muscle stem cells and vasculature to deepen the anatomical and kinetical understanding of the intercellular crosstalk between vascular networks and muscle stem cells. I propose to use multi-modalities across two-, three-photon microscopy and observe microvasculature and

myogenic progenitors in the hindlimb skeletal muscle of mice. We describe a step-by-step protocol and optimization process of chronic or long-lasting window to be able to optically access hindlimb muscle over the days of recovery. This multidisciplinary approach offers a great promise for the development of a robust in vivo tool to monitor muscle repair dynamics in real-time and will give the basement of monitoring muscle stem cells and their interaction in their native niche.

5.2 Results:

5.2.1 Window optimization for optical access

To develop intravital imaging to monitor muscle stem cells and vasculature in hindlimb muscle, we need to optimize a window to be optically accessible over the days of recovery in a living animal. Currently-available optical access is gained via a 3-mm diameter silicone ring attached to a cover glass that is used for the cardiac muscle (Jones et al., 2018). Webster et al., applied 2-3 cm diameter fluorodish that mounted over TA muscle to gain optical access but it requires to sacrifice the mice after imaging due to the restriction of mice movement after gluing the fluorodish window on hindlimb (Webster et al., 2016b). Here, we modified the current system to be able to chronically access skeletal muscles for a longer period without interfering with the mobility of mice.

In this step, we attempted to implant a small window that does not restrict the movement of muscle by employing different types of materials such as PDMS, silicone, 3D printed PLA (**Figure 2**). This step is particularly important to find the proper rigidity, lightness, cover glass attachment, view area, accessibility for objectives, and ability to hold water immersion. After implant several frames to the different locations in mice's legs, we traced the window if they are attached intact which is term as a chronic window. We discovered that the vastus lateralis which is located on the quadricep is the optimal location to insert the mice, minimizing the inconvenience in mice. Also, the 8 mm diameter silicone ring was the optimal window type that allows a wide view area and a sufficient amount of immersion on the glass cover (**Figure 2**). Detail procedure is commented on below.

Procedure

* All the animal engaged protocols were followed and approved by The Cornell University Institutional Animal Care and Use Committee (IACUC).

1. Window Frame Preparation

- a. Put glass cover on the frame with Loctite glue applied carefully only on the edge to avoid excessive glue which leaves an opaque membrane on the cover glass.
- b. Dip the frame with a glass cover in 70% ethanol and dry

2. Animal Preparation

- a. Measure the weight of mouse for injection and calculate the injection volume for glucose solution (5%), Dexamethason (0.1mg/mL), Bupivacaine (0.05%), Ketoprofen (2mg/mL), Gycopyrrolate (0.2mg/mL).
- b. Turn on the heating pad warm to 36.5 °C.
- c. Anesthetize the mouse and transfer the mouse to a heating pad-connected surgery board with a nosecone. Connect oxygen and isoflurane tubes to the surgery board
- d. Keep isoflurane level range from 1~2.5 during surgery.
* may be changed based on respiration and check the pinch-reaction.
- e. Apply one drop of ointment eye gel on both eyes
- f. Tape the mouse to fix (abdomen, one leg) and place a stage on the one leg which we implant the window.
- g. Shave leg hair and put 70% ethanol and inject the following solutions that are required for a survival surgery:
 - SC injection : Glucose solution (5%), Gycopyrrolate (0.2mg/mL),
 - IM local injection : Bupivacaine (0.05%), Ketoprofen (2mg/mL),
Dexamethason (0.1mg/mL)

3. Window Implantation

- a. Place the entire heating plate and surgery board with the mouse into clean surgery desk under a surgical microscope.
- b. Tape again to fasten the mouse's leg on a rubber stage that absorbs the pulsatile movement and then sanitize the implantation part with ethanol, povidone-iodine 3 times each in turn.
- c. Incise the skin roundly (minimize incision site) where you implant the window and stretch the subcutaneous space by disconnecting the fascia. This part can be done by putting and opening up the scissors under the skin.
- d. Place the window set (frame with a coverglass) which the coverglass toward the muscle. While holding the window set, apply the Vetbond adhesive under the skin that is in contact with the window frame by stretching the skin toward the top of the frame.
- e. Apply UV cure adhesive on the skin covering the frame edge and expose the gluing area to UV light for 30 seconds.
- f. Prepare dental cement by mixing acrylic resin liquid and powder.
- g. Place the dental cement on top of the frame edge before the dental cement is solidified. Let it dry and solidified for 1-2 minutes.
- h. Check if the coverglass is crystal clean with a surgical microscope.

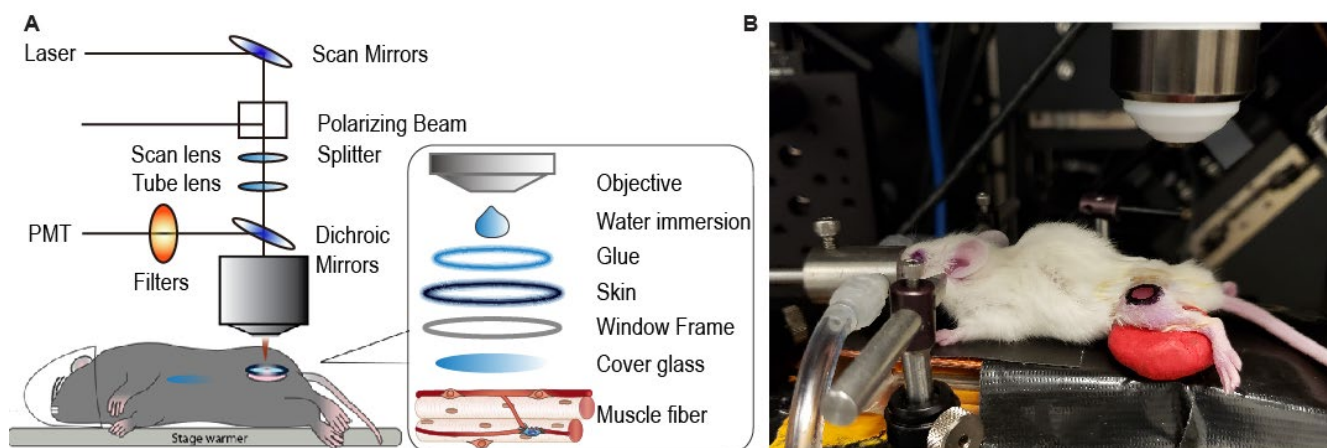


Figure 1. The scheme of mouse intravital imaging setup for hindlimb skeletal muscle using a multiphoton microscope. (A) The intravital imaging setup for hindlimb skeletal muscle includes an anesthetic table with a heating pad under objective, a stage to fix the muscle pulsatile movement of the hindlimb, a coverglass, window frame, glues, water immersion, and multi-photon microscope. **(B)** A mouse is positioned in the microscope setup.

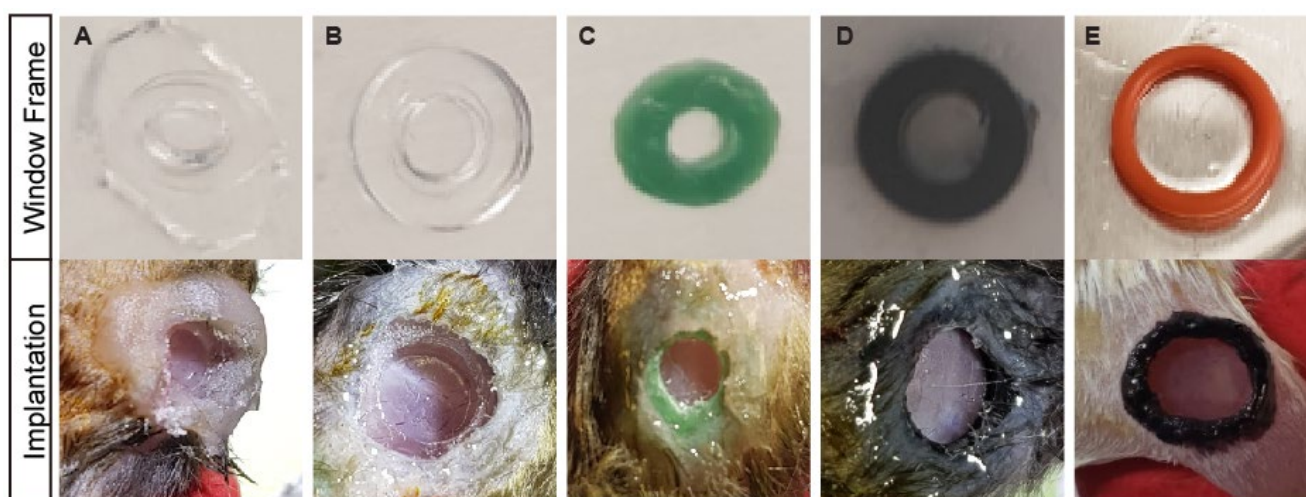


Figure 2. The window implantation optimization for optical access on hindlimb skeletal muscle using different materials and gluing systems. (A) Manually carved PDMS ring (upper) after implantation on hindlimb (bottom) **(B)** Punched PDMS ring **(C)** 3D printed PLA ring (4 mm inner circle, 6 mm outer circle) **(D)** 3D printed PLA ring (6 mm inner circle, 7 mm outer circle) **(E)** 8 mm diameter silicone ring and 8 mm glass cover

5.2.2 Optimization of labeling vascular system

To probe the vascular system, we tested if FITC conjugated dextran can label blood vessels, and compared with Cdh5-creERT;tdT mice using multiphoton microscopes (Cruz Hernández et al., 2019). Cdh5creERT mice were floxed with Td-tomato mice, which expresses a bright fluorescence signal in Cdh5 (Ve-cadherin) expressing vascular cells. The dextran conjugated with FITC injection through intravenous allows visualizing bloodstream. We found dextran-FITC injection was sufficiently colocalized with Cdh5-Tdt and sufficient support to visualize vasculature for long hours of imaging (**Figure 3**). Unexpectedly, the second harmonic generation which is previously described to visualize the fiber structure was not seen as apparent when we used a two-photon microscope (Olympus 10X/1030nm Satsuma laser) (Webster et al., 2016a).

5.2.3 Optimization of multiphoton microscopy for imaging MuSCs

Next, using the intravenous dextran fluorescence probe system, we labeled both vascular network and muscle progenitors after transplanting the GFP expressing myogenic progenitors (**Figure 4**). The myogenic progenitors were isolated from GFP-expressing mice and 200.000 cells were injected into the vastus lateralis muscle after notexin-induced muscle injury. To visualize the vasculature and skeletal muscle progenitors, we used a three-photon microscope (Olympus 25X, water immersion/ 1320nm laser). With this modality, we could reach 1-2 mm depth tissue from the cover glass, yet the best image can be acquired at - 0.9851mm. Nevertheless, we found that the successfully engrafted myogenic progenitors were in contact with blood vessels and the myofiber by third-harmonic generation structured with the vessels around (**Figure 4**).

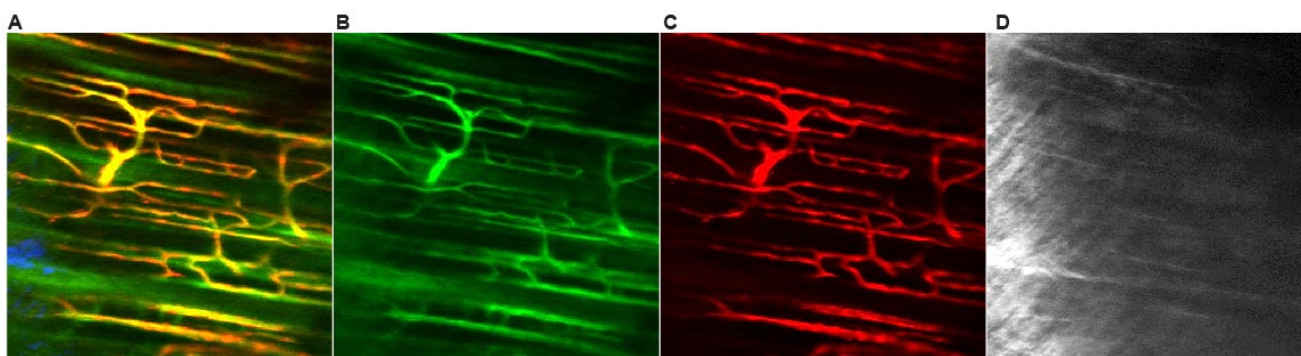


Figure 3. The intravital imaging of the vasculature in hindlimb skeletal muscle using Cdh5-cre Td-tomato expressing (A) Overlay of the images from FITC-dextran (green), Cdh5-TdT (red), and second harmonic channel (blue) (B) FITC-dextran labeled blood flux (C) Cdh5-Tdt (D) Second Harmony in gray

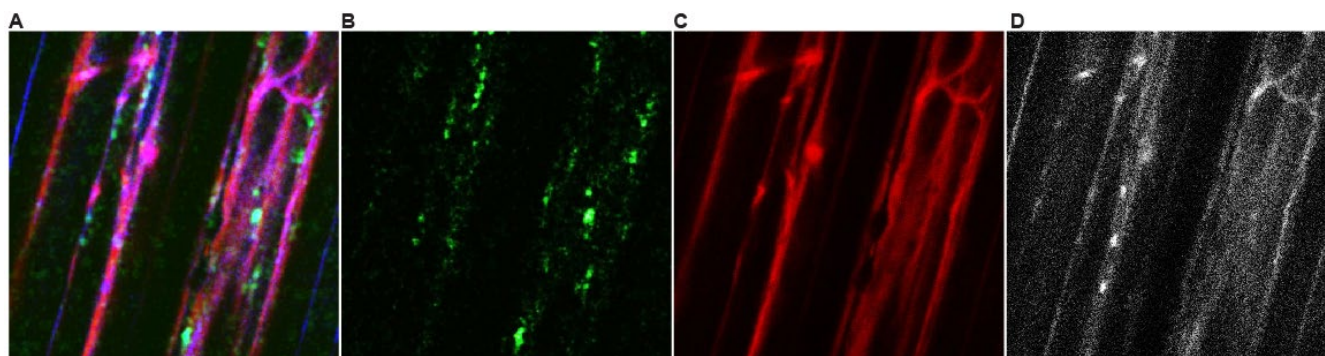


Figure 4. Images of the vasculature and myogenic progeny in hindlimb skeletal muscle. (A) Overlay of myoblasts engraftment (green), blood flow (red), and third harmonic channel (blue). (B) Green fluorescent protein-expressing myoblasts engrafted in muscle fiber. (C) Texas red dextran labeled blood flux. (D) Third harmonic in grey.

5.3 Discussion and Conclusion

From our previous chapters described above, we learned about interesting communications between vasculature or vessel forming cells and myogenic cells. We observed that the myokine, apelin remodels vasculature upon muscle injury and endothelial cells contribute to SKMP activation in a glucose-dependent manner. However, these conclusions are largely derived by histological and in-vitro experimental analysis, and we still lack an anatomical and kinetic understanding of how this relationship contributes to muscle repair through vascular patterning and muscle stem cell (MuSC) activation. Using multiphoton imaging is novel and differentiated, yet, essential for elucidating the role of microvasculature in muscle regeneration. Therefore, I initiated to develop a non-invasive live deep tissue imaging using multiphoton microscopy to probe the dynamics of vasculature and single satellite cells in skeletal muscle.

The section of the study mainly described and focused on the protocol optimized a window system to chronically monitor the vasculature and myogenic population in a living animal using multi-photon microscopy. We were able to install a chronic window that is attached intact in a hindlimb muscle without interfering with the mouse activity for longer than 4 days. Using this method, we obtained the microvasculature visualization system in skeletal muscle *in vivo* with and without transgenic reporter mice. Furthermore, we were able to visualize the SKMPs by reporter cell injection with a muscle injury, which will give an optimal system to monitor the engraftment process of skeletal muscle progenitors after cell transplantation. This will allow tracing satellite cells and vascularization dynamics during muscle regeneration in a live animal without sacrificing mice, which has not been possible in the previous *in-vivo* imaging (Verma et al., 2018a; Webster et al., 2016a, 2016b).

Although there are many biological questions we want to answer using this system, due to the Covid19 pandemic, the collaboration to use a multiphoton microscope had been restricted and further testing and optimizing detection methodology of endogenous MuSCs and vascular cells are postponed. The challenge was unforeseen and requires further research to complete. Although this dissertation chapter did not answer one of my fundamental biological questions, this project supports fundamental techniques to deepen the understanding of temporal and spatial mechanisms of muscle repair not only relating to muscle biology, but also for general research on cellular communication and vascular

remodeling during tissue repair. I believe that this approach can shift methodological paradigms to study other regulatory pathways during muscle regeneration as well as the role of the vasculature in the other fields of regenerative biology.

Section 6: Perspective

6.1 Summary and Perspective

This dissertation focuses on the inter-cellular regulation between myogenic cells and endothelial cells. By addressing the three specific chapters, we demonstrate the crosstalk of myogenic cells with endothelial cells and the vasculature to coordinate local niche interactions and systemic crosstalks. In the first chapter (**Section 3**), I demonstrated transcriptional mechanisms of apelin production in myofibers and their role in muscle regeneration through vascular remodeling. I addressed the following main outcomes in this session.

- We identified the myogenic transcription factor TEA domain family member 1 (*Tead1*) as a regulator of *Apln* transcription through a yeast one-hybrid screen of transcription factor binding to the apelin promoter. Myofiber-specific over-expression of *Tead1* suppresses apelin secretion at the whole-body level.
- Single-cell transcriptomic analysis of regenerating skeletal muscle revealed that *Ap1nr* (Apelin receptor) is enriched in muscle endothelial cells, whereas *Tead1* is enriched in myogenic cells. The elevated apelin secretion via *Tead1* knock-down in muscle cells stimulates endothelial cell proliferation in co-cultures.
- We showed that apelin peptide supplementation *in vivo* enhances endothelial cell expansion following muscle injury. Altogether, we conclude that paracrine crosstalk in which apelin secretion controlled by *Tead1* in myogenic cells influences endothelial remodeling during skeletal muscle repair.

Our experiments open translational opportunities by proving that apelin-mediated activation of angiogenesis can be further enhanced beyond its endogenous tone through therapeutic activation of apelin signaling *in vivo*. Importantly, our co-culture, conditioned medium and myofiber specific overexpression experiments also establish directionality in the apelin-mediated myogenic-angiogenic crosstalk by proving that *Tead1* regulation of apelin in myogenic cells directly modulates endothelial cells. Considering the importance of capillarization in skeletal muscle in muscle size and function, our results support a model

where the regulation of endothelial cell remodeling and angiogenesis by apelin contributes to the reported benefits of apelin treatment on muscle mass and muscle strength.

In the second chapter (**Section 4**), I show that *Ndr1* promotes muscle progenitor-endothelial cell interactions that lead to enhanced stem cell activation. The main outcomes are highlighted as follow:

- We discovered that endothelial cells synergistically enhance skeletal muscle progenitor proliferation in a low glycemic environment, while fibroblasts and macrophages had no effect.
- We observed that the crosstalk between SKMPs and endothelial cells was mediated by direct cell-cell contacts independent of soluble paracrine signals.
- Transcriptomic analysis revealed that the endothelial alpha/beta hydrolase N-Myc Downstream Regulated1 (NDRG1) is induced by a low glycemic environment and is associated with biological adhesion.
- SKMPs co-cultured with *Ndr1* knock-down endothelial cells lose their synergistic functional relationship in response to glucose levels. Collectively, our findings suggest that *Ndr1* is a key mediator of endothelial cell-mediated glycemic control of SKMPs and provides a link between systemic energy levels and the skeletal muscle stem cell niche.

Overall, our results support the notion that the vascular stem cell niche integrates systemic energy levels through ECs to control SKMP function. Our new findings raise the therapeutic potential of endothelial cells using low-glucose conditions for muscular diseases. As previous in-vivo experiments demonstrated that higher vascular density increases the frequency of muscle stem cells in MDX mice, our new target *Ndr1* in endothelial cells could be applicable to ameliorate muscular dystrophy which is caused by muscle stem cell malfunctioning.

In the last chapter (**Section 5**), I describe the development process of in vivo multi-photon intravital imaging of myogenic progenitors and microvessels to examine the effect of engraftment of muscle progenitors in intact mice. The main accomplishments are pointed below:

- We successfully optimized the long-lasting- chronic window frame to optically access hindlimb muscle during recovery.
- We developed an endogenous endothelial cell labeling system and monitored MuSC engraftment after cell transplantation in a living animal.
- We discovered that most of the muscle progenitors which successfully engrafted in skeletal muscle were located in close proximity to the vasculature.

This approach offers a great promise for the development of a robust tool to monitor muscle repair dynamics in real-time with spatial information of the vascular network. Altogether, my dissertation chapters bring together a complementary set of cellular mechanisms with reciprocal co-regulatory effects between myogenic and endothelial cell fates and established a competitive tool to investigate them in a living animal. I believe that this approach can shift methodological paradigms to study other regulatory pathways during muscle regeneration as well as the role of the vasculature in the other fields of regenerative biology.

6.2 Future Directions

From my dissertation chapters, we learned about intriguing reciprocal communication between myogenic and endothelial cells and established a competitive tool to monitor them in a living animal. Despite our findings, the observations open up numerous subsequent questions.

Most of my thesis outcomes are relying on the co-culture of endothelial cells and myogenic cells, which are mainly evaluated in a typical two-dimensional system *in-vitro*. To find more physiologically relevant interaction, we would need the multiple cell types in tissue with their topological locations. By using this conventional system, we can not evaluate the secondary effects coming from other tissue-resident cells that can be initiated

by endothelial cells. Therefore, building a three-dimensional artificial niche and vessels with their complete compartments could be useful to further dissect the mechanism of co-regulation between myogenic cells and endothelial cells. In this context, engineering artificial vessels with all the compartments such as smooth muscle cells and pericytes could be an intriguing next step in the future.

Other important questions we must ask include; Can we observe the specific states of myogenesis during different angiogenesis states in controlled environments? Can we observe the local genetic expression dynamically changes during these adaptations? In my dissertation, we could not profile the specific fates of myogenic cells in their crosstalk with endothelial cells. I believe that the new technical advance in multiplex in-situ will enable us to decode the specific regulatory circuits between the vascular niche and myogenic cell fates.

Furthermore, the vasculature in skeletal muscle provides a trophic function by rapid and transient vasodilation depending on the metabolic demands, which is possibly involved in myogenic cell function. With the current technologies, monitoring myogenic cells in the controlled vascular tone is still limited. Hence, developing a quantitative monitoring system of local hyperemia would be necessary to understand the fundamental metabolic function of vasculature in myogenic cell interaction.

Developing the therapeutic intervention using the intercellular targets must be one of the main future directions. In the context of aging, finding small molecules, mRNAs, microRNAs targeting intercellular signals is particularly beneficial as both vascular and muscle health drastically decline in aging. In addition, myogenic cell transplantation is in the active investigation in myogenic dystrophy diseases. However, people often face engraftment failure due to the inadequate vascularization of the implanted cells. By incorporating transplantation and angiogenic signals, we could potentially increase the success rate of cell engraftment. Lastly, the intravital imaging techniques would be further applicable to follow up the questions by providing temporal and spatial mechanisms of cellular communication with the vasculature. I am planning to keep working on developing bioimaging, asking stem cell biological questions, trying to solve them, and finding the intervention by applying what I learned from my Ph.D. research.

Appendix

The Exerkine Apelin Reverses Age-associated Sarcopenia

Claire Vinel¹, Laura Lukjanenko², Aurelie Batut¹, Simon Deleruyelle¹, Jean-Philippe Pradère¹, Sophie Le Gonidec¹, Alizée Dortignac¹, Nancy Geoffre¹, Ophelie Pereira¹, Sonia Karaz², **Umji Lee**², Mylène Camus³, Karima Chaoui³, Etienne Mouisel¹, Anne Bigot⁴, Vincent Mouly⁴, Mathieu Vigneau⁵, Allan F. Pagano⁶, Angèle Chopard⁶, Fabien Pillard¹, Sophie Guyonnet⁷, Matteo Cesari⁷, Odile Burlet-Schiltz³, Marco Pahor⁸, Jerome N. Feige², Bruno Vellas⁷, Philippe Valet^{1,9} and Cedric Dray^{1,9*}

¹Institut des Maladies Métaboliques et Cardiovasculaires, INSERM U1048, Université de Toulouse, Université Paul Sabatier, Toulouse, France.

²Aging Department, Nestlé Institute of Health Sciences SA, Ecole Polytechnique Fédérale de Lausanne Innovation Park, Lausanne, Switzerland.

³Institut de Pharmacologie et de Biologie Structurale–CNRS, Université de Toulouse, Université Paul Sabatier, Toulouse, France.

⁴Institut de Myologie, Université Pierre et Marie Curie, Paris 6 UM76, Univ. Paris 6/U974, UMR7215, CNRS, Pitié-Salpêtrière–INSERM, UMRS 974, Paris, France.

⁵Institut des Technologies Avancées en Science du Vivant–USR3505 Centre Pierre Potier, Toulouse, France.

⁶Université de Montpellier, Institut National de la Recherche Agronomique, UMR866 Dynamique Musculaire et Métabolisme, Montpellier, France.

⁷Gérontopole Toulouse-Purpan UMR 1027, Toulouse, France.

⁸Institute on Aging, College of Medicine, University of Florida, Gainesville, FL, USA.

Corresponding Author :

cedric.dray@inserm.fr

As a collaborative work with Toulouse University, we demonstrated that the plasma level of apelin was not only significantly declined with aging but was also dramatically reduced in sarcopenia patients, suggesting that apelin can be a biomarker of sarcopenia. Moreover, elderly patients with a higher level of apelin showed an increase in performance after exercise. The supplementation of apelin peptide in mice was able to enhance mitochondria biogenesis, autophagy and exerted anti-inflammatory effects. Particularly, we further identified that apelin signaling was perturbed in muscle stem cells in aging, and apelin restoration could enhance satellite cell function, enhancing muscle regeneration. Altogether, these results indicate that apelin can be a target for restoring muscle function in sarcopenia.

Status of the publication:

Published July 30, 2018, in Nature Medicine

<https://doi.org/10.1038/s41591-018-0131-6>

Author contribution :

This project is added to my thesis as I started my Ph.D. by joining this project in the Feige lab which leads muscle regeneration and muscle stem cell approaches in this manuscript. During the revisions, I tested the role of apelin to enhance muscle stem cell activity and regeneration in aged mice. I have characterized the histological phenotype in aged mice treated with apelin during muscle regeneration by quantifying Pax7 expressing MuSCs and proliferating Ki67⁺/Pax7⁺ cells (**Figure 5 I-K**). The systemic injection with apelin at 0.5 mol/kg, I.P significantly increases the number of Pax7⁺ muscle progenitors as well as the percentage of proliferating Pax7⁺/Ki67⁺ MuSCs at 7 days post-injury, at the peak of MuSC amplification. This result confirms that apelin has a beneficial effect on muscle regeneration in old mice by enhancing muscle stem cell activation.

Abstract

Sarcopenia, the degenerative loss of skeletal muscle mass, quality, and strength, lacks early diagnostic tools and new therapeutic strategies to prevent the frailty-to-disability transition often responsible for the medical institutionalization of elderly individuals. Herein we report that production of the endogenous peptide apelin, induced by muscle contraction, is reduced in an age-dependent manner in humans and rodents and is positively associated with the beneficial effects of exercise in older persons. Mice deficient in either apelin or its receptor (APLNR) presented dramatic alterations in muscle function with increasing age. Various strategies that restored apelin signaling during aging further demonstrated that this peptide considerably enhanced muscle function by triggering mitochondriogenesis, autophagy, and anti-inflammatory pathways in myofibers as well as enhancing the regenerative capacity by targeting muscle stem cells. Taken together, these findings revealed positive regulatory feedback between physical activity, apelin, and muscle function and identified apelin both as a tool for diagnosis of early sarcopenia and as the target of an innovative pharmacological strategy to prevent age-associated muscle weakness and restore physical autonomy.

Keywords; Sarcopenia, Myokine, Exerkine, Apelin, Mitochondriogenesis, Autophagy, Anti-inflammation

The exerkin apelin reverses age-associated sarcopenia

Claire Vinel¹, Laura Lukjanenko², Aurelie Batut¹, Simon Deleruyelle¹, Jean-Philippe Pradère¹, Sophie Le Gonidec¹, Alizée Dortignac¹, Nancy Geoffre¹, Ophelie Pereira¹, Sonia Karaz², Umji Lee², Mylène Camus³, Karima Chaoui³, Etienne Mouisel¹, Anne Bigot⁴, Vincent Mouly⁴, Mathieu Vigneau⁵, Allan F. Pagano⁶, Angèle Chopard⁶, Fabien Pillard¹, Sophie Guyonnet⁷, Matteo Cesari⁷, Odile Bulet-Schiltz³, Marco Pahor⁸, Jerome N. Feige², Bruno Vellas⁷, Philippe Valet^{1,9*} and Cedric Dray^{1,9*}

Sarcopenia, the degenerative loss of skeletal muscle mass, quality and strength, lacks early diagnostic tools and new therapeutic strategies to prevent the frailty-to-disability transition often responsible for the medical institutionalization of elderly individuals. Herein we report that production of the endogenous peptide apelin, induced by muscle contraction, is reduced in an age-dependent manner in humans and rodents and is positively associated with the beneficial effects of exercise in older persons. Mice deficient in either apelin or its receptor (APLNR) presented dramatic alterations in muscle function with increasing age. Various strategies that restored apelin signaling during aging further demonstrated that this peptide considerably enhanced muscle function by triggering mitochondriogenesis, autophagy and anti-inflammatory pathways in myofibers as well as enhancing the regenerative capacity by targeting muscle stem cells. Taken together, these findings revealed positive regulatory feedback between physical activity, apelin and muscle function and identified apelin both as a tool for diagnosis of early sarcopenia and as the target of an innovative pharmacological strategy to prevent age-associated muscle weakness and restore physical autonomy.

Maintaining the independence and physical functions of the elderly both preserves their lifestyle and dignity and considerably reduces the direct and indirect healthcare costs associated with disability^{1,2}. Sarcopenia, recently recognized as a disease by the World Health Organization³, is the degenerative loss of skeletal muscle strength and mass with aging, which contributes to the progressive loss of autonomy in the elderly. In addition, sarcopenia is tightly correlated with the development of other age-associated pathologies, such as osteoporosis, heart failure and cognitive disorders^{4,5}. Consequently, the loss of mobility and locomotion is increasingly considered to be one of the strongest predictors of negative health outcomes in the elderly population^{4,6–8}. In this context, different strategies have been proposed to preserve these functional capacities. Because of its positive effects on protein turnover and improved metabolism in myofibers and activation of satellite cells, physical exercise is currently considered the most effective approach to impede age-associated muscle atrophy. However, exercise is often impractical or inefficient for individuals with reduced functional capacities. Several pharmacological approaches have been proposed to counteract or slow the onset of sarcopenia, mainly focused on treatments that provide sex hormones, such as testosterone, growth hormone or dehydroepiandrosterone (DHEA), but their results are variable and frequently have side effects and/or only lead to marginal gains in muscle strength (for a review, see ref. ⁹). Thus the

development of new alternatives based on sarcopenia's pathophysiological mechanisms are worthy of further investigation.

One such dysfunction, which contributes to the decline of skeletal muscle during aging, is the mitochondrial-driven impairment of myofiber metabolism, characterized by decreasing energy supply and protein turnover and increasing reactive oxygen species production¹⁰. A better understanding of these mechanisms has been achieved through experiments involving caloric restriction and exercise, which have identified cellular pathways, such as AMP kinase (AMPK), peroxisome proliferator-activated receptor gamma coactivator 1 (PGC-1 α) and autophagy and mitophagy, associated with the decline of mitochondrial biogenesis and activity during aging^{11–13}. In parallel, physical exercise has revealed the importance of muscle cell progenitors (i.e., satellite cells) in muscle plasticity and that physical exercise contributes to muscle renewal by stimulating these stem cells¹⁴, although this renewal is limited in older individuals^{15,16}. Mitochondrial homeostasis could also play a critical role in the functional decline of these stem cells, in a manner similar to that which is seen in myofibers^{12,13}.

We identified apelin, a peptide that is 13 to 36 amino acids in length, as an exercise-induced myokine able to enhance both muscle cell metabolism and stem cell function during aging. Apelin has been used to induce beneficial metabolic effects by reducing obesity-related insulin resistance^{17–19}. Apelin increased

¹Institut des Maladies Métaboliques et Cardiovasculaires, INSERM U1048, Université de Toulouse, Université Paul Sabatier, Toulouse, France. ²Aging Department, Nestlé Institute of Health Sciences SA, Ecole Polytechnique Fédérale de Lausanne Innovation Park, Lausanne, Switzerland. ³Institut de Pharmacologie et de Biologie Structurale–CNRS, Université de Toulouse, Université Paul Sabatier, Toulouse, France. ⁴Institut de Myologie, Université Pierre et Marie Curie, Paris 6 UM76, Univ. Paris 6/U974, UMR7215, CNRS, Pitié-Salpêtrière–INSERM, UMRS 974, Paris, France. ⁵Institut des Technologies Avancées en Science du Vivant–USR3505 Centre Pierre Potier, Toulouse, France. ⁶Université de Montpellier, Institut National de la Recherche Agronomique, UMR866 Dynamique Musculaire et Métabolisme, Montpellier, France. ⁷Gérontopole Toulouse–Purpan UMR 1027, Toulouse, France. ⁸Institute on Aging, College of Medicine, University of Florida, Gainesville, FL, USA. ⁹These authors jointly directed this work: Philippe Valet, Cedric Dray. *e-mail: cedric.dray@inserm.fr

mitochondrial function and biogenesis by stimulating AMPK and AKT through its G_α subunit (G_α)_i-coupled receptor APJ (also known as APLNR) in muscle cells¹⁹. In the present study, we further establish the strong links between apelin and physical exercise^{20,21} and report, for the first time to our knowledge, that in vivo apelin production by myofibers is stimulated by exercise-associated muscle contraction in rodents and humans. During aging, apelin synthesis in skeletal muscle is reduced and plasma apelin levels decrease, suggesting that the peptide may play a role in sarcopenia. In addition, we have observed an accelerated onset of sarcopenia using both whole-body and muscle-specific apelin-deficient mice. Conversely, aged mice, supplemented with a daily injection of apelin or overexpressing apelin via an adenovirus-mediated gene transfer to skeletal muscle, exhibited improved muscle capacities and myofiber hypertrophy. We found that apelin-induced muscle enhancement is achieved through the stimulation of metabolic (AMPK, mitochondriogenesis), trophic (Forkhead box O3 (FOXO3)–MURF-1–atrogin axis) and regenerative pathways targeting either mature myofibers and/or satellite cells. Finally, this study clearly demonstrates that the impairment of the identified regulatory loop involving physical exercise, apelin and skeletal muscle dramatically contributes to sarcopenia while paving the way for the development of new diagnostic and therapeutic applications.

Results

Activity-induced muscle apelin production is blunted during aging. We found that age-related loss of muscle assessed by appendicular lean mass evaluation (as previously proposed²²) in the MAPT cohort²³ of elderly people is associated with a specific decrease in plasma apelin immunoreactivity levels (Supplementary Fig. 1 and Supplementary Tables 1 and 2). Compared to other cytokines and hormones (i.e., leptin, insulin, interleukin-6 (IL-6) and IL-8, nerve growth factor (NGF) or monocyte chemoattractant protein-1 (MCP-1)), plasma apelin immunoreactivity was specifically associated with sarcopenia independently of body weight and fat mass (Supplementary Fig. 1 and Supplementary Table 2). Consistent with these observations, in a mouse model of aging (at 3, 12 and 24 months of age), plasma apelin levels, as determined by immunoreactivity (Fig. 1a) or by the liquid chromatography–mass spectrometry (LC–MS) technique (Supplementary Fig. 2a–e), were lower in an age-dependent manner and were associated with a specific loss of skeletal muscle *Apln* and *Aplnr* mRNA expression (Fig. 1b and Supplementary Fig. 2f). The age-associated lower apelin expression was confirmed in isolated mouse muscle fibers from these groups of mice by mRNA expression and anti-apelin immunofluorescence labeling (Fig. 1c–e and Supplementary Fig. 2g), as well as in cultured human differentiated myocytes obtained from young (16–27 years old) and aged (68–83 years old) donors (Fig. 1f and Supplementary Fig. 2h).

Altogether, these data collected in humans and rodents highlight the tight relationship between aging and skeletal muscle apelin and led us to investigate the regulatory pathways underlying muscle apelin production. As we previously identified physical exercise as a potential enhancer of muscle apelin production in obese subjects²⁰, we first measured apelin secretion by human muscle cell lines stimulated by forskolin (Fig. 1g) or by an electric stimulus (Fig. 1h) in order to mimic the effects of muscle contraction in vitro. Although both stimulations showed significantly increased apelin secretion in culture medium of human cells originating from young donors, this upregulation was reduced in muscle cells from aged donors (Fig. 1g,h). This observation was confirmed in vivo by evaluating plasma venous–arterial differences in apelin immunoreactivity levels following sciatic nerve electrical stimulation–induced muscle contraction in mice. Indeed, a dramatic age-dependent decrease in muscle apelin release into the bloodstream after contraction

was observed (Fig. 1i) and could explain, at least in part, the deficiency of increased plasma apelin immunoreactivity during acute physical exercise in middle-aged (12 months) and aged (24 months) mice (Fig. 1j). However, 4 weeks of training promoted muscle apelin expression (Fig. 1k) and subsequently increased plasma apelin immunoreactivity (Fig. 1l) in young and middle-aged mice, suggesting that loss of exercise-induced muscle apelin production could be reversed by chronic exercise until middle age. Similarly, 5 d of forskolin treatment induced a dose-dependent increase of *Apln* gene expression in myotubes from young and aged donors, indicating that the intrinsic capacity of muscle cells to produce apelin was conserved regardless of aging (Fig. 1m). Conversely, a definitive link between apelin and muscle activity was provided by hindlimb unloaded mice exhibiting a specific association between apelin expression decrease and the degrees of atrophy among the hindlimb muscles (Fig. 1n and Supplementary Fig. 2i–m). Such an age-dependent loss of muscle apelin production, combined with plasma apelin deregulation, led us to investigate the consequences of apelin or its receptor depletion in mice to better understand the role of apelin in muscle homeostasis and function during aging.

Apln and *Aplnr* deficiency dramatically accelerated muscle aging.

Apelin-deficient mice (*Apln*^{−/−}) died prematurely (Supplementary Fig. 3a) compared to wild-type littermates, probably owing to cardiac deficiencies²⁴. Accordingly, we investigated the consequences of apelin deficiency on skeletal muscle in 12-month-old *Apln*^{−/−} mice. At this age, the lack of apelin induced an acceleration of muscle loss, as demonstrated by a decrease of lean tissue mass resulting from skeletal muscle fiber hypoplasia and atrophy compared to wild-type mice (Fig. 2a–c and Supplementary Fig. 3b–d). Moreover, apelin deficiency affected similarly different muscle fibers types since glycolytic and oxidative fiber areas were decreased to the same extent (Fig. 2c). Previous mechanistic studies have demonstrated that apelin plays a role in muscle mitochondriogenesis in the context of insulin resistance^{19,25}. To further investigate whether mitochondria were targeted by apelin deficiency during aging, we analyzed the shape, quantity and function of the organelle in apelin-deficient mice (Fig. 2d–h and Supplementary Fig. 3e). Intramyofibrillar mitochondria number was lower in apelin-deficient mice than in wild-type mice (Fig. 2d–f), alongside the accumulation of cristae implying mitochondria alterations (Fig. 2d). Moreover, activities of enzymes related to mitochondria, such as citrate synthase or aconitase, were also dramatically lower, independent of the number of organelles (Fig. 2g,h). This suggests that apelin could promote mitochondriogenesis and provide a beneficial impact on oxidative stress during aging. We next performed in situ contractility tests consisting of the evaluation of strength development in plantaris or tibialis anterior muscles following electric-stimulated contraction of the sciatic nerve. Compared to wild-type mice, we found that both muscles displayed a lower tetanic contractile capacity in apelin-deficient mice (Fig. 2i,j). Consequently, in vivo experiments demonstrated that *Apln*^{−/−} mice exhibited a weaker strength, as measured by grip test, as well as decreased speed and grid-hanging capacities than wild-type mice of the same age (Fig. 2k–m). The crucial role of apelin in muscle physiology during aging was confirmed by targeting *Aplnr* (Fig. 2k–m and Supplementary Fig. 3f). In contrast with apelin-deficient mice, maximal speed was not significantly altered by *Aplnr* reduction, whereas strength in the grip test and grid-hanging capacity were deteriorated to the same extent. Interestingly, this result suggests that a weak skeletal muscle expression of *Aplnr* (Supplementary Fig. 3f) was sufficient to preserve certain muscle functions, such as running, but not hanging capacity or strength. Altogether, these results clearly demonstrate that, as observed during aging, systemic loss of apelin–APLNR signaling accelerates muscle atrophy and that apelin and its receptor are necessary to maintain muscle physiology during aging. However, the

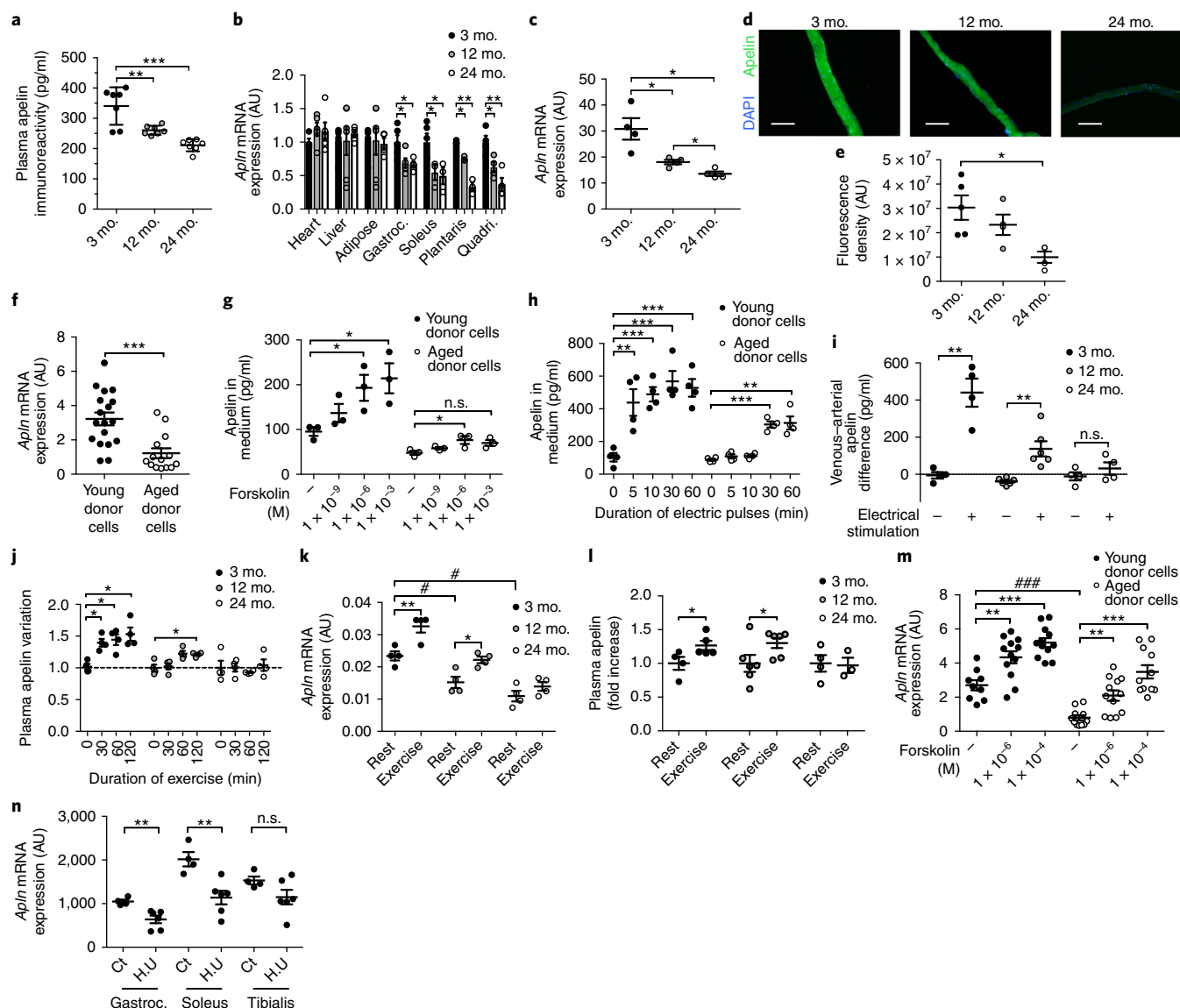


Fig. 1 | Aged skeletal muscle has a reduced capacity for apelin production. **a, b**, Plasma immunoreactivity ($n = 7$ mice per group) (**a**) and mRNA expression levels of apelin from the indicated tissues ($n = 5$ mice per group) (**b**) in middle-aged (12 months, gray circle) and aged (24 months, white circle) mice compared to young animals (3 months, black circle) ($n = 7$ mice per group). Gastroc., gastrocnemius muscle; Quadri., quadriceps muscle; AU, arbitrary units. **c–e**, *Apln* mRNA expression ($n = 5$ mice per group) (**c**), representative pictures ($n = 5$ mice per group for 3 mo. and $n = 4$ mice per group for 12 mo. and 24 mo.) of apelin immunolabeling (**d**) and associated fluorescence quantification in plantaris-isolated fibers in mice ($n = 5$ mice per group for 3 mo. and $n = 4$ mice per group for 12 mo. and 24 mo.) (**e**). Scale bars, 30 μm . **f**, Apelin expression in differentiated myotubes from aged and young human donors ($n = 3$ independent experiments from 3 different donors in each group). **g, h**, Apelin accumulation in medium from human myotubes after various doses of forskolin treatment (**g**) and duration of electrical pulse contractions (**h**) ($n = 3$ different donors in each group). **i**, Difference in plasma venous-arterial apelin immunoreactivity in the basal condition (-) or following electrical sciatic nerve stimulation (+) of young (3 mo., black circles), middle-aged (12 mo., gray circles) or aged (24 mo., white circles) mice ($n = 5$ mice per group). **j**, Ratio of plasma apelin immunoreactivity between baseline values and those after 30, 60 or 120 minutes of treadmill-mediated physical exercise in young (3 mo.), middle-aged (12 mo.) and aged (24 mo.) mice ($n = 4$ mice per group). Basal values of plasma apelin immunoreactivity are 385.2 ± 5.6 pg/ml; 260.4 ± 5.8 pg/ml and 211.6 ± 4.2 pg/ml for mice aged 3, 12 and 24 mo., respectively. **k, l**, *Apln* mRNA expression in tibialis muscle ($n = 4$ mice per group) (**k**) and plasma apelin protein levels compared to rest ($n = 6$ mice per group) (**l**) after a chronic bout of daily exercise (30 min treadmill per day, 28 d). Basal values of plasma apelin immunoreactivity are 306.9 ± 31.7 pg/ml; 258.2 ± 9.0 pg/ml and 208.2 ± 13.6 pg/ml for mice aged 3, 12 and 24 mo., respectively. **m**, *Apln* mRNA expression in differentiated human donor myotubes following a long-term forskolin treatment (5 d) ($n = 3$ independent experiments with 3 different donors in each group). **n**, *Apln* mRNA expression in skeletal muscles after 14 d of hindlimb unloading (H.U.) versus normal loaded control mice (Ct) ($n = 6$ mice per group). *Hprt* was used as a standard housekeeping gene, and *Apln* mRNA expression is presented relative to *Hprt* expression (**b, c, f, k, m, n**). Data presented are means \pm s.e.m. * $P < 0.05$; ** $P < 0.01$ and *** $P < 0.001$; one-way ANOVA with post hoc Tukey's multiple comparison test (**a, c, e**). * $P < 0.05$; ** $P < 0.01$ and *** $P < 0.001$; one-way ANOVA with post hoc Dunnett's multiple comparison test (**b, g, h, j, m**). * and # $P < 0.05$; ** $P < 0.01$ and *** and ### $P < 0.001$; two-tailed Student's *t*-test (**f, i, k, l, n**). n.s. (not significant) $P > 0.05$.

use of whole-body apelin-knockout mice did not allow discrimination between the local and systemic roles of apelin on muscle physiology during aging.

To that aim, we induced skeletal muscle-specific apelin knockdown in middle-aged mice by retro-orbitally delivering a GFP-expressing adeno-associated virus (AAV8-GFP) containing muscle creatine

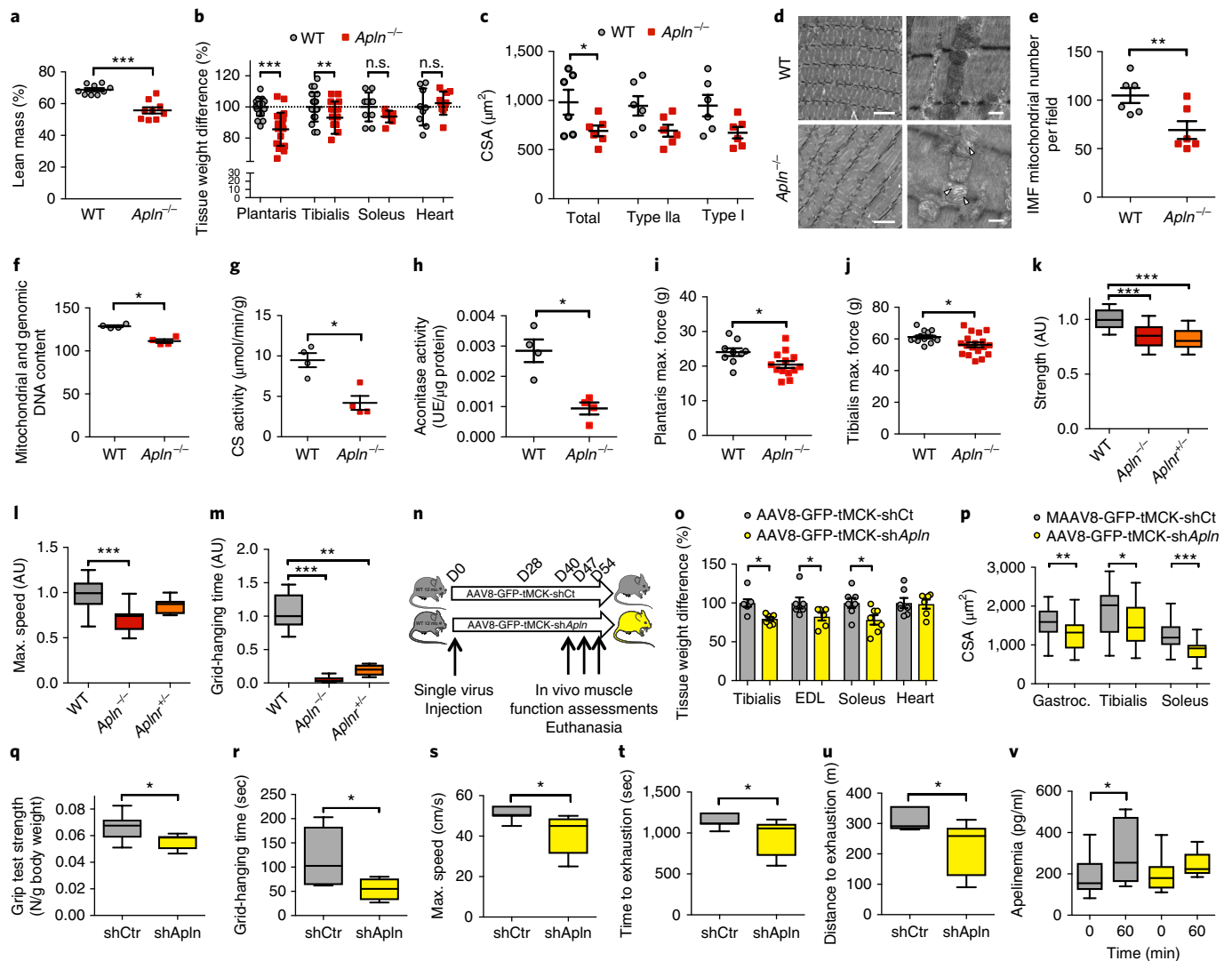


Fig. 2 | *Apln* and *Aplnr* deficiency have consequences on muscle aging. **a**, Percentage of total lean mass normalized to body weight of *Apln*^{-/-} mice (red squares) compared to control littermates (gray circles) at 12 months of age ($n = 9$ mice per group). **b**, Comparison of *Apln*^{-/-} mice muscle mass with controls ($n = 20$ mice per group for plantaris and tibialis and 9 mice per group for soleus and heart). **c**, Cross-sectional area (CSA) of total, glycolytic and oxidative fibers of plantaris muscle ($n = 6$ mice per group). **d**, **e** Representative electron photomicrographs of longitudinal section of tibialis muscle myofibers from 12-month-old wild-type and *Apln*^{-/-} mice (**d**) and associated quantification of intramyofibrillar (IMF) mitochondria number (**e**). White arrowheads indicate cristae accumulation in mitochondria. Scale bars: left panels, 5 μm ; right panels, 0.5 μm ($n = 6$ mice per group, 3 pictures/animal). **f**, Mitochondrial DNA content evaluated by the ratio of a mitochondrial encoded gene (*Cox1*) and a nuclear-encoded gene (*Ppia* encoding for cyclophilin A) in tibialis muscle ($n = 4$ mice per group). **g**, **h**, Citrate synthase (CS) (**g**) and aconitase (**h**) activities in tibialis muscle ($n = 4$ mice per group). **i**, **j**, Specific plantaris ($n = 9$ WT and 13 *Apln*^{-/-} mice) (**i**) and tibialis ($n = 11$ WT and 17 *Apln*^{-/-} mice) (**j**) maximal strength evaluated in situ by electrical sciatic nerve stimulation. **k**–**m**, Grip test strength (**k**), maximal speed (**l**) and grid-hanging capacities (**m**) evaluated in *Apln*^{-/-} (red boxes) and *Aplnr*^{-/-} (orange boxes) mice relative to 12-month-old wild-type mice (gray boxes) ($n = 8$ mice per group). **n**–**u**, Muscle-specific apelin knock down accelerates age-related muscle weakness. Protocol for retro-orbital AAV-tMCK-shRNA injection and associated experiments (**n**). Muscle mass comparison of 12-month-old AAV8-GFP-tMCK-sh*Apln*-treated mice (yellow circles) with control-treated littermates (gray circles) ($n = 8$ mice per group). **o**, Cross-sectional area of gastrocnemius, soleus, and tibialis in AAV8-GFP-tMCK-sh*Apln*-treated mice (yellow boxes) and control-treated littermates (gray boxes) ($n = 8$ mice per group) (**p**). Grip test strength (**q**), grid-hanging capacity (**r**), maximal speed (**s**) and time (**t**) and distance (**u**) to exhaustion evaluated in AAV8-GFP-tMCK-sh*Apln*-treated mice (yellow boxes) and control-treated littermates (gray boxes) ($n = 8$ mice per group). **v**, Blood apelin immunoreactivity before and after acute exercise (60 min) in AAV8-GFP-tMCK-sh*Apln*-treated mice (yellow boxes) and control-treated littermates (gray boxes) ($n = 8$ mice per group). Data presented are means \pm s.e.m. for **a**, **b**, **c**, **e**, **f**, **g**, **h**, **i**, **j** and **o**. Boxplots represent median (midline), 25% and 75% percentiles (upper and lower perimeters) and maximum and minimum (tails) for **k**, **l**, **m**, **p**, **q**, **r**, **s**, **t**, **u** and **v**. * $P < 0.05$; ** $P < 0.01$ and *** $P < 0.001$; two-tailed Student's *t*-test (**a**–**c**, **e**–**j**, **o**–**u**). ** $P < 0.01$ and *** $P < 0.001$; one-way ANOVA with post hoc Dunnett's multiple comparison test (**k**–**m**). * $P < 0.05$; Paired two-tailed Student's *t*-test (**v**). n.s. $P > 0.05$.

kinase (tMCK) promoter-driven shRNA targeting *Apln* (AAV8-GFP-tMCK-sh*Apln*), and we evaluated the consequences on muscle physiology (Fig. 2n–u and Supplementary Fig. 3g–l). As expected^{26–28}, AAV8-GFP-tMCK-sh*Apln* induced skeletal muscle-specific

knockdown of apelin expression in both primarily slow- and fast-twitch muscle fibers compared to controls (Supplementary Fig. 3g), suggesting that despite the preferential expression of the MCK promoter in fast-twitch fibers, we were able to achieve a

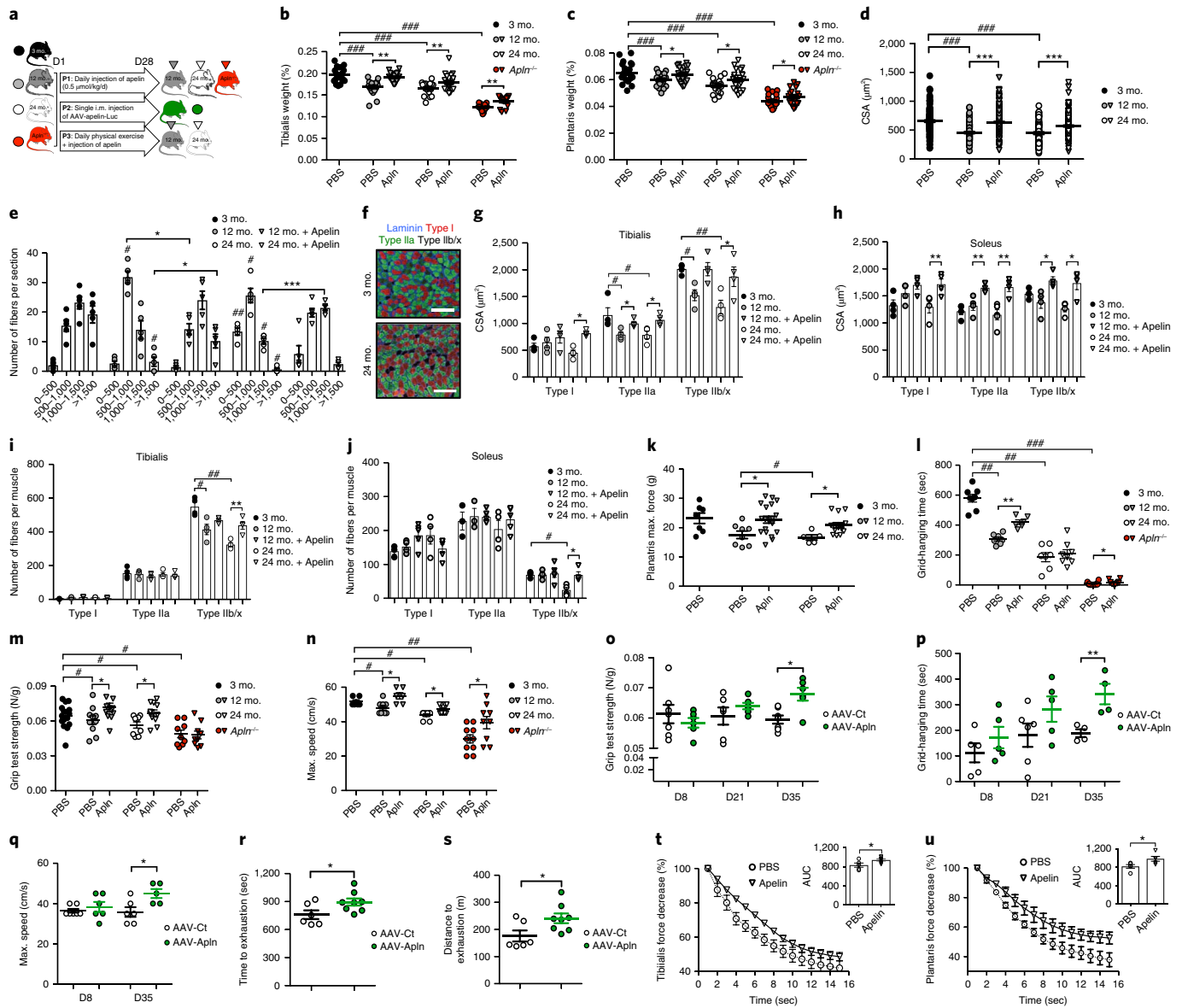


Fig. 3 | Chronic apelin supplementation reverses age-associated muscle weakness. **a**, Protocols for apelin supplementation. P1 consisted of a daily i.p. pyroglutamate-apelin-13 injection performed in wild-type (12 and 24 mo.) and in *Apln*^{-/-} (12 mo.) mice (gray, white and red triangles, respectively). P2 aimed to specifically increase muscle apelin production in aged mice (24 mo.) by intramuscular (i.m.) (tibialis and gastrocnemius) injection of an AAV1-apelin-Luc (green circles). P3 was designed to study the potential consequences of an i.p. apelin (0.5 μmol/kg/d, 28 d) injection on muscle physiology in aged mice (24 mo.) submitted to chronic exercise. **b,c**, Tibialis (**b**) and plantaris (**c**) masses relative to total body weight ($n=20$ mice per group pooled from 3 different experiments). *Apln*, daily i.p. pyroglutamate apelin-13-injected mice; PBS, daily i.p. PBS-injected mice. **d,e**, Mean of fibers cross-sectional area ($n=10$ mice per group; mean of 5 pictures per animal) (**d**) and distribution (in μm) ($n=4$ mice per group) (**e**) in tibialis. $\#P < 0.05$; two-tailed Student's *t*-test compared to 3-month-old mice. **f**, Representative pictures of myosin heavy chains isotypes (MHC) immunofluorescence in soleus muscle of young (3 mo., top) and aged (24 mo., bottom) mice. Scale bar, 100 μm. Triple-labeling with α-laminin (blue), α-MHC-I (red, Type I fibers), α-MHC-IIa (green, Type IIa fibers) allows the estimation of the Type IIb/x fibers amount (black, nonlabeled) ($n=4$ animals per group). **g-j**, Computational quantification of cross sectional area of each fiber type (**g,h**) and number of fibers per muscle (**i,j**) in tibialis and soleus muscles ($n=4$ mice per group). **k**, In situ specific plantaris maximal strength evaluated by electrical sciatic nerve stimulation ($n=8$ for PBS treatment and $n=18$ for apelin treatment). **l-n**, Grid-hanging capacity (**l**), maximal speed (**m**) and grip test strength (**n**) were evaluated in daily PBS- (circle) or apelin-treated (triangle) wild-type (3, 12 and 24 mo.; black, gray and white symbols, respectively) and *Apln*^{-/-} (12 mo., red symbols) mice ($n=10$ mice per group). **o-s**, Grip test strength ($n=6$ mice per group) (**o**), grid-hanging capacity ($n=6$ mice per group) (**p**), maximal speed ($n=6$ mice per group) (**q**) and time (**r**) and distance (**s**) to exhaustion ($n=6$ animals for AAV-Ct and $n=8$ for AAV-Apln) evaluated in aged-mice (24 mo.) after intramuscular injection of AAV1-control-Luc (white bars) or AAV1-apelin-Luc (green bars). D8 (8 d post injection), D21 (21 d post injection), and D35 (35 d post injection) represent the selected time points after full expression of the virus. **t,u**, Tibialis (**t**) and plantaris (**u**) in vivo concentric torque of aged (24 mo.) PBS- (circles) and apelin-treated (triangles) mice submitted to chronic physical exercise. Insert represents area under curve (AUC) ($n=8$ mice per group). Data are means ± s.e.m. * or $\#P < 0.05$; ** or $\#\#P < 0.01$; *** or $\#\#\#P < 0.001$; two-tailed Student's *t*-test.

considerable decrease of apelin expression in primarily slow muscles, such as soleus. Consequently, 54 days post injection (d.p.i.), mice treated with AAV8-GFP-tMCK-sh*Apln* exhibited a reduction

in muscle mass (Fig. 2o) and myofiber cross-sectional areas (Fig. 2p), without modification of regenerative processes (Supplementary Fig. 3h,i), fibrosis (Supplementary Fig. 3j,k) or number of fibers per

muscle (Supplementary Fig. 3l). In vivo, the muscle-specific knock-down of *Apln* resulted in a significant decrease in all the tested parameters, such as strength in the grip test (Fig. 2q), grid-hanging time (Fig. 2r), maximal speed (Fig. 2s) and time and distance to exhaustion (Fig. 2t,u) compared to control (AAV8-GFP-tMCK-shCt)-injected mice. Interestingly, although basal values of plasma apelin immunoreactivity were unchanged, exercise-induced apelin production was dramatically lost in mice lacking apelin in skeletal muscle (Fig. 2v). This result supports a strong impact of skeletal muscle on the variation of plasma apelin levels in response to physical exercise. Finally, considering the age-dependent decrease of apelin and its receptor in muscle, all these results suggest that altered muscle apelin production could promote, at least partially, age-associated muscle weakness leading us to investigate the effects of apelin supplementation during aging.

Apelin supplementation reverses age-associated sarcopenia.

We performed apelin supplementations in mice using a systemic pharmacological approach or by specifically targeting muscles (Fig. 3a). Middle-aged (12 months) and aged (24 months) mice were intraperitoneally (i.p.) injected with pyroglutamate apelin-13 (0.5 μmol per kg body weight per d) daily for 28 d. I.p. injection of apelin significantly promoted a physiological (600 pg/ml) and transient (5 min after injection) increase of plasma immunoreactivity (Supplementary Fig. 4a). Despite the flash half-life of apelin, this increase is consistent with functional effects regarding the pharmacological characteristics of the peptide^{29–32} and the similar results obtained by chronic infusion or daily injection of apelin in the field of cardiovascular disease^{33,34}. Apelin treatment increased the weight of both studied muscles (Fig. 3b,c) in aged wild-type and *Apln*^{-/-} mice, which was associated with fiber hypertrophy (Fig. 3d,e). Apelin treatment also induced a shift toward a greater proportion of larger fibers (Fig. 3e). When compared to saline-treated mice, 12-month-old apelin-supplemented animals displayed a significant increase in the number of large diameter fibers (>1,500 μm) and a decrease in the number of smaller fibers (500–1,000 μm) (Fig. 3e). The oldest apelin-treated mice exhibited an increase in the number of larger fibers (diameter between 500 μm and 1,500 μm) without developing hypertrophic fibers (>1,500 μm) (Fig. 3e). Accordingly, area determination depending on fiber typology (Fig. 3f) measured in both glycolytic (tibialis, Fig. 3g) and oxidative (soleus, Fig. 3h) muscles, revealed that apelin promoted a strong increase in the cross sectional area of all the fibers types, independently of age. In parallel, apelin treatment promoted the emergence of type IIb/x fibers, which are the most sensitive to age-induced apoptosis³⁵ (Fig. 3i,j and Supplementary Fig. 4b,c).

Considering that loss of fast-fiber type is considered to be a protective mechanism during aging³⁶ and that fiber size is not systematically correlated with functional gain, we performed in situ and in vivo experiments to assess the consequence of such a restoration on muscle activity (Fig. 3k–n). In situ, plantaris and tibialis muscles from aged apelin-treated mice displayed an enhanced tetanic force related to age-matched controls (Fig. 3k and Supplementary Fig. 4d). In addition, daily apelin administration in aged mice led to a considerable increase in muscle function as evaluated by grid-hanging ability, maximal speed and strength measurements compared to PBS-treated mice (Fig. 3l–n). This observation was reinforced by the specific overexpression of apelin in gastrocnemius and tibialis muscles from 24-month-old mice (protocol P2; Fig. 3a,o–s and Supplementary Fig. 4e–j) achieved by intramuscular injection of an adenovirus expressing apelin and luciferase (AAV1-apelin-Luc) (Supplementary Fig. 4e–g). Muscle-specific apelin overexpression induced a significant gain in strength (Fig. 3o), grid-hanging capacities (Fig. 3p), maximal speed (Fig. 3q) and time and distance to exhaustion (Fig. 3r,s) together with a specific increase

in the weight of injected muscles (Supplementary Fig. 4h–j). These results strongly suggest that local apelin production is sufficient to enhance muscle efficacy during aging, possibly via an autocrine regulatory loop.

Together with the regulation of muscle apelin production by exercise, we hypothesized that there was a potential cumulative effect of apelin and physical exercise during aging on muscle physiology. Therefore, we performed apelin supplementation treatments in conjunction with exercise over a 28 d period in aged mice (Protocol P3; Fig. 3a). No additive effect of apelin was observed on muscle function, as apelin-treated mice did not display any additional gain in muscle mass (Supplementary Fig. 4k,l) or force (Supplementary Fig. 4m,n) compared to exercised, PBS-treated controls. This result could be explained by the fact that, despite aging, physical exercise still enhanced gains in muscle mass and allowed muscles to functionally recover several capacities, as already described^{37,38}. Nevertheless, beyond functional capacities, muscle homeostasis was still targeted by apelin treatment during physical exercise, as resistance to fatigue was improved in aged animals (Fig. 3t,u) and in 12-month-old mice supplemented with apelin (Supplementary Fig. 4o,p). Muscle fatigue is characterized by the accumulation of reactive oxygen species and alterations in metabolic and trophic functions in fibers, as well as a poor cell renewal due to modifications in activation to satellite cells alteration^{39–41}, suggesting a potential role for apelin in these pathways.

Apelin promotes mitochondriogenesis and protein synthesis through AMPK, AKT and P70S6K activation in sarcopenic myofibers.

In nonmuscle cells, apelin has been shown to be a potential trigger of various pathways that are also involved in muscle aging, such as AMPK, AKT, P70S6K or mTOR^{19,42,43}. We first performed in vitro short-term apelin treatment of muscle cells from young and aged donors and assessed potential apelin-dependent signaling (Fig. 4a). Acute apelin (1 nM) treatment of cells from young donors increased AMPK and AKT phosphorylation (Fig. 4a). Downstream of AKT, apelin triggered the mTOR–P70 S6 kinase (P70S6K)–4E-binding protein-1 (4E-BP1) cascade. Surprisingly, most of these effects were maintained and, moreover, sustained in cells from aged donors. Indeed, apelin targeted mTOR and P70S6K phosphorylation, which are involved in muscle anabolic pathways during aging. Unexpectedly, 4E-BP1 and FOXO-3 hyperphosphorylation was suppressed by apelin in cells from aged donors, evidencing a supplemental argument in favor of protein synthesis and revealing a new pathway for apelin in skeletal muscle. Validation of this hypothesis was provided by puromycin incorporation experiments with mature myotubes whereby apelin treatment was shown to be able to promote protein synthesis in young and aged cells (Fig. 4b). To confirm the crucial role of AMPK, we chronically treated 12-month-old mice, lacking AMPK activity specifically in skeletal muscle (AMPK-DN), with apelin (Fig. 4c,d). Cross-sectional area and grip test experiments validated the requirement of AMPK to promote apelin effects on muscle hypertrophy and strength during aging. Besides effects on protein synthesis and, accordingly, AMPK activation, chronic apelin treatment also enhanced mitochondria biogenesis by increasing mitochondrial DNA synthesis (Fig. 4e) and function by improving citrate synthase and aconitase activities (Fig. 4f,g) in both aged and apelin-deficient mice. All these improvements were accompanied by a redefinition of mitochondrial shape and size (Fig. 4h,i) and of their function via an increase in mitochondrial respiratory capacities in intramuscular AAV1-apelin-Luc-injected aged mice (Fig. 4j). These results definitively demonstrated a beneficial role for apelin in age-associated mitochondrial disorders; however, a broad range of intracellular pathways related to metabolism, oxidative stress, autophagy and inflammation could also be involved.

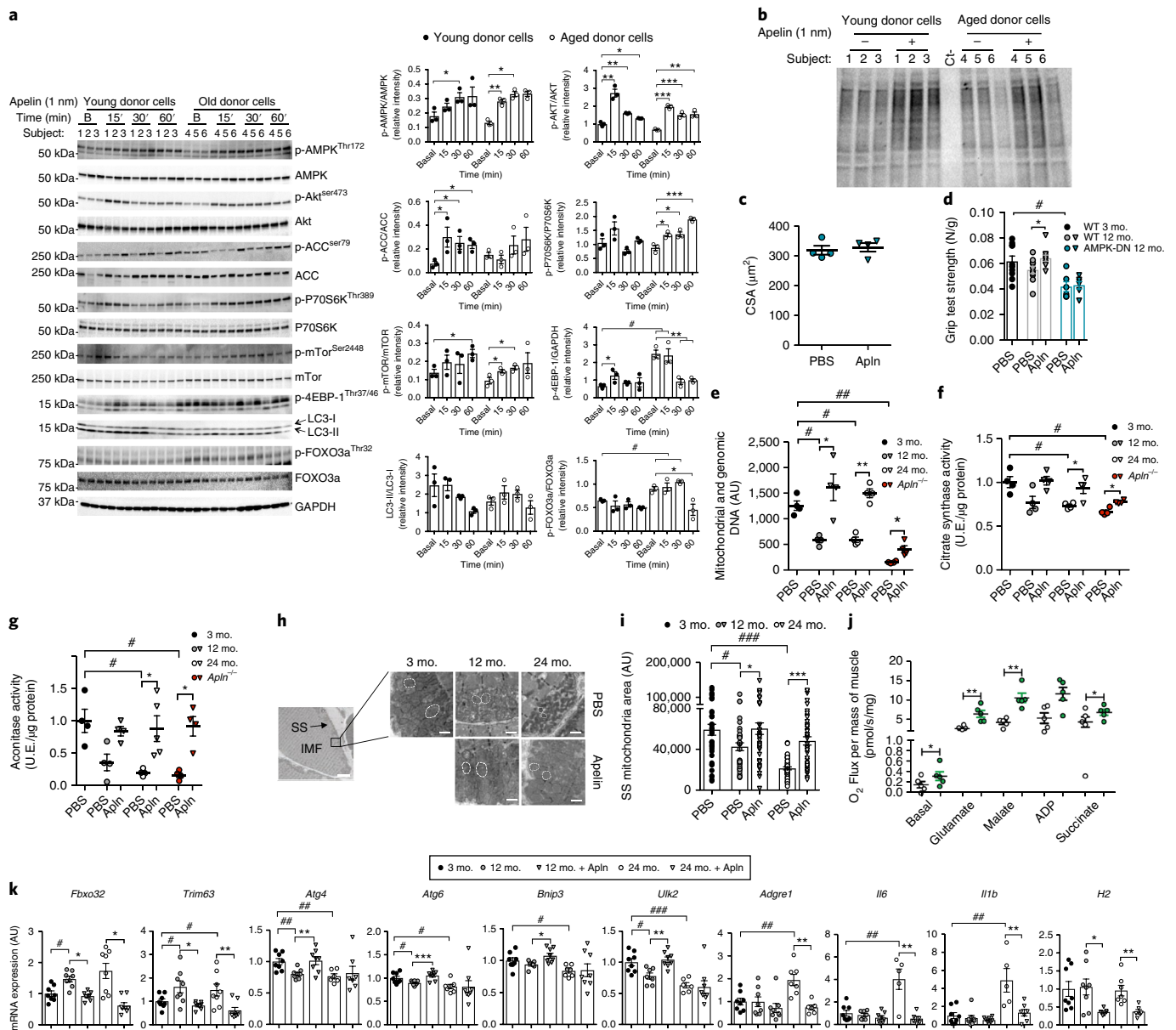


Fig. 4 | APLNR-mediated pathways in aged muscle cells. **a**, Left, Kinetic activation of different proteins by apelin (1 nM) treatment in young and aged donor's differentiated myotubes. Uncropped gels are presented in Supplementary Fig. 6. B, basal. Right, Quantification of western blots by densitometry analysis ($n=3$ different donors). **b**, Western blotting of puromycin incorporation into young and aged donors' differentiated myotubes chronically treated (4 d) with apelin (1 nM). The uncropped gel is presented in Supplementary Fig. 6. **c**, Cross-sectional area of tibialis muscle from AMPK-DN middle-aged (12 mo.) mice treated daily treated with PBS or apelin ($n=4$ mice per group). **d**, Grip test strength measured in wild-type (WT) (12 months old, gray) ($n=6$ mice) and AMPK-DN (12- months old, blue) ($n=5$ mice) treated with apelin (triangles) or PBS (circles). Young mice (3 months old, black circle) strength is given as a positive control ($n=10$ mice). **e**, Mitochondrial DNA in tibialis muscle from 3-, 12- and 24-month-old mice treated with apelin or PBC ($n=4$ mice per group). **f, g**, Citrate synthase (**f**) and aconitase (**g**) activities in tibialis ($n=4$ mice per group). U.E., unit of enzyme. **h**, Representative electron micrographs of longitudinal section of tibialis myofibers from 3-, 12- and 24-month-old mice chronically treated with apelin or PBS ($n=6$ mice per group, 3 pictures per mouse). IMF, intramyofibrillar; SS, subsarcolemal. The dashed lines indicate the shape of the organelle. Scale bars, $1\ \mu\text{m}$. **i**, Quantification of mean mitochondrial area in tibialis muscle ($n=6$ mice per group, 3 images per mouse). **j**, Mitochondrial respiration in permeabilized myofibers prepared from tibialis of AAV1-control-Luc-treated (white circles) or AAV1-apelin-Luc-treated (green circles) aged (24-month-old) mice at 35 d post injection ($n=5$ mice per group). **k**, Tibialis mRNA expression of genes involved in muscle wasting (*Fbxo32*, *Trim63*), autophagy (*Atg4*, *Atg6*, *Bnip3* and *Ulk2*) and inflammatory (*Adgre1*, *Il6*, *Il1b* and *H2*) pathways ($n=6$ mice per group). Expression is shown relative to that of *Hprt*. Data presented are means \pm s.e.m. * or # $P < 0.05$; ** or ## $P < 0.01$; *** or ### $P < 0.001$; two-tailed unpaired Student's *t*-test.

By studying muscle transcription for different signaling pathways, we first showed that long-term apelin treatment induces a systematic increase in muscle *Aplnr* expression, confirming a feedback regulatory mechanism between the peptide and its own receptor as previously described²⁵ (Supplementary Fig. 5a). In a broader

approach, a microfluidic array was employed to monitor gene expression changes in tibialis from mice subjected to chronic apelin treatment (Fig. 4k and Supplementary Fig. 5b). As expected, middle-aged apelin-treated mice displayed increased expression of genes related to mitochondria biogenesis (*Tfam* and *Ppargc1*), oxidative

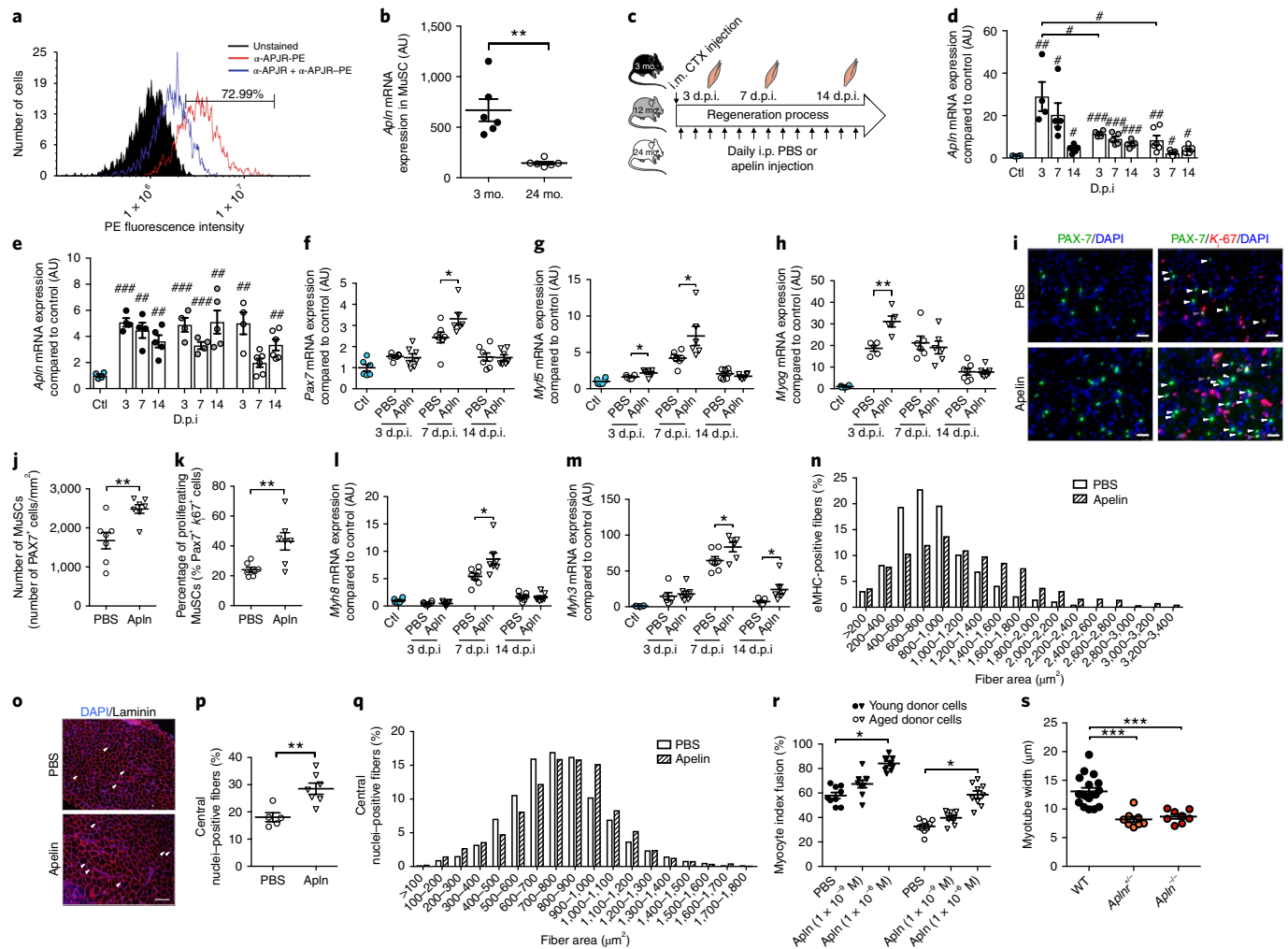


Fig. 5 | Satellite cells are targeted by apelin during muscle regeneration in aged mice. **a**, Flow cytometry evaluation of APLNR (APJ) immunoreactivity on PAX-7⁺ cells in tibialis. Sorted muscle stem cells were unstained as a negative control (black curve) or stained with phycoerythrin (PE)-coupled APLNR antibody (red curve). Specificity of the staining was evaluated by preincubating sorted MuSCs for 30 min with the unlabeled APLNR antibody followed by an incubation with the APLNR-PE coupled antibody (blue curve). **b**, *Aplnr* mRNA expression of PAX-7⁺ cells in tibialis of young and aged mice ($n=6$ mice per group). **c**, Protocol of cardiotoxin (CTX)-induced muscle regeneration experiments. d.p.i., days post injection. **d,e**, Expression of *Aplnr* (**d**) and *Aplnr* (**e**) mRNA in tibialis of 3-, 12- and 24-month-old mice (black, gray and white circles, respectively; $n=5$ mice per group). Blue circles represent the mice not treated by cardiotoxin. **f-h**, *Pax7* (**f**), *Myf5* (**g**) and *Myog* (**h**) expression in tibialis of 24-month-old mice treated with apelin (triangles) or PBS (circles) ($n=6$ mice per group). Blue circles represent the mice not treated by cardiotoxin and/or apelin. **i**, Representative immunofluorescence pictures of PAX-7 and PAX-7 and K₆₇ labeling in tibialis of cardiotoxin-injected aged mice (24 months old) treated with apelin or PBS. Yellow arrows represent the proliferative PAX-7-K₆₇-double-positive cells. Scale bars, 25 μm . ($n=5$ mice per group, 1 picture per mouse). **j,k**, Number of PAX-7⁺ (**j**) and PAX-7⁺K₆₇⁺ (**k**) cells in tibialis of cardiotoxin-injected aged mice (24 months old) treated with apelin (0.5 $\mu\text{mol/kg/day}$) or PBS over 7 d ($n=7$ mice per group). **l,m**, *Myh3* (**l**) and *Myh8* (**m**) expression in tibialis of 24-month-old mice treated with apelin (triangles) or PBS (circles) ($n=6$ mice per group). Blue circles represent the mice not treated by cardiotoxin and/or apelin. **n**, Distribution of embryonic myosin heavy chain (eMHC)-positive fibers in 24-month-old mice treated with apelin (hatched bars) or PBS (white bars) ($n=4$ mice per group). **o**, Representative immunofluorescence labeling of laminin and DAPI for central nuclei quantification. White arrowheads indicate the presence of central nuclei ($n=4$ mice per group, 3 pictures per mouse). Scale bars, 70 μm . **p**, Mean percentage ($n=5$ mice for PBS, $n=7$ mice for Apn) and distribution (**q**) of fibers with central nuclei ($n=4$ mice) in 24-month-old mice treated with apelin (triangles) or PBS (circles). **r**, Myocyte index fusion calculated in young (black bars) and aged (white bar) donor muscle cells treated with apelin or PBS (1×10^{-9} and 1×10^{-6} mol/L) over 10 d ($n=3$ independent experiments, 3 donors per group). **s**, Determination of myotube width in primary culture from WT (black circles), *Aplnr*^{+/+} (orange circles) and *Aplnr*^{-/-} mice (red circles) hindlimb ($n=3$ mice per group, 3 wells per mouse, 3 pictures per well). *Aplnr* mRNA expression is presented relative to *Hprt* expression (**b,d,e,f,g,h,l,m**). Data presented are means \pm s.e.m. * or # $P < 0.05$; ** or ## $P < 0.01$; *** or ### $P < 0.001$; two-tailed unpaired Student's *t*-test.

damage response (*Sod1* (*Sox*) and *Cox5a* (*Cox*)) and metabolism (*Prkaa2* (*Prkaa*), *Gsk3b*, *Sreb1*, *Slc2a1*, *Mixl1* (*Mixpl*), *Sirt3*, *Sirt4* and *Sirt5*) (Supplementary Fig. 5b). Consistent with a reduction of FOXO-3a hyperphosphorylation in cells from aged donors, apelin blunted *Fbxo32* and *Trim63* overexpression in chronically treated aged mice (Fig. 4k). Notably, in muscles, apelin also promoted transcriptional activation of autophagy genes by increasing expression

of *Atg4*, *Becn1* (*Atg6*), *Bnip3* and *Ulk2* (Fig. 4k). However, pharmacological apelin treatment did not stimulate the transcription of these genes in 24-month-old mice, in which inflammation-related genes (*Emr1* (*Adgre*), *Il6*, *Il1b* and *H2*) were found to be decreased in expression (Fig. 4k) suggesting that apelin could trigger different mechanisms depending on the age and/or state of the muscle and that a reduction in inflammation could be a prerequisite to the

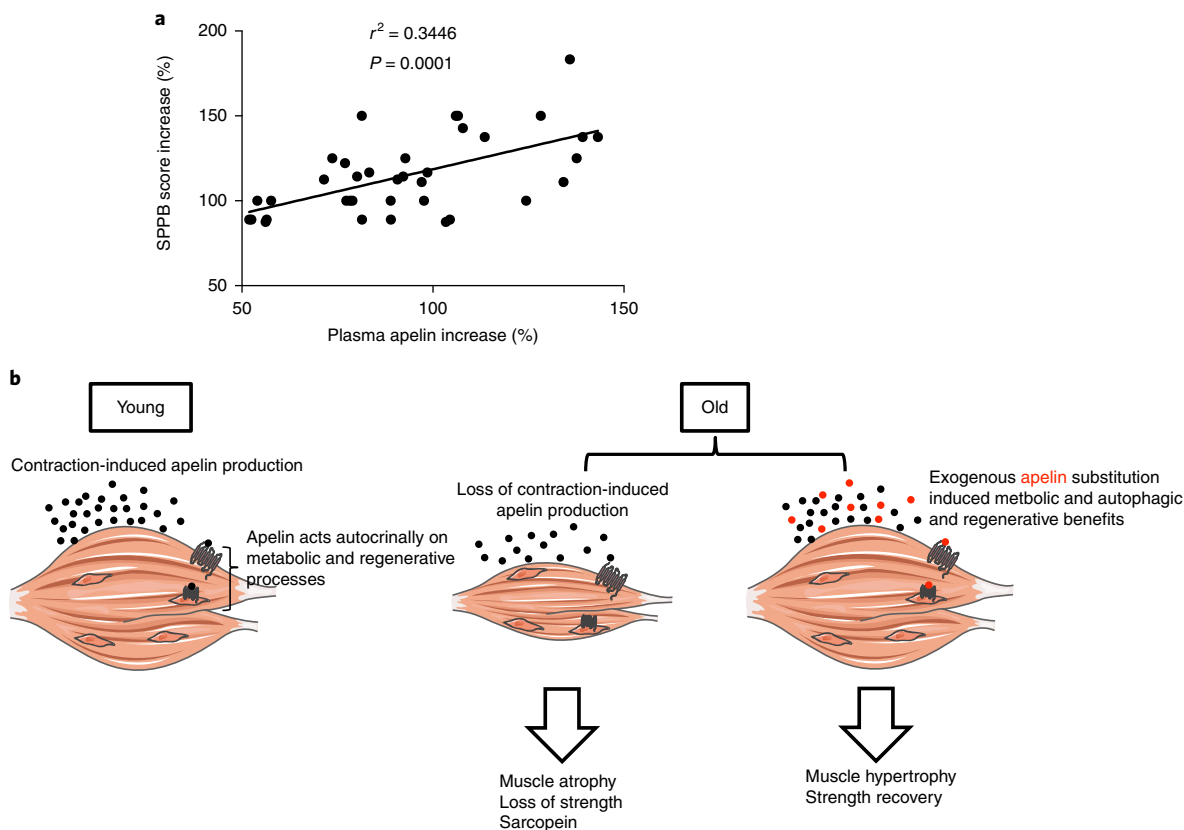


Fig. 6 | Apelin is correlated with beneficial exercise in humans. **a**, Correlation between the capacity of individuals from the LIFE-P cohort to increase their plasma apelin immunoreactivity level between 0 and 6 months (x axis) and the variation of SPPB score during this training phase (y axis). The line indicates linear regression, and the Spearman correlation coefficient is shown. **b**, Graphic description of apelin regulation and action in sarcopenic muscle. Apelin is produced and secreted by a contractile skeletal muscle. This regulation is dropped during aging, leading to muscle atrophy, loss of strength and age-associated sarcopenia. After exogenous apelin supplementation in aged muscle cells and mice, mitochondria functions are enhanced, as well as inflammation or autophagy. In parallel, apelin also acts on satellite cells to promote the regeneration process.

promotion of other pathways that enhance muscle physiology during late phases of aging.

Apelin targets muscle stem cells to enhance muscle regeneration.

In adults, muscle stem cells (MuSCs) are quiescent but become activated and proliferate to generate myoblasts that fuse into myofibers in response to physiological or pathological stimuli (for example, stretching, exercise or mechanical injury). Loss of MuSC function is a hallmark of aging and can emerge as defects in the maintenance of quiescence, self-renewal ability or activation–proliferation potential^{44,45}. In the context of a regulatory loop involving apelin, exercise and myogenesis, we hypothesized that apelin potentially plays a role in muscle regeneration during aging. By taking advantage of Pax7-ZsGreen reporter mice generated by inserting a T2A-ZsGreen-NLS reporter downstream of exon 9 of the Pax7 locus through homologous recombination, we first evaluated the presence of *Aplnr* on Pax7-positive MuSCs by flow cytometry (Fig. 5a). MuSCs, sorted from young and old mice as previously described⁴⁵, demonstrated a fourfold reduction in *Aplnr* expression in MuSCs from old mice (Fig. 5b). Cardiotoxin-mediated regeneration experiments, in which MuSCs are activated to induce the regenerative response (Fig. 5c), revealed a strong upregulation of *Apln* and *Aplnr* expression in reconstructing muscle during regeneration, providing evidence for a crucial role of apelin and its receptor in this process (Fig. 5d,e). However, this response was blunted in aged mice (Fig. 5d,e).

We next treated cardiotoxin-injected aged mice with apelin daily and analyzed the consequences of this supplementation on regeneration. Compared to controls, mice supplemented pharmacologically

with apelin had increased expression of satellite cell markers, such as *Pax7*, *Myf5* and *Myog* (Fig. 5f–h). Additionally, apelin treatment of cardiotoxin-injected aged mice increased the number of MuSCs and their proliferative capacity, as shown by increased numbers of PAX-7-positive and PAX-7-K67-double-positive MuSCs (Fig. 5i–k). Moreover, apelin was able to significantly enhance myogenic differentiation and repair (Fig. 5l–s). Indeed, compared to PBS-treated mice, mRNA expression of *Myh3* and *Myh8* (markers transiently expressed in adult muscles during the regeneration process) was enhanced by apelin treatment (Fig. 5l,m) and associated with a shift toward larger positive embryonic MHC (eMHC) fibers (Fig. 5n), suggesting that the regenerative process was more active. To reinforce these results, we measured the diameter of newly synthesized centrally nucleated fibers, considered to be a marker of the regenerative processes (Fig. 5o–q) and found that the number of centrally nucleated fibers (Fig. 5p), as well as the area of these regenerating fibers, was higher in apelin-treated mice compared to controls (Fig. 5q). Finally, the enhanced fusion index observed in human differentiated myotubes chronically treated with apelin (Fig. 5r), together with the reduced width of myotubes obtained from *Apln*^{-/-} or *Aplnr*^{+/-} MuSC primary cultures (Fig. 5s) definitively supported a prodifferentiating role for the apelin peptide in skeletal muscle.

Measuring apelin to assess the benefit of exercise in older individuals.

By acting simultaneously on both muscle fiber and satellite cell differentiation, contraction-induced muscle apelin could help mediate the benefit of physical exercise with increasing age. To evaluate this hypothesis, we measured plasma apelin immunoreactivity

in a group of elderly people subjected to a 1-year program of regular physical exercise (LIFE-Study⁴⁶). Compared to their basal level (i.e., before the study) of plasma apelin immunoreactivity, we observed that individuals who displayed increased plasma apelin levels 6 months after the beginning of the trial also demonstrated the most improved Short Physical Performance Battery test (SPPB) score (Fig. 6a).

This result evidences a positive regulatory loop between muscle contraction, apelin and muscle physiology, which may be altered during the aging process (Fig. 6b). More broadly, this result indicated that plasma apelin immunoreactivity level measured after acute physical exercise in the elderly could represent a potential diagnostic tool able to predict the benefit of physical exercise. Therefore, apelin supplementation in the elderly subpopulation that demonstrate reduced capacities toward apelin production represents an innovative approach that may partly limit or reverse age-associated muscle desensitization to the benefits of physical exercise.

Discussion

Age-related sarcopenia and loss of muscle strength are important risk factors for disabling conditions, such as cognitive decline, congestive heart failure and osteoporosis^{4,47}. It is important to identify and characterize individuals at risk of developing sarcopenia and propose preventive strategies to avert transition to disability and medical institutionalization of older individuals. Our study has revealed the existence of a regulatory feedback mechanism between muscle contraction, apelin production and myogenesis. In addition, we also demonstrated that these mechanisms are altered during aging, thus potentially contributing to the onset of sarcopenia. Finally, apelin may represent a promising therapeutic target in the field of aging, a potential new tool for the early diagnosis of sarcopenia and a prognostic marker for the benefits of exercise in the elderly.

A crucial role for the apelin peptide in muscle physiology during aging was first revealed by murine models deficient in apelin or its receptor. In the heart, it has recently been described that apelin deficiency leads to premature cardiac aging⁴⁸. Herein we found loss of skeletal muscle mass and functional alterations in mice deficient for apelin (whole body and muscle-specific) or its receptor (heterologous knockout). As muscle atrophy was not observed in young knockout mice, we hypothesized that apelin-associated changes regarding metabolism, oxidative processes, innervation and angiogenesis were age dependent. It has been previously demonstrated that targeting of skeletal muscle cells by apelin improves metabolic functions through an AMPK–mitochondriogenesis-dependent axis^{19,49}. Additionally, different *Aplnr*-expressing cell types exhibited apelin-induced activation of intracellular pathways such as AMPK, mTOR, P70S6 kinase and AKT^{42,43,50}. The aging process has already been clearly shown to lead to alteration of mitochondria-related metabolism in muscle and that defects in AMPK, P70S6 kinase and AKT signaling are major mediators of this effect on the mitochondria^{51,52}. Our results show that apelin supplementation in aged mice improved various processes related to muscle rejuvenation in an AMPK-dependent manner but without overt overactivation of this pathway. Apelin affected processes including mitochondrial function and biogenesis, antioxidant enzymes, autophagy and inflammation. Furthermore, apelin induced activation of anabolic pathways promoting protein synthesis (AKT, mTOR, P70S6K and 4E-BP1) and has been shown, for what we believe is the first time, to inhibit the activation of age-related proteolysis actors such as FOXO3a in aged, human differentiated myotubes. Together with the reduction of *Fbxo32* and *Trim63* expression in muscle observed in vivo, this result paves the way for new insight into the signaling pathway of apelin in the field of muscle atrophy. Although other muscle atrophy-associated processes, such as innervation or angiogenesis^{36,53}, also need to be investigated and could partly explain the observed

effects of apelin, our results highlight two fundamental mechanisms of muscle aging that are targeted by apelin: mitohormesis and proteogenesis–proteolysis. Consequently, we hypothesized that apelin could participate in type IIb/x fibers synthesis in glycolytic muscle by decreasing mitochondria-induced damage that is associated with aging, whereas fiber hypertrophy is most likely mediated by the effect of apelin on protein balance in both glycolytic and oxidative twitch muscles.

Our work also described the beneficial effects of apelin during muscle regeneration in aged mice and human cell lines. Apelin triggered mechanisms that permit the differentiation of MuSCs and led to an improvement of regenerative processes. It has been previously shown that $G_{\alpha i}$ signaling acts as a strong inducer of muscle hypertrophy, myoblast differentiation and muscle regeneration⁵⁴, thus coupling of APLNR to $G_{\alpha i}$ reinforced our results. By using a model of inducible depletion of satellite cells, it has been previously demonstrated that regenerative processes did not affect sarcopenia in mice¹⁶. However, in the context of resistance training associated with fiber damages and regeneration, apelin should promote the potentiation of cell renewal processes, congruent with our results demonstrating lower fatigability when the peptide was administered to mice together in conjunction with physical exercise. Additional experiments are necessary to determine whether the positive regulatory loop involving muscle contraction, apelin and myogenesis is related to a particular form of exercise and to identify the underlying molecular mechanisms initiating the activation of satellite cells by apelin. Regardless, our results are supportive of the hypothesis that apelin both acts on mature muscle fibers to promote trophic benefits and participates in muscle reconstruction during acute phases of regeneration after damage due to different forms of resistance training or post trauma.

Contracting muscle cells, of both human and murine origin, produce apelin. Although skeletal muscle has been previously shown to synthesize apelin^{20,55,56}, we have now extended this observation by establishing a link between apelin and exercise and have shown, for we believe the first time, that muscle contraction promotes apelin secretion into bloodstream, although it was previously shown that chronic exercise leads to an increase in plasma apelin with a decrease in soleus apelin⁵⁷. Our data confirm the increase in plasma and show that mRNA expression of the muscle tissue increases, suggesting that myocyte apelin content was probably emptied by exercise, as seen previously in enterocytes stimulated by glucose⁵⁸. Basal apelin levels have been shown to be decreased with age in mice⁴⁸ and humans, when adjusted for sex²¹, but our current study represents the first report of a reduction in exercise-stimulated muscle apelin production with age. We also show that muscle apelin production correlates with exercise efficiency during aging, indicating a potential use for apelin as a marker of the health benefits of exercise in the elderly. Compared to other exercise-induced muscle markers, such as IL-6 (ref. 59), apelin appears to be more specific, and its reduced production with age constitutes a powerful tool to identify muscle weakness. Thus, we propose apelin measurement after acute exercise as a new index of exercise achievement, which will potentially help clinicians better manage the physical exercise practice of the elderly in the future.

However, it is worth remarking that different apelin isoforms (apelin-13, 17 or 36 amino acids) are found in plasma or biological fluids, reflecting the need to better characterize the forms produced by contractile muscle through more accurate techniques in order to validate apelin production as a new biomarker of age-related exercise success. Finally, from a therapeutic perspective, it appears fundamental to better understand the associated mechanisms regulating muscle contraction and apelin production and how this regulation is altered with age. Supporting this view, mechanic contraction itself could be involved, as cardiomyocyte stretching resulted in apelin production and *Aplnr* expression⁶⁰ whereas inflammation and/or senescence could be potent repressors of muscle apelin or APLNR⁴⁸.

Our findings directly implicate apelin signaling as a positive factor relating to the benefit of exercise that deteriorates with aging, suggesting that it represents a target for various aspects in the development of health improvement strategies. To determine which part of the benefit is due to apelin, it will be interesting to perform different types of exercise in absence of apelin and measure the consequence on sarcopenia onset. In addition to approaches incorporating physical activity, which we show can bolster endogenous apelin, it is possible that various nutritional approaches could be developed to either supply exogenous apelin or even stimulate endogenous production. In addition, development of APLNR agonists that provide both long-term activity and muscle specificity warrant further investigation as pharmacological strategies. Apelin, and possibly its receptor, represent future markers as well as therapeutic targets for strategies that aim to ameliorate health problems related to age-associated sarcopenia.

Methods

Methods, including statements of data availability and any associated accession codes and references, are available at <https://doi.org/10.1038/s41591-018-0131-6>.

Received: 2 March 2017; Accepted: 8 June 2018;

Published online: 30 July 2018

References

- Janssen, I., Shepard, D. S., Katzmarzyk, P. T. & Roubenoff, R. The healthcare costs of sarcopenia in the United States. *J. Am. Geriatr. Soc.* **52**, 80–85 (2004).
- Han, K. et al. Sarcopenia as a determinant of blood pressure in older Koreans: findings from the Korea National Health and Nutrition Examination Surveys (KNHANES) 2008–2010. *PLoS One* **9**, e86902 (2014).
- Anker, S. D., Morley, J. E. & von Haehling, S. Welcome to the ICD-10 code for sarcopenia. *J. Cachexia Sarcopenia Muscle* **7**, 512–514 (2016).
- Pasco, J. A. et al. Sarcopenia and the common mental disorders: a potential regulatory role of skeletal muscle on brain function? *Curr. Osteoporos. Rep.* **13**, 351–357 (2015).
- Martinez, B. P. et al. Frequency of sarcopenia and associated factors among hospitalized elderly patients. *BMC Musculoskelet. Disord.* **16**, 108 (2015).
- Robertson, D. A., Savva, G. M. & Kenny, R. A. Frailty and cognitive impairment—a review of the evidence and causal mechanisms. *Ageing Res. Rev.* **12**, 840–851 (2013).
- Rockwood, K. & Mitnitski, A. Frailty in relation to the accumulation of deficits. *J. Gerontol. A Biol. Sci. Med. Sci.* **62**, 722–727 (2007).
- Samper-Ternent, R., Al Snih, S., Raji, M. A., Markides, K. S. & Ottenbacher, K. J. Relationship between frailty and cognitive decline in older Mexican Americans. *J. Am. Geriatr. Soc.* **56**, 1845–1852 (2008).
- Giannoulis, M. G., Martin, F. C., Nair, K. S., Umpleby, A. M. & Sonksen, P. Hormone replacement therapy and physical function in healthy older men. Time to talk hormones? *Endocr. Rev.* **33**, 314–377 (2012).
- Hepple, R. T. Mitochondrial involvement and impact in aging skeletal muscle. *Front. Aging Neurosci.* **6**, 211 (2014).
- Johnson, M. L., Robinson, M. M. & Nair, K. S. Skeletal muscle aging and the mitochondrion. *TEM* **24**, 247–256 (2013).
- Cartee, G. D., Hepple, R. T., Bamman, M. M. & Zierath, J. R. Exercise promotes healthy aging of skeletal muscle. *Cell Metab.* **23**, 1034–1047 (2016).
- Ryu, D. et al. Urolithin A induces mitophagy and prolongs lifespan in *C. elegans* and increases muscle function in rodents. *Nat. Med.* **22**, 879–888 (2016).
- Snijders, T. et al. The skeletal muscle satellite cell response to a single bout of resistance-type exercise is delayed with aging in men. *Age (Dordr.)* **36**, 9699 (2014).
- Bernet, J. D. et al. p38 MAPK signaling underlies a cell-autonomous loss of stem cell self-renewal in skeletal muscle of aged mice. *Nat. Med.* **20**, 265–271 (2014).
- Fry, C. S. et al. Inducible depletion of satellite cells in adult, sedentary mice impairs muscle regenerative capacity without affecting sarcopenia. *Nat. Med.* **21**, 76–80 (2015).
- Castan-Laurell, I. et al. Apelin, diabetes, and obesity. *Endocrine* **40**, 1–9 (2011).
- Dray, C. et al. Apelin and APJ regulation in adipose tissue and skeletal muscle of type 2 diabetic mice and humans. *Am. J. Physiol. Endocrinol. Metab.* **298**, E1161–E1169 (2010).
- Dray, C. et al. Apelin stimulates glucose utilization in normal and obese insulin-resistant mice. *Cell Metab.* **8**, 437–445 (2008).
- Besse-Patin, A. et al. Effect of endurance training on skeletal muscle myokine expression in obese men: identification of apelin as a novel myokine. *Int. J. Obes. (Lond.)* **38**, 707–713 (2014).
- Fujie, S. et al. Reduction of arterial stiffness by exercise training is associated with increasing plasma apelin level in middle-aged and older adults. *PLoS One* **9**, e93545 (2014).
- Newman, A. B. et al. Sarcopenia: alternative definitions and associations with lower extremity function. *J. Am. Geriatr. Soc.* **51**, 1602–1609 (2003).
- Vellas, B. et al. Mapt Study: a multidomain approach for preventing Alzheimer's disease: design and baseline data. *J. Prev. Alzheimers Dis.* **1**, 13–22 (2014).
- Kuba, K. et al. Impaired heart contractility in Apelin gene-deficient mice associated with aging and pressure overload. *Circ. Res.* **101**, e32–e42 (2007).
- Yamamoto, T. et al. Apelin-transgenic mice exhibit a resistance against diet-induced obesity by increasing vascular mass and mitochondrial biogenesis in skeletal muscle. *Biochim. Biophys. Acta* **1810**, 853–862 (2011).
- Wang, B. et al. Construction and analysis of compact muscle-specific promoters for AAV vectors. *Gene Ther.* **15**, 1489–1499 (2008).
- Tai, P. W. et al. Differentiation and fiber type-specific activity of a muscle creatine kinase intronic enhancer. *Skelet. Muscle* **1**, 25 (2011).
- Hauser, M. A. et al. Analysis of muscle creatine kinase regulatory elements in recombinant adenoviral vectors. *Mol. Ther.* **2**, 16–25 (2000).
- Katugampola, S. D., Maguire, J. J., Matthewson, S. R. & Davenport, A. P. [(125)I]-(Pyr(1))Apelin-13 is a novel radioligand for localizing the APJ orphan receptor in human and rat tissues with evidence for a vasoconstrictor role in man. *Br. J. Pharmacol.* **132**, 1255–1260 (2001).
- Pitkin, S. L., Maguire, J. J., Bonner, T. I. & Davenport, A. P. International Union of Basic and Clinical Pharmacology. LXXIV. Apelin receptor nomenclature, distribution, pharmacology, and function. *Pharmacol. Rev.* **62**, 331–342 (2010).
- Yang, P. et al. Elabela/toddler is an endogenous agonist of the apelin APJ receptor in the adult cardiovascular system, and exogenous administration of the peptide compensates for the downregulation of its expression in pulmonary arterial hypertension. *Circulation* **135**, 1160–1173 (2017).
- Medhurst, A. D. et al. Pharmacological and immunohistochemical characterization of the APJ receptor and its endogenous ligand apelin. *J. Neurochem.* **84**, 1162–1172 (2003).
- Jia, Y. X. et al. Apelin protects myocardial injury induced by isoproterenol in rats. *Regul. Pept.* **133**, 147–154 (2006).
- Chun, H. J. et al. Apelin signaling antagonizes Ang II effects in mouse models of atherosclerosis. *J. Clin. Invest.* **118**, 3343–3354 (2008).
- Jacobs, R. A. et al. Fast-twitch glycolytic skeletal muscle is predisposed to age-induced impairments in mitochondrial function. *J. Gerontol. A Biol. Sci. Med. Sci.* **68**, 1010–1022 (2013).
- Demontis, F., Piccirillo, R., Goldberg, A. L. & Perrimon, N. Mechanisms of skeletal muscle aging: insights from *Drosophila* and mammalian models. *Dis. Model. Mech.* **6**, 1339–1352 (2013).
- Stewart, V. H., Saunders, D. H. & Greig, C. A. Responsiveness of muscle size and strength to physical training in very elderly people: a systematic review. *Scand. J. Med. Sci. Sports* **24**, e1–e10 (2014).
- Pahor, M. et al. Effect of structured physical activity on prevention of major mobility disability in older adults: the LIFE study randomized clinical trial. *JAMA* **311**, 2387–2396 (2014).
- Westerblad, H. & Allen, D. G. Emerging roles of ROS/RNS in muscle function and fatigue. *Antioxid. Redox Signal.* **15**, 2487–2499 (2011).
- Snijders, T. et al. A single bout of exercise activates skeletal muscle satellite cells during subsequent overnight recovery. *Exp. Physiol.* **97**, 762–773 (2012).
- Allen, D. G., Lamb, G. D. & Westerblad, H. Skeletal muscle fatigue: cellular mechanisms. *Physiol. Rev.* **88**, 287–332 (2008).
- Masri, B., Morin, N., Cornu, M., Knibiehler, B. & Audigier, Y. Apelin (65–77) activates p70 S6 kinase and is mitogenic for umbilical endothelial cells. *FASEB J.* **18**, 1909–1911 (2004).
- Xie, F. et al. Apelin-13 promotes cardiomyocyte hypertrophy via PI3K–Akt–ERK1/2–p70S6K and PI3K-induced autophagy. *Acta Biochim. Biophys. Sin. (Shanghai)* **47**, 969–980 (2015).
- García-Prat, L., Sousa-Victor, P. & Muñoz-Cánoves, P. Functional dysregulation of stem cells during aging: a focus on skeletal muscle stem cells. *FEBS J.* **280**, 4051–4062 (2013).
- Lukjanenko, L. et al. Loss of fibronectin from the aged stem cell niche affects the regenerative capacity of skeletal muscle in mice. *Nat. Med.* **22**, 897–905 (2016).
- Pahor, M. et al. Effects of a physical activity intervention on measures of physical performance: results of the lifestyle interventions and independence for Elders Pilot (LIFE-P) study. *J. Gerontol. A Biol. Sci. Med. Sci.* **61**, 1157–1165 (2006).
- Papachristou, E. et al. The relationships between body composition characteristics and cognitive functioning in a population-based sample of older British men. *BMC Geriatr.* **15**, 172 (2015).

48. Rai, R. et al. Downregulation of the apelinergic axis accelerates aging, whereas its systemic restoration improves the mammalian healthspan. *Cell Rep.* **21**, 1471–1480 (2017).
49. Attané, C. et al. Apelin stimulates glucose uptake but not lipolysis in human adipose tissue ex vivo. *J. Mol. Endocrinol.* **46**, 21–28 (2011).
50. Zhang, H. et al. Apelin inhibits the proliferation and migration of rat PASCs via the activation of PI3K/Akt/mTOR signal and the inhibition of autophagy under hypoxia. *J. Cell. Mol. Med.* **18**, 542–553 (2014).
51. Paturi, S. et al. Effects of aging and gender on muscle mass and regulation of Akt–mTOR–p70s6k related signaling in the F344BN rat model. *Mech. Ageing Dev.* **131**, 202–209 (2010).
52. Sandri, M. et al. Signalling pathways regulating muscle mass in ageing skeletal muscle: the role of the IGF1–Akt–mTOR–FoxO pathway. *Biogerontology* **14**, 303–323 (2013).
53. Ambrose, C. Muscle weakness during aging: a deficiency state involving declining angiogenesis. *Ageing Res. Rev.* **23**(Pt B), 139–153 (2015).
54. Minetti, G. C. et al. G_m2 signaling is required for skeletal muscle growth, regeneration, and satellite cell proliferation and differentiation. *Mol. Cell. Biol.* **34**, 619–630 (2014).
55. Bertrand, C. et al. Effects of dietary eicosapentaenoic acid (EPA) supplementation in high-fat fed mice on lipid metabolism and apelin/APJ system in skeletal muscle. *PLoS One* **8**, e78874 (2013).
56. Yue, P. et al. Apelin is necessary for the maintenance of insulin sensitivity. *Am. J. Physiol. Endocrinol. Metab.* **298**, E59–E67 (2010).
57. Son, J. S. et al. Effects of exercise-induced apelin levels on skeletal muscle and their capillarization in type 2 diabetic rats. *Muscle Nerve* **56**, 1155–1163 (2017).
58. Dray, C. et al. The intestinal glucose–apelin cycle controls carbohydrate absorption in mice. *Gastroenterology* **144**, 771–780 (2013).
59. Pedersen, B. K. & Fischer, C. P. Beneficial health effects of exercise—the role of IL-6 as a myokine. *Trends Pharmacol. Sci.* **28**, 152–156 (2007).
60. Chandrasekaran, B. et al. Myocardial apelin production is reduced in humans with left ventricular systolic dysfunction. *J. Card. Fail.* **16**, 556–561 (2010).

Acknowledgements

We thank V. Minville, I. Castan-Laurell, A. Yart, B. Masri, and L. Casteilla for their fruitful discussions. We also specially thank all of the personnel of the ANEXPLO animal facility (Toulouse, France) and transcriptomic GeTQ platform (Toulouse, France);

J. Rouquette, head of the ITAV Imaging Service (Centre Pierre Potier, Toulouse, France); Federico S. and the NIH flow cytometry facility (Lausanne, Switzerland). We thank J. Iacovani and J. Christensen for corrections to the article and M. Rossell for technical assistance. Mice deficient for AMPK activity (DN-AMPK) in skeletal muscles were kindly provided by the laboratory of M. J. Birnbaum (University of Pennsylvania Medical School, Philadelphia, USA). This work has been funded by INSERM (Institut National de la Santé et de la Recherche Médicale), the Région Occitanie and the Fondation de la Recherche Médicale (FRM). This project was supported in part by European funds (Fonds Européens de Développement Régional, FEDER), Toulouse Métropole, and the French Ministry of Research through the Investissement d'Avenir Infrastructures Nationales en Biologie et Santé program (ProFI, Proteomics French Infrastructure project, ANR-10-INBS-08).

Author contributions

C.D. and P.V. conceived the study. C.V., S.L.G., A.D., O.P. and S.D. performed all animal experiments. C.V., L.L., S.K., U.L. and J.F.N. designed, performed and analyzed the regeneration experiments. C.D., C.V. and J.-P.P. performed all the western blots. C.V., A.D., O.P. and N.G. performed all the transcriptomics. V.M. and A.B. provided human cells. A.B. performed all the culture cell experiments. B.V., M.C., M.P., F.P. and S.G. were involved in human samples collection and analysis. A.C. and A.F.P. performed the hindlimb unloading experiments. M.C., K.C. and O.S. designed and performed the HPLC experiments. M.V. analyzed muscle fiber composition. E.M. participated in performing the specific muscle contraction tests. C.D. supervised the design and execution of the study, interpreted the results and wrote the manuscript.

Competing interests

The authors declare no competing interests.

Additional information

Supplementary information is available for this paper at <https://doi.org/10.1038/s41591-018-0131-6>.

Reprints and permissions information is available at www.nature.com/reprints.

Correspondence and requests for materials should be addressed to C.D.

Publisher's note: Springer Nature remains neutral with regard to jurisdictional claims in published maps and institutional affiliations.

Methods

Human cohorts. We determined the minimum number of participants according to the plasma apelin variability published by Castan-Laurell et al.⁶¹. A minimum sample size of 17 participants per group is necessary to detect a statistical difference of 0.1 ng/ml in apelin concentration between the groups, assuming $\alpha = 0.05$, $\beta = 0.90$ and s.d. within each group = 0.02.

Multidomain Alzheimer Preventive Trial. *Study design.* MAPT²³ was a phase 3, multicentered, randomized, placebo-controlled trial using a four-arm design. The study protocol has been approved by the French Ethical Committee located in Toulouse (CPP SOOM II) at the date of December 6, 2007 and was authorized by French health authority (Ministry of Health) on December 31, 2007. Written consent was obtained from all participants. The protocol is registered on a public-access clinical trial database (NCT00672685).

Participants. With respect to Newman's index to characterize sarcopenia (see Supplementary Table 1), we only considered samples obtained before the intervention and collected 27 individuals without muscle weakness and 33 individuals with sarcopenia.

Lifestyle Interventions and Independence for Elders Pilot. *Study Design.* LIFE-P³⁸ was a single-blind, multicentered, randomized controlled trial of physical activity or health education intervention in sedentary older adults. The study protocol was approved by the institutional review boards of the University of Florida and Wake Forest University Health Sciences. Participants gave written informed consent. The protocol is consistent with the principles of the Declaration of Helsinki and is registered at www.clinicaltrials.gov (NCT00116194). In our study, apelin measurements were taken from 34 individuals who performed physical exercise. SPPB score (based on chair stands, balance, and walk tests) was obtained as previously described.

Plasma sample assays. Arterial or venous total blood was centrifuged at 14,000 r.p.m., and then serum was collected and frozen at -80°C . Serum apelin, insulin and leptin concentrations were measured using a nonselective apelin-12 EIA kit that recognizes the C-terminal sequence of 12 amino acids shared among all of the apelin isoforms (Phoenix Pharmaceuticals; Belmont, CA), an ultrasensitive mouse/human insulin ELISA (Mercodia, Uppsala, Sweden) and mouse/human leptin ELISA (R&D system), respectively. Samples for apelin quantification were supplemented with aprotinin (0.6 TIU/ml of total fluid) and purified by a 10-kDa cutoff column before snap freezing (Amicon Ultra, 10,000 molecular weight cutoff, Millipore, Temecula, CA). Plasma glucose was colorimetrically determined by RTU kit (Biomerieux). Nerve growth factor (NGF), IL-6, IL-8, tumor necrosis factor (TNF)- α , MCP-1 and hepatocyte growth factor (HGF) were measured using Luminex technology (Millipore).

Animals. All experimental procedures were performed in accordance with institutional guidelines for animal studies and were approved by an ethics committee (US006/CREFRE, CEEA-122 INSERM). C57Bl6/J WT mice aged 3–24 months were obtained from Janvier Laboratory (St-Berthevin, France). Apelin-deficient (*Apln*^{-/-}) mice were generated as previously described and backcrossed to C57Bl6/J background mice ten times. *Aplnr* heterozygous (*Aplnr*^{+/-}) mice were generated from a cross between C57Bl6/J WT littermates and mice heterozygous for the *Aplnr* mutation (Deltagen, San Carlos, CA, USA). Mice groups were randomly constituted. Mice were housed conventionally in a constant temperature (20–22°C) and humidity (50–60%) animal room, with a 12 h–12 h light–dark cycle and free access to food and water. During the different protocols, mice were excluded if they died prematurely or if they displayed tumors after necropsy. All mice were fed a normal diet. All mice were euthanized in a fed state by cervical vertebra dislocation.

Nanoflow liquid chromatography–tandem mass spectrometry analysis. Blood samples from young (3 months) and aged (24 months) mice were collected using a 22-gauge needle to avoid hemolysis and were immediately centrifuged at 14,000 r.p.m. over 30 min at 4°C. After the centrifugation, the extracted serum was immediately acidified using HCl (12 M, 10%), and the proteases were neutralized by adding leupeptin (40 μM), AEBSEF-HCl (2 mM), bestatin (100 μM), E64 (30 μM), EDTA (10 μM), pepstatin A (100 μM) and aprotinin (5 μM). The prepared serum was injected on a NanoRS 3500 chromatographic system (Dionex, Amsterdam, The Netherlands) coupled to a Q-Exactive HF-X mass spectrometer (Thermo Fisher Scientific, Bremen, Germany). 5 μl of sample was loaded on a C18 precolumn (300- μm inner diameter \times 5 mm; Dionex) at 20 $\mu\text{l}/\text{min}$ in 5% acetonitrile, 0.05% TFA. After 3 min of desalting, the precolumn was switched online with the analytical C18 column (75- μm inner diameter \times 50 cm; in-house packed with Reprosil C18) equilibrated in 95% solvent A (5% acetonitrile, 0.2% formic acid) and 5% solvent B (80% acetonitrile, 0.2% formic acid). Peptides were eluted using a 2–40% gradient of solvent B over 60 min at a flow rate of 300 nL/min. Full mass spectrometry (MS) scans were acquired in the Orbitrap on the 350–1500 m/z range with the resolution set to 60,000. An inclusion list corresponding to several charge states (2+, 3+, 4+) of [Pyr-1]-apelin-13 was used to select these ions for HCD

fragmentation, and the resulting fragment ions were analyzed in the Orbitrap with the resolution set to 15,000. Dynamic exclusion was used within 20 s to prevent repetitive selection of the same peptide.

A standard sample of [Pyr-1]-apelin 13 was injected on a NanoRS 3500 chromatographic system (Dionex, Amsterdam, The Netherlands) coupled to an LTQ-Orbitrap Velos mass spectrometer (Thermo Fisher Scientific, Bremen, Germany). The chromatographic conditions were the same as above for serum samples, except that peptides were eluted using a 5–50% gradient of solvent B over 105 min. The LTQ-Orbitrap Velos was operated in data-dependent acquisition mode with the XCalibur software. Survey scan MS were acquired in the Orbitrap on the 350–1800 m/z range with the resolution set to a value of 60,000. The ten most intense ions per survey scan were selected for collision-induced dissociation (CID) fragmentation, and the resulting fragments were analyzed in the linear trap (LTQ).

The Mascot software (version 2.6.1) was used to automatically extract peak lists from raw files. Data were searched against Mouse entries of the Swissprot protein database (UniProtKB/Swiss-Prot Knowledgebase release 2018_02, Mouse, <https://www.uniprot.org/uniprot/Q9R0R4>).

qPCR. Total RNA (1 μg) was isolated from muscle using GeneJet RNA Purification kit (K0732, Fermentas, Thermo Scientific) and was reverse-transcribed using random hexamers and Superscript II reverse transcriptase (MultiScribe, Applied Biosystems). Real time PCR was performed as previously described starting with 6.25 ng cDNA and both sense and antisense oligonucleotides in a final volume of 10 μl in a 384-well plate using the SYBR green universal PCR master mix (Eurogentec). Analysis of *Hprt* (Hypoxanthine-guanine phosphoribosyltransferase) mRNA was performed to normalize gene expression.

Immunohistology. Muscle frozen sections (10 μm) were immunolabeled for the different myosin heavy chains (MHCs). Primary antibodies were MHC-1 (BA-D5), MHC-2a (SC-71), eMHC (F1.652) from Developmental Studies Hybridoma Bank (DSHB, University of Iowa, IA) and Laminin (Abcam, no. Ab11575). Briefly, sections were blocked for 1 h in PBS plus 4% BSA, 2% goat serum and 0.01% Triton X-100. Sections were then incubated overnight with primary antibodies. After washes in PBS, sections were incubated for 1 h with secondary antibodies anti-Ig2b AF 488, anti-IgG1 AF 546 and anti-rabbit AF 350 (Life Technology). Slides were finally mounted in ProLong Gold antifade Reagent (Molecular probes by Life Technology). Images were captured using a digital camera (Nanozoomer, Hamamatsu) attached to a motorized fluorescence microscope or using Olympus VS120 Virtual Microscopy Slide Scanning System. The area covered by eMHC-positive fibers and the degenerated area were manually determined across the entire sections using the VS-ASW FL software measurement tools. The size of myofibers with central nuclei was calculated from laminin–DAPI staining on all fibers of the section and area determination were performed across the entire sections using an automated image processing algorithm developed internally using the MetaXpress software (Molecular Devices). Finally, virus infection efficiency was assessed by labeling muscle frozen sections with GFP antibody (CS no. 2956, clone D5.1, Cell Signaling) for AAV8-eGFP-tMCK-sh*Apln* or with Luciferase pAb (G7451, Promega) for AAV1-apelin-Luc-CMV. Apelin immunostaining in isolated fibers was performed as previously described³⁸.

Human cell culture. Human myoblasts isolated from muscle from three young healthy volunteers (subject 1: 25 years old; subject 2: 16 years old; subject 3: 27 years old) or from 3 aged healthy volunteers (subject 4: 79 years old; subject 5: 68 years old; subject 6: 83 years old) were immortalized as previously described⁶². Biopsies were provided anonymously by MYOBANK, a tissue bank affiliated to EUROBIOBANK. Human myoblasts were cultured in Skeletal Muscle Cell Media (PromoCell, no. C-23060) supplemented with 20% FBS at 37°C in a humidified atmosphere containing 5% CO₂. When cells were confluent, they were switched to the differentiation medium (DMEM with 50 $\mu\text{g}/\text{ml}$ Gentamicin (Thermo Fischer Scientific, no. 15750045), 10 $\mu\text{g}/\text{ml}$ insulin from bovine pancreas (Sigma-Aldrich, no. I5500), and 100 $\mu\text{g}/\text{ml}$ apo-Transferrin human (Sigma-Aldrich, no. T4382) without any further medium change. Mycoplasma contamination was checked monthly by specific qPCR and DAPI labeling.

Venous–arterial difference. Mice were anesthetized with pentobarbital (0.1 mg/g body weight, CEVA, France) and warmed on a 37°C isothermal pad. Mice were shaved, and a skin incision was performed in the femoral area in order to identify the femoral vein. For arterial blood collection, carotid arteries were dissected. Indwelling catheters were gently placed in both vessels under microscope and fixed by surgical glue (3M-Vetbond). Sciatic nerve and tibialis tendon were then isolated to allow the electric-mediated (frequency of 75–150 Hz, train of stimulation of 200 msec, every 2 s) isotonic contraction (see the section 'In situ tibialis anterior and plantaris specific strength' below). After 10 min of recovery, arterial and venous blood was collected over 10 min through catheters ('stimulation -') and kept at 4°C. Then, 10 min of electric contractions (every 2 seconds) were performed and blood was collected during this time ('stimulation +') and kept at 4°C.

Acute and chronic physical training. Prior to training, randomized mice were first submitted to the acclimation phase consisting of 5 min of treadmill

exploration (0 cm/second) followed by 5 min at slow speed (10 cm/second). The next day, maximal speed capacity was measured by rising the speed by 5 cm/second every 2 min until exhaustion. Mice were considered to be exhausted when the animal's hindlimbs remained on the electric grid for more than 10 seconds. Acute exercise consisted of a 30-, 60- or 120-min bout of exercise (65% of maximal speed, 10% slope). Chronic training consisted of a daily 30 min bout of exercise (65% of maximal speed, 10% slope) for 6 d per week over 28 consecutive d.

Muscle atrophy induced by hindlimb unloading. Unloading associated muscle atrophy was performed according to the protocol described by McMahon et al.⁶³. Briefly, tails of the mice were cleaned and were loosely surrounded by adhesive tapes cross-sectionally. A string was fixed at the dorsal side of the tail to maintain blood flow. The string was fastened to a mobile system fixed at the roof of the cage at a height allowing the forelimbs to support the mouse's body weight yet preventing the hind limbs from touching the floor and the sides of the cage. The mice could reach food and water freely by using their forelimbs. The protocol was carried out over 14 consecutive d.

Body lean mass composition. To determine lean mass, mice were placed in a clear plastic holder, without anesthesia or sedation, and were inserted into the EchoMRI-3-in-1 system (Echo Medical Systems, Houston, TX).

Skeletal muscle function exploration. Time and distance to exhaustion. After two consecutive days of acclimation, running performance was tested in mice by measuring their ability to run until exhaustion. Mice were placed on a treadmill, the speed of which was increased every 2 min by 5 cm/second with the slope at 13%. Mice were considered to be exhausted when the animal's hindlimbs remained on the electric grid for more than 10 s. Time and distance were automatically collected at the end of the protocol.

Strength by grip test. Mice were allowed to grasp a horizontal grid connected to a dynamometer with all four limbs and were pulled backwards five times. The force applied to the grid each time before the animal lost its grip was recorded in Newton. The average of the five measures is normalized to the whole body weight of each mouse.

Inverted grid test. Mice were placed in the center of the wire grid system, and the grid was rotated to an inverted position over 2 s, with the mouse head declining first. The grid was held steadily 40–50 cm above a padded surface. The grid-hanging time capacity was determined by the time the mice spent hanging on the grid.

Maximal speed by running performances. Maximal speed capacity was evaluated by placing mice on a treadmill and raising the treadmill speed 5 cm/second every 2 min until exhaustion. Mice were considered to be exhausted when the animal's hindlimbs remained on the electric grid for more than 10 s.

In situ tibialis anterior and plantaris specific strength. Mice were anesthetized with pentobarbital i.p. injection (0.1 mg/g body weight; CEVA, France). Muscle distal tendons were isolated from other surrounded muscles, cut and bound with silk attached to a force transducer (50 g and 500 g respectively for plantaris and tibialis; AD Instruments, France) using the PowerLab system (26T, AD Instruments) and software (LabChart 4, AD Instruments). Bipolar electrical probes were placed on isolated sciatic nerves, which were stimulated using the supramaximal square wave pulse. Force-generation capacity was evaluated by measuring the maximal force generated in response to isometric contraction under electrical stimulation (frequency of 75–150 Hz, train of stimulation of 200 milliseconds). Maximal isometric force was determined at L0 (length at which maximal tension was obtained during the tetanus). Force was normalized to the muscle mass (mg). Fatigue resistance was determined after a 2 minute resting period. Sciatic nerves were stimulated at 10 Hz over 500 milliseconds every 2 seconds for 1 minute. All contractions were made at the initial length L0. Contractions were expressed as a percentage of the initial maximal (isometric) force. Fatigability corresponded to the time allowing 50% decrease of force.

Microscopic image analysis and quantification. For electron microscope analysis, muscle was cut into small pieces and fixed in 1% glutaraldehyde solution. The tissue was then cut and mounted on copper grids and observed with a Hitachi HU 12 A transmission electron microscope equipped with a high-resolution camera. Mitochondria number was determined by counting the number of organelles per field. Mitochondria area was evaluated by measuring the average surface of the organelles per field.

Mitochondrial DNA content. The content of mitochondrial DNA (mtDNA) was calculated using real-time qPCR by measuring the threshold cycle ratio of a mitochondrial encoded gene (*mt-Co1*; *Cox1*) and a nuclear-encoded gene (*Ppia*).

Enzyme activities. Frozen muscle cryosections were dropped into 100 μ l of ice-cold homogenization buffer (0.25 M sucrose, 10 mM Tris, pH 7.4). Following

centrifugation (650 r.p.m., 4 °C, 15 min), supernatant was discarded, and samples were centrifuged again (25,000 r.p.m., 4 °C, 15 min). The pellet was suspended with homogenization buffer, before another centrifugation (25,000 r.p.m., 4 °C, 15 min). Finally, pellet-containing mitochondria were suspended with 0.1 M Tris, pH 8. For enzyme activities, samples were quickly frozen and defrosted three times in liquid nitrogen, centrifuged (5 min, 13,600 r.p.m., 4 °C), then supernatant was kept for enzyme activities. Citrate synthase activity was measured by adding to muscle mitochondria homogenate, 150 μ l of Tris Buffer 100 mM (pH 8), 25 μ l DTNB (1 mM, Sigma D-8130), 40 μ l Acetyl CoA (Sigma A-2056), 10% Triton and 15 μ l of Oxaloacetate 3 mM (Sigma O-4126). Absorbance was read at 412 nm, and citrate activity was assessed in μ mol/min/g = ((Abs/min) \times total volume)/13.6 \times sample volume \times dilution factor). For aconitase activity, muscle mitochondria homogenate was mixed with aconitate (10 mM), Mg²⁺ (60 mM), β -NADP (0.1 mg/ml), tetrazolium salt (0.1 mg/ml), phenazine methosulfate (25 μ g/ml), Fe(NH₄)₂(SO₄)₂ (10 μ g/ml), isocitrate dehydrogenase (0.04 U/ml) and Tris (150 mM, pH 8). Sample absorbance, as well as a standard curve of pig aconitase, was read at 575 nm for 30 min at 37 °C.

Muscle-specific apelin deletion. shRNA directed against murine apelin gene (NM_013912.3) was integrated into AAV8 under tMCK promoter dependency coupled with a triple enhancer and with eGFP (AAV8-eGFP-MCK-shApln) (Vector Biolabs). As already demonstrated^{26–28}, high skeletal muscle specificity was obtained by adding a triple tandem of 2RS5 enhancer sequences (3-Ebox) ligated to the truncated regulation region of the MCK promoter, generating the tMCK promoter. The cardiac transcriptional factor Nkx-2.5 does not bind to the E-box, explaining why the multimerized E-boxes, especially the modified 2RS5 E-boxes, increased gene expression in skeletal muscle but not in the heart. Control mice were treated with a similar construction containing a scramble peptide sequence instead of shApln (AAV8-eGFP-MCK-shCt). After titration in mouse, 10-month-old C57Bl6/j randomized mice were submitted to a single retro-orbital injection (5 μ l) of the virus diluted in PBS to a final concentration of 5 \times 10¹¹ particles. Forty d.p.i., blood was collected before and after a treadmill single boot exercise in order to measure plasma apelin immunoreactivity. Forty-seven d.p.i., mice were submitted to physical tests to evaluate strength, grid-hanging capacities, time and distance to exhaustion performed on treadmill and maximal speed. Finally, at 54 d.p.i., mice were euthanized, and tissues were collected.

Apelin supplementation. Chronic i.p. injection. 3-, 12- and 24-month-old C57Bl6/j mice, 12-month-old *Apln*^{-/-}, *Apln*^{+/-} and DN-AMPK mice randomized to different groups according to their weights were daily i.p. injected with [pyr1]apelin-13 (Bachem, Switzerland) at 0.5 μ mol/kg/day for 28 d, as previously described. Age- and genotype-matched control mice were injected with PBS. Investigators were blinded to the group allocation (injection of apelin or PBS) during the protocol and the associated experiments. All mice were euthanized 24 h after the last apelin or PBS injection. The investigators were blinded regarding the treatment.

AAV-mediated skeletal muscle apelin overexpression. Murine apelin sequence (NM_013912.3) was integrated to AAV1 under cytomegalovirus promoter dependency with secretion signal. Apelin was coexpressed with F-Luciferase interconnected by a p2A peptide (AAV1-apelin-Luc). Control mice were injected with a similar construction containing a scramble peptide sequence instead of apelin (AAV1-Luc-Ct). Randomized 24-month-old C57Bl6/j mice were injected in the tibialis anterior and gastrocnemius muscles with 10¹¹ particles of AAV1-apelin-Luciferase in 50 μ l of 1 \times PBS. Investigators were blinded to the group allocation during the protocol and the associated experiments. Mice were euthanized 8 weeks after injection.

In vivo animal imaging of luciferase expression. Seven days after AAV injection, mice were anesthetized with 2% isoflurane and oxygen. The D-luciferin substrate (Promega) was injected intraperitoneally at a dose of 150 μ g/g of body weight. The mice were then placed in a light-tight chamber, and images were generated using a cryogenically cooled charge-coupling device camera IVIS 100 (Xenogen, Alameda, CA). For each mouse, the images were taken 8–12 min after the substrate injection. Light and dark images of mice were collected, and the dark images were pseudocolored using the Xenogen software. The visual output represents the number of photons emitted/second/cm² as a false color image where the maximum is red and the minimum is dark blue.

Western blotting. Muscle and cells samples were lysed (Precellys 24, Ozyme France) and loaded (30 mg protein per lane) on a 4–20% SDS-PAGE gel and transferred to nitrocellulose membrane (GE Healthcare, Life Sciences, Whatman). Membranes were blotted with anti-p-AMPK α ^{Thr172} (CS no. 2535, clone 40H9), AMPK α (CS no. 2757), p-Akt^{Ser473} (CS no. 4060, clone D9E), Akt (CS no. 4685, clone 11E7), p-mTOR^{Ser2448} (CS no. 5536, clone D9C2), mTOR (CS no. 2983, clone 7C10), p-p70S6 kinase^{Thr389} (CS no. 9234, clone 108D2), p70S6 kinase (CS no. 9202), p-FoxO1^{Thr24}/FoxO3a^{Thr32} (CS no. 9464), FoxO3a (CS no. 2497), LC3B (CS no. 2775), p-46-4E-BP1^{Thr37} (CS no. 2855, clone 236B4), p-Acetyl-CoA Carboxylase^{Ser79} (CS no. 3661), Acetyl-CoA Carboxylase (CS no. 3662) and GAPDH (CS no. 5174, clone D16H11) (Cell Signaling Technology). MyHCIIa

western blotting was performed with MHC-2a (SC-71) antibody Developmental Studies Hybridoma Bank (DSHB, University of Iowa, IA). Immunoreactive proteins were detected using the Clarity Western ECL Substrate (BioRad) and quantified using Image Lab software (BioRad).

Protein synthesis by in vitro SUNSET. The SUNSET assay was used to monitor the rate of protein synthesis. Briefly, 10 min prior harvesting the cells, puromycin was added to culture medium at 1 $\mu\text{g}/\text{ml}$. As a control, no puromycin was added. Cell extracts were then processed for western blotting using anti-puromycin 12D10 antibody (Millipore).

Mitochondrial respiration. The skeletal muscle tissue was subjected to mechanical dissection with pointed forceps in relaxing buffer on ice. The relaxing buffer contained 2.77 mM CaK₂-EGTA, 7.23 mM K₂EGTA, 20 mM imidazole, 20 mM taurine, 6.56 mM MgCl₂, 5.77 mM ATP, 15 mM phosphocreatine, 0.5 mM dithiothreitol and 50 mM K-MES, pH 7.1. Skeletal muscle fibers were permeabilized by gentle agitation for 30 min at 4 °C in the relaxing solution supplemented with 50 $\mu\text{g}/\text{mL}$ of saponin. Fibers were then twice washed in ice-cold respiration medium. Respiration was measured at 30 °C in a high-resolution respirometer (Oroboros, Oxygraph; Innsbruck, Austria), and data are given as pmol O₂/sec/mg (wet weight of muscle). The respiration medium consisted of 110 mM sucrose, 60 mM K-lactobionate, 0.5 mM EGTA, 1 g/L BSA essentially fatty acid free, 3 mM MgCl₂, 20 mM taurine, 10 mM KH₂PO₄ and 20 mM K-HEPES, pH 7.1. The software DatLab (Oroboros Instruments) was used for data analysis. Respiration was assessed with glutamate (10 mM) and malate (2 mM), followed by ADP (3.5 mM). Rotenone (0.5 M) was added to inhibit complex I then succinate (10 mM) was added. Malate and glutamate provide NADH for complex I, succinate provides FADH₂ for complex II.

Fluidigm by Biomark qPCR. qPCR was performed with 6.5 ng of cDNA and 100 μM of both sense and antisense oligonucleotides as already described. The complete list of sequences and the results are available upon request.

Flow cytometry detection of APLNR. The rabbit anti-mouse Aplnr (Abcam ab214369, Cambridge, UK) was conjugated to PE by means of the Lightning Link PE-kit (Innova Biosciences, Cambridge, UK) following the manufacturer's instructions. Muscle stem cells (MuSCs) were sorted from PAX-7-ZsGreen reporter mice, which were generated by inserting a T2A-ZsGreen-NLS reporter downstream of exon 9 of the *Pax7* locus through homologous recombination. In this model, the ZsGreen fluorescent protein is expressed specifically in the nucleus of PAX-7⁺ muscle stem cells independently of the PAX-7 protein but under the control of the endogenous PAX-7 promoter. Correct transgene insertion was verified by long-range PCR and the neomycin selection cassette was removed through a Flp-mediated recombination system. The reporter was further validated by demonstrating that MuSCs sorted from skeletal muscle based on ZsGreen fluorescence are CD34⁺SCA1⁺ α 7Int⁺ by flow cytometry, positive for PAX-7 by qPCR and myogenic ex vivo.

Hind-limb skeletal muscle was digested with Dispase II (2.5 U/ml) (Roche), Collagenase B (0.2%) (Roche) and MgCl₂ (5 mM) at 37 °C after tissue mincing, and muscle stem cells were FACS-sorted at 4 °C using a Beckman Coulter Astrios Cell sorter using their positivity for the Zs-Green-PAX-7 reporter. Sorted muscle stem cells were then kept on ice and were left unstained as a negative control or were stained for 30 min on ice with PE-coupled APLNR antibody (APJ-PE; 0.5 $\mu\text{g}/\text{uL}$), and washed with HBSS⁺. Specificity of the staining was evaluated by preincubating sorted MuSCs for 30 min with the unlabeled APLNR antibody followed by a 30 min incubation with the APLNR-PE coupled antibody at 1 $\mu\text{g}/\text{uL}$. Samples were then reanalyzed on the Beckman Coulter Astrios Cell sorter for APLNR detection based on PE fluorescence.

Cardiotoxin injury-induced skeletal muscle regeneration. Mice were i.p injected with buprenorphin (Centravet, 0.1 mg/kg) 30 min before injury and the day after. The day of the injury, mice were anesthetized with isoflurane inhalation and hindlimbs were shaved. Then, 10 μM of cardiotoxin (CTX, Latoxan, no. L8102) was injected through two injections of 25 μl into left tibialis muscle and two injections of 50 μl into left gastrocnemius muscle, using a 22-gauge needle (Hamilton). Mice were euthanized 3, 7 and 14 d after injury by cervical dislocation, and muscles (PBS- and CTX-injected) were cut in two parts. One part was snap frozen into liquid nitrogen for total RNA extraction and the other part was embedded into

optimum cutting temperature (OCT) compound and frozen in isopentan cooled with liquid nitrogen for histological analysis.

Histology of muscle stem cells. Mouse muscle samples were dissected and cryopreserved in OCT frozen in liquid nitrogen-cooled isopentan. Samples were then sectioned at 10 μm on a cryostat and post-fixed with 4% paraformaldehyde (PFA) for 15 min at room temperature. After permeabilization with cold 100% methanol for 6 min at -20 °C, sections were boiled in citrate buffer (10 mM, pH 6.0) for 10 min. Following blocking with 4% BSA and goat anti-mouse Fab (1/100) for 30 min, primary antibodies were incubated at 4 °C overnight (mouse anti-PAX-7 (purified IgG1 from DSHB hybridoma), 1:500 and rabbit anti-K₁-67 polyclonal (Abcam no. ab15580), 1:200). Secondary antibodies (biotinylated goat anti-mouse IgG, 1/1,000; goat anti-rabbit A648 1/2,000) were incubated for 1 h at room temperature. Subsequently, streptavidin-A555 was incubated at 1/2,000 for 30 min to amplify the PAX-7 signal, and Hoechst was used to detect nuclei. The stained sections were mounted, imaged using a 10 \times objective on an Olympus VS120 fluorescence slide scanner and quantified manually in three randomly selected injured areas of each sample using the VS-ASV 2.8 software (Olympus). The total number of MuSCs was quantified as the total number PAX-7⁺DAPI⁺ nuclei per area analyzed, and the percentage of proliferating MuSCs was quantified as the number of PAX-7⁺K₁-67⁺DAPI⁺ nuclei normalized to the total number of MuSCs.

Mouse muscle stem cell primary culture. WT, *Aplnr*^{-/-} and *Aplnr*^{+/-} mice were euthanized, and their hindlimbs were rapidly collected and dissected into cold PBS. Then, muscles were digested according to Rosenblatt's protocol and stem cells (MuSCs) were purified by magnetic beads sorting using a commercial kit (Satellite Cell Isolation Kit, mouse, MACS, Miltenyl Biotec, Germany). MuSCs were then plated on 1% collagen-treated dishes in proliferation medium (40% DMEM, 40% HAM's medium, 1% penicillin/streptomycin, 20% fetal bovine serum) supplemented with FGF₂ (50 $\mu\text{g}/\text{ml}$). After 5 d, myocytes were differentiated into myotubes adding DMEM with 1% horse serum. After 7 d of differentiation, myotubes were rinsed with PBS and fixed into 4% formalin. Fiber width was determined by averaging 10 different measures all along the myotube in a field of 20 \times .

Fusion index. Cells were cultivated over 4 d (until confluence) and treated with apelin or PBS over 10 d. Then cells were fixed with 4% formalin (Sigma). DAPI coloration is done and myocytes index fusion is calculated by dividing the number of nuclei into a myotube by the total number of nuclei in a field \times 100.

Statistical analysis. Data are expressed as the mean \pm s.e.m. Statistical analyses were performed using Student's *t*-test (two-tailed paired or unpaired) or one-way ANOVA followed by the post hoc Dunnett's and Tukey's test with GraphPad Prism 5 software (GraphPad Software). *P* values less than 0.05 (* or #), 0.01 (** or ##) or 0.001 (***) or ### were statistically significant. A logistic regression was performed to discriminate if age, apelin, BMI and sex were independently correlated to the sarcopenic status. Goodness of fit of the model was assessed using the Hosmer-Lemeshow test. Statistical analysis was realized by MedCalc statistical software (Mariakerke, Belgium).

Reporting Summary. Further information on experimental design is available in the Nature Research Reporting Summary linked to this article.

Data availability. All of the data generated or analyzed during this study are included in this published article (and its Supplementary Information file) and are available from the corresponding author.

References

- Castan-Laurell, I. et al. Effect of hypocaloric diet-induced weight loss in obese women on plasma apelin and adipose tissue expression of apelin and APJ. *Eur. J. Endocrinol.* **158**, 905–910 (2008).
- Mamchaoui, K. et al. Immortalized pathological human myoblasts: towards a universal tool for the study of neuromuscular disorders. *Skelet. Muscle* **1**, 34 (2011).
- McMahon, C. D. et al. Myostatin-deficient mice lose more skeletal muscle mass than wild-type controls during hindlimb suspension. *Am. J. Physiol. Endocrinol. Metab.* **285**, E82–E87 (2003).

Reporting Summary

Nature Research wishes to improve the reproducibility of the work that we publish. This form provides structure for consistency and transparency in reporting. For further information on Nature Research policies, see [Authors & Referees](#) and the [Editorial Policy Checklist](#).

Statistical parameters

When statistical analyses are reported, confirm that the following items are present in the relevant location (e.g. figure legend, table legend, main text, or Methods section).

n/a Confirmed

- The exact sample size (n) for each experimental group/condition, given as a discrete number and unit of measurement
- An indication of whether measurements were taken from distinct samples or whether the same sample was measured repeatedly
- The statistical test(s) used AND whether they are one- or two-sided
Only common tests should be described solely by name; describe more complex techniques in the Methods section.
- A description of all covariates tested
- A description of any assumptions or corrections, such as tests of normality and adjustment for multiple comparisons
- A full description of the statistics including central tendency (e.g. means) or other basic estimates (e.g. regression coefficient) AND variation (e.g. standard deviation) or associated estimates of uncertainty (e.g. confidence intervals)
- For null hypothesis testing, the test statistic (e.g. F , t , r) with confidence intervals, effect sizes, degrees of freedom and P value noted
Give P values as exact values whenever suitable.
- For Bayesian analysis, information on the choice of priors and Markov chain Monte Carlo settings
- For hierarchical and complex designs, identification of the appropriate level for tests and full reporting of outcomes
- Estimates of effect sizes (e.g. Cohen's d , Pearson's r), indicating how they were calculated
- Clearly defined error bars
State explicitly what error bars represent (e.g. SD, SE, CI)

Our web collection on [statistics for biologists](#) may be useful.

Software and code

Policy information about [availability of computer code](#)

Data collection

Data analysis

For manuscripts utilizing custom algorithms or software that are central to the research but not yet described in published literature, software must be made available to editors/reviewers upon request. We strongly encourage code deposition in a community repository (e.g. GitHub). See the Nature Research [guidelines for submitting code & software](#) for further information.

Data

Policy information about [availability of data](#)

All manuscripts must include a [data availability statement](#). This statement should provide the following information, where applicable:

- Accession codes, unique identifiers, or web links for publicly available datasets
- A list of figures that have associated raw data
- A description of any restrictions on data availability

Field-specific reporting

Please select the best fit for your research. If you are not sure, read the appropriate sections before making your selection.

Life sciences Behavioural & social sciences

For a reference copy of the document with all sections, see [nature.com/authors/policies/ReportingSummary-flat.pdf](https://www.nature.com/authors/policies/ReportingSummary-flat.pdf)

Life sciences

Study design

All studies must disclose on these points even when the disclosure is negative.

Sample size	Mouse sample sized was estimated by pilot experiments that showed trends of effects and their sizes. In most cases, an n=5 was the minimal amount used, only where effect size was large an n=3 yielded significant results. Human sample size See Methods, chapter "human cohorts". We determined the minimal number of participants according to the plasma apelin variability published by Castan-Laurell et al. (Eur. J. Endocrinol., 2009) We calculated a sample size of 17 participants per group to detect a minimal difference of 0.1ng/ml in apelin concentration between the groups assuming alpha = 0.05, beta = 0.90, SD within each group = 0.02.
Data exclusions	Because animals are gaed, mice were excluded for poor body condition (e.g.weight loose, important injuries). Exclusion crieria were pre-established before the study.
Replication	All replications were successful.
Randomization	Mice were randomly allocated to groups. To insure randomization, we weighted animals and distributed them equally in the different groups.
Blinding	All the treatements and the functionnal experiments were done by blinded investigators

Materials & experimental systems

Policy information about [availability of materials](#)

n/a	Involved in the study
<input type="checkbox"/>	<input checked="" type="checkbox"/> Unique materials
<input type="checkbox"/>	<input checked="" type="checkbox"/> Antibodies
<input type="checkbox"/>	<input checked="" type="checkbox"/> Eukaryotic cell lines
<input type="checkbox"/>	<input checked="" type="checkbox"/> Research animals
<input type="checkbox"/>	<input checked="" type="checkbox"/> Human research participants

Unique materials

Obtaining unique materials

Antibodies

Antibodies used

Validation

Eukaryotic cell lines

Policy information about [cell lines](#)

Cell line source(s)

Authentication

Mycoplasma contamination

Commonly misidentified lines
(See [ICLAC](#) register)

Name any commonly misidentified cell lines used in the study and provide a rationale for their use.

Research animals

Policy information about [studies involving animals](#); [ARRIVE guidelines](#) recommended for reporting animal research

Animals/animal-derived materials

Mus musculus, C57Bl6/j background, male, aged from 3 to 24 month old

Human research participants

Policy information about [studies involving human research participants](#)

Population characteristics

All the characteristics of the human cohort are listed online MAPT: NCT00672685
LIFE-P: NCT00116194

Method-specific reporting

n/a	Involvement in the study
<input checked="" type="checkbox"/>	<input type="checkbox"/> ChIP-seq
<input checked="" type="checkbox"/>	<input type="checkbox"/> Flow cytometry
<input checked="" type="checkbox"/>	<input type="checkbox"/> Magnetic resonance imaging

Bibliography

1. Abou-Khalil, R., Le Grand, F., Pallafacchina, G., Valable, S., Authier, F.-J., Rudnicki, M.A., Gherardi, R.K., Germain, S., Chretien, F., Sotiropoulos, A., et al. (2009). Autocrine and Paracrine Angiopoietin 1/Tie-2 Signaling Promotes Muscle Satellite Cell Self-Renewal. *Cell Stem Cell* 5, 298–309.
2. Abreu, P. (2018). Bioenergetics mechanisms regulating muscle stem cell self-renewal commitment and function. *Biomed. Pharmacother.* 103, 463–472.
3. Abreu, P., Mendes, S.V.D., Ceccatto, V.M., and Hirabara, S.M. (2017). Satellite cell activation induced by aerobic muscle adaptation in response to endurance exercise in humans and rodents. *Life Sci.* 170, 33–40.
4. AbuSamra, D.B. (2015). CD34 Is a Ligand for Vascular Selectins on Human Hematopoietic Stem/Progenitor Cells. *Blood* 126, 2399–2399.
5. Ahsan, S., Raval, M.H., Ederer, M., Tiwari, R., Chareunsouk, A., and Rodgers, J.T. (2020). Metabolism of glucose and glutamine is critical for skeletal muscle stem cell activation. *BioRxiv* 2020.07.28.225847.
6. Alfaro, L.A.S., Dick, S.A., Siegel, A.L., Anonuevo, A.S., McNagny, K.M., Megeney, L.A., Cornelison, D.D.W., and Rossi, F.M.V. (2011). CD34 promotes satellite cell motility and entry into proliferation to facilitate efficient skeletal muscle regeneration. *Stem Cells Dayt. Ohio* 29, 2030–2041.
7. Ance, S., Stuelsatz, P., and Feige, J.N. (2021). Muscle Stem Cell Quiescence: Controlling Stemness by Staying Asleep. *Trends Cell Biol.*
8. Armingol, E., Officer, A., Harismendy, O., and Lewis, N.E. (2021). Deciphering cell–cell interactions and communication from gene expression. *Nat. Rev. Genet.* 22, 71–88.
9. Attane, C., Foussal, C., Le Gonidec, S., Benani, A., Daviaud, D., Wanecq, E., Guzman-Ruiz, R., Dray, C., Bezair, V., Rancoule, C., et al. (2012). Apelin Treatment Increases Complete Fatty Acid Oxidation, Mitochondrial Oxidative Capacity, and Biogenesis in Muscle of Insulin-Resistant Mice. *Diabetes* 61, 310–320.
10. Auffray, C., Fogg, D., Garfa, M., Elain, G., Join-Lambert, O., Kayal, S., Sarnacki, S., Cumano, A., Lauvau, G., and Geissmann, F. (2007). Monitoring of Blood Vessels and Tissues by a Population of Monocytes with Patrolling Behavior. *Science* 317, 666–670.
11. Barnouin, Y., McPhee, J.S., Butler-Browne, G., Bosutti, A., De Vito, G., Jones, D.A., Narici, M., Behin, A., Hogrel, J.-Y., and Degens, H. (2017). Coupling between skeletal muscle fiber size and capillarization is maintained during healthy aging. *J. Cachexia Sarcopenia Muscle* 8, 647–659.

12. Baumgartner-Parzer, S.M., Wagner, L., Pettermann, M., Grillari, J., Gessl, A., and Waldhäusl, W. (1995). High-Glucose–Triggered Apoptosis in Cultured Endothelial Cells. *Diabetes* 44, 1323–1327.
13. Beauchamp, J.R., Heslop, L., Yu, D.S.W., Tajbakhsh, S., Kelly, R.G., Wernig, A., Buckingham, M.E., Partridge, T.A., and Zammit, P.S. (2000). Expression of Cd34 and Myf5 Defines the Majority of Quiescent Adult Skeletal Muscle Satellite Cells. *J. Cell Biol.* 151, 1221–1234.
14. Bengal, E., Perdiguero, E., Serrano, A.L., and Muñoz-Cánoves, P. (2017). Rejuvenating stem cells to restore muscle regeneration in aging. *F1000Research* 6, 76.
15. Benninger, R.K.P., and Piston, D.W. (2013). Two-Photon Excitation Microscopy for the Study of Living Cells and Tissues. *Curr. Protoc. Cell Biol.* 59.
16. Bentzinger, C.F., Wang, Y.X., Dumont, N.A., and Rudnicki, M.A. (2013). Cellular dynamics in the muscle satellite cell niche. *EMBO Rep.* 14, 1062–1072.
17. Berger, M., Hagg, S.A., Goodman, M.N., and Ruderman, N.B. (1976). Glucose metabolism in perfused skeletal muscle. Effects of starvation, diabetes, fatty acids, acetoacetate, insulin and exercise on glucose uptake and disposition. *Biochem. J.* 158, 191–202.
18. Bertrand, C., Pignalosa, A., Wanecq, E., Rancoule, C., Batut, A., Deleruyelle, S., Lionetti, L., Valet, P., and Castan-Laurell, I. (2013). Effects of dietary eicosapentaenoic acid (EPA) supplementation in high-fat fed mice on lipid metabolism and apelin/APJ system in skeletal muscle. *PLoS One* 8, e78874.
19. Besse-Patin, A., Montastier, E., Vinel, C., Castan-Laurell, I., Louche, K., Dray, C., Daviaud, D., Mir, L., Marques, M.-A., Thalamas, C., et al. (2014). Effect of endurance training on skeletal muscle myokine expression in obese men: identification of apelin as a novel myokine. *Int. J. Obes.* 38, 707–713.
20. Blanco-Bose, W.E., Yao, C.-C., Kramer, R.H., and Blau, H.M. (2001). Purification of Mouse Primary Myoblasts Based on $\alpha 7$ Integrin Expression. *Exp. Cell Res.* 265, 212–220.
21. Blau, H.M., Pavlath, G.K., Hardeman, E.C., Chiu, C.-P., Silberstein, L., Webster, S.G., Miller, S.C., and Webster, C. (1985). Plasticity of the Differentiated State. *Science* 230, 758–766.
22. Blau, H.M., Cosgrove, B.D., and Ho, A.T.V. (2015). The central role of muscle stem cells in regenerative failure with aging. *Nat. Med.* 21, 854–862.
23. Bloor, C.M. (2005). Angiogenesis during exercise and training. *Angiogenesis* 8, 263–271.
24. Bockman, E.L. (1983). Blood flow and oxygen consumption in active soleus and gracilis muscles in cats. *Am. J. Physiol.* 244, H546–551.
25. Boucher, J., Masri, B., Daviaud, D., Gesta, S., Guigné, C., Mazzucotelli, A., Castan-Laurell, I., Tack, I., Knibiehler, B., Carpené, C., et al. (2005). Apelin, a Newly

- Identified Adipokine Up-Regulated by Insulin and Obesity. *Endocrinology* *146*, 1764–1771.
26. Bowerman, M., Murray, L.M., Scamps, F., Schneider, B.L., Kothary, R., and Raoul, C. (2018). Pathogenic commonalities between spinal muscular atrophy and amyotrophic lateral sclerosis: Converging roads to therapeutic development. *Eur. J. Med. Genet.* *61*, 685–698.
 27. Brack, A.S., and Rando, T.A. (2012). Tissue-specific stem cells: Lessons from the skeletal muscle satellite cell. *Cell Stem Cell* *10*, 504–514.
 28. Brack, A.S., Conboy, M.J., Roy, S., Lee, M., Kuo, C.J., Keller, C., and Rando, T.A. (2007). Increased Wnt signaling during aging alters muscle stem cell fate and increases fibrosis. *Science* *317*, 807–810.
 29. Bracy, D.P., Zinker, B.A., Jacobs, J.C., Lacy, D.B., and Wasserman, D.H. (1995). Carbohydrate metabolism during exercise: influence of circulating fat availability. *J. Appl. Physiol. Bethesda Md* *1985* *79*, 506–513.
 30. Brocca, L., McPhee, J.S., Longa, E., Canepari, M., Seynnes, O., De Vito, G., Pellegrino, M.A., Narici, M., and Bottinelli, R. (2017). Structure and function of human muscle fibres and muscle proteome in physically active older men: Skeletal muscle adaptations in human ageing. *J. Physiol.* *595*, 4823–4844.
 31. Broholm, C., Mortensen, O.H., Nielsen, S., Akerstrom, T., Zankari, A., Dahl, B., and Pedersen, B.K. (2008). Exercise induces expression of leukaemia inhibitory factor in human skeletal muscle. *J. Physiol.* *586*, 2195–2201.
 32. Brooks, G.A. (1997). Importance of the “crossover” concept in exercise metabolism. *Clin. Exp. Pharmacol. Physiol.* *24*, 889–895.
 33. Brooks, G.A. (1998). Mammalian fuel utilization during sustained exercise. *Comp. Biochem. Physiol. B Biochem. Mol. Biol.* *120*, 89–107.
 34. Brzoska, E., Kowalewska, M., Markowska-Zagrajek, A., Kowalski, K., Archacka, K., Zimowska, M., Grabowska, I., Czerwińska, A.M., Czarnecka-Góra, M., Stremińska, W., et al. (2012). Sdf-1 (CXCL12) improves skeletal muscle regeneration via the mobilisation of Cxcr4 and CD34 expressing cells. *Biol. Cell* *104*, 722–737.
 35. Buas, M.F., and Kadesch, T. (2010). Regulation of skeletal myogenesis by Notch. *Exp. Cell Res.* *316*, 3028–3033.
 36. Buckingham, M. (2007). Skeletal muscle progenitor cells and the role of Pax genes. *C. R. Biol.* *330*, 530–533.
 37. Buranasin, P., Mizutani, K., Iwasaki, K., Pawaputanon Na Mahasarakham, C., Kido, D., Takeda, K., and Izumi, Y. (2018). High glucose-induced oxidative stress impairs proliferation and migration of human gingival fibroblasts. *PLoS ONE* *13*, e0201855.
 38. Burzyn, D., Kuswanto, W., Kolodin, D., Shadrach, J.L., Cerletti, M., Jang, Y., Sefik, E., Tan, T.G., Wagers, A.J., Benoist, C., et al. (2013). A Special Population of Regulatory T Cells Potentiates Muscle Repair. *Cell* *155*, 1282–1295.

39. Butler, A., Hoffman, P., Smibert, P., Papalexi, E., and Satija, R. (2018). Integrating single-cell transcriptomic data across different conditions, technologies, and species. *Nat. Biotechnol.* *36*, 411–420.
40. Cafforio, G., Pistolesi, S., D'Avino, C., Galluzzi, F., Patricelli, A., Solito, B., Fontanini, G., and Siciliano, G. (2005). Inclusion body myopathy associated with motor neuron syndrome: three case reports. *Clin. Neuropathol.* *24*, 36–41.
41. Carbone, J.W., McClung, J.P., and Pasiakos, S.M. (2012). Skeletal Muscle Responses to Negative Energy Balance: Effects of Dietary Protein. *Adv. Nutr.* *3*, 119–126.
42. Castan-laurell, I., Dray, C., Knauf, C., Kunduzova, O., and Valet, P. (2012). Apelin, a promising target for type 2 diabetes treatment? *Trends Endocrinol. Metab.* *23*, 234–241.
43. Castets, P., Ham, D.J., and Rüegg, M.A. (2020). The TOR Pathway at the Neuromuscular Junction: More Than a Metabolic Player? *Front. Mol. Neurosci.* *13*, 162.
44. Catoire, M., Mensink, M., Kalkhoven, E., Schrauwen, P., and Kersten, S. (2014). Identification of human exercise-induced myokines using secretome analysis. *Physiol. Genomics* *46*, 256–267.
45. Cerletti, M., Jang, Y.C., Finley, L.W.S., Haigis, M.C., and Wagers, A.J. (2012). Short-term calorie restriction enhances skeletal muscle stem cell function. *Cell Stem Cell* *10*, 515–519.
46. Chakkalakal, J.V., Jones, K.M., Basson, M.A., and Brack, A.S. (2012). The aged niche disrupts muscle stem cell quiescence. *Nature* *490*, 355–360.
47. Chakkalakal, J.V., Christensen, J., Xiang, W., Tierney, M.T., Boscolo, F.S., Sacco, A., and Brack, A.S. (2014). Early forming label-retaining muscle stem cells require p27kip1 for maintenance of the primitive state. *Development* *141*, 1649–1659.
48. Chang, Y.-H., Tsai, J.-N., Chen, T.-L., Ho, K.-T., Cheng, H.-Y., Hsiao, C.-W., and Shiau, M.-Y. (2019). Interleukin-4 Promotes Myogenesis and Boosts Myocyte Insulin Efficacy. *Mediators Inflamm.* *2019*, e4182015.
49. Chapman, N.A., Dupré, D.J., and Rainey, J.K. (2014). The apelin receptor: Physiology, pathology, cell signalling, and ligand modulation of a peptide-activated class A GPCR. *Biochem. Cell Biol. Biochim. Biol. Cell.* *92*, 431–440.
50. Chargé, S.B.P., and Rudnicki, M.A. (2004). Cellular and Molecular Regulation of Muscle Regeneration. *Physiol. Rev.* *84*, 209–238.
51. Charnaux, N., Brule, S., Hamon, M., Chaigneau, T., Saffar, L., Prost, C., Lievre, N., and Gattegno, L. (2005). Syndecan-4 is a signaling molecule for stromal cell-derived factor-1 (SDF-1)/ CXCL12. *FEBS J.* *272*, 1937–1951.
52. Chazaud, B. (2020). Inflammation and Skeletal Muscle Regeneration: Leave It to the Macrophages! *Trends Immunol.* *41*, 481–492.

53. Chen, S.-E., Jin, B., and Li, Y.-P. (2007a). TNF- α regulates myogenesis and muscle regeneration by activating p38 MAPK. *Am. J. Physiol. Cell Physiol.* **292**, C1660-1671.
54. Chen, Y.-H., Lin, S.-J., Lin, F.-Y., Wu, T.-C., Tsao, C.-R., Huang, P.-H., Liu, P.-L., Chen, Y.-L., and Chen, J.-W. (2007b). High Glucose Impairs Early and Late Endothelial Progenitor Cells by Modifying Nitric Oxide-Related but Not Oxidative Stress-Mediated Mechanisms. *Diabetes* **56**, 1559–1568.
55. Choi, J., Rakhilin, N., Gadamsetty, P., Joe, D.J., Tabrizian, T., Lipkin, S.M., Huffman, D.M., Shen, X., and Nishimura, N. (2018). Intestinal crypts recover rapidly from focal damage with coordinated motion of stem cells that is impaired by aging. *Sci. Rep.* **8**.
56. Choudhury, R.R., Hyvola, N., and Lowe, M. (2005). Phosphoinositides and membrane traffic at the trans-Golgi network. *Biochem. Soc. Symp.* 31–38.
57. Christov, C., Chrétien, F., Abou-Khalil, R., Bassez, G., Vallet, G., Authier, F.-J., Bassaglia, Y., Shinin, V., Tajbakhsh, S., Chazaud, B., et al. (2007a). Muscle Satellite Cells and Endothelial Cells: Close Neighbors and Privileged Partners. *Mol. Biol. Cell* **18**, 1397–1409.
58. Christov, C., Chrétien, F., Abou-Khalil, R., Bassez, G., Vallet, G., Authier, F.-J., Bassaglia, Y., Shinin, V., Tajbakhsh, S., Chazaud, B., et al. (2007b). Muscle Satellite Cells and Endothelial Cells: Close Neighbors and Privileged Partners. *Mol. Biol. Cell* **18**, 1397–1409.
59. Clark, M.G., Rattigan, S., Clerk, L.H., Vincent, M.A., Clark, A.D., Youd, J.M., and Newman, J.M. (2000). Nutritive and non-nutritive blood flow: rest and exercise. *Acta Physiol. Scand.* **168**, 519–530.
60. Clarke, M. (2010). Muscle sliding filaments: Sliding filament model for muscle contraction. *Nat. Rev. Mol. Cell Biol.* **9**, s7–s7.
61. Clifford, P.S., Kluess, H.A., Hamann, J.J., Buckwalter, J.B., and Jasperse, J.L. (2006). Mechanical compression elicits vasodilatation in rat skeletal muscle feed arteries. *J. Physiol.* **572**, 561–567.
62. Collins, B.C., Mader, T.L., Cabelka, C.A., Iñigo, M.R., Spangenburg, E.E., and Lowe, D.A. (2018). Deletion of estrogen receptor α in skeletal muscle results in impaired contractility in female mice. *J. Appl. Physiol.* **124**, 980–992.
63. Collins, B.C., Arpke, R.W., Larson, A.A., Baumann, C.W., Xie, N., Cabelka, C.A., Nash, N.L., Juppi, H.-K., Laakkonen, E.K., Sipilä, S., et al. (2019). Estrogen Regulates the Satellite Cell Compartment in Females. *Cell Rep.* **28**, 368-381.e6.
64. Collins, P.J., McCully, M.L., Martínez-Muñoz, L., Santiago, C., Wheeldon, J., Caucheteux, S., Thelen, S., Cecchinato, V., Laufer, J.M., Purvanov, V., et al. (2017). Epithelial chemokine CXCL14 synergizes with CXCL12 *via* allosteric modulation of CXCR4. *FASEB J.* **31**, 3084–3097.

65. Conboy, I.M., and Rando, T.A. (2002). The Regulation of Notch Signaling Controls Satellite Cell Activation and Cell Fate Determination in Postnatal Myogenesis. *Dev. Cell* 3, 397–409.
66. Contreras, O., Rebolledo, D.L., Oyarzún, J.E., Olguín, H.C., and Brandan, E. (2016). Connective tissue cells expressing fibro/adipogenic progenitor markers increase under chronic damage: relevance in fibroblast-myofibroblast differentiation and skeletal muscle fibrosis. *Cell Tissue Res.* 364, 647–660.
67. Cornier, M.-A., Dabelea, D., Hernandez, T.L., Lindstrom, R.C., Steig, A.J., Stob, N.R., Van Pelt, R.E., Wang, H., and Eckel, R.H. (2008). The metabolic syndrome. *Endocr. Rev.* 29, 777–822.
68. Cosgrove, B.D., Sacco, A., Gilbert, P.M., and Blau, H.M. (2009). A home away from home: challenges and opportunities in engineering in vitro muscle satellite cell niches. *Differ. Res. Biol. Divers.* 78, 185–194.
69. Cosgrove, B.D., Gilbert, P.M., Porpiglia, E., Mourkioti, F., Lee, S.P., Corbel, S.Y., Llewellyn, M.E., Delp, S.L., and Blau, H.M. (2014a). Rejuvenation of the aged muscle stem cell population restores strength to injured aged muscles. *Nat. Med.* 20, 255–264.
70. Cosgrove, B.D., Gilbert, P.M., Porpiglia, E., Mourkioti, F., Lee, S.P., Corbel, S.Y., Llewellyn, M.E., Delp, S.L., and Blau, H.M. (2014b). Rejuvenation of the muscle stem cell population restores strength to injured aged muscles. *Nat. Med.* 20, 255–264.
71. Covault, J., and Sanes, J.R. (1986). Distribution of N-CAM in synaptic and extrasynaptic portions of developing and adult skeletal muscle. *J. Cell Biol.* 102, 716–730.
72. Crane, J.D., MacNeil, L.G., Lally, J.S., Ford, R.J., Bujak, A.L., Brar, I.K., Kemp, B.E., Raha, S., Steinberg, G.R., and Tarnopolsky, M.A. (2015). Exercise-stimulated interleukin-15 is controlled by AMPK and regulates skin metabolism and aging. *Aging Cell* 14, 625–634.
73. Cruz Hernández, J.C., Bracko, O., Kersbergen, C.J., Muse, V., Haft-Javaherian, M., Berg, M., Park, L., Vinarcsik, L.K., Ivasyk, I., Rivera, D.A., et al. (2019). Neutrophil adhesion in brain capillaries reduces cortical blood flow and impairs memory function in Alzheimer’s disease mouse models. *Nat. Neurosci.* 22, 413–420.
74. De Micheli, A.J., Laurilliard, E.J., Heinke, C.L., Ravichandran, H., Fraczek, P., Soueid-Baumgarten, S., De Vlaminc, I., Elemento, O., and Cosgrove, B.D. (2020). Single-Cell Analysis of the Muscle Stem Cell Hierarchy Identifies Heterotypic Communication Signals Involved in Skeletal Muscle Regeneration. *Cell Rep.* 30, 3583-3595.e5.
75. Deyo, R.A., and Mirza, S.K. (2016). Herniated Lumbar Intervertebral Disk. *N. Engl. J. Med.* 374, 1763–1772.
76. Dorrens, J., and Rennie, M.J. (2003). Effects of ageing and human whole body and muscle protein turnover: Ageing and human whole body and muscle protein turnover. *Scand. J. Med. Sci. Sports* 13, 26–33.

77. Drouin, G., Couture, V., Lauzon, M.-A., Balg, F., Faucheux, N., and Grenier, G. (2019). Muscle injury-induced hypoxia alters the proliferation and differentiation potentials of muscle resident stromal cells. *Skelet. Muscle* 9, 18.
78. D'Souza, D.M., Al-Sajee, D., and Hawke, T.J. (2013). Diabetic myopathy: impact of diabetes mellitus on skeletal muscle progenitor cells. *Front. Physiol.* 4.
79. Duan, C., Ren, H., and Gao, S. (2010). Insulin-like growth factors (IGFs), IGF receptors, and IGF-binding proteins: Roles in skeletal muscle growth and differentiation. *Gen. Comp. Endocrinol.* 167, 344–351.
80. Dumont, N.A., Wang, Y.X., von Maltzahn, J., Pasut, A., Bentzinger, C.F., Brun, C.E., and Rudnicki, M.A. (2015). Dystrophin expression in muscle stem cells regulates their polarity and asymmetric division. *Nat. Med.* 21, 1455–1463.
81. Duscha, B.D., Kraus, W.E., Keteyian, S.J., Sullivan, M.J., Green, H.J., Schachat, F.H., Pippen, A.M., Brawner, C.A., Blank, J.M., and Annex, B.H. (1999). Capillary density of skeletal muscle. *J. Am. Coll. Cardiol.* 33, 1956–1963.
82. Eadie, B.D., Redila, V.A., and Christie, B.R. (2005). Voluntary exercise alters the cytoarchitecture of the adult dentate gyrus by increasing cellular proliferation, dendritic complexity, and spine density. *J. Comp. Neurol.* 486, 39–47.
83. Egerman, M.A., and Glass, D.J. (2014). Signaling pathways controlling skeletal muscle mass. *Crit. Rev. Biochem. Mol. Biol.* 49, 59–68.
84. Egginton, S. (2001). Unorthodox angiogenesis in skeletal muscle. *Cardiovasc. Res.* 49, 634–646.
85. Englund, D.A., Murach, K.A., Dungan, C.M., Figueiredo, V.C., Vechetti, I.J., Dupont-Versteegden, E.E., McCarthy, J.J., and Peterson, C.A. (2020). Depletion of resident muscle stem cells negatively impacts running volume, physical function, and muscle fiber hypertrophy in response to lifelong physical activity. *Am. J. Physiol. Cell Physiol.* 318, C1178–C1188.
86. Ennen, J.P., Verma, M., and Asakura, A. (2013). Vascular-targeted therapies for Duchenne muscular dystrophy. *Skelet. Muscle* 3, 9.
87. Farmawati, A., Kitajima, Y., Nedachi, T., Sato, M., Kanzaki, M., and Nagatomi, R. (2013). Characterization of contraction-induced IL-6 up-regulation using contractile C2C12 myotubes. *Endocr. J.* 60, 137–147.
88. Flück, M., and Hoppeler, H. (2003). Molecular basis of skeletal muscle plasticity—from gene to form and function. In *Reviews of Physiology, Biochemistry and Pharmacology*, (Berlin, Heidelberg: Springer Berlin Heidelberg), pp. 159–216.
89. Frontera, W.R., and Ochala, J. (2015). Skeletal muscle: a brief review of structure and function. *Calcif. Tissue Int.* 96, 183–195.
90. Fry, C.S., Lee, J.D., Mula, J., Kirby, T.J., Jackson, J.R., Liu, F., Yang, L., Mendias, C.L., Dupont-Versteegden, E.E., McCarthy, J.J., et al. (2015). Inducible depletion of satellite cells in adult, sedentary mice impairs muscle regenerative capacity without affecting sarcopenia. *Nat. Med.* 21, 76–80.

91. Fuchs, E., and Blau, H.M. (2020). Tissue Stem Cells: Architects of Their Niches. *Cell Stem Cell* 27, 532–556.
92. Fulco, M., Cen, Y., Zhao, P., Hoffman, E.P., McBurney, M.W., Sauve, A.A., and Sartorelli, V. (2008). Glucose Restriction Inhibits Skeletal Myoblast Differentiation by Activating SIRT1 through AMPK-Mediated Regulation of Nampt. *Dev. Cell* 14, 661–673.
93. Furuichi, Y., Kawabata, Y., Aoki, M., Mita, Y., Fujii, N.L., and Manabe, Y. (2021). Excess Glucose Impedes the Proliferation of Skeletal Muscle Satellite Cells Under Adherent Culture Conditions. *Front. Cell Dev. Biol.* 9.
94. Galli, S.J., Borregaard, N., and Wynn, T.A. (2011). Phenotypic and functional plasticity of cells of innate immunity: macrophages, mast cells and neutrophils. *Nat. Immunol.* 12, 1035–1044.
95. Gates, L.A., Shi, J., Rohira, A.D., Feng, Q., Zhu, B., Bedford, M.T., Sagum, C.A., Jung, S.Y., Qin, J., Tsai, M.-J., et al. (2017). Acetylation on histone H3 lysine 9 mediates a switch from transcription initiation to elongation. *J. Biol. Chem.* 292, 14456–14472.
96. Gibbs, B.F., Wierdecky, J., Welker, P., Henz, B.M., Wolff, H.H., and Grabbe, J. (2001). Human skin mast cells rapidly release preformed and newly generated TNF- α and IL-8 following stimulation with anti-IgE and other secretagogues: Human skin mast cells and TNF- α and IL-8. *Exp. Dermatol.* 10, 312–320.
97. Girardi, F., Taleb, A., Ebrahimi, M., Datye, A., Gamage, D.G., Peccate, C., Giordani, L., Millay, D.P., Gilbert, P.M., Cadot, B., et al. (2021). TGF β signaling curbs cell fusion and muscle regeneration. *Nat. Commun.* 12, 750.
98. Goel, A.J., Rieder, M.-K., Arnold, H.-H., Radice, G.L., and Krauss, R.S. (2017). Niche Cadherins Control the Quiescence-to-Activation Transition in Muscle Stem Cells. *Cell Rep.* 21, 2236–2250.
99. Gomasasca, M., Banfi, G., and Lombardi, G. (2020). Myokines: The endocrine coupling of skeletal muscle and bone. *Adv. Clin. Chem.* 94, 155–218.
100. Gon, Y., Maruoka, S., Kishi, H., Kozu, Y., Kazumichi, K., Nomura, Y., Takeshita, I., Oshima, T., and Hashimoto, S. (2017). NDRG1 is important to maintain the integrity of airway epithelial barrier through claudin-9 expression: NDRG1 maintains epithelial barrier integrity. *Cell Biol. Int.* 41, 716–725.
101. Görgens, S.W., Eckardt, K., Jensen, J., Drevon, C.A., and Eckel, J. (2015). Exercise and Regulation of Adipokine and Myokine Production. *Prog. Mol. Biol. Transl. Sci.* 135, 313–336.
102. Gorski, T., and De Bock, K. (2019). Metabolic regulation of exercise-induced angiogenesis. *Vasc. Biol.* 1, H1–H8.
103. Goueli, B.S., Powell, M.B., Finger, E.C., and Pfeffer, S.R. (2012). TBC1D16 is a Rab4A GTPase activating protein that regulates receptor recycling and EGF receptor signaling. *Proc. Natl. Acad. Sci.* 109, 15787–15792.

104. Gratchev, A., Guillot, P., Hakiy, N., Politz, O., Orfanos, C.E., Schledzewski, K., and Goerdts, S. (2001). Alternatively activated macrophages differentially express fibronectin and its splice variants and the extracellular matrix protein beta1G-H3. *Scand. J. Immunol.* **53**, 386–392.
105. Gubelmann, C., Waszak, S.M., Isakova, A., Holcombe, W., Hens, K., Iagovitina, A., Feuz, J., Raghav, S.K., Simicevic, J., and Deplancke, B. (2013). A yeast one-hybrid and microfluidics-based pipeline to map mammalian gene regulatory networks. *Mol. Syst. Biol.* **9**, 682.
106. Halevy, O., Piestun, Y., Allouh, M.Z., Rosser, B.W.C., Rinkevich, Y., Reshef, R., Rozenboim, I., Wleklinski-Lee, M., and Yablonka-Reuveni, Z. (2004). Pattern of Pax7 expression during myogenesis in the posthatch chicken establishes a model for satellite cell differentiation and renewal. *Dev. Dyn. Off. Publ. Am. Assoc. Anat.* **231**, 489–502.
107. Hamann, J.J., Buckwalter, J.B., and Clifford, P.S. (2004). Vasodilatation is obligatory for contraction-induced hyperaemia in canine skeletal muscle. *J. Physiol.* **557**, 1013–1020.
108. Han, S., Wang, G., Qi, X., Lee, H.M., Englander, E.W., and Greeley, G.H. (2008a). A possible role for hypoxia-induced apelin expression in enteric cell proliferation. *Am. J. Physiol.-Regul. Integr. Comp. Physiol.* **294**, R1832–R1839.
109. Han, S., Wang, G., Qi, X., Lee, H.M., Englander, E.W., and Greeley, G.H. (2008b). A possible role for hypoxia-induced apelin expression in enteric cell proliferation. *Am. J. Physiol.-Regul. Integr. Comp. Physiol.* **294**, R1832–R1839.
110. Hänninen, O., and Atalay, M. (1998). Oxidative metabolism in skeletal muscle. In *Oxidative Stress in Skeletal Muscle*, A.Z. Reznick, L. Packer, C.K. Sen, J.O. Holloszy, and M.J. Jackson, eds. (Basel: Birkhäuser), pp. 29–42.
111. Hawley, J.A., Tipton, K.D., and Millard-Stafford, M.L. (2006). Promoting training adaptations through nutritional interventions. *J. Sports Sci.* **24**, 709–721.
112. Hempel, A., Maasch, C., Heintze, U., Lindschau, C., Dietz, R., Luft, F.C., and Haller, H. (1997). High Glucose Concentrations Increase Endothelial Cell Permeability via Activation of Protein Kinase C α . *Circ. Res.* **81**, 363–371.
113. Hens, K., Feuz, J.-D., Isakova, A., Iagovitina, A., Massouras, A., Bryois, J., Callaerts, P., Celniker, S.E., and Deplancke, B. (2011a). Automated protein-DNA interaction screening of *Drosophila* regulatory elements. *Nat. Methods* **8**, 1065–1070.
114. Hens, K., Feuz, J.-D., Isakova, A., Iagovitina, A., Massouras, A., Bryois, J., Callaerts, P., Celniker, S.E., and Deplancke, B. (2011b). Automated protein-DNA interaction screening of *Drosophila* regulatory elements. *Nat. Methods* **8**, 1065–1070.
115. Hernandez-Torres, F., Rodríguez-Outeiriño, L., Franco, D., and Aranega, A.E. (2017). Pitx2 in Embryonic and Adult Myogenesis. *Front. Cell Dev. Biol.* **5**, 46.

116. Hirayama, J., Yamagata, M., Ogata, S., Shimizu, K., Ikeda, Y., and Takahashi, K. (2006). Relationship between low-back pain, muscle spasm and pressure pain thresholds in patients with lumbar disc herniation. *Eur. Spine J.* 15, 41–47.
117. Hjorth, M., Norheim, F., Meen, A.J., Pourteymour, S., Lee, S., Holen, T., Jensen, J., Birkeland, K.I., Martinov, V.N., Langleite, T.M., et al. (2015). The effect of acute and long-term physical activity on extracellular matrix and serglycin in human skeletal muscle. *Physiol. Rep.* 3, e12473.
118. Ho, T.K., Tsui, J., Xu, S., Leoni, P., Abraham, D.J., and Baker, D.M. (2010). Angiogenic effects of stromal cell-derived factor-1 (SDF-1/CXCL12) variants in vitro and the in vivo expressions of CXCL12 variants and CXCR4 in human critical leg ischemia. *J. Vasc. Surg.* 51, 689–699.
119. Huh, H.D., Kim, D.H., Jeong, H.-S., and Park, H.W. (2019). Regulation of TEAD Transcription Factors in Cancer Biology. *Cells* 8.
120. Hurley, M.V. (1999). THE ROLE OF MUSCLE WEAKNESS IN THE PATHOGENESIS OF OSTEOARTHRITIS. *Rheum. Dis. Clin. N. Am.* 25, 283–298.
121. Huxley, A.F., and Niedergerke, R. (1954). Structural Changes in Muscle During Contraction: Interference Microscopy of Living Muscle Fibres. *Nature* 173, 971–973.
122. Irintchev, A., Zeschnigk, M., Starzinski-Powitz, A., and Wernig, A. (1994). Expression pattern of M-cadherin in normal, denervated, and regenerating mouse muscles. *Dev. Dyn.* 199, 326–337.
123. Janssen, I., Shepard, D.S., Katzmarzyk, P.T., and Roubenoff, R. (2004). The healthcare costs of sarcopenia in the United States. *J. Am. Geriatr. Soc.* 52, 80–85.
124. Japp, A.G., and Newby, D.E. (2008). The apelin–APJ system in heart failure: Pathophysiologic relevance and therapeutic potential. *Biochem. Pharmacol.* 75, 1882–1892.
125. Jejurikar, S.S., and Kuzon, Jr., W.M. (2003). Satellite cell depletion in degenerative skeletal muscle. *Apoptosis* 8, 573–578.
126. Jeon, K., Kim, T., and Lee, S.-H. (2016). Effects of muscle extension strength exercise on trunk muscle strength and stability of patients with lumbar herniated nucleus pulposus. *J. Phys. Ther. Sci.* 28, 1418–1421.
127. Jesse, T.L., LaChance, R., Iademarco, M.F., and Dean, D.C. (1998). Interferon Regulatory Factor-2 Is a Transcriptional Activator in Muscle Where It Regulates Expression of Vascular Cell Adhesion Molecule-1. *J. Cell Biol.* 140, 1265–1276.
128. Joe, A.W.B., Yi, L., Natarajan, A., Le Grand, F., So, L., Wang, J., Rudnicki, M.A., and Rossi, F.M.V. (2010). Muscle injury activates resident fibro/adipogenic progenitors that facilitate myogenesis. *Nat. Cell Biol.* 12, 153–163.

129. Jones, J.S., Small, D.M., and Nishimura, N. (2018). In Vivo Calcium Imaging of Cardiomyocytes in the Beating Mouse Heart With Multiphoton Microscopy. *Front. Physiol.* *9*, 969.
130. Jørgensen, L.H., Jepsen, P.L., Boysen, A., Dalgaard, L.B., Hvid, L.G., Ørtenblad, N., Ravn, D., Sellathurai, J., Møller-Jensen, J., Lochmüller, H., et al. (2017). SPARC Interacts with Actin in Skeletal Muscle in Vitro and in Vivo. *Am. J. Pathol.* *187*, 457–474.
131. Joshi, S., Davidson, G., Le Gras, S., Watanabe, S., Braun, T., Mengus, G., and Davidson, I. (2017). TEAD transcription factors are required for normal primary myoblast differentiation in vitro and muscle regeneration in vivo. *PLOS Genet.* *13*, e1006600.
132. Kachhap, S.K., Faith, D., Qian, D.Z., Shabbeer, S., Galloway, N.L., Pili, R., Denmeade, S.R., DeMarzo, A.M., and Carducci, M.A. (2007). The N-Myc down regulated Gene1 (NDRG1) Is a Rab4a effector involved in vesicular recycling of E-cadherin. *PLoS One* *2*, e844.
133. Kadoglou, N.P.E., Vrabas, I.S., Kapelouzou, A., Lampropoulos, S., Sailer, N., Kostakis, A., Liapis, C.D., and Angelopoulou, N. (2012). The impact of aerobic exercise training on novel adipokines, apelin and ghrelin, in patients with type 2 diabetes. *Med. Sci. Monit. Int. Med. J. Exp. Clin. Res.* *18*, CR290–CR295.
134. Kanzleiter, T., Rath, M., Görgens, S.W., Jensen, J., Tangen, D.S., Kolnes, A.J., Kolnes, K.J., Lee, S., Eckel, J., Schürmann, A., et al. (2014). The myokine decorin is regulated by contraction and involved in muscle hypertrophy. *Biochem. Biophys. Res. Commun.* *450*, 1089–1094.
135. Karagounis, L.G., and Hawley, J.A. (2010). Skeletal muscle: increasing the size of the locomotor cell. *Int. J. Biochem. Cell Biol.* *42*, 1376–1379.
136. Karlsen, A., Bechshøft, R.L., Malmgaard-Clausen, N.M., Andersen, J.L., Schjerling, P., Kjaer, M., and Mackey, A.L. (2019). Lack of muscle fibre hypertrophy, myonuclear addition, and satellite cell pool expansion with resistance training in 83-94-year-old men and women. *Acta Physiol.* *227*, e13271.
137. Kidoya, H., and Takakura, N. (2012). Biology of the apelin-APJ axis in vascular formation. *J. Biochem. (Tokyo)* *152*, 125–131.
138. Kim, G., and Kim, J.H. (2020). Impact of Skeletal Muscle Mass on Metabolic Health. *Endocrinol. Metab.* *35*, 1–6.
139. Kim, J.-S., Lee, Y.-H., and Yi, H.-K. (2016a). Gradual downhill running improves age-related skeletal muscle and bone weakness: implication of autophagy and bone morphogenetic proteins: Gradual downhill running improves age-related skeletal weakness. *Exp. Physiol.* *101*, 1528–1540.
140. Kim, M., Kim, T., Johnson, R.L., and Lim, D.-S. (2015). Transcriptional Co-repressor Function of the Hippo Pathway Transducers YAP and TAZ. *Cell Rep.* *11*, 270–282.

141. Kim, Y.J., Tamadon, A., Park, H.T., Kim, H., and Ku, S.-Y. (2016b). The role of sex steroid hormones in the pathophysiology and treatment of sarcopenia. *Osteoporos. Sarcopenia* 2, 140–155.
142. Korsunsky, I., Millard, N., Fan, J., Slowikowski, K., Zhang, F., Wei, K., Baglaenko, Y., Brenner, M., Loh, P., and Raychaudhuri, S. (2019a). Fast, sensitive and accurate integration of single-cell data with Harmony. *Nat. Methods* 16, 1289–1296.
143. Korsunsky, I., Millard, N., Fan, J., Slowikowski, K., Zhang, F., Wei, K., Baglaenko, Y., Brenner, M., and Loh, P. (2019b). Fast, sensitive and accurate integration of single-cell data with Harmony. *Nat. Methods*.
144. Krauss, R.S., Cole, F., Gaio, U., Takaesu, G., Zhang, W., and Kang, J.-S. (2005). Close encounters: regulation of vertebrate skeletal myogenesis by cell-cell contact. *J. Cell Sci.* 118, 2355–2362.
145. Krishnasamy, P., Hall, M., and Robbins, S.R. (2018). The role of skeletal muscle in the pathophysiology and management of knee osteoarthritis. *Rheumatology* 57, iv22–iv33.
146. Kuang, S., and Rudnicki, M.A. (2008). The emerging biology of satellite cells and their therapeutic potential. *Trends Mol. Med.* 14, 82–91.
147. Kwon, J.H., Moon, K.M., and Min, K.-W. (2020). Exercise-Induced Myokines can Explain the Importance of Physical Activity in the Elderly: An Overview. *Healthcare* 8, 378.
148. Lakka, H.-M., Laaksonen, D.E., Lakka, T.A., Niskanen, L.K., Kumpusalo, E., Tuomilehto, J., and Salonen, J.T. (2002). The metabolic syndrome and total and cardiovascular disease mortality in middle-aged men. *JAMA* 288, 2709–2716.
149. Larsson, L., and Ansved, T. (1995). Effects of ageing on the motor unit. *Prog. Neurobiol.* 45, 397–458.
150. Larsson, L., Sjödén, B., and Karlsson, J. (1978). Histochemical and biochemical changes in human skeletal muscle with age in sedentary males, age 22–65 years. *Acta Physiol. Scand.* 103, 31–39.
151. Latroche, C., Gitiaux, C., Chrétien, F., Desguerre, I., Mounier, R., and Chazaud, B. (2015). Skeletal Muscle Microvasculature: A Highly Dynamic Lifeline. *Physiology* 30, 417–427.
152. Latroche, C., Weiss-Gayet, M., Muller, L., Gitiaux, C., Leblanc, P., Liot, S., Ben-Larbi, S., Abou-Khalil, R., Verger, N., Bardot, P., et al. (2017). Coupling between Myogenesis and Angiogenesis during Skeletal Muscle Regeneration Is Stimulated by Restorative Macrophages. *Stem Cell Rep.* 9, 2018–2033.
153. Lazure, F., Blackburn, D.M., Corchado, A.H., Sahinyan, K., Karam, N., Sharanek, A., Nguyen, D., Lepper, C., Najafabadi, H.S., Perkins, T.J., et al. (2020). Myf6/MRF4 is a myogenic niche regulator required for the maintenance of the muscle stem cell pool. *EMBO Rep.* 21, e49499.

154. Leal, L.G., Lopes, M.A., and Batista, M.L. (2018). Physical Exercise-Induced Myokines and Muscle-Adipose Tissue Crosstalk: A Review of Current Knowledge and the Implications for Health and Metabolic Diseases. *Front. Physiol.* **9**, 1307.
155. Lee, J.H., Budanov, A.V., and Karin, M. (2013). Sestrins Orchestrate Cellular Metabolism to Attenuate Aging. *Cell Metab.* **18**, 792–801.
156. Lehman, W., Craig, R., and Vibert, P. (1994). Ca²⁺-induced tropomyosin movement in Limulus thin filaments revealed by three-dimensional reconstruction. *Nature* **368**, 65–67.
157. Lepper, C., Partridge, T.A., and Fan, C.-M. (2011). An absolute requirement for Pax7-positive satellite cells in acute injury-induced skeletal muscle regeneration. *Dev. Camb. Engl.* **138**, 3639–3646.
158. Li, L., Yang, G., Li, Q., Tang, Y., Yang, M., Yang, H., and Li, K. (2006). Changes and Relations of Circulating Visfatin, Apelin, and Resistin Levels in Normal, Impaired Glucose Tolerance, and Type 2 Diabetic Subjects. *Exp. Clin. Endocrinol. Diabetes* **114**, 544–548.
159. Liang, G., Lin, J.C.Y., Wei, V., Yoo, C., Cheng, J.C., Nguyen, C.T., Weisenberger, D.J., Egger, G., Takai, D., Gonzales, F.A., et al. (2004). Distinct localization of histone H3 acetylation and H3-K4 methylation to the transcription start sites in the human genome. *Proc. Natl. Acad. Sci. U. S. A.* **101**, 7357–7362.
160. Lin, R.-Z., Moreno-Luna, R., Li, D., Jaminet, S.-C., Greene, A.K., and Melero-Martin, J.M. (2014). Human endothelial colony-forming cells serve as trophic mediators for mesenchymal stem cell engraftment via paracrine signaling. *Proc. Natl. Acad. Sci.* **111**, 10137–10142.
161. Lindner, D., Zietsch, C., Becher, P.M., Schulze, K., Schultheiss, H.-P., Tschöpe, C., and Westermann, D. (2012). Differential expression of matrix metalloproteases in human fibroblasts with different origins. *Biochem. Res. Int.* **2012**, 875742.
162. Liu, M., Stevens-Lapsley, J.E., Jayaraman, A., Ye, F., Conover, C., Walter, G.A., Bose, P., Thompson, F.J., Borst, S.E., and Vandenborne, K. (2010). Impact of treadmill locomotor training on skeletal muscle IGF1 and myogenic regulatory factors in spinal cord injured rats. *Eur. J. Appl. Physiol.* **109**, 709–720.
163. Liu, W., Zhang, B., Hu, Q., Qin, Y., Xu, W., Shi, S., Liang, C., Meng, Q., Xiang, J., Liang, D., et al. (2017). A new facet of NDRG1 in pancreatic ductal adenocarcinoma: Suppression of glycolytic metabolism. *Int. J. Oncol.* **50**, 1792–1800.
164. Londhe, P., and Davie, J.K. (2013). Interferon- γ Resets Muscle Cell Fate by Stimulating the Sequential Recruitment of JARID2 and PRC2 to Promoters to Repress Myogenesis. *Sci. Signal.* **6**, ra107–ra107.
165. Low, M., Eisner, C., and Rossi, F. (2017). Fibro/Adipogenic Progenitors (FAPs): Isolation by FACS and Culture. In *Muscle Stem Cells: Methods and Protocols*, E. Perdiguero, and D. Cornelison, eds. (New York, NY: Springer), pp. 179–189.

166. Lukjanenko, L., Brachat, S., Pierrel, E., Lach-Trifilieff, E., and Feige, J.N. (2013). Genomic Profiling Reveals That Transient Adipogenic Activation Is a Hallmark of Mouse Models of Skeletal Muscle Regeneration. *PLoS ONE* 8, e71084.
167. Lukjanenko, L., Karaz, S., Stuelsatz, P., Gurriaran-Rodriguez, U., Michaud, J., Dammone, G., Sizzano, F., Mashinchian, O., Ancel, S., Migliavacca, E., et al. (2019). Aging Disrupts Muscle Stem Cell Function by Impairing Matricellular WISP1 Secretion from Fibro-Adipogenic Progenitors. *Cell Stem Cell* 24, 433-446.e7.
168. Luo, W., Ai, L., Wang, B.-F., Wang, L.-Y., Gan, Y.-M., and Zhou, Y. (2020). [Effects of mice macrophages on skeletal muscle cells under high glucose treatment]. *Zhongguo Ying Yong Sheng Li Xue Za Zhi Zhongguo Yingyong Shenglixue Zazhi Chin. J. Appl. Physiol.* 36, 124–129.
169. Luque, E., Peña, J., Martin, P., Jimena, I., and Vaamonde, R. (1995). Capillary Supply During Development of Individual Regenerating Muscle Fibers. *Anat. Histol. Embryol.* 24, 87–89.
170. Lv, X., Zheng, B., Li, S., Han, A., Wang, C., Shi, J., Zhang, X., Liu, Y., Li, Y., and Wen, J. (2013). Synthetic retinoid Am80 up-regulates apelin expression by promoting interaction of RAR α with KLF5 and Sp1 in vascular smooth muscle cells. *Biochem. J.* 456, 35–46.
171. Macosko, E.Z., Basu, A., Satija, R., Nemes, J., Shekhar, K., Goldman, M., Tirosh, I., Bialas, A.R., Kamitaki, N., Martersteck, E.M., et al. (2015). Highly Parallel Genome-wide Expression Profiling of Individual Cells Using Nanoliter Droplets. *Cell* 161, 1202–1214.
172. Mademtoglou, D., Asakura, Y., Borok, M.J., Alonso-Martin, S., Mourikis, P., Kodaka, Y., Mohan, A., Asakura, A., and Relaix, F. (2018). Cellular localization of the cell cycle inhibitor Cdkn1c controls growth arrest of adult skeletal muscle stem cells. *ELife* 7, e33337.
173. Maggio, M., Lauretani, F., and Ceda, G.P. (2012). Sex hormones and sarcopenia in older persons: *Curr. Opin. Clin. Nutr. Metab. Care* 1.
174. Maloney, P.R., Khan, P., Hedrick, M., Gosalia, P., Milewski, M., Li, L., Roth, G.P., Sergienko, E., Suyama, E., Sugarman, E., et al. (2010). Functional antagonists of the Apelin (APJ) receptor. In *Probe Reports from the NIH Molecular Libraries Program*, (Bethesda (MD): National Center for Biotechnology Information (US)), p.
175. von Maltzahn, J., Jones, A.E., Parks, R.J., and Rudnicki, M.A. (2013). Pax7 is critical for the normal function of satellite cells in adult skeletal muscle. *Proc. Natl. Acad. Sci.* 110, 16474–16479.
176. Marcell, T.J. (2003). Sarcopenia: causes, consequences, and preventions. *J. Gerontol. A Biol. Sci. Med. Sci.* 58, M911-916.
177. Mashinchian, O., Pisconti, A., Le Moal, E., and Bentzinger, C.F. (2018). Chapter Two - The Muscle Stem Cell Niche in Health and Disease. In *Current Topics in Developmental Biology*, D. Sassoon, ed. (Academic Press), pp. 23–65.

178. Matsakas, A., Yadav, V., Lorca, S., and Narkar, V. (2013). Muscle ERRy mitigates Duchenne muscular dystrophy via metabolic and angiogenic reprogramming. *FASEB J. Off. Publ. Fed. Am. Soc. Exp. Biol.* 27, 4004–4016.
179. Mazzucotelli, A., Ribet, C., Castan-Laurell, I., Daviaud, D., Guigné, C., Langin, D., and Valet, P. (2008). The transcriptional co-activator PGC-1alpha up regulates apelin in human and mouse adipocytes. *Regul. Pept.* 150, 33–37.
180. McGinnis, C.S., Murrow, L.M., and Gartner, Z.J. (2019). DoubletFinder: Doublet Detection in Single-Cell RNA Sequencing Data Using Artificial Nearest Neighbors. *Cell Syst.* 8, 329-337.e4.
181. McKellar, D.W., Walter, L.D., Song, L.T., Mantri, M., Wang, M.F.Z., Vlaminc, I.D., and Cosgrove, B.D. (2020a). Strength in numbers: Large-scale integration of single-cell transcriptomic data reveals rare, transient muscle progenitor cell states in muscle regeneration. *BioRxiv* 2020.12.01.407460.
182. McKellar, D.W., Walter, L.D., Song, L.T., Mantri, M., Wang, M.F.Z., De Vlaminc, I., and Cosgrove, B.D. (2020b). Strength in numbers: Large-scale integration of single-cell transcriptomic data reveals rare, transient muscle progenitor cell states in muscle regeneration. *BioRxiv* 2020.12.01.407460.
183. Melotte, V., Qu, X., Ongenaert, M., van Criekinge, W., de Bruïne, A.P., Baldwin, H.S., and van Engeland, M. (2010). The N-myc downstream regulated gene (NDRG) family: diverse functions, multiple applications. *FASEB J.* 24, 4153–4166.
184. Migliavacca, E., Tay, S.K.H., Patel, H.P., Sonntag, T., Civiletto, G., McFarlane, C., Forrester, T., Barton, S.J., Leow, M.K., Antoun, E., et al. (2019). Mitochondrial oxidative capacity and NAD + biosynthesis are reduced in human sarcopenia across ethnicities. *Nat. Commun.* 10, 5808.
185. Miller, W., Rosenbloom, K., Hardison, R.C., Hou, M., Taylor, J., Raney, B., Burhans, R., King, D.C., Baertsch, R., Blankenberg, D., et al. (2007). 28-Way vertebrate alignment and conservation track in the UCSC Genome Browser. *Genome Res.* 17, 1797–1808.
186. Miranda, M., Morici, J.F., Zanoni, M.B., and Bekinschtein, P. (2019). Brain-Derived Neurotrophic Factor: A Key Molecule for Memory in the Healthy and the Pathological Brain. *Front. Cell. Neurosci.* 13, 363.
187. Mounier, R., Chrétien, F., and Chazaud, B. (2011). Chapter five - Blood Vessels and the Satellite Cell Niche. In *Current Topics in Developmental Biology*, G. k. Pavlath, ed. (Academic Press), pp. 121–138.
188. Mul, J.D., Stanford, K.I., Hirshman, M.F., and Goodyear, L.J. (2015). Exercise and Regulation of Carbohydrate Metabolism. In *Progress in Molecular Biology and Translational Science*, (Elsevier), pp. 17–37.
189. Muñoz-Cánoves, P., Neves, J., and Sousa-Victor, P. (2020). Understanding muscle regenerative decline with aging: new approaches to bring back youthfulness to aged stem cells. *FEBS J.* 287, 406–416.

190. Murphy, M.M., Lawson, J.A., Mathew, S.J., Hutcheson, D.A., and Kardon, G. (2011). Satellite cells, connective tissue fibroblasts and their interactions are crucial for muscle regeneration. *Dev. Camb. Engl.* *138*, 3625–3637.
191. Nalbandian, M., Radak, Z., and Takeda, M. (2020). Lactate Metabolism and Satellite Cell Fate. *Front. Physiol.* *0*.
192. Nazari, A., and Chehelcheraghi, F. (2020). Using Apelin and exercise to protect the cardiac cells: synergic effect in ischemia reperfusion injuries treatment in rats. *Bratisl. Med. J.* *121*, 14–21.
193. Nederveen, J.P., Snijders, T., Joanisse, S., Wavell, C.G., Mitchell, C.J., Johnston, L.M., Baker, S.K., Phillips, S.M., and Parise, G. (2017). Altered muscle satellite cell activation following 16 wk of resistance training in young men. *Am. J. Physiol. Regul. Integr. Comp. Physiol.* *312*, R85–R92.
194. Nyimanu, D., Kay, R.G., Sulentic, P., Kuc, R.E., Ambery, P., Jermutus, L., Reimann, F., Gribble, F.M., Cheriyan, J., Maguire, J.J., et al. (2019). Development and validation of an LC-MS/MS method for detection and quantification of in vivo derived metabolites of [Pyr 1]apelin-13 in humans. *Sci. Rep.* *9*, 19934.
195. Obeso, J., Weber, J., and Auerbach, R. (1990). A hemangioendothelioma-derived cell line: its use as a model for the study of endothelial cell biology. *Lab. Investig. J. Tech. Methods Pathol.* *63*, 259–269.
196. Ochoa, O., Sun, D., Reyes-Reyna, S.M., Waite, L.L., Michalek, J.E., McManus, L.M., and Shireman, P.K. (2007). Delayed angiogenesis and VEGF production in CCR2^{-/-} mice during impaired skeletal muscle regeneration. *Am. J. Physiol. Regul. Integr. Comp. Physiol.* *293*, R651-661.
197. Olson, L.E., and Soriano, P. (2009). Increased PDGFR α Activation Disrupts Connective Tissue Development and Drives Systemic Fibrosis. *Dev. Cell* *16*, 303–313.
198. Ouchi, N., Oshima, Y., Ohashi, K., Higuchi, A., Ikegami, C., Izumiya, Y., and Walsh, K. (2008). Follistatin-like 1, a Secreted Muscle Protein, Promotes Endothelial Cell Function and Revascularization in Ischemic Tissue through a Nitric-oxide Synthase-dependent Mechanism. *J. Biol. Chem.* *283*, 32802–32811.
199. Pannérec, A., Springer, M., Migliavacca, E., Ireland, A., Piasecki, M., Karaz, S., Jacot, G., Métairon, S., Danenberg, E., Raymond, F., et al. (2016). A robust neuromuscular system protects rat and human skeletal muscle from sarcopenia. *Aging* *8*, 712–728.
200. Parise, G., and Yarasheski, K.E. (2000). The utility of resistance exercise training and amino acid supplementation for reversing age-associated decrements in muscle protein mass and function. *Curr. Opin. Clin. Nutr. Metab. Care* *3*, 489–495.
201. Pavlou, S., Lindsay, J., Ingram, R., Xu, H., and Chen, M. (2018). Sustained high glucose exposure sensitizes macrophage responses to cytokine stimuli but reduces their phagocytic activity. *BMC Immunol.* *19*, 24.

202. Pedersen, B.K. (2013). Muscle as a secretory organ. *Compr. Physiol.* **3**, 1337–1362.
203. Pedersen, B.K., and Febbraio, M.A. (2012). Muscles, exercise and obesity: skeletal muscle as a secretory organ. *Nat. Rev. Endocrinol.* **8**, 457–465.
204. Periasamy, M., Herrera, J.L., and Reis, F.C.G. (2017). Skeletal Muscle Thermogenesis and Its Role in Whole Body Energy Metabolism. *Diabetes Metab. J.* **41**, 327.
205. Pisters, M.F., Veenhof, C., van Dijk, G.M., and Dekker, J. (2014). Avoidance of activity and limitations in activities in patients with osteoarthritis of the hip or knee: a 5 year follow-up study on the mediating role of reduced muscle strength. *Osteoarthritis Cartilage* **22**, 171–177.
206. Pourteymour, S., Eckardt, K., Holen, T., Langleite, T., Lee, S., Jensen, J., Birkeland, K.I., Drevon, C.A., and Hjorth, M. (2017). Global mRNA sequencing of human skeletal muscle: Search for novel exercise-regulated myokines. *Mol. Metab.* **6**, 352–365.
207. Pretheeban, T., Lemos, D.R., Paylor, B., Zhang, R.-H., and Rossi, F.M. (2012). Role of stem/progenitor cells in reparative disorders. *Fibrogenesis Tissue Repair* **5**, 20.
208. Puchert, M., Adams, V., Linke, A., and Engele, J. (2016). Evidence for the involvement of the CXCL12 system in the adaptation of skeletal muscles to physical exercise. *Cell. Signal.* **28**, 1205–1215.
209. Qiu, H., Wang, F., Liu, C., Xu, X., and Liu, B. (2011). TEAD1-dependent expression of the FoxO3a gene in mouse skeletal muscle. *BMC Mol. Biol.* **12**, 1.
210. Rai, R., Ghosh, A.K., Eren, M., Mackie, A.R., Levine, D.C., Kim, S.-Y., Cedernaes, J., Ramirez, V., Procissi, D., Smith, L.H., et al. (2017). Downregulation of the Apelinergic Axis Accelerates Aging, whereas Its Systemic Restoration Improves the Mammalian Healthspan. *Cell Rep.* **21**, 1471–1480.
211. Ramis, M.R., Sarubbo, F., Moranta, D., Tejada, S., Lladó, J., Miralles, A., and Esteban, S. (2021). Neurochemical and Cognitive Beneficial Effects of Moderate Physical Activity and Catechin in Aged Rats. *Antioxidants* **10**, 621.
212. Ratajczak, M.Z. (2003). Expression of Functional CXCR4 by Muscle Satellite Cells and Secretion of SDF-1 by Muscle-Derived Fibroblasts is Associated with the Presence of Both Muscle Progenitors in Bone Marrow and Hematopoietic Stem/Progenitor Cells in Muscles. *Stem Cells* **21**, 363–371.
213. Reilly, G.C., and Engler, A.J. (2010). Intrinsic extracellular matrix properties regulate stem cell differentiation. *J. Biomech.* **43**, 55–62.
214. Relaix, F., Rocancourt, D., Mansouri, A., and Buckingham, M. (2005). A Pax3/Pax7-dependent population of skeletal muscle progenitor cells. *Nature* **435**, 948–953.

215. Relaix, F., Bencze, M., Borok, M.J., Der Vartanian, A., Gattazzo, F., Mademtzoglou, D., Perez-Diaz, S., Prola, A., Reyes-Fernandez, P.C., Rotini, A., et al. (2021). Perspectives on skeletal muscle stem cells. *Nat. Commun.* *12*, 692.
216. Rhoads, R.P., Johnson, R.M., Rathbone, C.R., Liu, X., Temm-Grove, C., Sheehan, S.M., Hoying, J.B., and Allen, R.E. (2009). Satellite cell-mediated angiogenesis in vitro coincides with a functional hypoxia-inducible factor pathway. *Am. J. Physiol. Cell Physiol.* *296*, C1321-1328.
217. Rice, W.L., Kaplan, D.L., and Georgakoudi, I. (2010). Two-Photon Microscopy for Non-Invasive, Quantitative Monitoring of Stem Cell Differentiation. *PLoS ONE* *5*, e10075.
218. Ripamonti, U., and Hari Reddi, A. (1997). Tissue Engineering, Morphogenesis, and Regeneration of the Periodontal Tissues By Bone Morphogenetic Proteins. *Crit. Rev. Oral Biol. Med.* *8*, 154–163.
219. Roberts, M.D., Haun, C.T., Vann, C.G., Osburn, S.C., and Young, K.C. (2020). Sarcoplasmic Hypertrophy in Skeletal Muscle: A Scientific “Unicorn” or Resistance Training Adaptation? *Front. Physiol.* *11*, 816.
220. Rose, A.J., and Richter, E.A. (2005). Skeletal Muscle Glucose Uptake During Exercise: How is it Regulated? *Physiology* *20*, 260–270.
221. Rozo, M., Li, L., and Fan, C.-M. (2016). Targeting β 1-integrin signaling enhances regeneration in aged and dystrophic muscle in mice. *Nat. Med.* *22*, 889–896.
222. Rubio-Ruiz, M.E., Guarner-Lans, V., Pérez-Torres, I., and Soto, M.E. (2019). Mechanisms Underlying Metabolic Syndrome-Related Sarcopenia and Possible Therapeutic Measures. *Int. J. Mol. Sci.* *20*, E647.
223. Ryall, J.G. (2013). Metabolic reprogramming as a novel regulator of skeletal muscle development and regeneration. *FEBS J.* *280*, 4004–4013.
224. Ryall, J.G., Dell’Orso, S., Derfoul, A., Juan, A., Zare, H., Feng, X., Clermont, D., Koulnis, M., Gutierrez-Cruz, G., Fulco, M., et al. (2015). The NAD(+)-dependent SIRT1 deacetylase translates a metabolic switch into regulatory epigenetics in skeletal muscle stem cells. *Cell Stem Cell* *16*, 171–183.
225. Saber, J., Lin, A.Y.T., and Rudnicki, M.A. (2020). Single-cell analyses uncover granularity of muscle stem cells. *F1000Research* *9*.
226. Saclier, M., Yacoub-Youssef, H., Mackey, A.L., Arnold, L., Ardjoune, H., Magnan, M., Sailhan, F., Chelly, J., Pavlath, G.K., Mounier, R., et al. (2013). Differentially activated macrophages orchestrate myogenic precursor cell fate during human skeletal muscle regeneration. *Stem Cells Dayt. Ohio* *31*, 384–396.
227. Salmon, W.D., and Daughaday, W.H. (1957). A hormonally controlled serum factor which stimulates sulfate incorporation by cartilage in vitro. *J. Lab. Clin. Med.* *49*, 825–836.

228. Sambasivan, R., Yao, R., Kissenpfennig, A., Van Wittenberghe, L., Paldi, A., Gayraud-Morel, B., Guenou, H., Malissen, B., Tajbakhsh, S., and Galy, A. (2011). Pax7-expressing satellite cells are indispensable for adult skeletal muscle regeneration. *Dev. Camb. Engl.* *138*, 3647–3656.
229. Sartori, R., Romanello, V., and Sandri, M. (2021). Mechanisms of muscle atrophy and hypertrophy: implications in health and disease. *Nat. Commun.* *12*, 330.
230. Scapini, P., Lapinet-Vera, J.A., Gasperini, S., Calzetti, F., Bazzoni, F., and Cassatella, M.A. (2000). The neutrophil as a cellular source of chemokines. *Immunol. Rev.* *177*, 195–203.
231. Schnoor, M., Cullen, P., Lorkowski, J., Stolle, K., Robenek, H., Troyer, D., Rauterberg, J., and Lorkowski, S. (2008). Production of Type VI Collagen by Human Macrophages: A New Dimension in Macrophage Functional Heterogeneity. *J. Immunol.* *180*, 5707–5719.
232. Schultz, E. (1996). Satellite Cell Proliferative Compartments in Growing Skeletal Muscles. *Dev. Biol.* *175*, 84–94.
233. Shea, K.L., Xiang, W., LaPorta, V.S., Licht, J.D., Keller, C., Basson, M.A., and Brack, A.S. (2010). Sprouty1 Regulates Reversible Quiescence of a Self-Renewing Adult Muscle Stem Cell Pool during Regeneration. *Cell Stem Cell* *6*, 117–129.
234. Shefer, G., Rauner, G., Yablonka-Reuveni, Z., and Benayahu, D. (2010). Reduced Satellite Cell Numbers and Myogenic Capacity in Aging Can Be Alleviated by Endurance Exercise. *PLoS ONE* *5*, e13307.
235. Shorter, E., Sannicandro, A.J., Poulet, B., and Goljanek-Whysall, K. (2019). Skeletal Muscle Wasting and Its Relationship With Osteoarthritis: a Mini-Review of Mechanisms and Current Interventions. *Curr. Rheumatol. Rep.* *21*, 40.
236. Snijders, T., Nederveen, J.P., Joannisse, S., Leenders, M., Verdijk, L.B., van Loon, L.J.C., and Parise, G. (2017). Muscle fibre capillarization is a critical factor in muscle fibre hypertrophy during resistance exercise training in older men. *J. Cachexia Sarcopenia Muscle* *8*, 267–276.
237. Southard, S., Kim, J.-R., Low, S., Tsika, R.W., and Lepper, C. (2016). Myofiber-specific TEAD1 overexpression drives satellite cell hyperplasia and counters pathological effects of dystrophin deficiency. *ELife* *5*, e15461.
238. Stein, C., Bardet, A.F., Roma, G., Bergling, S., Clay, I., Ruchti, A., Agarinis, C., Schmelzle, T., Bouwmeester, T., Schübeler, D., et al. (2015). YAP1 Exerts Its Transcriptional Control via TEAD-Mediated Activation of Enhancers. *PLoS Genet.* *11*.
239. Stein, S., Thomas, E.K., Herzog, B., Westfall, M.D., Rocheleau, J.V., Jackson, R.S., Wang, M., and Liang, P. (2004). NDRG1 Is Necessary for p53-dependent Apoptosis*. *J. Biol. Chem.* *279*, 48930–48940.
240. Stoll, T., Germann, D., and Hagmann, H. (2001). Physiotherapy in lumbar disc herniation. *Ther. Umsch.* *58*, 487–492.

241. Stuart, T., Butler, A., Hoffman, P., Hafemeister, C., Papalexi, E., Mauck, W.M., Hao, Y., Stoeckius, M., Smibert, P., and Satija, R. (2019). Comprehensive Integration of Single-Cell Data. *Cell* *177*, 1888-1902.e21.
242. Su, A.I., Wiltshire, T., Batalov, S., Lapp, H., Ching, K.A., Block, D., Zhang, J., Soden, R., Hayakawa, M., Kreiman, G., et al. (2004). A gene atlas of the mouse and human protein-encoding transcriptomes. *Proc. Natl. Acad. Sci. U. S. A.* *101*, 6062–6067.
243. Szigeti, K., and Lupski, J.R. (2009). Charcot–Marie–Tooth disease. *Eur. J. Hum. Genet.* *17*, 703–710.
244. Szokodi, I., Tavi, P., Földes, G., Voutilainen-Myllylä, S., Ilves, M., Tokola, H., Pikkarainen, S., Piuholta, J., Rysä, J., Tóth, M., et al. (2002a). Apelin, the Novel Endogenous Ligand of the Orphan Receptor APJ, Regulates Cardiac Contractility. *Circ. Res.* *91*, 434–440.
245. Szokodi, I., Tavi, P., Földes, G., Voutilainen-Myllylä, S., Ilves, M., Tokola, H., Pikkarainen, S., Piuholta, J., Rysä, J., Tóth, M., et al. (2002b). Apelin, the novel endogenous ligand of the orphan receptor APJ, regulates cardiac contractility. *Circ. Res.* *91*, 434–440.
246. Takahashi, A., Kureishi, Y., Yang, J., Luo, Z., Guo, K., Mukhopadhyay, D., Ivashchenko, Y., Branellec, D., and Walsh, K. (2002). Myogenic Akt Signaling Regulates Blood Vessel Recruitment during Myofiber Growth. *Mol. Cell. Biol.* *22*, 4803–4814.
247. Tanideh, N., Shahin Sheikhan, H., Salesi, M., Tamadon, A., Rostamzad, K., and Kardeh, A. (2014). Effects of endurance exercise and estrogen supplementation on the proliferation of satellite cells. *Comp. Clin. Pathol.* *23*, 1645–1649.
248. Tatemoto, K., Hosoya, M., Habata, Y., Fujii, R., Kakegawa, T., Zou, M.X., Kawamata, Y., Fukusumi, S., Hinuma, S., Kitada, C., et al. (1998). Isolation and characterization of a novel endogenous peptide ligand for the human APJ receptor. *Biochem. Biophys. Res. Commun.* *251*, 471–476.
249. Tatemoto, K., Takayama, K., Zou, M.-X., Kumaki, I., Zhang, W., Kumano, K., and Fujimiya, M. (2001). The novel peptide apelin lowers blood pressure via a nitric oxide-dependent mechanism. *Regul. Pept.* *99*, 87–92.
250. Tedesco, F.S., Dellavalle, A., Diaz-Manera, J., Messina, G., and Cossu, G. (2010). Repairing skeletal muscle: regenerative potential of skeletal muscle stem cells. *J. Clin. Invest.* *120*, 11–19.
251. Theret, M., Gsaier, L., Schaffer, B., Juban, G., Ben Larbi, S., Weiss-Gayet, M., Bultot, L., Collodet, C., Foretz, M., Desplanches, D., et al. (2017). AMPK α 1-LDH pathway regulates muscle stem cell self-renewal by controlling metabolic homeostasis. *EMBO J.* *36*, 1946–1962.
252. Theret, M., Rossi, F.M.V., and Contreras, O. (2021). Evolving Roles of Muscle-Resident Fibro-Adipogenic Progenitors in Health, Regeneration, Neuromuscular Disorders, and Aging. *Front. Physiol.* *0*.

253. Thomas, K., Engler, A.J., and Meyer, G.A. (2015). Extracellular matrix regulation in the muscle satellite cell niche. *Connect. Tissue Res.* *56*, 1–8.
254. Tidball, J.G. (2017). Regulation of muscle growth and regeneration by the immune system. *Nat. Rev. Immunol.* *17*, 165–178.
255. Tomasek, J.J., Gabbiani, G., Hinz, B., Chaponnier, C., and Brown, R.A. (2002). Myofibroblasts and mechano-regulation of connective tissue remodelling. *Nat. Rev. Mol. Cell Biol.* *3*, 349–363.
256. Trombetta, J.M., Bradshaw, A.D., and Johnson, R.H. (2010). SPARC/Osteonectin Functions to Maintain Homeostasis of the Collagenous Extracellular Matrix in the Periodontal Ligament. *J. Histochem. Cytochem.* *58*, 871–879.
257. Tsika, R.W., Schramm, C., Simmer, G., Fitzsimons, D.P., Moss, R.L., and Ji, J. (2008). Overexpression of TEAD-1 in Transgenic Mouse Striated Muscles Produces a Slower Skeletal Muscle Contractile Phenotype. *J. Biol. Chem.* *283*, 36154–36167.
258. Uchugonova, A., Gorjup, E., Riemann, I., Sauer, D., and König, K. (2008). Two-photon imaging of stem cells. 68601W.
259. Uezumi, A., Fukada, S., Yamamoto, N., Takeda, S., and Tsuchida, K. (2010). Mesenchymal progenitors distinct from satellite cells contribute to ectopic fat cell formation in skeletal muscle. *Nat. Cell Biol.* *12*, 143–152.
260. Uezumi, A., Ito, T., Morikawa, D., Shimizu, N., Yoneda, T., Segawa, M., Yamaguchi, M., Ogawa, R., Matev, M.M., Miyagoe-Suzuki, Y., et al. (2011). Fibrosis and adipogenesis originate from a common mesenchymal progenitor in skeletal muscle. *J. Cell Sci.* *124*, 3654–3664.
261. Urciuolo, A., Quarta, M., Morbidoni, V., Gattazzo, F., Molon, S., Grumati, P., Montemurro, F., Tedesco, F.S., Blaauw, B., Cossu, G., et al. (2013). Collagen VI regulates satellite cell self-renewal and muscle regeneration. *Nat. Commun.* *4*, 1964.
262. Van den Bossche, J., O'Neill, L.A., and Menon, D. (2017). Macrophage Immunometabolism: Where Are We (Going)? *Trends Immunol.* *38*, 395–406.
263. Verma, M., Asakura, Y., Murakonda, B.S.R., Pengo, T., Latroche, C., Chazaud, B., McLoon, L.K., and Asakura, A. (2018a). Muscle Satellite Cell Cross-Talk with a Vascular Niche Maintains Quiescence via VEGF and Notch Signaling. *Cell Stem Cell* *23*, 530-543.e9.
264. Verma, M., Asakura, Y., Murakonda, B.S.R., Pengo, T., Latroche, C., Chazaud, B., McLoon, L.K., and Asakura, A. (2018b). Muscle Satellite Cell Cross-Talk with a Vascular Niche Maintains Quiescence via VEGF and Notch Signaling. *Cell Stem Cell* *23*, 530-543.e9.
265. Vinel, C., Lukjanenko, L., Batut, A., Deleruyelle, S., Pradère, J.-P., Le Gonidec, S., Dortignac, A., Geoffre, N., Pereira, O., Karaz, S., et al. (2018). The exerkin apelin reverses age-associated sarcopenia. *Nat. Med.* *24*, 1360–1371.

266. Vinel, C., Schanstra, J.P., Boizard, F., Péreira, O., Auriiau, J., Dortignac, A., Breuil, B., Feuillet, G., Nkuipou-Kenfack, E., Zürbig, P., et al. (2019). Apelin affects the mouse aging urinary peptidome with minimal effects on kidney. *Sci. Rep.* **9**, 10647.
267. Wahren, J., Felig, P., Ahlborg, G., and Jorfeldt, L. (1971). Glucose metabolism during leg exercise in man. *J. Clin. Invest.* **50**, 2715–2725.
268. Wang, G., Qi, X., Wei, W., Englander, E.W., and Greeley, G.H. (2006). Characterization of the 5'-regulatory regions of the rat and human apelin genes and regulation of breast apelin by USF. *FASEB J.* **20**, 2639–2641.
269. Wang, S.J., Greer, P., and Auerbach, R. (1996). Isolation and propagation of yolk-sac-derived endothelial cells from a hypervascular transgenic mouse expressing a gain-of-function *fps/fes* proto-oncogene. *In Vitro Cell. Dev. Biol. Anim.* **32**, 292–299.
270. Wang, X., Shen, Q.W., Wang, J., Zhang, Z., Feng, F., Chen, T., Zhang, Y., Wei, H., Li, Z., Wang, X., et al. (2016). KLF7 Regulates Satellite Cell Quiescence in Response to Extracellular Signaling. *Stem Cells Dayt. Ohio* **34**, 1310–1320.
271. Webster, M.T., Manor, U., Lippincott-Schwartz, J., and Fan, C.-M. (2016a). Intravital Imaging Reveals Ghost Fibers as Architectural Units Guiding Myogenic Progenitors during Regeneration. *Cell Stem Cell* **18**, 243–252.
272. Webster, M.T., Harvey, T., and Fan, C.-M. (2016b). Quantitative 3D Time Lapse Imaging of Muscle Progenitors in Skeletal Muscle of Live Mice. *Bio-Protoc.* **6**, e2066.
273. Whitham, M., and Febbraio, M.A. (2016). The ever-expanding myokinome: discovery challenges and therapeutic implications. *Nat. Rev. Drug Discov.* **15**, 719–729.
274. Williams, B.D., Plag, I., Troup, J., and Wolfe, R.R. (1995). Isotopic determination of glycolytic flux during intense exercise in humans. *J. Appl. Physiol. Bethesda Md* **1985** **78**, 483–490.
275. Winbanks, C.E., Chen, J.L., Qian, H., Liu, Y., Bernardo, B.C., Beyer, C., Watt, K.I., Thomson, R.E., Connor, T., Turner, B.J., et al. (2013). The bone morphogenetic protein axis is a positive regulator of skeletal muscle mass. *J. Cell Biol.* **203**, 345–357.
276. Wolfe, R.R. (2006). The underappreciated role of muscle in health and disease. *Am. J. Clin. Nutr.* **84**, 475–482.
277. Wosczyzna, M.N., Biswas, A.A., Cogswell, C.A., and Goldhamer, D.J. (2012). Multipotent progenitors resident in the skeletal muscle interstitium exhibit robust BMP-dependent osteogenic activity and mediate heterotopic ossification. *J. Bone Miner. Res. Off. J. Am. Soc. Bone Miner. Res.* **27**, 1004–1017.
278. Wu, C., Macleod, I., and Su, A.I. (2013). BioGPS and MyGene.info: organizing online, gene-centric information. *Nucleic Acids Res.* **41**, D561–565.

279. Wu, L., Chen, L., and Li, L. (2017). Apelin/APJ system: A novel promising therapy target for pathological angiogenesis. *Clin. Chim. Acta Int. J. Clin. Chem.* **466**, 78–84.
280. Xu, S., Liu, S., Xu, L., Deng, S., He, Y., Li, S., and Ni, G. (2018). Response of decorin to different intensity treadmill running. *Mol. Med. Rep.*
281. Xuan, Y.H., Huang, B.B., Tian, H.S., Chi, L.S., Duan, Y.M., Wang, X., Zhu, Z.X., Cai, W.H., Zhu, Y.T., Wei, T.M., et al. (2014). High-Glucose Inhibits Human Fibroblast Cell Migration in Wound Healing via Repression of bFGF-Regulating JNK Phosphorylation. *PLoS ONE* **9**, e108182.
282. Yablonka-Reuveni, Z. (2011). The skeletal muscle satellite cell: still young and fascinating at 50. *J. Histochem. Cytochem. Off. J. Histochem. Soc.* **59**, 1041–1059.
283. Yaffe, D., and Saxel, O. (1977). Serial passaging and differentiation of myogenic cells isolated from dystrophic mouse muscle. *Nature* **270**, 725–727.
284. Yamada, M., Hokazono, C., Tokizawa, K., Marui, S., Iwata, M., Lira, V.A., Suzuki, K., Miura, S., Nagashima, K., and Okutsu, M. (2019). Muscle-derived SDF-1 α /CXCL12 modulates endothelial cell proliferation but not exercise training-induced angiogenesis. *Am. J. Physiol.-Regul. Integr. Comp. Physiol.* **317**, R770–R779.
285. Yang, J. (2014). Enhanced Skeletal Muscle for Effective Glucose Homeostasis. In *Progress in Molecular Biology and Translational Science*, (Elsevier), pp. 133–163.
286. Yang, W., and Hu, P. (2018). Skeletal muscle regeneration is modulated by inflammation. *J. Orthop. Transl.* **13**, 25–32.
287. Yao, C.C., Ziober, B.L., Sutherland, A.E., Mendrick, D.L., and Kramer, R.H. (1996). Laminins promote the locomotion of skeletal myoblasts via the alpha 7 integrin receptor. *J. Cell Sci.* **109** (Pt 13), 3139–3150.
288. Yin, H., Price, F., and Rudnicki, M.A. (2013a). Satellite Cells and the Muscle Stem Cell Niche. *Physiol. Rev.* **93**, 23–67.
289. Yin, H., Price, F., and Rudnicki, M.A. (2013b). Satellite cells and the muscle stem cell niche. *Physiol. Rev.* **93**, 23–67.
290. Young, M.D., and Behjati, S. (2018). SoupX removes ambient RNA contamination from droplet based single cell RNA sequencing data. *BioRxiv* 303727.
291. Yucel, N., Wang, Y.X., Mai, T., Porpiglia, E., Lund, P.J., Markov, G., Garcia, B.A., Bendall, S.C., Angelo, M., and Blau, H.M. (2019). Glucose Metabolism Drives Histone Acetylation Landscape Transitions that Dictate Muscle Stem Cell Function. *Cell Rep.* **27**, 3939-3955.e6.
292. Zaiss, D.M.W., Gause, W.C., Osborne, L.C., and Artis, D. (2015). Emerging functions of amphiregulin in orchestrating immunity, inflammation and tissue repair. *Immunity* **42**, 216–226.

293. Zammit, P.S., Relaix, F., Nagata, Y., Ruiz, A.P., Collins, C.A., Partridge, T.A., and Beauchamp, J.R. (2006). Pax7 and myogenic progression in skeletal muscle satellite cells. *J. Cell Sci.* *119*, 1824–1832.
294. Zarei, S., Carr, K., Reiley, L., Diaz, K., Guerra, O., Altamirano, P., Pagani, W., Lodin, D., Orozco, G., and Chinea, A. (2015). A comprehensive review of amyotrophic lateral sclerosis. *Surg. Neurol. Int.* *6*, 171.
295. Zhang, J., Ren, C.X., Qi, Y.F., Lou, L.X., Chen, L., Zhang, L.K., Wang, X., and Tang, C. (2006). Exercise training promotes expression of apelin and APJ of cardiovascular tissues in spontaneously hypertensive rats. *Life Sci.* *79*, 1153–1159.
296. Zhang, J., Liu, Q., Fang, Z., Hu, X., Huang, F., Tang, L., and Zhou, S. (2016). Hypoxia induces the proliferation of endothelial progenitor cells via upregulation of Apelin/APLNR/MAPK signaling. *Mol. Med. Rep.* *13*, 1801–1806.
297. Zhang, J., Muri, J., Fitzgerald, G., Gorski, T., Gianni-Barrera, R., Masschelein, E., D’Hulst, G., Gilardoni, P., Turiel, G., Fan, Z., et al. (2020). Endothelial Lactate Controls Muscle Regeneration from Ischemia by Inducing M2-like Macrophage Polarization. *Cell Metab.* *31*, 1136-1153.e7.
298. Zheng, G.X.Y., Terry, J.M., Belgrader, P., Ryvkin, P., Bent, Z.W., Wilson, R., Ziraldo, S.B., Wheeler, T.D., McDermott, G.P., Zhu, J., et al. (2017). Massively parallel digital transcriptional profiling of single cells. *Nat. Commun.* *8*, 14049.
299. Zhou, X., and Wang, T. (2012). Using the Wash U Epigenome Browser to examine genome-wide sequencing data. *Curr. Protoc. Bioinforma.* Ed. Board Andreas Baxevanis *AI 0 10*, Unit10.10.
300. Ziemkiewicz, N., Hilliard, G., Pullen, N.A., and Garg, K. (2021). The Role of Innate and Adaptive Immune Cells in Skeletal Muscle Regeneration. *Int. J. Mol. Sci.* *22*, 3265.
301. Zierer, J., Pallister, T., Tsai, P.-C., Krumsiek, J., Bell, J.T., Lauc, G., Spector, T.D., Menni, C., and Kastenmüller, G. (2016). Exploring the molecular basis of age-related disease comorbidities using a multi-omics graphical model. *Sci. Rep.* *6*, 37646.
302. Zurlo, F., Larson, K., Bogardus, C., and Ravussin, E. (1990). Skeletal muscle metabolism is a major determinant of resting energy expenditure. *J. Clin. Invest.* *86*, 1423–1427.
303. (2014). Medical gallery of Blausen Medical 2014. *WikiJournal Med.* *1*.
304. Muscle Groups | SEER Training.

Curriculum Vitae

Umji Lee

Cornell University, Ithaca,
 NY, USA, 14850
 +1-607-279-6184
dldjawl4@gmail.com
ul35@cornell.edu

1. Education

- Cornell University**, Ithaca, New York, USA (2019 – present)
 Visiting Ph.D. student in Biomedical Engineering
- Swiss Federal Institute of Technology**, Lausanne, Switzerland (2016 – present)
 Ph.D. student in Bioengineering and Biotechnology
- Swiss Federal Institute of Technology**, Lausanne, Switzerland (2013 – 2016)
 Master of Science in Life Sciences and Technologies, Molecular Medicine
- Seoul National University of Science and Technology**, Korea (2008 – 2012)
 Bachelor of Engineering in Food Science and Technology

2. Research Experience

- Ph.D Student**, *Benjamin Cosgrove Laboratory*,
Cornell University, USA (2019 – present)
- Investigating crosstalk between vascular niche and muscle stem cells in hyperglycemic and normal glycemic metabolic conditions
 - Developing the intravital skeletal muscle imaging to tracing spatiotemporal in-vivo dynamics using a multi-photon microscope (Program funded by SNSF grant)
- Ph.D Student**, *Jerome Feige Laboratory*,
Nestle Institute of Health Sciences, CH (2016 – 2019)
- Investigated transcriptional mechanism of Apelin regulation in muscle regeneration.
- Master Student**, *Cowan Chad Laboratory, Harvard University USA* (2016)
- Studied endothelial dysfunction induced by hyperglycemia through DUSP1 in MAPK signaling using human Pluripotent Stem Cells (hiPSC)

Research Assistant, Florian Bentzinger Laboratory,
Nestle Institute of Health Sciences, CH (2015)

- Studied niche dependent metabolic reprogramming of muscle stem cells

Research Assistant, R&N Bio - Stem Cell Research Center,
Seoul, South Korea (2013)

- Optimization of method for culturing mesenchymal stem cells derived from amnion membrane

Publications

1. Lee, U., Laurillard, E., Hong, H., McKellar, D., Heinke C. J., Feige, J, Bentzinger, C.F., Cosgrove, B. Glycemic Levels Regulate Skeletal Muscle Progenitor Function through the Alpha/Beta Hydrolase Ndrp1 in Endothelial Cells (In submission **Skeletal Muscle**) (2021)

2. Lee, U., Stuelsatz, P., Karaz, S., McKellar, D., Russeil, J., Deak, M., Lepper, C., Deplancke, B., Cosgrove, B., Feige, J. Paracrine apelin promotes skeletal muscle vasculogenesis via myogenic Tead1 transcription factor (In revision **iScience**) (2021)

3. Vinel, C., Lukjanenko, L., Batut, A., Deleruyelle, S., Pradère, J.-P., Le Gonidec, S., Dortignac, A., Geoffre, N., Pereira, O., Karaz, S., **Lee, U.,** Camus, M., Chaoui, K., Mouisel, E., Bigot, A., Mouly, V., Vigneau, M., Pagano, A.F., Chopard, A., Pillard, F., Guyonnet, S., Cesari, M., Burlet-Schiltz, O., Pahor, M., Feige, J.N., Vellas, B., Valet, P., Dray, C. The exerkin apelin reverses age-associated sarcopenia **Nature Medicine** (2018) <https://doi.org/10.1038/s41591-018-0131-6>

4. Lukjanenko, L., Jung, M.J., Hegde, N., Perruisseau-Carrier, C., Migliavacca, E., Rozo, M., Karaz, S., Jacot, G., Schmidt, M., Li, L., Metairon, S., Raymond, F., **Lee, U.,** Sizzano, F., Wilson, D.H., Dumont, N.A., Palini, A., Fässler, R., Steiner, P., Descombes, P., Rudnicki, M.A., Fan, C.-M., von Maltzahn, J., Feige, J.N., Bentzinger, C.F., Loss of fibronectin from the aged stem cell niche affects the regenerative capacity of skeletal muscle in mice **Nature Medicine** (2016) 22, 897–905. <https://doi.org/10.1038/nm.4126>

5. Patent KR101588394B1 Media Composition for Improving Renewal Ability and Method for Culturing Stem Cells, R&N Bio Inc., Korea (2013)

Teaching Activities & Memberships

Biomechanics in Physiology (Fall 2018)

Drug Discovery (Fall 2018)

Mise A Niveau : Mathematics 2 (Linear Algebra and Analytic Geometry) (Spring 2018)

Membership in Life Sciences Switzerland (LS2)	(2017-2021)
Membership in Switzerland-Korea Science Association	(2013-Current)

Awards & Fellowships

SNSF Mobility Grant, Fellowship (CHF75,000 corresponding \$84,451)	(2019-2021)
Travel Grant 2019 LS2 (CHF 1500)	(2019)
Best Poster Award, Europe-Korea Conference, Glasgow, Scotland	(2018, August)
Mogam Science Study Abroad Scholarship (\$20,000), Korea	(2013, Sep)
Czech Technical University Exchange Program Scholarship, Korea	(2011-2012)

Posters & Oral Presentations

Apelin promotes capillary remodeling during muscle regeneration via Tead1 transcription factor, Myogenesis Gordon Conference, Lucca, Italy (June 2019)

TEAD1 modulation on apelin directs myogenesis and vascular repatterning, Face Industry Research, Lausanne, Switzerland (Feb 2019)

A High-Throughput Screening of Transcription Factors Regulating Apelin to Reprogram Skeletal Muscle, Invited Talk at Cornell University, Ithaca, USA (Sep 2018)

A High-Throughput Screening of Transcription Factors Regulating Apelin to Reprogram Skeletal Muscle Europe-Korea Conference, Glasgow, Scotland (August 2018)

A High-Throughput Screening of Transcription Factors Regulating Apelin to Reprogram Skeletal Muscle by Inducing Apelinergic Nexus, LIMNA (Lausanne Integrative Metabolism Nutrition Alliance) Symposium, Lausanne (May 2018)

Language

Korean (Native), English (proficient, C1), French (independent, B1), Czech (basic, A1)

References

Benjamin Cosgrove (Ph.D); bdc68@cornell.edu
Assistant Professor, Cornell University

Jerome Feige (Ph.D); Jerome.feige@rd.nestle.com
Head of Musculoskeletal Health Department, Nestle Research

Florian Bentzinger (Ph.D); CF.Bentzinger@USherbrooke.ca
Assistant Professor, University of Sherbrooke

Cowan Chad (Ph.D); chad_cowan@harvard.edu
Associate Professor, Harvard University